QUANTITATIVE MEASUREMENT AND MODELING OF SENSITIZATION DEVELOPMENT IN STAINLESS STEELS

Stephen M. Bruemmer
B.S., University of Illinois, 1975
M.S., University of Illinois, 1977

A dissertation submitted to the faculty
of the Oregon Graduate Center
in partial fulfillment of the
requirements for the degree
Doctor of Philosophy
in
Materials Science and Engineering

May 1988

The dissertation "Quantitative Measurement and Modeling of Sensitization Development in Stainless Steels" by Stephen M. Bruemmer has been examined and approved by the following Examination Committee:

David G. Atteridge, Thesis Advisor
Associate Professor

William E. Wood
Professor and Department Head

Lawrence E. Murr
Professor

Paul Davis
Professor

ACKNOWLEDGMENTS

The author gratefully acknowledges the support from the Division of Engineering Technology, Office of Nuclear Regulatory Research, U.S. Nuclear Regulatory Commission both at Pacific Northwest Laboratory and at the Oregon Graduate Center which made this research possible. Separate funding from the U.S. Department of Energy through Pacific Northwest Laboratory is also appreciated as part of the Advanced Education and Staff-Faculty Interchange Programs and from the Advanced Nuclear Reactor Technology Support Office.

This work would not have been possible without the help, interactions and discussions with many individuals at Pacific Northwest Laboratory (PNL) and the Oregon Graduate Center (OGC). Special recognition is given to Larry Charlot (PNL), who performed the Analytical Electron Microscopy and assisted in many efforts important to this thesis, and Bruce Arey (PNL), who conducted most of the electrochemical experiments. Technical interactions with my thesis advisor and co-worker, Dave Atteridge, and Joseph Muscara of the Nuclear Regulatory Commission were essential to the development of the topic and content contained in this thesis. Additional technical support is also acknowledged from Jack Humason (PNL) and Ashok Advani (OGC).

Appreciation is extended to the PNL-300 Area, Text Processing Group including Benita Gottsch, Joyce Zama, Deb Perez and Shirley Flink for final manuscript typing and lay-up.

Personal thanks are extended to those at PNL who helped make my degree program a reality including Russ Jones, Adrian Roberts, Gary McVay and Pat Hart. The support and friendship from the faculty and staff of the Materials Science and Engineering Department at OGC are also recognized with special regards to Bill Wood and Larry Murr. Finally, special thanks to Dave and Jessie Atteridge for their empathy and hospitality during my stay.

This thesis is dedicated to the women in my life: Soozi, Megan and Kelli, who have shared the trials, tribulations and joys of the university experience. Without them, this effort would not have been possible.

TABLE OF CONTENTS

FIGURES

TABLES

ABSTRACT

Quantitative Measurement and Modeling of Sensitization Development in Stainless Steels

Stephen M. Bruemmer, Ph.D.
Oregon Graduate Center, 1988

Supervising Professor: David G. Atteridge

The current state-of-the-art to quantitatively measure and model sensitization development in austenitic stainless steels is assessed and critically analyzed. A modeling capability is evolved and validated using a diverse experimental data base. Quantitative predictions are demonstrated for simple and complex thermal and thermomechanical treatments. Commercial stainless steel heats ranging from high-carbon Type 304 and 316 to low-carbon Type 304L and 316L have been examined including many heats which correspond to extra-low-carbon, nuclear-grade compositions. Within certain limits the electrochemical potentiokinetic reactivation (EPR) test was found to give accurate and reproducible measurements of the degree of sensitization (DOS) in Type 304 and 316 stainless steels. EPR test results are used to develop the quantitative data base and evolve/validate the quantitative modeling capability.

This thesis represents a first step to evolve methods for the quantitative assessment of structural reliability in stainless steel

components and weldments. Assessments will be based on component-specific information concerning material characteristics, fabrication history and service exposure. Methods will enable fabrication (e.g., welding and repair welding) procedures and material aging effects to be evaluated and ensure adequate cracking resistance during the service lifetime of reactor components. This work is being conducted by the Oregon Graduate Center with interactive input from personnel at Pacific Northwest Laboratory.

1.0 INTRODUCTION

1.1 OVERVIEW

Sensitization in stainless alloys is one of the most studied phenomena related to environmental degradation of engineering materials. Qualitative understanding and methods of prevention were recognized more than 60 years ago. However, failures manifested by intergranular corrosion or stress corrosion continue to be observed. These failures have significant economic consequences and potential safety implications in many industries. Initial problems in nuclear reactor systems began in the mid-60s, but were not considered a generic problem until about 10 years later.

Intergranular (IG) stress corrosion cracking (SCC) has been the predominant degradation mode and has been limited to Boiling Water Reactor (BWR) piping for the most part. Although cracking has been observed in Pressurized Water Reactor (PWR) systems, it is much more severe in BWRs due to the choice of piping material and the higher oxidizing environment. Cracking often is observed in weldment heat affected zone (HAZ) regions or in sections of pipe that have been improperly heat treated. IGSCC cracks have been documented in piping throughout the BWR system including the full range of pipe sizes (3- to 28-in. diameter).

The current state-of-the-art offers many options to minimize IGSCC susceptibility through material, stress state or environment

modifications. In each case, concerns are still raised as to the effectiveness of the particular modification. More quantitative information and understanding needs to be developed to ensure adequate SCC resistance after modification treatment and that it will remain effective after prolonged service exposure. Few guidelines or the necessary information to develop such guidelines exist at the present time to address such problems. Concerns related to welding/repair welding of current and replacement piping and aging effects on component structural reliability need to be examined and resolved. This report details one aspect required in such an analysis, the quantitative measurement and modeling of sensitization.

1.2 OBJECTIVES

Sensitization leads to preferential IG corrosion and/or SCC in both iron and nickel-base stainless alloys. This attack is caused by local regions depleted in chromium along grain boundaries. Until recently quantitative measurement of this phenomena was not possible and, as a result, our understanding and ability to accurately model sensitization was limited. The current capabilities of analytical electron microscopy (AEM) enable a direct analysis of grain boundary chromium depletion. In addition, an indirect electrochemical technique (EPR) has been developed which allows a rapid, inexpensive measurement of a material's degree of sensitization (DOS). These experimental characterization methods create the opportunity to quantitatively analyze and model the sensitization phenomena.

The objectives of this work center on three specific areas impacted by the discussion above:

1. Quantitative Measurement of DOS - the EPR test will be evaluated and quantified by comparison to direct measurements of chromium depletion using AEM,
2. Quantitative Sensitization Data Base - a comprehensive matrix of DOS information will be generated, analyzed and organized to assess and model predictive capabilities, and
3. Quantitative Modeling of Sensitization - a theoretically based model will be evolved to quantitatively predict material DOS as a function of material composition, condition, heat treatment and thermomechanical history.

2.0 BACKGROUND

2.1 DEFINITION OF SENSITIZATION

Quantification of sensitization is a misnomer since the term "sensitization" has been used as a qualitative description indicating simply that an alloy is sensitive to IG corrosion. The first step to quantify this phenomena is to adequately define it. Several observations related to the loss in corrosion resistance prompted the phenomenological description of sensitization:

1. Bulk carbon and chromium concentration has a large effect on a stainless alloy's susceptibility to IG attack
2. A critical temperature regime exists where susceptibility develops which depends on alloy composition
3. Sufficient time is required within the critical temperature regime which again depends on alloy composition.

These general observations have led to the qualitative definition of sensitization as a loss in corrosion resistance due to heat treatment in or through a specific temperature range (500 to 850°C for unstabilized austenitic stainless steels). As a result, any microstructure or localized microchemistry that promotes IG attack has been called "sensitized." This is fundamentally incorrect and has led to

considerable confusion in the literature. Somehow sensitization became analogous to IG corrosion susceptibility of which sensitization is only a small subset.

The development of transmission electron microscopy (TEM) and analytical TEM has enabled a clear understanding of the sensitization process and corroborated the theories of Bain, Aborn and Rutherford[1] proposed more than 50 years ago. Grain boundary regions become susceptible to attack due to the local depletion of chromium. Chromium depletion is prompted by the precipitation and growth of chromium-rich carbides on grain boundaries and differences between carbon and chromium diffusivities. Thus, sensitization is controlled by the thermodynamics of carbide precipitation and the kinetics of chromium diffusion. It occurs in a temperature range where carbides are thermodynamically stable and chromium diffusion is sufficiently rapid for nucleation and growth in a finite time frame. This understanding leads to a mechanistic and more quantitative definition:

> Sensitization refers to the existence of an intergranular chromium-depleted region which results from the precipitation of chromium-rich second phases at grain boundaries.

An interesting aspect of this definition is that it has nothing to do with corrosion resistance. The point here is that sensitization specifies a microstructural/microchemical condition and does not indicate corrosion behavior. An alloy's performance in a corrosive

environment depends on many parameters apart from material characteristics. Certainly, the aggressiveness of the environment itself determines corrosion behavior. Stress state can also directly impact whether a material is resistant or susceptible to attack. Therefore, a second part of the sensitization definition can be added to illustrate the qualitative relationship to localized attack, i.e.,

> This grain boundary chromium-depleted region may promote intergranular corrosion or stress corrosion cracking in certain aqueous environments.

The important concept is that intergranular corrosion or SCC susceptibility is not automatically specified, even if the degree of sensitization is known quantitatively. Different material-environment-stress conditions will lead to different relationships between chromium depletion and susceptibility to intergranular attack. It becomes essential to identify the controlling mechanism(s) for each material-environment-stress system of interest in order to properly assess susceptibility. This area will be discussed in more detail in Section 3.0.

2.2 ENGINEERING IMPORTANCE OF SENSITIZATION

Stainless steel is the most versatile, corrosion-resistant alloy for engineering structures. Applications encompass a wide range of temperatures from cryogenic to elevated and in various industries including power production, chemical and petrochemical, food

processing, dairy and waste handling/processing. In each case, resistance to general corrosion in aggressive environmental conditions justifies its selection. Unfortunately, like most metal systems which form passive films for corrosion resistance, stainless steels are susceptible to localized attack under certain environmental conditions. The primary forms of this localized attack are pitting, intergranular corrosion and SCC. Sensitization is often directly responsible for the latter two and can also have an effect on pit initiation.

The engineering significance of the sensitization phenomena is best illustrated considering the SCC problems encountered in BWR piping. As mentioned previously, cracking in BWRs was first observed more than 25 years ago. Reported pipe cracks have increased at least up through 1983 with about 70 in 1975, 130 in 1978 and 550 in 1983.[2] A wide variety of piping systems have been affected including recirculation, residual heat removal, isolation condenser and control rod drive return lines. The large number of pipes exhibiting cracks has prompted replacement of the entire recirculation system in some plants.

Extensive sensitization-related research has been conducted over the last 20 years. Examples of this work, both basic and applied, are given in References 2 through 20. Although in practice, the problem of sensitization-induced pipe cracking is not eliminated, research has led to an applications-oriented understanding and effective measures to minimize this type of cracking. As with most engineering problems,

adequate solutions are developed without a complete mechanistic understanding to ensure long-term resistance.

The materials solution to BWR SCC problems has centered on the development of extra-low carbon grades of Type 304 and 316 stainless steel. These grades reduce the maximum carbon level to 0.02 wt% and specify higher nitrogen levels (<0.1 wt%) to achieve mechanical properties comparable to Type 304 stainless steel. A new grade of stainless steel was created, i.e., nuclear grade. Type 316 nuclear grade stainless steel has prompted the most interest and use as a replacement material. Although nuclear grades are not immune to IGSCC, they are quite resistant to sensitization during typical welding procedures. Sensitization behavior of such low-carbon stainless steels and the effect of nitrogen additions will be examined in Section 4.2.3.

2.3 PARAMETERS CONTROLLING SENSITIZATION

From the basic definition in Section 2.1, sensitization (i.e., chromium depletion) occurs due to the precipitation of second phases at grain boundaries. Thus, initial understanding of the parameters controlling sensitization must begin with precipitation phenomena in stainless steels.

2.3.1 Precipitate Phases in Austenitic Stainless Steel

A large number of different second phases can form in the 300 series stainless steels including carbides, nitrides and various intermetallics. The dominant carbide is the $M_{23}C_6$-type and nitride

is Cr_2N, while sigma, chi and laves intermetallics can form in low carbon, Type 316. Intermetallic phases may influence corrosion behavior (e.g., grain boundary sigma in certain oxidizing solutions), but do not directly influence sensitization due to relatively low chromium content. Precipitation characteristics of these phases in Type 316 is discussed in some detail by Lai[21] and will not be reviewed here.

The face-centered-cubic $M_{23}C_6$ carbide, which tends to be predominately chromium, controls sensitization development in most 300 series alloys. Precipitation of the carbide is a function of thermal treatment and bulk composition (primarily carbon) of the heat. A typical method of illustrating precipitation behavior is by a time-temperature-precipitation (TTP) diagram as shown in Figure 1. Carbide nucleation and growth occurs first at the interface between delta ferrite and austenite, followed by precipitation at austenite grain

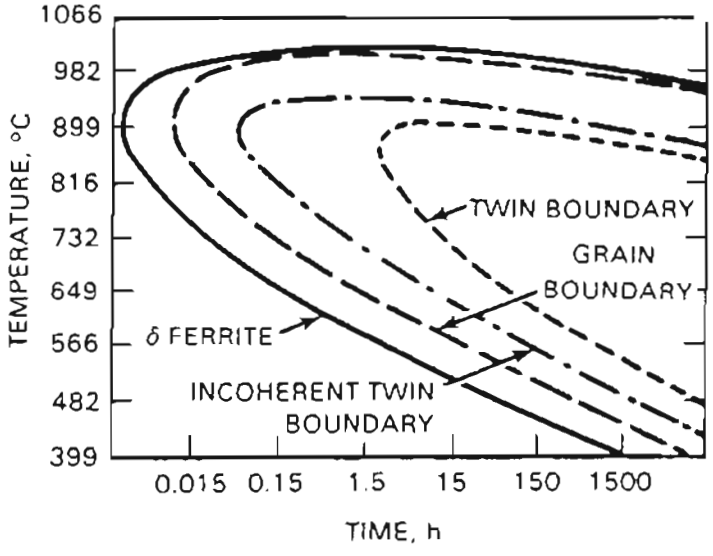

FIGURE 1. Time-Temperature-Precipitation Curves for $M_{23}C_6$ in 0.038% C, Type 304 Stainless Steel from Stickler and Vinckier.[22]

boundaries, incoherent twin boundaries and finally, at coherent twins. The trends shown in Figure 1 for a Type 304SS[22] also have been demonstrated for Type 316,[23] duplex alloys[24] and high-chromium stainless steels.[24] Obviously, delta ferrite will not be present in all alloys, but is possible in many "austenitic" stainless steels depending on bulk composition and processing treatment. Carbon is an extremely effective austenite stabilizer and its content is a critical factor in determining whether ferrite will remain in Type 304 and 316 stainless steels.

Carbide precipitation occurs readily in stainless steels due to the low solid solubility of carbon. Cooling from high temperature will trap an excess or supersaturated amount of carbon which can then precipitate during lower temperature aging. Carbon solubility (S_C) depends on bulk composition, but relatively consistent predictions can be made using empirical relationships determined for a particular type of stainless steel as a function of heat treatment temperature. Perhaps, the best relationship for Type 304 stainless steel was reported by Natesan and Kassner:[25]

$$S_C \text{ (wt\%)} = 1088 \exp(-23653/RT) \qquad (1)$$

Composition effects on the maximum temperature at which carbides precipitate has been reported[20] based on the solubility data of Petrova and Shvartsman:[26]

$$T_{max} \text{ (}^{\circ}\text{C)} = 5500/(2.92 - 0.01 \text{ wt\% Ni} - \ln \text{ wt\% C}) \qquad (2)$$

This equation was developed for $M_{23}C_6$ carbides in austenitic steels containing 20% Cr and 9-40% Ni.

Molybdenum additions have several effects on carbide precipitation including decreasing carbon solubility and increasing the maximum temperature where carbides can form. Converting the relationship of Deighton[27] for Type 316 into a form to determine wt%, the solubility equation becomes:

$$S_C \text{ (wt\%)} = 0.0001 \exp (17.88 - 14426/T) \qquad (3)$$

These relationships predict that the solubility limit is exceeded in a 0.08 wt% alloy at ~980 (304) and ~1015°C (316), while in a 0.02 wt% alloy limits are ~820 (304) and ~870°C (316). Carbide precipitation is therefore favored at temperatures below these values.

The morphology, density and distribution of the $M_{23}C_6$ precipitates also depends on the particular type of boundary. These differences appear to depend on grain boundary misorientation and structure. Carbide morphologies can be classified as two-dimensional "sheets;" as dendrites which are initially lamellar; or as small geometric particles.[28] Geometric carbides are common resulting from precipitates nucleating at grain boundaries and growing preferentially into one grain. A crystallographic orientational relationship is established with the matrix to minimize interfacial energy. Carbides nucleate on high energy sites in the grain boundary, probably at ledges[29,31] or sites of ledge annihilation.[32]

A primary reason that $M_{23}C_6$ prompts chromium depletion is due to its high chromium content. The chromium content in the carbide increases with time at most temperatures. According to Cihal,[20] initial chromium levels in a growing carbide are on the order of 50 at%, while the equilibrium concentration is closer to 65 at%. Experimental measurements on extracted carbides from Type 304 and 316 stainless steels show compositions of $Cr_{16}Fe_7C_6$ and $Cr_{16}Fe_5Mo_2C_6$, respectively.[21,33,34] In any case, $M_{23}C_6$ carbides incorporate large amounts of chromium leading to the situation where localized depletion can occur.

Recent suggestions[35] that carbides growing at low temperatures (300 to 500°C) may be predominately iron-rich is not consistent with the relative stability of a $Fe_{23}C_6$ versus $Cr_{23}C_6$ precipitate. Thermodynamically, the precipitation of the iron-rich carbide is not favored and significant chromium contents are required to stabilize $M_{23}C_6$. Additional information concerning thermodynamic stabilities of various carbides and nitrides in stainless steels are summarized in Reference 20. Most of the remaining discussion will concentrate on the chromium-rich $M_{23}C_6$ carbide (next section) because of its critical importance in sensitization development.

Another precipitate that must be considered is chromium nitride, Cr_2N. This phase can be important in nitrogen- and nuclear-grade stainless steels. Type 304LN and 316LN both will exhibit significant nitride precipitation after heat treatments in the 550 to 750°C temperature range. Nitrides can also form in the nuclear-grade heats

since bulk nitrogen levels can be up to 0.1 wt%. The nitride appears to contain some iron ($Cr_{1.94}Fe_{0.04}N_{0.9}$) in small amounts.[36] Mixed carbo-nitrides may also be possible at lower temperatures, but no definite observations have been reported. Of interest to sensitization is that Cr_2N also incorporates large amounts of chromium and can promote depletion of chromium from the matrix. Nitrogen levels need to be quite high to promote significant nitride precipitation and chromium depletion. Data from several sources[37-42] suggest that more than about 0.15 wt% is required. This area will be addressed in Section 4.23.

Martensite can also form in unstabilized stainless steels under certain conditions. At moderate levels of plastic deformation (i.e., cold work), the planar dislocation structures typical of this low stacking fault energy alloy evolves into cell structures which can contain eta-martensite. With increasing deformation, alpha-martensite can form at eta intersections and becomes quite significant at higher strains. Martensite has been shown to accelerate carbide precipitation (by nucleation and growth at martensite boundaries) and therefore, sensitization kinetics,[43-45] but has a much more complicated effect on SCC.[16,18,46-48]

2.3.2 Thermodynamics of $M_{23}C_6$ Carbide Precipitation

The tendency for a second phase to precipitate from solution depends on its free energy of formation, i.e., whether precipitation is thermodynamically favored. As the free energy, ΔG, becomes more

negative, the driving force for precipitation increases. Free energies for any reaction of the type:

$$x\ M + y\ C = M_x C_y \tag{4}$$

can be expressed at equilibrium as:

$$\Delta G = -\ RT\ \ln K \tag{5}$$

where x and y are constants for a given reaction between two elements, M and C, and K, the equilibrium constant, is described by:

$$K = \frac{a_{M_x C_y}}{(a_M)^x\ (a_C)^y} \tag{6}$$

The terms represented by a's in Equation (6) are activities of the elements in solution and in the second phase. For the $M_{23}C_6$ precipitate controlling sensitization development, the above can be written as:

$$K = \exp\ (-\Delta G)/RT = a_{M_{23}C_6}/(a_{Cr})^{23}(a_C)^6 \tag{7}$$

Since, under standard conditions, the activity of the second phase can be considered unity, the thermodynamic stability and the tendency for precipitation of the carbide is directly related to the activities of Cr and C in solution. Activities are, in turn, proportional to elemental composition (e.g., X_{Cr} and X_C). In ideal

solutions activities equal compositions, while in real solutions they are related through the activity coefficient, γ, by:

$$a = \gamma \cdot X \tag{8}$$

The composition (X) reflected in Equation (8) is not the initial bulk level, but the composition in thermodynamic equilibrium with the second phase (carbide). This concept is important since it is a controlling factor in the development of the chromium-depleted region adjacent to the carbide. Kinetics prompt the formation of the region to accommodate this thermodynamic level of chromium which tends to be significantly less than the bulk content in the "sensitizing" temperature range. An expression can be written from the above to determine the chromium concentration in equilibrium with a $Cr_{23}C_6$ carbide as:

$$X_{Cr} = (1/K)^{1/23} (\gamma_{Cr}) (\gamma_C X_C)^{6/23} \tag{9}$$

This interfacial chromium concentration represents the first step in modeling chromium depletion and sensitization. Its calculation requires knowledge of X_C and the activity coefficients for chromium and carbon. Carbon content can be assumed to be effectively equilibrated since carbon diffuses much more rapidly than chromium. Activity coefficients can be determined using the methodology of Wagner,[49] but it is only consistent for γ_C calculations. As a result, Tedmon et al.[50] treated γ_{Cr} as an adjustable parameter based on corrosion test data. Chromium and nickel concentration effects

on γ_C are illustrated in Figures 2a and 2b. The relationship between γ_{Cr} and bulk chromium content is shown in Figure 2c.

Approximation of γ_{Cr} using an adjustable parameter which is based on indirect corrosion tests leaves much to be desired. It is limited from an empirical as well as a theoretical point of view. Fullman[51,52] and Was[53] have used the Kohler approach[54] to predict γ_{Cr} in austenitic alloys by breaking down the complex interactions into a series of binary parameters. Combining this approach with thermochemical and phase relations data,[55,56] γ's for chromium, nickel and iron can be determined as a function of alloy composition. Additional information concerning specific formulations can be obtained by referring to Fullman's work[51] for austenitic stainless steels or Was's work[53] for a nickel-base stainless alloy. Mozhi et al.[40] has also applied this same approach to help examine nitrogen effects on sensitization in Type 304 stainless steel heats.

Up to this point, simple $Cr_{23}C_6$ carbides have been considered. Most previous modeling efforts have used this approximation primarily out of convenience and a lack of information to describe the more complex carbides. Since the metal component in the $M_{23}C_6$ carbide is predominately chromium, this assumption has not made a significant difference in qualitative predictive capabilities. The presence of other carbide-forming elements besides chromium (e.g., molybdenum, titanium and niobium) can have a strong effect on γ_C and γ_{Cr}.

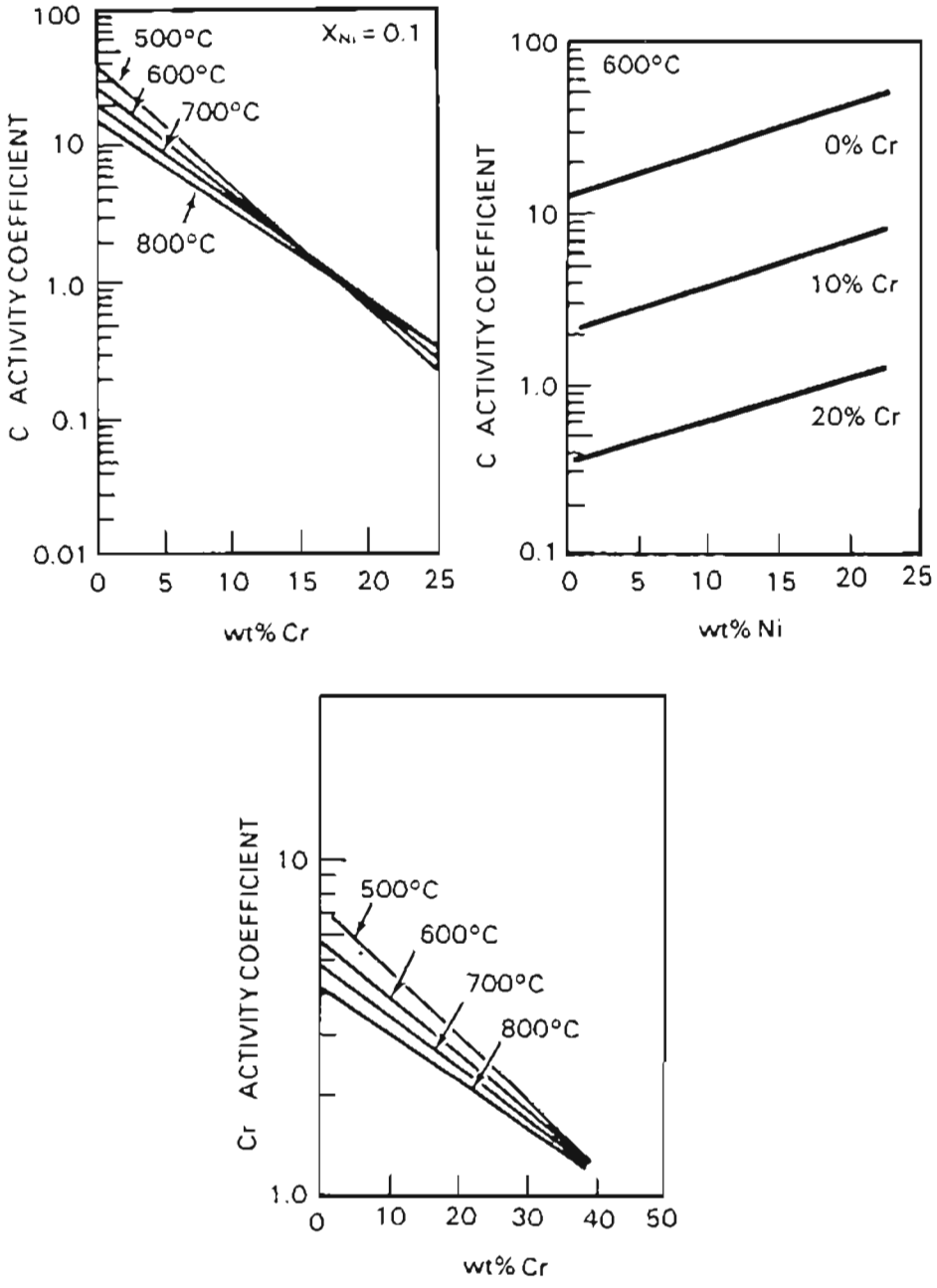

FIGURE 2. Bulk Composition Effects on Carbon (γ_C) and Chromium (γ_{Cr}) Activity Coefficients in Austenitic Stainless Steel: (a) γ_C versus Cr; (b) γ_C versus Ni; and (c) γ_{Cr} versus Cr.[52]

Fullman[51,52] analyzed available thermodynamic data on binary carbides and Fe-Cr-Ni-M-C interactions to predict chromium concentrations in equilibrium with a complex $(Cr,Fe,M)_{23}C_6$ carbide. Partial molar free energies, using ideal solution approximations, were taken from a number of sources to describe the thermochemistry of complex carbides. Data for binary $M_{23}C_6$ carbides often had to be estimated from a series of stable carbides of different compositions. Elemental effects on the free energy of carbide formation was extrapolated leading to an assessment of bulk composition effects on chromium depletion and sensitization. Results of these predictions will be discussed in Section 2.6.1.

2.3.3 Kinetics of Carbide Precipitation and Sensitization

The time-temperature-precipitation diagrams presented in Figure 1 illustrate that kinetics as well as thermodynamics play a critical role in the reaction process. At temperatures below the nose of the C-curve, diffusion kinetics represent the rate-limiting step for carbide precipitation and subsequent sensitization development. Kinetics can be limited by the diffusion rate of a critical element through the lattice, along grain boundaries or pipe diffusion via dislocations. Since the carbide of interest to sensitization is the Cr-rich $M_{23}C_6$, chromium and carbon diffusion kinetics predominate.

Lattice diffusivities for chromium and carbon in austenitic stainless steels have been reported by several investigators. A common limitation in most experiments is the need to extrapolate high

temperature (>900°C) results into a lower temperature regime (500 to 850°C) where sensitization is observed. Even more difficulties can occur when attempting to predict low temperature behavior (<400°C). Chromium[57,58] and carbon[59] diffusivity equations which appear to be most applicable at "sensitizing" temperatures are:

$$\text{Type 304} < \begin{cases} D_{Cr} = 0.08 \exp(-58500/RT) & (10) \\ D_{C} = 6.18 \exp(-22450/RT) & (11) \end{cases}$$

$$\text{Type 316} < \begin{cases} D_{Cr} = 0.33 \exp(-63900/RT) & (12) \\ D_{C} = 0.19 \exp(-18820/RT) & (13) \end{cases}$$

Comparisons based on these relationships predicts faster migration of both elements in Type 304 versus 316 and a large difference (many orders of magnitude) between chromium and carbon diffusion rates. For example, at 650°C chromium diffusivities are about 1×10^{-15} and 2×10^{-16} cm/s for Types 304 and 316, while carbon diffusivities are 2×10^{-5} and 6×10^{-6} for 304 and 316, respectively. These large discrepancies between the rate at which chromium and carbon arrive at the growing carbide promote the development of the chromium depleted zone.

The kinetics of carbide precipitation in austenitic stainless steel has been examined and modeled by Logan.[60] Adapting the approach of Grobner[61] and theories of Christian[62] and Becker,[63] carbide nucleation rates were predicted based on thermodynamics and kinetics defining a critical nucleus. The nucleation rate (J_N) can be expressed as:

temperature (>900°C) results into a lower temperature regime (500 to 850°C) where sensitization is observed. Even more difficulties can occur when attempting to predict low temperature behavior (<400°C). Chromium[57,58] and carbon[59] diffusivity equations which appear to be most applicable at "sensitizing" temperatures are:

$$\text{Type 304} < \begin{cases} D_{Cr} = 0.08 \exp(-58500/RT) & (10) \\ D_{C} = 6.18 \exp(-22450/RT) & (11) \end{cases}$$

$$\text{Type 316} < \begin{cases} D_{Cr} = 0.33 \exp(-63900/RT) & (12) \\ D_{C} = 0.19 \exp(-18820/RT) & (13) \end{cases}$$

Comparisons based on these relationships predicts faster migration of both elements in Type 304 versus 316 and a large difference (many orders of magnitude) between chromium and carbon diffusion rates. For example, at 650°C chromium diffusivities are about 1×10^{-15} and 2×10^{-16} cm/s for Types 304 and 316, while carbon diffusivities are 2×10^{-5} and 6×10^{-6} for 304 and 316, respectively. These large discrepancies between the rate at which chromium and carbon arrive at the growing carbide promote the development of the chromium depleted zone.

The kinetics of carbide precipitation in austenitic stainless steel has been examined and modeled by Logan.[60] Adapting the approach of Grobner[61] and theories of Christian[62] and Becker,[63] carbide nucleation rates were predicted based on thermodynamics and kinetics defining a critical nucleus. The nucleation rate (J_N) can be expressed as:

$$J_N = C \exp\left(-\frac{Q_D + F}{RT}\right) \qquad (14)$$

where C is a constant, Q_D is the activation energy for diffusion of the rate limiting element and F is the energy necessary to form a stable nucleus. Thus, a kinetic term, Q_D, and a thermodynamic term, F, control the rate of nucleation. Two competing energy considerations determine the magnitude of F: the free energy change due to the reaction (Equation 5) and energy required to stabilize the new interfacial surface area created by the precipitating phase. More specific information concerning individual model components is discussed in Section 5.1.2.

The primary interest in this model is that a quantitative prediction of nucleation kinetics can be made and evaluated. Logan used it as a basis for geometry-independent and geometry-dependent precipitate growth and sensitization prediction. In order to take into account geometric effects, finite element modeling was required. Although only a small amount of actual precipitation or sensitization data was examined to validate model predictions,[63] comparisons indicated this approach could be used to match the time-temperature dependence of certain stainless steels. A limitation of the predictive capability appeared to rest on the need to calibrate specific constants in the model based on precipitation/sensitization response. The capabilities of this approach will be evaluated in detail versus $M_{23}C_6$ nucleation data in Section 5.1.2.

the width of the depleted zone increases. Eventually, chromium levels will equilibrate leaving a stable structure with carbides, but no adjacent regions depleted in chromium. This phenomena is called "desensitization" and will be modeled and discussed in Section 5.1.4 and 5.2.3.

Stawstrom and Hillert[57] outlined the basic methodology to predict chromium depletion development. The model assumes for simplicity that carbide precipitation occurs as a continuous film along grain

boundaries. This allows the problem to be solved considering only one-dimensional diffusion. Chromium depletion width (W_{Cr}) can be estimated by:

$$W_{Cr} = 2\sqrt{2 \cdot D_{Cr} \cdot t} \tag{15}$$

Assuming some critical chromium content exists for grain boundary attack (X'_{Cr}), then the width controlling attack (W'_{Cr}) can be determined if the chromium content at the carbide interface, X_{Cr}, is known:

$$W'_{Cr} = 2\sqrt{D_{Cr} \cdot t}\,\frac{X'_{Cr} - X_{Cr}}{Cr - X_{Cr}} \tag{16}$$

where Cr is the bulk chromium level in the heat. More detailed formulations have been reported, but they appear to give comparable predictions. However, this may be due to the lack of a quantitative data base to properly assess predictive capabilities.

2.4 SENSITIZATION AND MATERIAL ELECTROCHEMISTRY

Sensitization by definition specifies a sharp difference in material microchemistry at and near grain boundaries. While the matrix remains at about its initial composition (except for carbon), grain boundary regions exhibit $M_{23}C_6$ carbides, a chromium depleted zone which extends some distance from the boundary and potentially impurity (e.g., phosphorus and sulfur) enrichment at the interface. Thus, four distinct microchemistries may exist in sensitized stainless

steel. Each can affect the mechanical and electrochemical response of the material, thereby impacting IGSCC susceptibility. In most cases, the chromium depleted zone dominates due to its effect on material electrochemistry. The variation in chromium concentration from 16 to 18% for most of the material to as low as 8% near grain boundaries creates a situation where localized attack can occur.

Corrosion is an electrochemical process. As a result, basic corrosion (and SCC) behavior is commonly studied using electrochemical methods. Stainless alloys obtain their corrosion resistance by the presence of chromium. For ternary alloys of iron-nickel-chromium, levels of about 12% or more chromium prompt a significant improvement in general corrosion resistance as indicated in Figure 3. The current density (i.e., corrosion rate) sharply drops in the "passive" region of the polarization curve (~300 to 700 mV, Figure 3a) with increasing bulk chromium content. Chromium additions lead to a reduction in the rate of dissolution in both this passive region and in the "active" potential region at lower potentials (~-50 to 100 mV). At the same time, the potential range over which the material is passive increases and the active range decreases.

These characteristics of electrochemical polarization behavior indicate critical thermodynamic and kinetic aspects defining a materials corrosion resistance. The passive range shows the thermodynamic stability region for protective oxide film formation, while current densities define the kinetics of continuing metal dissolution. Chromium has a strong effect because it incorporates into the film making

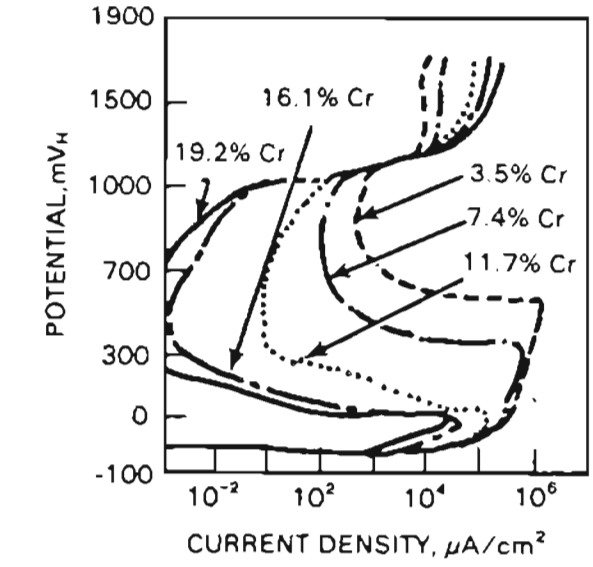

(a)

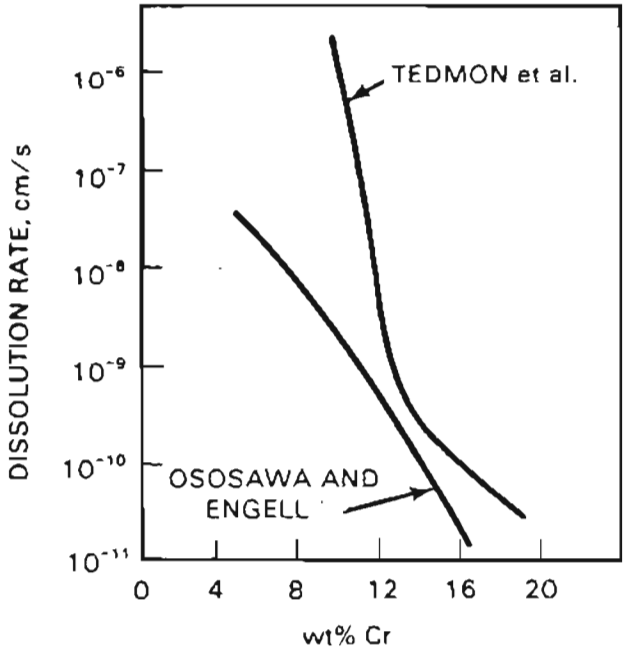

(b)

FIGURE 3. Electrochemical Polarization Behavior (a) and Bulk Dissolution Rates (b) or Fe-10%Ni Alloys as a Function of Chromium Content.[69,70]

it more protective. Enrichment of chromium in the M_2O_3 film increases with bulk chromium concentrations, reaching a rather high metal fraction.[67,68]

The importance of this effect of chromium is that a sensitized material can contain a continuous path of low-chromium, less-passive material which may be susceptible to attack. Such a localized region of active behavior surrounded by a passive matrix can lead to high rates of dissolution. For example, compare the current densities in Figure 3a for a stainless alloy with 16 to 19% Cr (matrix) versus that for a 7.4% alloy (grain boundary) at potentials of ~100 to 300 mV. The simulated grain boundary composition shows dissolution rates more than a million times larger than the matrix. Potentials of this magnitude, near the active-passive transition, have been shown to promote IGSCC and exist in certain service environments such as for BWR piping.[8-10,13-15,71-73]

Electrochemistry of chromium-depleted grain boundaries has been inferred from studies on bulk alloys with compositions representing those typical of boundary regions.[69,70,74,75] All of these investigations reach a similar conclusion as noted above, dissolution rates of a chromium-depleted composition are expected to be much larger than for the matrix. Attempts have also been made to isolate electrochemical response from grain boundary regions in sensitized and nonsensitized materials.[76,77] Results were qualitatively consistent with bulk alloy measurements in that depleted grain boundary regions showed higher dissolution rates.

Other elements can have an effect on the passivation characteristics of stainless steels. Molybdenum is the most important of these for the common alloys. Additions of about 0.5% or more lowers active and passive current densities[20] and improves corrosion resistance. It can directly impact depassivation/repassivation of the film which controls pitting attack and SCC. Molybdenum does not appear to incorporate into the protective film as does chromium, but has been observed to enrich metal surfaces.[78,79] Depletion of molybdenum also occurs during sensitization of Type 316 stainless steel and further degrades localized corrosion resistance. Silicon,[80,81] titanium[82] and copper[20] can improve corrosion resistance under certain conditions, but are not typically present in sufficient quantities except in specialized grades.

Grain boundary reactivity in corrosive environments can also be influenced by the presence and compositions of precipitates and by solute segregation. Electrochemical behavior of second-phase precipitates at grain boundaries has not been extensively studied. Hisamatsu and Ogawa[83] found that the dissolution rate of $M_{23}C_6$-type carbides increased as iron replaced chromium in the carbide. Chromium-rich carbides in sensitized stainless steels are not attacked in most solutions even though the depleted region is aggressively dissolved. These carbides are most likely cathodic to the low chromium region and, if anything, accelerate dissolution of the depleted zone.

Equilibrium solute segregation of impurities, such as phosphorus and sulfur, has been observed in stainless steels[83-91] and

alloys.[92-100] Grain boundary segregation of these elements is known to promote IG corrosion and SCC in many iron and nickel-base alloys. In stainless alloys, phosphorus segregation appears to dominate because of its relatively high impurity level in most grades. Phosphorus enrichment at grain interfaces promotes attack in highly oxidizing environments, e.g., boiling nitric acid.[83,95,99] It also has been implicated in IGSCC of low carbon heats[101] and as the potential controlling species for irradiation-induced SCC.[102-104] Thus, the presence of second phases and segregants at grain boundaries must be considered to assess the overall effect of interfacial microchemistry on IG corrosion and SCC.

2.5 TECHNIQUES TO MEASURE SENSITIZATION

Many different techniques have been used to assess the degree of sensitization (DOS) of austenitic stainless steels. Environments and conditions for these tests vary among tests which leads to a marked difference in material response. As a result, the understanding of what is being measured is critical to interpret information from each test and assess a material's IG corrosion resistance. Obviously, if a technique is sensitive to something besides chromium depletion (e.g., precipitates or impurity segregants), but chromium depletion controls IG attack, test results will not properly assess corrosion resistance. It will indicate some aspect of the material microstructure or microchemistry, unfortunately this aspect may have nothing to do with a particular degradation mechanism in service.

2.5.1 ASTM Standard Corrosion Tests

Five standard corrosion practices have been available for many years to determine if a stainless steel is sensitized.[105] These tests have been standardized by the American Society for Testing and Materials (ASTM A262). Of the five, only Practice E, the copper sulfate-sulfuric acid test is sensitive to only chromium depletion, applicable to common grades and can give at least semiquantitative information concerning DOS. A key accelerant in this test (often referred to as the Strauss test) is the presence of metallic copper in solution with the stainless steel specimen. Copper accelerates IG attack by stabilizing the stainless steel's electrochemical potential near the active-passive transition region, Figure 4. As already discussed, dissolution rates for chromium depleted zones are much greater than for the matrix.

Several methods have been used to quantify DOS after exposure to the Strauss test solution. Depth of penetration measurements are the most common, often determined after specimen fracture. The most limiting aspects of this technique is the extensive exposure times required and its destructive nature. Slightly sensitized (low DOS) materials may necessitate multiple solution exposures of 72 hours each to assess material condition.

Perhaps, the most often used of the standard practices is the oxalic acid etch test (Practice A). It is a rapid method to identify nonsusceptible materials. Stainless steels which give an unacceptable

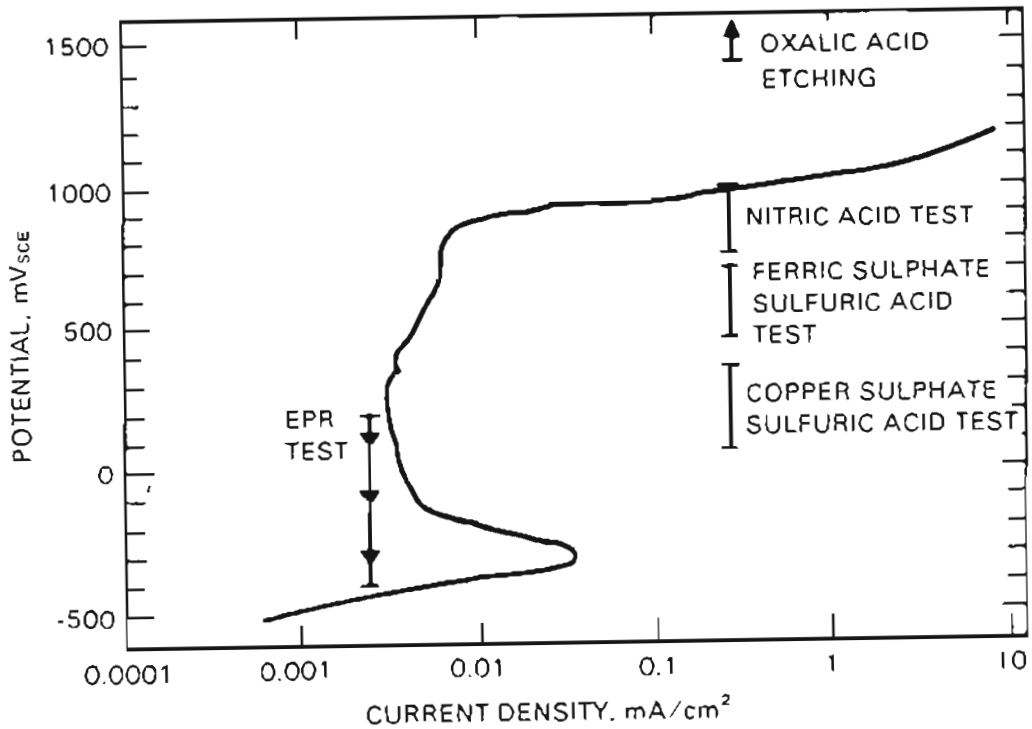

FIGURE 4. Electrochemical Potential Regimes for Sensitization Tests Relative to the Active-Passive Polarization Behavior of Austenitic Stainless Steel.

etch structure must be evaluated by a more quantitative test. However, this technique has been shown to produce excellent results for most practical purposes.[106,107] Materials which exhibit grain boundary etching (dual or ditched structure) have IG carbides and are probably sensitized. The problem with the oxalic acid etch is that carbides are preferentially attacked and results do not directly reflect chromium depletion. Since carbide precipitation and growth is necessary to produce depletion, avoiding carbides at grain boundaries will effectively avoid sensitization. This test would not differentiate between a desensitized (carbides but not sufficient chromium

depletion to cause attack) and sensitized material. Stainless steels can exhibit this desensitized structure after short high-temperature heat treatment (>800°C) or long times at moderate temperatures (700-800°C). Although the oxalic acid test is referred to as a corrosion test, it consists of an electrochemical etch at highly anodic potentials (Figure 4).

Another of the standard tests which is commonly used is the nitric acid or Huey test. Stainless steels are polarized into transpassive potentials by the boiling nitric acid solution as indicated in Figure 4. This solution is quite aggressive prompting attack of not only chromium depleted regions, but also carbides, sigma-phase and segregated phosphorus. Solution aggressiveness increases with time as Cr^{+6} ions are produced by the corrosion process. Thus, exposure steps are limited to 48-hour periods. Because of the highly oxidizing conditions present in the Huey test, it is most applicable for screening materials to be used in comparable environments, e.g., nitric acid. The Huey test has been used to indicate the presence of grain boundary phosphorus segregation as noted in Section 2.4.

The final two standard practices, the ferric sulfate-sulfuric acid and nitric-hydrofluoric acid tests, are not applied to document sensitization as routinely as for the other tests. This is particularly true for the nitric-hydrofluoric, which was developed for molybdenum grades. Handling of hydrofluoric acid solutions appears to limit its use. The ferric sulfate, or Streicher, test is occasionally used, but is not as effective as the copper sulfate test. Carbides,

chromium depletion and possibly impurity segregation are attacked by this solution. It is also highly oxidizing due to the presence of Fe^{+3} ions and approaches transpassive potentials (Figure 4).

In summary, the only ASTM standard practice which is capable of measuring DOS for stainless steels is the copper sulfate-sulfuric acid test. All other solutions attack additional microstructural or microchemical components besides the chromium depleted zone. A critical aspect of the Strauss test is that it polarizes stainless steels into the active-passive transition potential regime. While quantification of Strauss test results are difficult, semiquantitative measurements of DOS can be made which reflect actual chromium depletion.

2.5.2 Electrochemical Methods

The differences in electrochemical dissolution and passivation behavior between high- and low-chromium stainless steels outlined in Section 2.4 have led to several electrochemical methods for the determination of DOS. Constant potential etching has been the simplest of these employing various solutions such as sulfuric and perchloric acids.[108-111] Electrochemical potential is controlled in the active-passive transition region where maximum differences between the depleted zone and the bulk is found. Chung and Smialowska[111] selected a potential corresponding to a second anodic peak prompted by dissolution of the chromium depleted zone. DOS was evaluated by the current density achieved at this potential or the integrated current over some etching time. A difficulty with constant potential etching

is the selection of an optimum potential for general testing. Even for heats within the same grade of stainless steel, this potential probably shifts significantly from heat to heat. Thus, calibration would be required for each heat to make quantitative DOS comparisons.

A method to avoid this single potential limitation is by using electrochemical potentiodynamic tests, i.e., scan across potentials, thereby collecting data throughout the active-passive region of interest. Considerable effort has been put forth in this area to develop methods and procedures.[112-124] Several base solutions have been employed, but the most common is sulfuric acid. Typically, a reverse scan at a controlled rate is used starting at a potential where the entire specimen is passive. Reactivation, or scanning from the passive-to-active regimes, leads to localized film breakdown and attack of regions sufficiently depleted in chromium. If the material is nonsensitized, the passive film will stay intact and suppress the large active peak observed for sensitized stainless steels.

Quantitative measurement of DOS has been based on the charge transfer accumulated during the reactivation scan[114] or by comparison of the reverse scan to the forward potential scan.[121] Since measured values depend on a variety of test, environment and material parameters, these must be kept constant to properly assess DOS. Clarke[114] designated this method as the electrochemical potentiokinetic reactivation or EPR. Test procedures were standardized for Type 304 and 316 stainless steels using simply the reactivation scan. Later, Umemura et al.[121] documented a comparable approach for the

"dual" scan technique (forward and reverse scans). Both methods show excellent correlations with the ASTM standard corrosion tests and the Strauss test in particular. EPR test results have also been shown to agree with IGSCC susceptibility in certain environments including high-temperature oxygenated water.[116,125]

The EPR test method exhibits numerous advantages over the ASTM standard practices described above. It is a rapid and nondestructive (only light surface attack) method of determining DOS and IG corrosion and SCC. Potentiokinetic reactivation can discriminate between DOS values for various heats within the same grade and for Type 304 versus 316 stainless steels. Most importantly, EPR appears to only attack chromium depleted zones similar to the Strauss test. All of these factors make the EPR test ideal for parametric studies of sensitization in the laboratory, as well as assessing a material's condition prior to, or during, service. Field cells have been developed which allow DOS analysis of engineering components such as welded piping in BWR systems.[114,121]

2.6 APPROACHES TO MODEL SENSITIZATION

Sensitization has been modeled both phenomenologically and mechanistically. Phenomenological modeling was pioneered by Cihal[126] and is based on the normalization of bulk compositional effects on IG corrosion and SCC susceptibility. As a result, it is limited to qualitative predictions for heat-to-heat comparative purposes. Mechanistic modeling began with the proposal that chromium depletion explained

sensitization phenomena.[1] Forty years later, Stawstrom and Hillert[57] and Tedmon et al.[50] formulized many of the relationships needed to predict the development of the chromium-depleted zone and enable a quantitative description of DOS to be made. Both of these approaches will be reviewed briefly in this section to indicate current capabilities to assess sensitization.

2.6.1 Phenomenological Modeling: Composition Equivalence

Sensitization has long been realized to depend on material bulk composition and carbon content in particular. Cihal[125] attempted to "quantify" composition effects by normalizing heat-to-heat differences through the use of effective carbon and chromium concentrations. Carbon was normalized in relation to nickel and chromium by molybdenum:

$$C_{eff} = C + 0.002\ (Ni - 10) \tag{17}$$

$$Cr_{eff} = Cr + (1.0 \text{ to } 1.7)\ Mo \tag{18}$$

where concentrations of each element are expressed in weight percent. Equivalent IG corrosion and SCC resistance (K_{eq}) could then be defined for alloys with equal values of:

$$K_{eq} = Cr_{eff} - 100\ C_{eff} \tag{19}$$

This equivalence concept enables the assessment and ranking of individual stainless steel heats. Higher values of K_{eq} indicates

improved IGSCC resistance and vice versa. Since equivalence must be based on sensitization, it relates to the chromium depletion that can be reached. Redefining K_{eq} as a "composite" chromium value,[6,127] combining Equations (16), (17), and (18) and dropping the constant for simplicity gives:

$$Cr^* = Cr + (1.0 \text{ to } 1.7)\ Mo - 100\ C - 0.2\ Ni \qquad (20)$$

where Cr* is the composite chromium concentration in weight percent. Values range from about 9% for high-carbon stainless steels to about 16% for low-carbon heats.

The concept that Cihal equivalence parameters must be related to local chromium concentrations prompted Fullman[53] to calculate parameters based on thermodynamics of carbide formation (Section 2.3.2). By considering the effect of individual alloying elements on carbon activity and carbide stability, chromium-equivalency parameters for many elements were determined. Making a few assumptions,[6] Cr* can be defined as:

$$\begin{aligned} Cr^* = Cr &+ 1.45\ Mo - 0.19\ Ni - 100\ C - 0.51\ Al \\ &- 0.2\ Co + 0.01\ Cu + 0.13\ Mn - 0.22\ Si \\ &+ 0.61\ Ti + 0.34\ V + 0.22\ W \end{aligned} \qquad (21)$$

Most of these elements have only a small effect on Cr* unless they are present in levels much higher than typical.

Bruemmer[6,127] evaluated the above composition-based relationships and others by comparison to a large data base of time-temperature-sensitization measurements (>100 heats).

Times-to-sensitize, as measured by the indirect techniques reviewed in Section 2.5, were compared to Cr* predictions. Linear regression analysis was performed on data as a function of heat treatment temperature with the best overall fit found using a slightly modified version of Cihal's parameters:

$$Cr^* = Cr + 1.6\ Mo - 0.2\ Ni - 100\ C \qquad (22)$$

An example of the correlation between predicted Cr* and measured time to sensitize is presented in Figure 5 for 650°C data. The equation in the figure represents this correlation and shows that time-to-sensitize can be estimated through Cr* although significant scatter (as much as two orders of magnitude) exist. Indications that a much better data fit could be obtained if second order (e.g., C*Ni, C*Cr and Mo*Mo) terms were allowed in the Cr* equation, have been reported.[7] Unfortunately, more detailed relationships have not been developed and validated.

2.6.2 Mechanistic Modeling: Chromium Depletion

The compositional modeling described above simply indicates the relative potential of a stainless steel heat to sensitize. It gives no direct information concerning whether a material will become sensitized as a result of heat treatment or, if it does, the resultant DOS. Such information requires mechanistic understanding and modeling. The basis of such modeling must begin with the thermodynamics and kinetics of carbide precipitation and chromium depletion profile

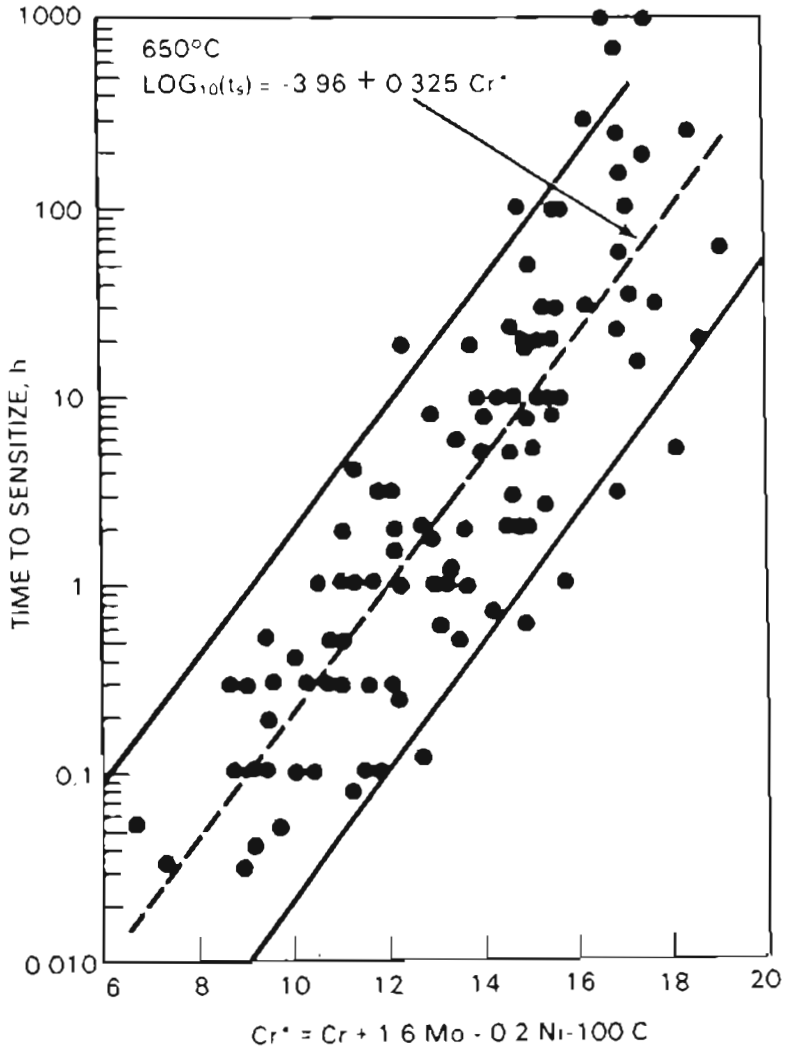

FIGURE 5. Correlation Between Composition Normalization Parameter, Cr*, and Isothermal Time-to-Sensitize Data.(6)

evolution. These areas have been reviewed in Sections 2.3.2 and 2.3.3 and pertinent equations were presented. Formulations directed specifically for DOS prediction, or more accurately, the prediction of the depth and width of the chromium-depleted zone as a function of time and temperature, were documented in Equations (9) and (14).

Predictions using the general approach of Stawstrom and Hillert[57] and some more detailed models will be discussed here.

Numerous investigators[20,40,41,46,53,58,60,64-66] have attempted to explain experimental sensitization data using the Stawstrom and Hillert approach. The success of these predictions has been somewhat mixed. Qualitatively, they have shown that the correct process prompting IG attack, chromium depletion, is being modeled. As a result, time-to-sensitize data can be modeled reasonably well in many cases. However, this success is often dependent on empirical adjustment of selected baseline parameters such as the critical values for chromium depletion (minimum and width) for attack to occur. Prediction of heat-to-heat variability is possible only qualitatively. There have been few attempts to evaluate more quantitative predictive capabilities due in part to the inability to generate an adequate DOS data base for comparison.

Exceptions to this lack of quantitative prediction has been shown in recent work by Was,[53] Briant and Hall[94] and Lackey[46] where theoretical predictions were compared to actual measured chromium depletion profiles. These profiles were measured using analytical electron microscopy (AEM) which is capable of directly determining chromium concentrations across grain boundaries. Unfortunately, grain boundaries typically exhibit significant variability in carbide morphology and density and in chromium depletion. It becomes extremely difficult to make any statistically relevant comparison. AEM can be used to document the minimum chromium contents if the width

of the profile is sufficient (>~20 nm). This data can be compared to predictions of interfacial chromium content from carbide thermodynamics such as that shown in Figure 6. In general, current models underpredict chromium minimums at lower temperatures (>~600°C) and overpredict minimums at higher temperatures (>~700°C). AEM will be discussed in more detail in Section 3.2 and in relation to model predictions of chromium depletion in Section 5.2.1.

The chromium depletion comparisons mentioned above have been limited to single heats after selected heat treatments. The most

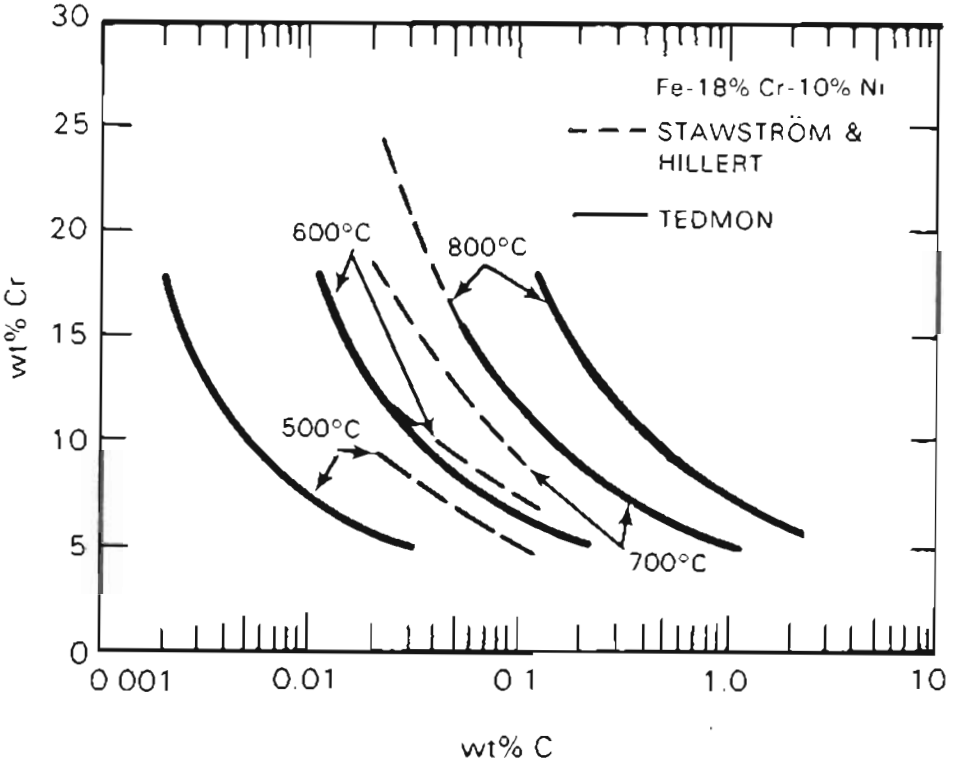

FIGURE 6. Relationship Between Chromium and Carbon Concentrations at the Carbide-Matrix Interface Predicted Using Methods of Stawstrom and Hillert[51] and Tedmon et al.[52]

complete example for stainless steels is the work of Lackey[46] on a high-carbon Type 304. Depletion profiles were mapped after several heat treatment times and temperatures. Measured and predicted (using Stawstrom and Hillert model) depletion widths are shown in Figure 7 for the total depletion width (W_{Cr} from Equation 13) in (a) and the critical width below 13% (W'_{Cr} from Equation 14) in (b). Although experimental data documents the increase in depletion with heat treatment at both 600 and 675°C, it does not match the trend predicted by the $\sqrt{D_{Cr}t}$ term. Depletion width is overpredicted for most times except initial W_{Cr} predictions as illustrated in Figure 7a. Lackey suggested that this inconsistency could partially be explained by the importance of grain boundary diffusion versus lattice diffusion in carbide growth. This aspect of sensitization development was proposed by Tedmon et al.[50] who incorporated both grain boundary and lattice diffusivities to describe kinetics.

The important conclusion from the application of chromium depletion modeling to date is that quantitative predictive capability has not been demonstrated. On the contrary, even though the basic theoretical approach appears to be available, DOS cannot be predicted as a function of thermal history for stainless steel heats. Modeling has primarily been used to show trends and make qualitative assessments of behavior. Very little parameter optimization has been attempted to improve predictive capability. One critical aspect which needs more accurate description, at least in comparison to experiment, is the

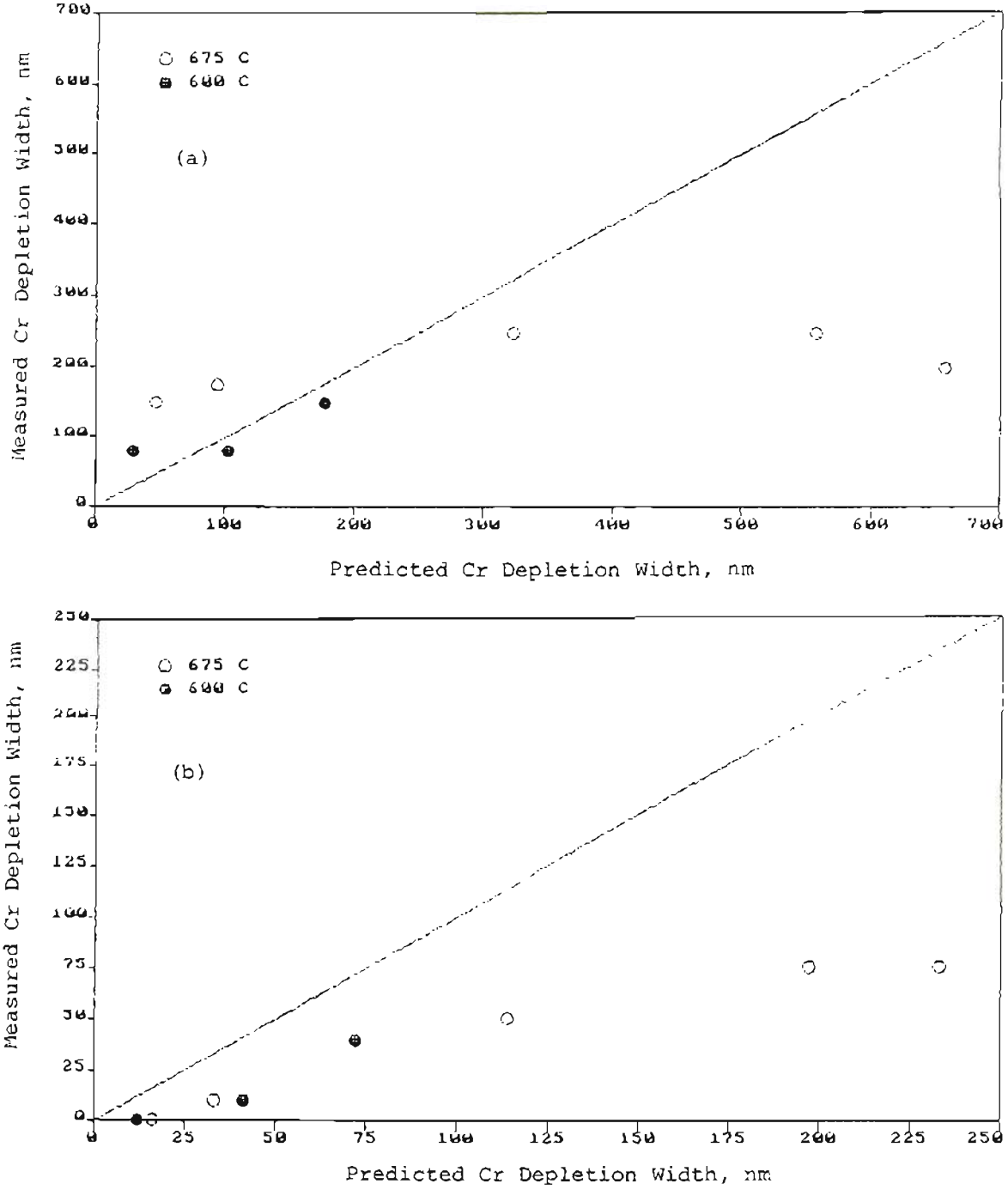

FIGURE 7. Comparison of Measured (by AEM) and Predicted Chromium Depletion from Data of Lackey[46]
(a) Total Width and (b) Width below 13%.

minimum chromium depletion levels in the depleted zone. However, perhaps the most pressing need for quantitative model evolution is the development of a data base which can be used to evaluate model predictions.

3.0 QUANTITATIVE MEASUREMENT OF SENSITIZATION

3.1 DIRECT MEASUREMENT OF CHROMIUM DEPLETION

Since sensitization refers to the presence of a chromium depleted region at grain boundaries, the best method to assess DOS would be to directly map this region. Several microanalytical techniques are currently available with either the resolution, elemental sensitivity and selectivity necessary, but few combine all of these capabilities. The most flexible technique is AEM using a scanning transmission electron microscope (STEM) equipped with an energy dispersive X-ray spectrometer (EDS). Chromium depletion phenomena in stainless alloys has been documented and studied by many investigators.[40,41,53,93,94,99,100,125,128-134] In order to compare direct and indirect DOS measurement capabilities and assess the effect of DOS on IGSCC, selected experiments were designed and performed to interrelate STEM-EDS, EPR and IGSCC results.

3.1.1 Experimental Procedure

Three austenitic stainless steels with relatively high carbon concentrations were selected for analysis. Bulk compositions were determined by chemical analysis from two sources and averaged since differences between sources were minor. These compositions are listed in Table 1. Heats were solution annealed at 1100°C for 1 hour, water

TABLE 1. Bulk Composition of Stainless Steels, wt%

Alloy	C	Cr	Ni	Mo	Mn	Si	N	P
304-C6	0.062	18.5	8.75	0.20	1.72	0.39	0.07	0.013
304-C7	0.072	18.5	9.33	0.43	1.74	0.46	0.04	0.046
316-C10	0.050	17.4	10.91	2.17	1.71	0.63	--	0.013

quenched, and isothermally heat treated at various temperatures between 480 and 900°C. Heat treatment times ranged from 0.5 to 5000 hours. Average grain sizes of the Type 304 and 316 heats were found to be approximately 120 microns after solution annealing.

Microchemistry data was obtained using a Philips EM 400T STEM equipped with a Kevex EDS detector interfaced to a Tracor Northern analyzer. An incident probe of 10 nm was typically used leading to a through-thickness resolution for the thin-foil (~100 to 150 nm in thickness within analysis regions) specimens of about 25 nm. Chromium profiles were mapped by:

(a) Tilting the specimen into a position to orient the grain boundary edge-on to the detector.

(b) Accumulating EDS Spectra at locations perpendicular to the boundary, starting on the boundary between suitably spaced carbides and determining chromium content in steps typically 25 nm apart.

(c) A minimum of five high-angle grain boundaries were examined for each material condition. No attempt was made to document boundary orientation or generate statistically relevant values for chromium minimums or depletion widths.

More detailed information concerning the procedure and basis for the STEM-EDS measurements is given elsewhere.[134,135] The purpose in this section is to present chromium depletion data for an in-depth evaluation of EPR measurement capability in the following sections.

3.1.2 STEM-EDS Measurements of Chromium Depletion

Grain boundary chromium depletion profiles varied with heat treatment time and temperature. The most consistent time sequence was carried out at 700°C and showed depletion widths increasing with heat treatment time for both Type 304 and 316 heats. An example of this dependence is documented for the C6 heat in Figure 8. The total width of depletion increased from about 70 nm after 1 h, to 100 nm after 10 h and finally to 500 nm after 100 h. The density and size of carbides ($M_{23}C_6$) along grain boundaries also increased with time. A major change between 1 and 10 h was the increase in carbide density on specific boundaries and a significant rise in the fraction of interfaces containing carbides. Extending exposure to 100 h prompted a large increase in carbide size. Microstructures indicating boundaries with a high density of carbides is presented in Figure 9. These microstructures are typical for the 10 and 100 h specimens, but reflect a higher density for the 1 h specimen.

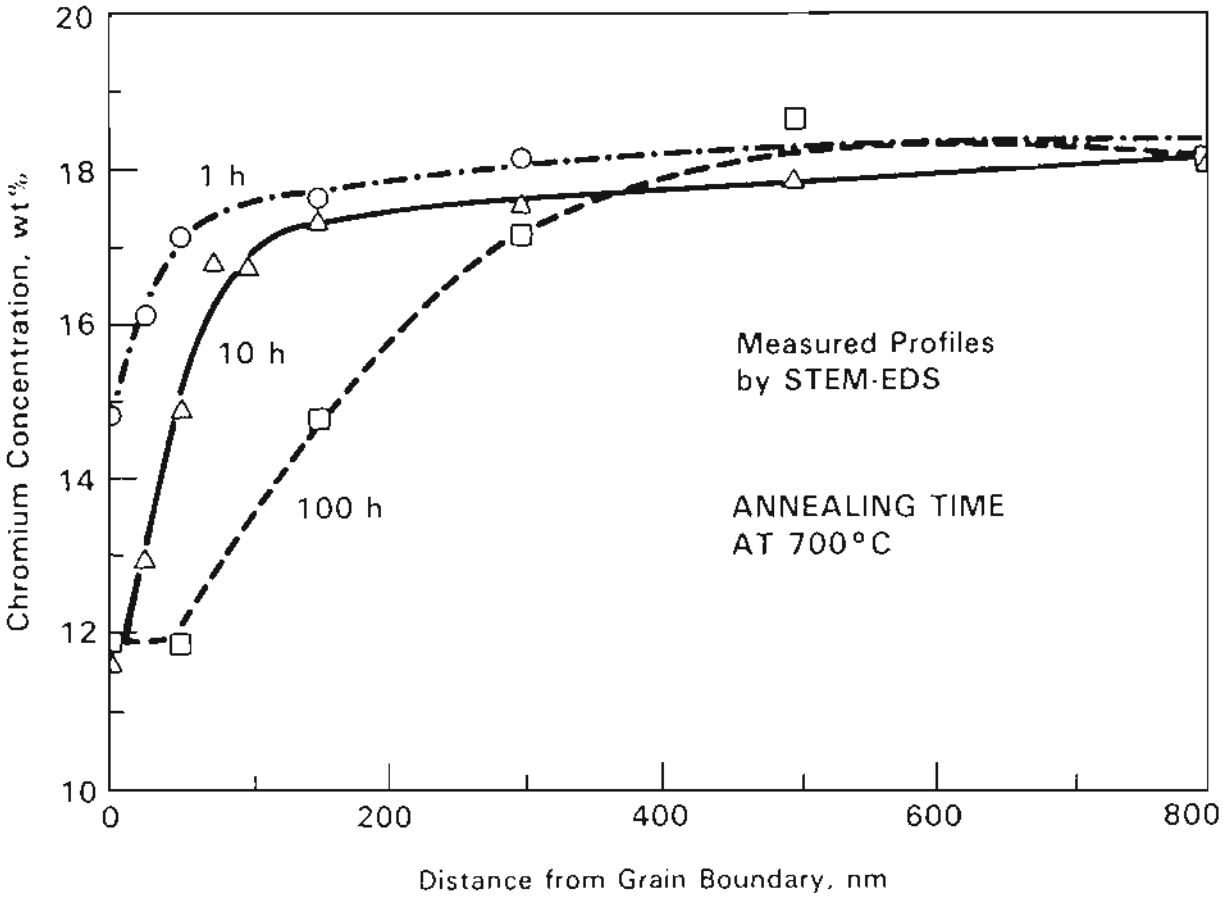

FIGURE 8. Measured Chromium Concentration as a Function of Distance from the Grain Boundary in Type 304, Heat C6 Specimens Heat Treated at 700°C.

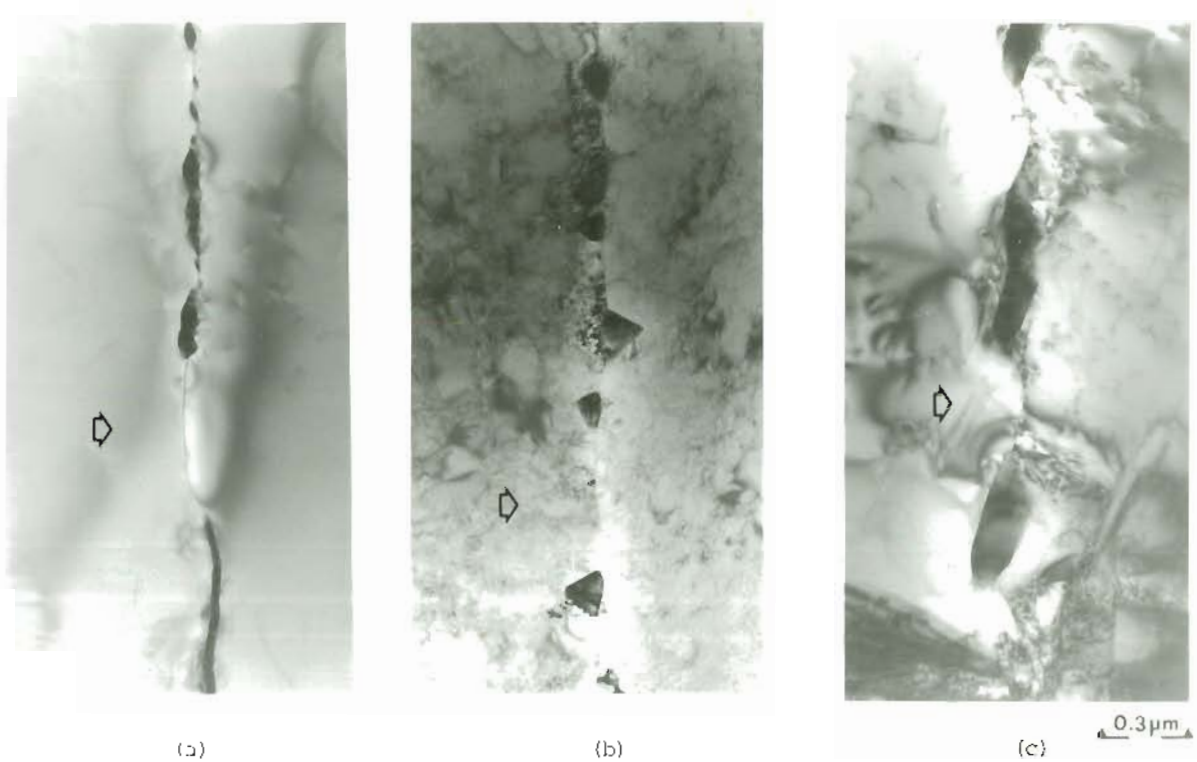

FIGURE 9. Transmission Electron Micrographs Documenting Carbide Distributions in Type 304 Specimens Heat Treated at 700°C for (a) 1 h, (b) 10 h and (c) 100 h.

The change in carbide precipitation characteristics with time suggests that initial grain boundary structure and energy controls nucleation and early stages of sensitization development. Depletion profiles are significantly different boundary-to-boundary (among high angle grain boundaries) in the 1-h specimen, consistent with this concept. As heat treatment time increased, precipitation at high-angle boundaries becomes much more consistent, and no large boundary-to-boundary variability is noted. This is also true for general comparisons for chromium depletion profiles. Widths appeared to be similar within a range of about 20%. Differences still existed even after 100 h between high-angle and low-angle boundaries, e.g., twins. Carbides at twin boundaries were only observed after the longest heat treatment time.

Minimum chromium concentrations at grain boundaries also showed differences among the 700°C specimens. Measured minimums decreased from about 12.5 wt% after 1 h, to 11.4 wt% after 10 h, and then increased again to nearly 12 wt% due to the 100 h anneal. The difference between 1 and 10-h specimens resulted from the limitation in resolution for the STEM-EDS technique. Chromium depletion profiles for the 1-h specimens were very sharp and narrow (Figure 8). Since approximately a volume corresponding to a two-dimensional width of 25 nm is sampled by the electron beam, minimums reflected the average measurement of chromium level over a region where chromium is changing

significantly. In order to estimate actual minimums at the grain boundary (C_{GB}), values were interpolated from measured minimums (C_M) using a relationship from Was, et al. (53):

$$C_{GB} = (C_M - (D/3A) * C_A)/(1 - D/3A) \quad (23)$$

where D is the diameter of the region analyzed and C_A is the measured concentration at a distance A from the boundary. Thus, the shape of the depletion profile is used to indicate the "true" minimum concentration.

Interpolated minimums indicate that minimum chromium levels do not decrease with time as suggested by measured values in Figure 8. Calculations using Equation (23) give chromium concentrations of slightly below 11 wt% after 1 or 10-h anneals and increases by about 1 wt% after 100 h. The increase after long heat treatment times is consistent with the change in bulk carbon content (decreasing). This prompted a thermodynamic change in the interfacial chromium content. As a result, even though depletion width and sensitization increased with time, desensitization somewhat negated the effect by increasing minimum chromium levels. Grain boundary minimums and depletion widths are summarized for the various heat treatments examined in Table 2.

The importance of kinetics on sensitization development is also indicated by examining depletion widths as a function of heat treatment temperature. Depletion evolved much more slowly at 600 versus 700°C, for example. This difference is evidenced by comparing

TABLE 2. Summary of Minimum Grain Boundary Chromium Concentrations and Chromium Depletion Widths

Heat	Heat Treatment °C/h	Grain Boundary Cr Content, wt%		Typical Depletion Width, nm			EPR-DOS C/cm^2
		Range of Measurements	Interpolated Minimum[a]	13% Cr	Below 14% Cr	15% Cr	
C6	STEP COOL[b]	10.4-13.8	9.2	30	50	60	44
	480/5000	9.6-14.7	8.9	70	80	110	34
	500/100	14.4-17.2	10.3	<10	10	20	16
	700/1 + 500/100	11.0-12.9	10.8	50	150	300	63
	600/9	13.1-14.5	10.1	<10	12	20	10
	600/57	11.9-15.3	10.3	20	40	50	43
	600/100	11.4-11.9	10.4	30	50	100	46
	625/25	11.0-12.7	10.0	20	30	30	35
	700/1	12.5-14.1	10.8	10	15	20	14
	700/10	11.4-13.0	10.8	20	40	50	60
	700/100	11.9-12.9	11.8	100	275	320	82
	800/10	14.5-16.1	14.4	0	0	320	1
	600/57 + 800/0.03	12.6-13.7	12.1	10	50	60	21
	600/57 + 825/0.03	12.9-14.6	12.5	<10	40	60	14
	600/57 + 850/0.03	13.7-16.7	13.3	0	35	70	4
	600/57 + 900/0.03	13.8-14.2	13.7	0	20	80	0.5
C7	STEP COOL	11.2-13.4	9.5	20	30	40	23
	480/5000	8.7-14.9	8.4	90	100	130	66
	600/9	13.0-13.4	10.4	<10	10	20	9
	625/25	11.4-12.6	10.1	10	25	30	25
C10	STEP COOL	12.6-13.5	10.5	10	25	40	15
	600/100	11.5-12.0	11.1	60	150	180	51
	700/1	15.9-16.4	14.6	0	0	<10	3
	700/10	10.4-11.6	10.0	50	85	120	35
	700/100	11.7-12.3	11.6	200	400	500	100
	800/10	11.9-13.7	11.8	100	150	250	35
	900/0.5	14.1-16.0	13.6	0	10	30	0

(a) Interpolated minimums are determined from depletion profiles using Equation 23.
(b) STEP COOL TREATMENT (°C/h): 700/1 + 600/25 + 500/110 + 400/200.

measurements after 100 h. Chromium-depletion widths decreased by a factor of three due to the slower kinetics at 600°C. A heat treatment of 5000 h at 480°C resulted in a depletion width comparable to that after only 100 h at 600°C. The reverse trend can be seen as data from higher temperatures are examined. Widths at 700°C were 3 to 6 times smaller than at 800°C for an identical thermal exposure (10 h).

Differences in depletion widths are qualitatively consistent with temperature effects on chromium diffusivity which controls the development of the depleted zone. Chromium diffusivity relationships were discussed in Section 2.3.3 and in Equations (10) and (12). Inputting appropriate temperatures into these equations shows that chromium diffusivity increases by about a factor of 35 from 600 to 700°C and a factor of 14 from 700 to 800°C for Type 304 (C6) stainless steel (slightly larger increases are noted for Type 316). Remembering that for the simplest comparison (Equation 15), depletion width is proportional to the square root of chromium diffusivity, differences in measured depletion widths between these temperatures should be on the order of 3 to 6 times. Quantitative predictions of depletion profiles will be presented and evaluated in Section 5.2.4.

Temperature also had an effect on minimum grain boundary chromium concentrations. Minimums increased with increasing temperature as can be seen by comparing data at 480, 600, 700 and 800°C in Table 2. Concentrations increased from about 9% at 480°C, to 10% at 600°C and to nearly 11% at 700°C. There are insufficient data to document the same trend in the Type 316 heat, but measurements at 700,

800 and 900°C indicate it exists. However, since desensitization becomes significant at higher temperatures even after only short times, minimums may not reflect thermodynamic values. For example, just as minimums increased with annealing to 100 h at 700°C, a comparable increase from the true thermodynamic minimum has certainly occurred after 10 h at 800°C. Thus, most, if not all, of the interpolated minimums represent values at least slightly greater than thermodynamic equilibrium concentrations established after carbide nucleation.

In order to obtain better estimates of minimum grain boundary chromium concentrations at high temperatures, a dual heat treatment of 57 h at 600°C followed by two minutes at 800, 825 or 850 was performed. Isothermal heat treatments at temperatures of 800°C and greater resulted in large, well-spaced carbides and significant grain boundary migration. Both of these effects lead to boundary-to-boundary variations in depletion as well as some variation in depletion characteristics along a single grain boundary. Longer annealing times decreased this variability somewhat, but by that time desensitization directly impacts minimum chromium concentrations. The dual treatment (illustrated in Figure 10) eliminated most of these problems.

Heat treatment at 600°C established a nearly uniform distribution of small carbides along high-angle boundaries and a relatively consistent, boundary-to-boundary, depletion profile. The high density of carbides effectively pinned the boundaries during the subsequent

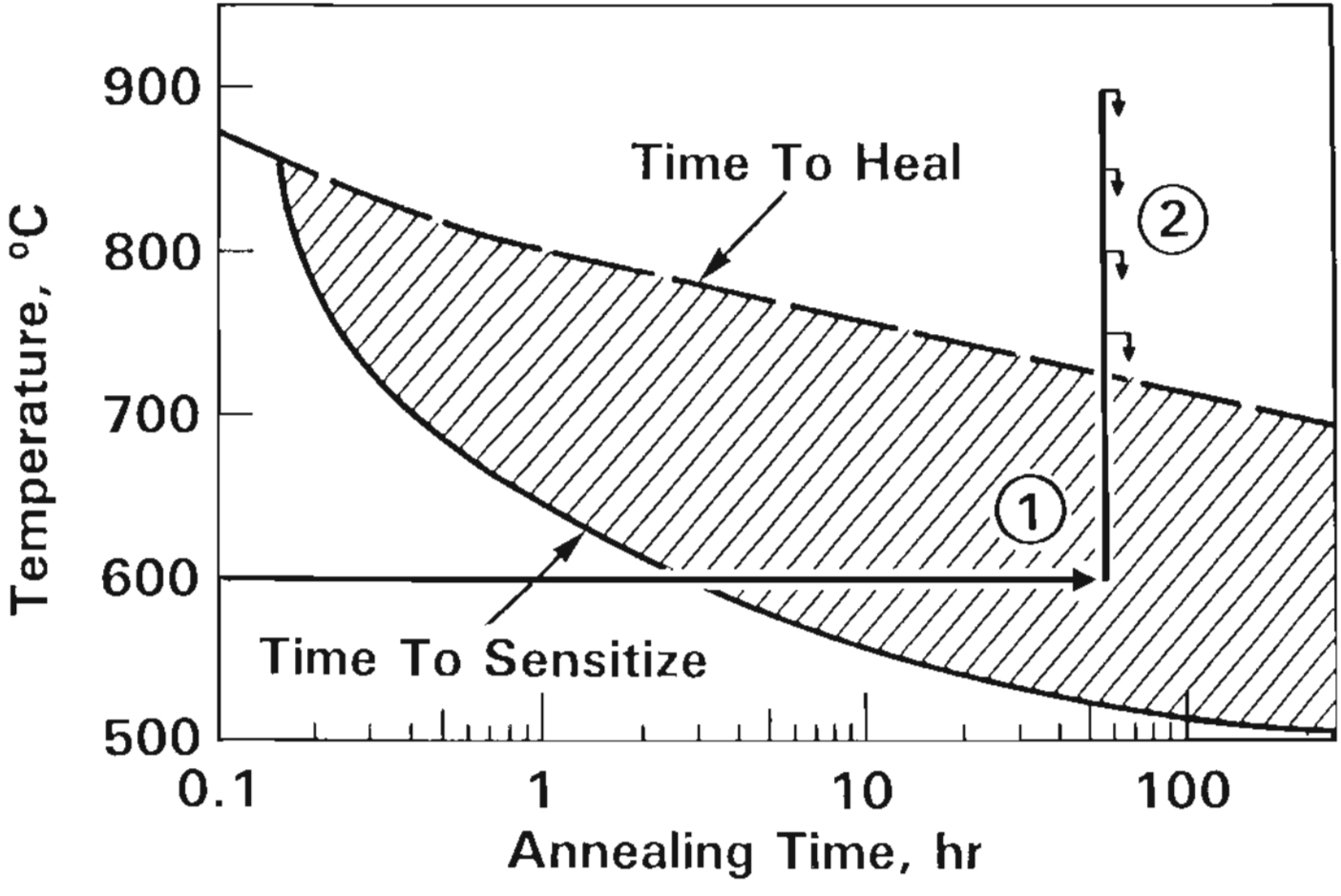

FIGURE 10. Heat Treatment Sequence for the Variable Chromium Minimum Series Tests.

high temperature anneal. This same high intergranular carbide density and initially stable depletion profile prompted a consistent change in depletion with temperature of the second treatment.

Minimums increased from about 10 wt% at 600°C to 12.1, 12.5 and 13.3 wt% for final treatments at 800, 825 and 850°C, respectively. Depletion widths also exhibited a small increase as illustrated in Figure 11. Although it is likely that the dual treatment specimens better indicate thermodynamic minimums, it is not certain that this value is achieved or exceeded during the two minute anneal. Diffusivity calculations suggest that chromium will migrate from about 30 to 100 nm which should be sufficient to reestablish local chromium equilibrium at the higher temperature.

An attempt was also made to extend the temperature range over which chromium minimums could be established by using a step-cool heat treatment. In this case, the purpose was to nucleate carbides and initial depletion at higher temperatures and then heat treat long enough to promote a minimum representative of lower temperatures. Typically, it would require thousands of hours to nucleate and grow carbides sufficiently for depletion to be measured at temperatures below about 500°C. Results for the 480°C/5000 h specimens indicate how slow the kinetics become at these lower temperatures. The step-cool treatment consisted of 700°C/1 h + 600°C/25 h + 500°C/110 h + 400°C/200 h, with specimens furnace cooled between individual steps.

Measured minimums after step cooling were similar or slightly larger for Type 304 heats than those measured after the 480°C heat

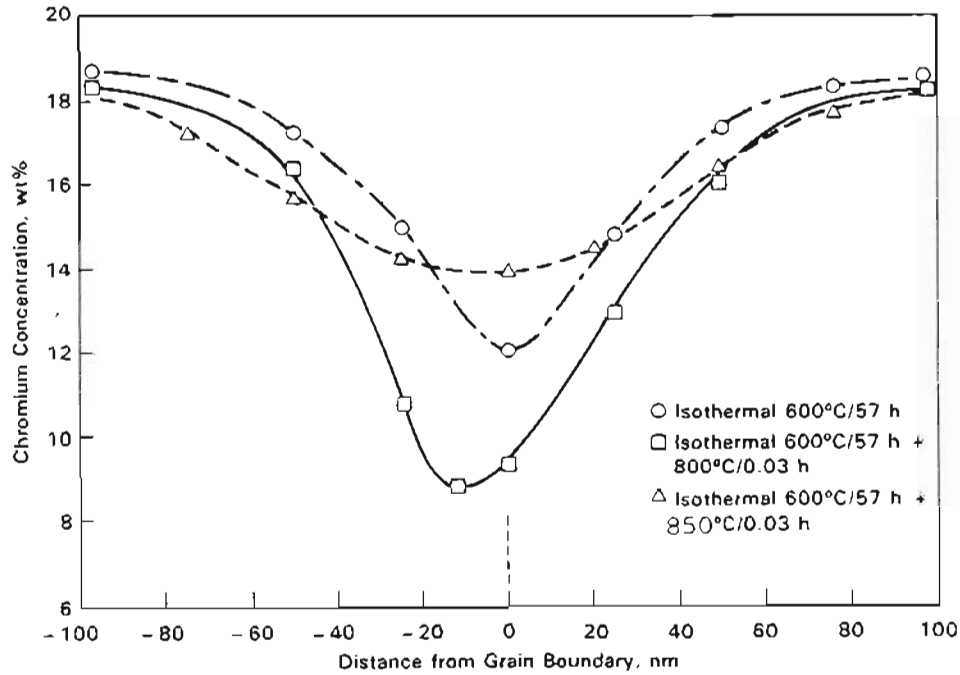

FIGURE 11. Measured Chromium Depletion Profiles in Type 304 Stainless Steel Illustrating the Effect of the Second (Dual) Heat Treatment

treatment. It is not known whether this indicates that interfacial chromium levels do not continue to decrease at lower temperatures or simply that the kinetics of our final thermal step at 400°C were insufficient to establish minimums reflecting the new equilibrium. Schmidt et al. (35) suggested that carbides may be increasingly iron-rich as temperature is reduced. This would help explain the isolated step-cool data, but is inconsistent with the overall data trend. Minimum chromium contents as a function of temperature will be modeled and further evaluated in Section 5.2.1.

Although most of the discussions above refer to the more complete data base for the C6, Type 304 heat, measurements on C7 and the

Type 316 heat (C10) are supportive. The 480°C/5000 h, C7 specimen shows the smallest minimum chromium concentration at 8.4 wt%. Measured minimums were consistently lower than for the C6 specimen, perhaps due to the higher carbon content in the C7 heat. The Type 316 heat tends to show smaller chromium minimums at high temperatures (>700°C) reflecting the effect of molybdenum. Molybdenum increases the upper temperature where carbide precipitation and sensitization will occur and decreases kinetics as noted earlier.

Grain boundary regions were also depleted in molybdenum relative to the matrix concentration (~2.2 wt%). However, this depletion was not consistent with heat treatment and rarely could be effectively mapped across boundaries. The minimum molybdenum levels measured were on the order of 1.0 to 1.5 wt% in the 700 C/10 h specimen, but significant boundary-to-boundary variations were observed. Addition experimentation and analysis required to adequately document molybdenum profiles was not performed.

3.2 INDIRECT MEASUREMENT OF SENSITIZATION

Chemical and electrochemical methods to measure sensitization were reviewed in Section 2.5. Of the methods considered, electrochemical potentiokinetic reactivation (EPR) was identified as possessing the most potential for quantitative DOS analysis. The need for a rapid, inexpensive test for quantitative DOS measurement is obvious. In this section EPR test procedure and results on selected heats will be presented for comparison to STEM-EDS measurements of chromium

depletion. By comparing the indirect EPR-DOS to direct information concerning depletion, the potential for using EPR to quantiatively measure DOS will be assessed. The EPR test will also be used in the following section to develop a large parametric data base documenting sensitization as a function of material and heat treatment variables.

3.2.1 Experimental Procedure

Several different approaches for EPR testing have been proposed, but the most common have followed the work of Novak et al.[113] and Clarke[114-116]. This approach has been described in detail and is under consideration to become an ASTM recommended practice. In addition, equipment for simplified laboratory and field use has been developed and is being sold commercially. As a result, suggested procedures of Clarke were followed.

Potentiokinetic scans were made using either a Princeton Applied Research potentiostat/galvanostat (Model 173) and a universal programmer (Model 175) or a semi-automatic system for EPR measurement called "Sensitest" which consists of a Instruspec Model WC-5. After initial calibration experiments, the majority of all tests were performed using the WC-5 unit. This unit incorporates the functions of a potentiostat, electrometer and programmer, as well as integrating current-time measurements.

Test solution for these experiments was kept constant at 0.05M H_2SO_4 + 0.01M KSCN. Temperature effects on EPR-DOS measurements were evaluated[7] and indicated that small variations can lead to

significant changes in measured DOS. Because of this, test temperature was specified to ±0.5°C with all testing performed at 30°C. Solutions were prepared on approximately a weekly basis since KSCN will tend to oxidize over a period of time. Tests were conducted in a standard laboratory corrrosion cell containing about 0.5 liter of solution. Cell solution was changed every 10 to 20 tests depending on the DOS (i.e., amount of material dissolved) of specimens examined.

Stainless steel specimens were mounted and metallographically polished to a 1 μm diamond finish. Surface area was controlled to a circular area 0.38 cm in diameter by a precut masking tape. Specimen was placed in solution with the analysis surface facing downward and care was taken to ensure no air bubbles were trapped on the specimen surface. The specimen was electrically connected through the mounting material to the potentiostat. A platinum rod, about 0.3 cm in diameter was used as the counter electrode with a saturated calomel electrode as the reference. Initial comparisons between deaerated and non-deaerated solutions showed no effective differences in measured EPR-DOS or reactivation behavior. As a result, remaining tests were all performed in non-deaerated solution.

EPR tests were conducted in the following sequence:

(1) Establish and record corrosion potential, E_{corr}

(2) Shift potential to a passive potential of 0.2 V, SCE and hold for 2 minutes

(3) Scan in the cathodic direction at a rate of 6 V/h for Type 304 or 3 V/h for Type 316.

Each of these steps is done automatically with the WC-5 unit. Corrosion potential must be stable before the passivation step is initiated. The reactivation scan will also be stopped if passivation step is ineffective (i.e., current must drop below a somewhat arbitrary level). Stainless steels of this work typically exhibited E_{corr} between -0.37 and -0.47 V, SCE.

Typical reactivation scans are shown in Figure 12 illustrating observed differences in the maximum reactivation current, (I_r), the Flade potential (E_F) and in the integrated charge transfer (Q) as a function of DOS. The Q values are normalized by the specimen area and grain size as described previously (Section 2.5.2) to define EPR-DOS

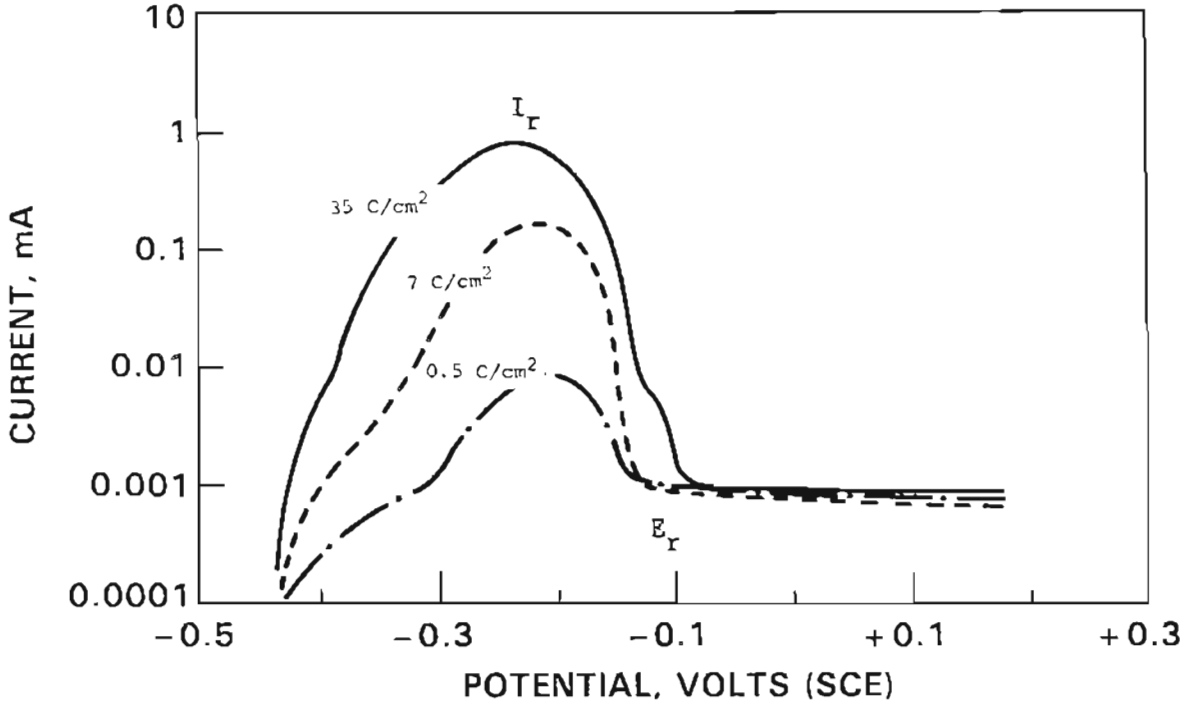

FIGURE 12. Examples of Potentiokinetic Reactivation Scale for C6 Specimens with Different Levels of Sensitization, EPR-DOS Values are Indicated

which is identical to the Pa term used by Clarke.[114] EPR-DOS or the charge transfer per unit area is reported as coulombs (C)/cm^2. Increasing EPR-DOS values reflect the increase in intragranular attack as shown in Figure 13.

A minimum of two EPR tests were conducted per material condition. In most cases, duplicate results were quite consistent showing differences less than about 20%. If larger variations were observed, additional tests were performed to improve confidence of EPR-DOS value reported. Average values are used throughout this report. EPR-DOS measurements which exhibited higher test-to-test variability were limited to a few specimens with low levels of sensitization (EPR-DOS < 2 C/cm^2). These difficulties were, in part, due to attack within the matrix resulting in part from dissolution of nonmetallic inclusions. At low EPR-DOS numbers, the charge transfer due to intragranular attack can be significant in certain heats.

3.2.2 EPR Measurements of DOS

Sensitization development in heats C6 and C10 was measured after heat treatments from 500 to 800°C and times ranging from 0.1 to 100 h. At moderate temperatures (600 and 700°C) both heats exhibited a continuous increase in EPR-DOS with annealing time (Figure 14). The Type 304 heat shows larger values at shorter times due to the more rapid chromium diffusivity in Type 304 versus 316 stainless steel. Measurable EPR-DOS requires times of about 1 and 10 h for heat C10 at temperatures of 700 and 600°C, respectively. This compares to about

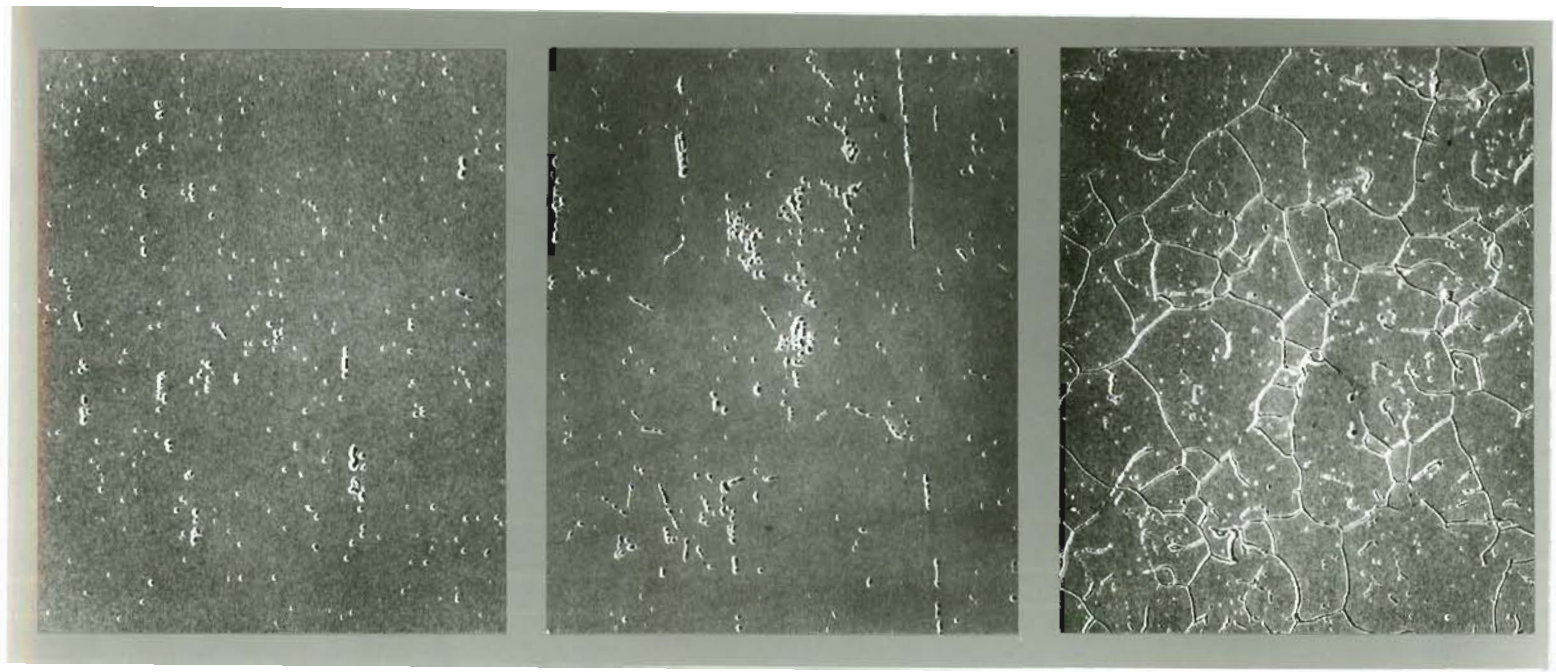

(a) (b) (c)

FIGURE 13. Optical Micrographs Illustrating Attack in the EPR Test for Three DOS Levels: (a) 0.5, (b) 7 and (c) 35 C/cm^2.

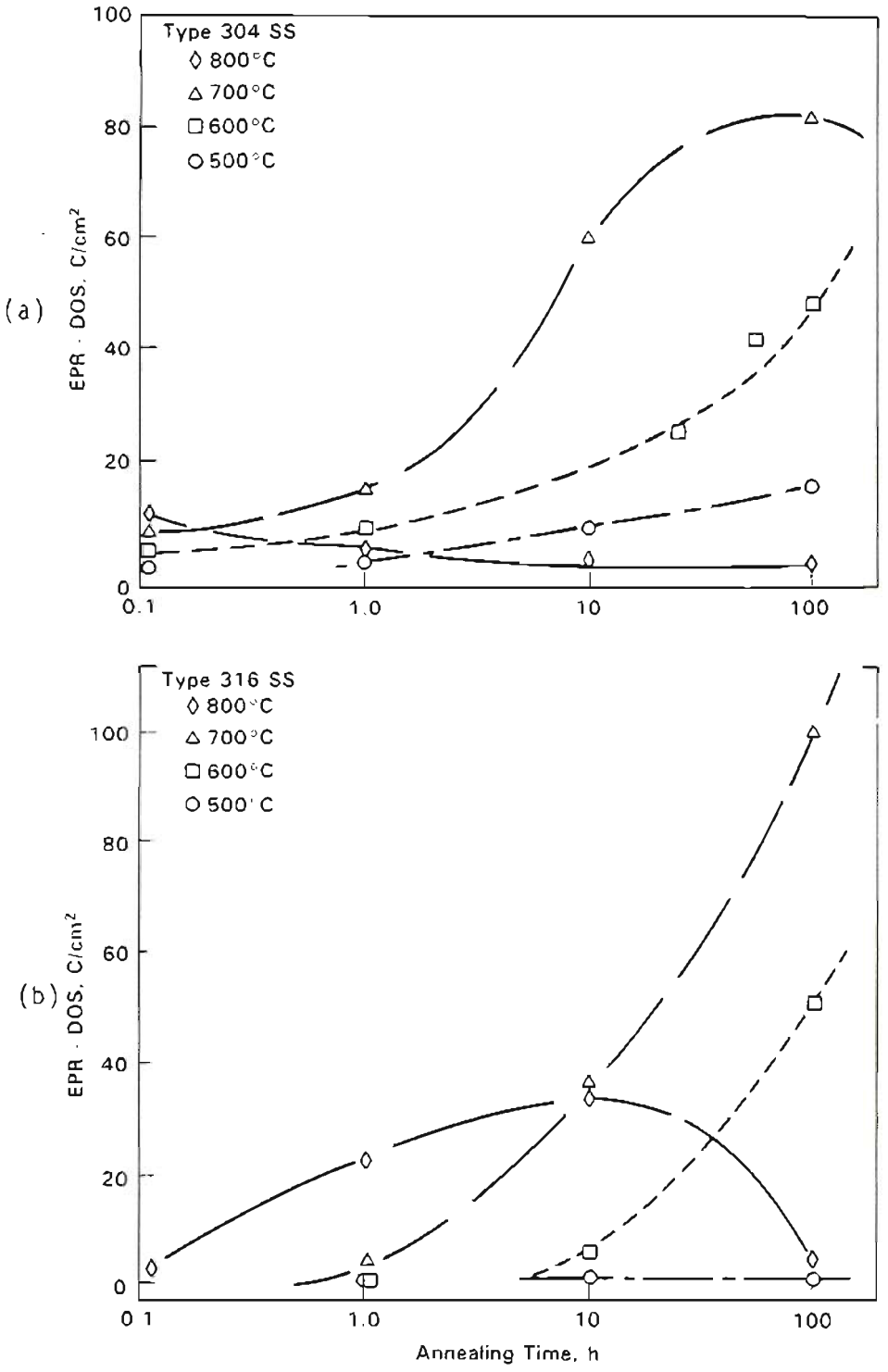

FIGURE 14. Sensitization Development in Type 304 - Heat C6 (a) and 316 - Heat C10 (b) Stainless Steels as a Function of Heat Treatment Temperature and Time

0.1 and less than 1 h for heat C6 at the same temperatures. The 500°C data, where only the Type 304 heat exhibits sensitization within a 100-h anneal, also reflect differences in sensitization kinetics.

Another distinction in the sensitization response of the two stainless steels is due to desensitization. Again diffusivity differences are the key determining behavior. Just as the more rapid kinetics for Type 304 led to higher EPR-DOS, it also prompts desensitization to become a factor at shorter times in the C6 over the C10 heat. EPR-DOS values decrease with increasing heat treatment time (indicating desensitization) after only minutes at 800°C and appear to do the same after about 100 h at 700°C. The Type 316 - C10 heat, on the other hand, shows increasing EPR-DOS up to about 10 h at 800°C and through 100 h at 700°C. No indication of desensitization was observed for either heat at lower temperatures. These data are illustrated in Figure 14 and summarized in Table 3.

Information listed in Table 3 can also be used to construct time-temperature-sensitization (TTS) diagrams for the two heats as presented in Figure 15. Comparing the two diagrams points out the basic thermodynamic and kinetic differences between Type 304 and 316 stainless steel. As discussed in the background, molybdenum additions increase the stability of carbides to higher temperatures and shift TTP and TTs curves upward. This can be seen for the C10 versus C6 TTS behavior in Figure 15. The upward shift in maximum sensitization temperature would be even greater if the carbon contents (which has a large effect on TTS) were equal between the heats (C615 > C10).

TABLE 3. Average EPR-DOS Measurements for Type 304 and 316 Heats, C/cm^2

	500°C		700°C			
Heat	10 h	100 h	0.1 h	1 h	10 h	100 h
C6	0	16	8	14	60	82
C10	0	0	0	3	35	100

	600°C			800°C			
Heat	1 h	10 h	100 h	0.1 h	1 h	10 h	100 h
C6	0	10	46	6	12	1	0
C10	0	5	51	1	21	35	0

Kinetic differences, described in some detail above, are illustrated by the shift in the "nose" of the curve to longer times and increasing the minimum temperature where measurable sensitization is documented for the C10 heat.

In order to better assess chromium depletion effects on EPR-DOS, C6 specimens given dual heat treatments (600°C plus high temperature anneal) were examined. EPR-DOS dropped rapidly as the temperature of the second treatment increased. The initial EPR-DOS after the 600°C/57 h exposure was 43 C/cm^2 which became 21,14,4 and 0.5 C/cm^2 after 2 minute anneals at 800, 825, 850 and 900°C, respectively. Therefore, the second treatments are prompting desensitization in each case.

Sensitization development in a large number of other stainless steel heats has also been determined by EPR and will be presented in Section 4.0. Several specific heat treatments from this expanded data base are of interest in this section since they have matching STEM-EDS measurements of chromium depletion. As a result, although primary

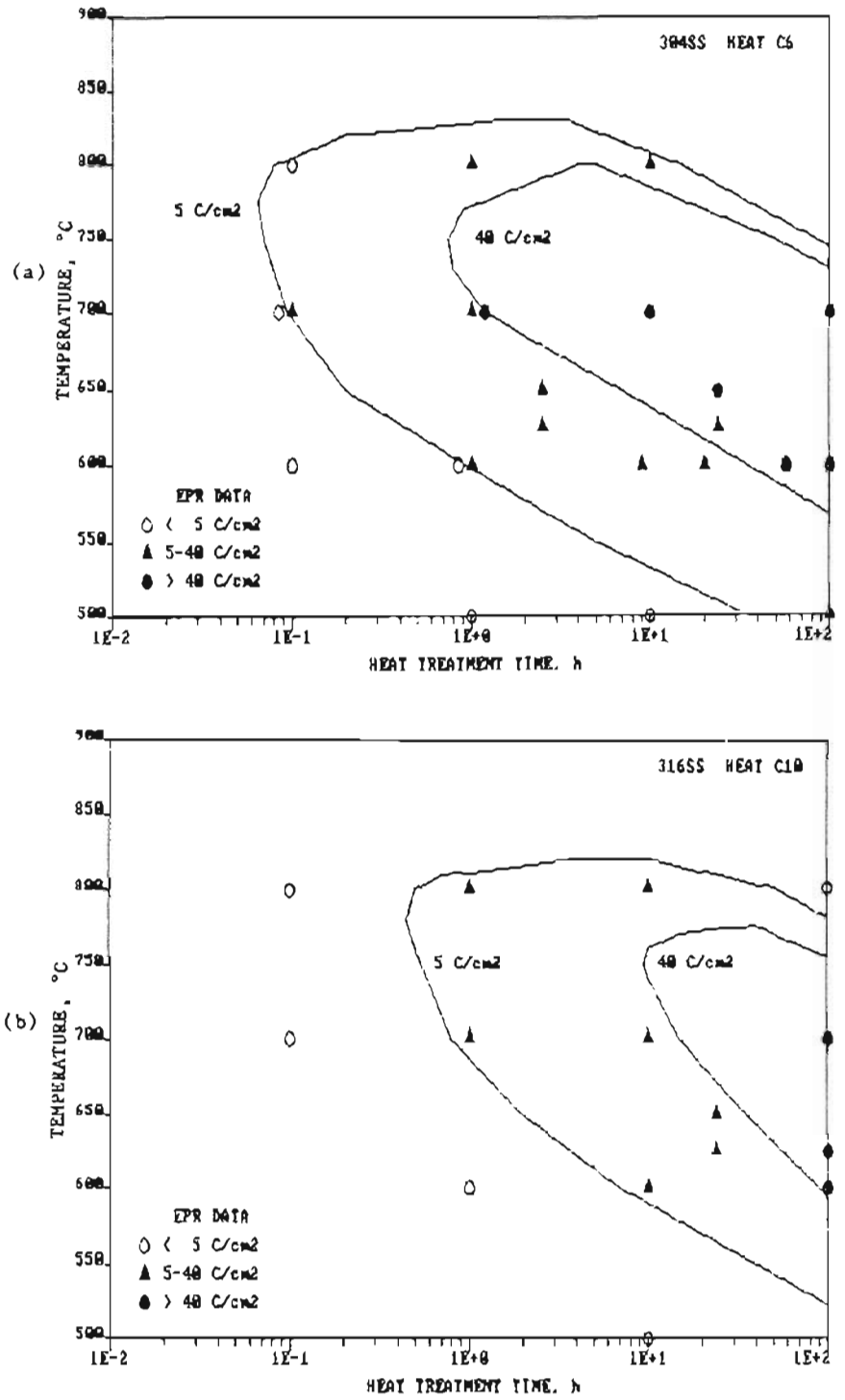

FIGURE 15. Time-Temperature-Sensitization Curves for Heats C6 (a) and C10 (b) Based on EPR-DOS Measurements

comparisons will be made based on C6 and C10 data, additional heats (e.g., C7) and heat treatments will also be used to expand assessment statistics.

3.2.3 Correlation of EPR and Chromium Depletion Measurements

Chromium depletion effects on DOS as measured by the EPR test can now be directed evaluated. The attempt is made to isolate specific aspects of the depletion profile, chromium grain boundary minimum and depletion width, and their effect on EPR-DOS. To do this, relevant data on the primary three heats, C6, C7 and C10, have been incorporated for comparison in Table 2. Chromium depletion widths below 13, 14 and 15 wt% are listed because they span the range typically thought to be critical for corrosion susceptibility.

The importance of minimum chromium concentration can be seen in Table 2 (Section 3.1.2) by examining EPR-DOS values for specimens exhibiting interpolated concentrations below and above about 13 wt%. EPR-DOS values are typically quite large when minimums drop below 13 wt%, while the opposite is true when minimums are above about 13 wt%. In general, as minimums reach near 13.5 wt%, EPR-DOS becomes approximately zero. This behavior is documented graphically in Figure 16.

The dual treatment specimens were heat treated for the purpose of examining this "critical" chromium level for attack in the EPR test. They show clearly that minimums can control DOS since depletion widths are not changing significantly in the series. Thus, increasing the minimum from 10.3 (600°C) to 12.1 (600 + 800°C) wt% cut measured

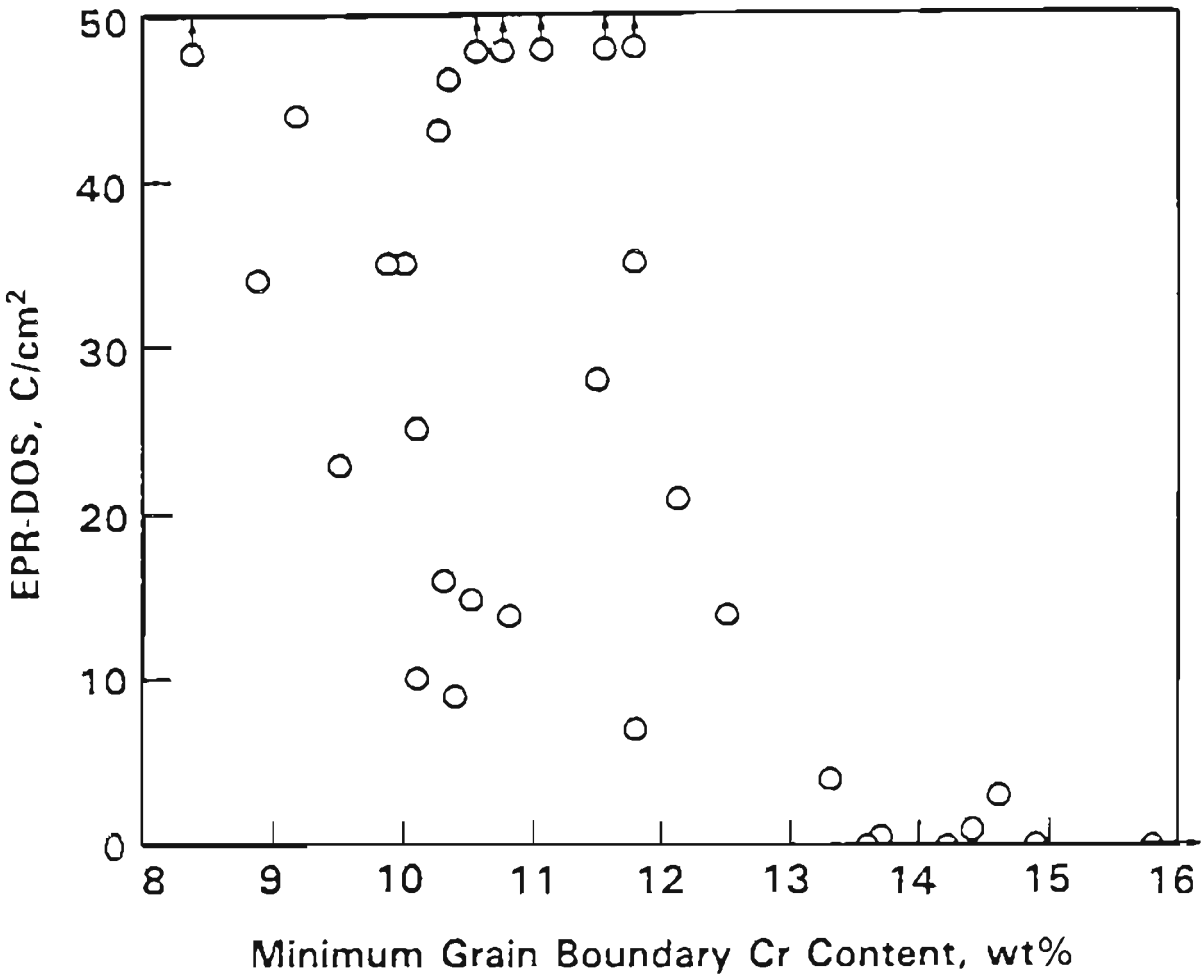

FIGURE 16. Comparison Between Minimum Grain Boundary Chromium Concentration from STEM-EDS Data and DOS Measured by EPR

EPR-DOS by 50%. Pushing the chromium minimums to higher levels progressively reduced EPR-DOS until it reaches levels near zero after the 600 + 900°C heat treatment. Because of the statistical limitations using STEM-EDS, a critical width for EPR attack cannot be precisely defined. In addition, the critical concentration may be dependent on depletion width. Taking these considerations into account, it is

still possible to make conclusions concerning this critical concentration. This concentration is certainly less than 14 wt% and greater than 12 wt% based on the present data and it appears likely than the value is within 12.5 to 13.5 wt%. As a result, previously proposed levels of 12% determined from corrosion tests on bulk alloys[50] and 15% estimated from anodic polarization curves of sensitized stainless steel[111] are not representative for the EPR test. Critical grain boundary chromium concentration for IG corrosion resistance will depend on environmental and material variables, while values for IGSCC may also be different due to the added complexity of stress state on film stability, passivation/repassivation and metal dissolution.

Although the minimum chromium content impacts EPR-DOS, depletion width controls its magnitude in most cases. Examining either Type 304 or 316 at 700°C illustrates that even though minimums increase with time, EPR-DOS rises rapidly due to the increase in depletion width. The overall effect of chromium depletion width on EPR-DOS is presented in Figure 17 integrating all of the available data. A much better correlation can be observed for the two lower critical chromium levels (17b and c) than for 15 wt% (17a). This is consistent with only regions depleted in chromium below about 13.5 wt% being attacked in the EPR test. Slightly less scatter is observed for widths below 14 wt%, but both the 13 and 14 wt% data show reasonable agreement. The limitation in assessing EPR-DOS based on depletion width is that minimums have already been demonstrated to be important.

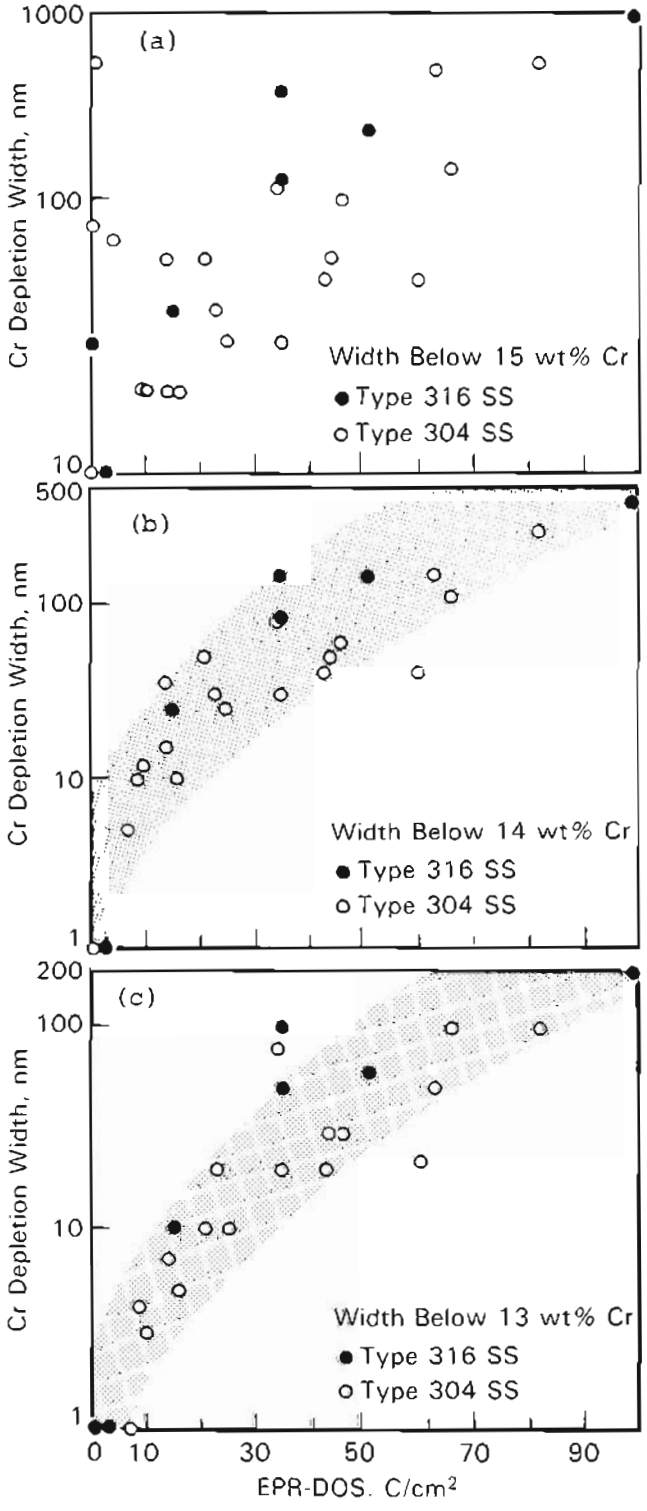

FIGURE 17. Correlations Between Chromium Depletion Width Measured by STEM-EDS and EPR-DOS for Depletion at 15 (a), 14 (b) and 13 (c) wt%

Therefore, EPR-DOS should be a function of both depletion width and depth. Examples from Table 4 show that comparable EPR-DOS can be achieved from sharply different depletion widths. Comparing C6 specimens after 500°C/100 h or 700°C/1 h versus the dual treatment of 600 + 825°C points out that a moderate DOS (~15 C/cm^2) can be obtained with narrow (~20 nm) or relatively broad (50 nm) depletion widths. To investigate the combined effects of width and depth, a volume depletion parameter (VP) was calculated similar to that formulated by Was (136):

$$VP = \frac{(X'_{Cr} - X_{Cr})\, W'_{Cr}}{2\, X'_{Cr}} \qquad (24)$$

where X'_{Cr} is the critical chromium concentration for attack in the EPR test, X_{Cr} is the measured minimum chromium concentration and W'_{Cr} is the width of the depleted zone at X'_{Cr}. This parameter represents the two-dimensional area of a triangle approximating the depletion profile and is normalized by the critical chromium content.

Correlations between VP and EPR-DOS are shown in Figure 18 for the 15, 14 and 13 wt% data. A marked improvement in the relative fit using VP instead of W'_{Cr} (Figure 17) is not observed, but it does reduce scatter, particularly for the 15 and 14 wt% data. The remaining data scatter is inherent due to the previously mentioned limitations in measurement capabilities. Regression analysis shows that the most consistent "fit" is determined using the 14 wt% data in Figure 18(b). This correlation can be used to predict EPR-DOS from depletion by:

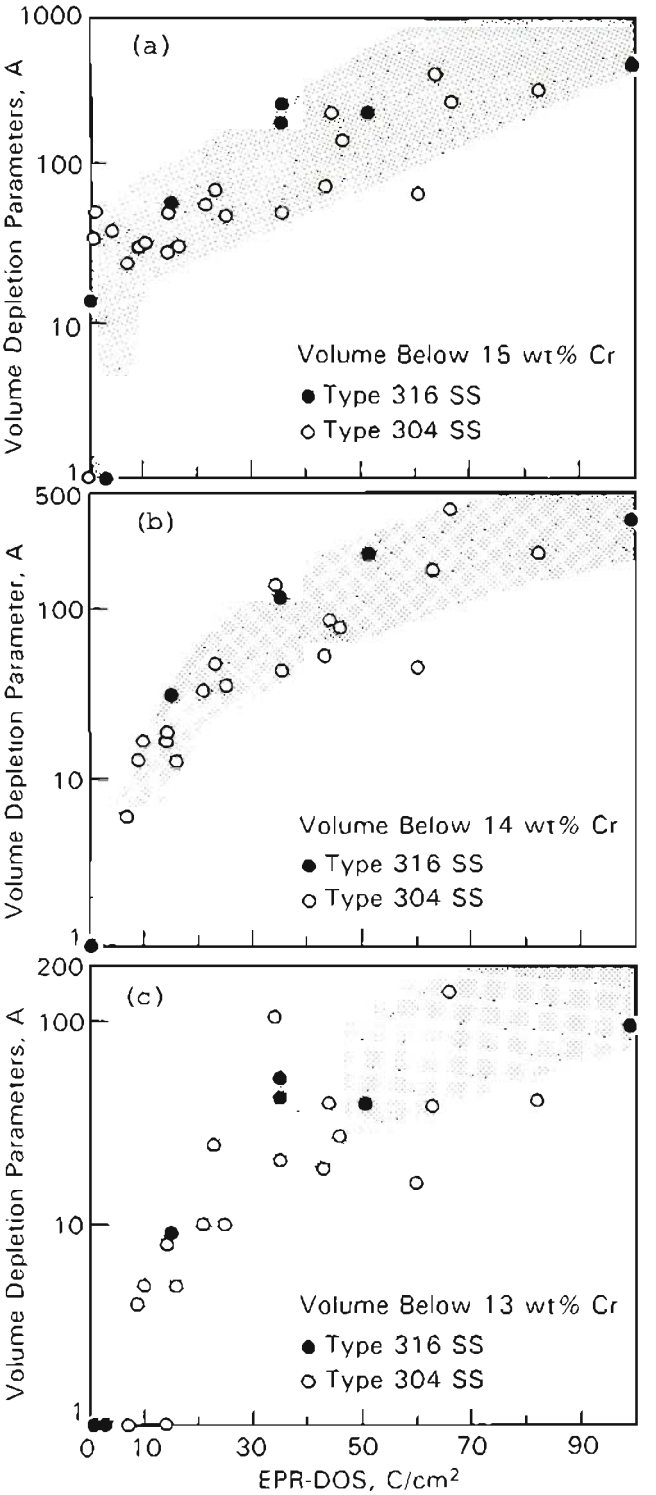

FIGURE 18. Correlations Between Volume Depletion Parameter and EPR-DOS for Depletion at 15 (a), 14 (b) and 13 (c) wt%

$$\text{EPR-DOS} = 0.42\ VP - 5\times10^{-4}\ VP^2 + 2\times10^{-7}\ VP^3 \qquad (25)$$

where VP is in angstroms and EPR-DOS is in C/cm^2.

The observation that the best fit to the experimental depletion data was found using widths at 14 wt% is somewhat inconsistent with previous conclusions for the critical chromium concentration. If EPR attacks regions below 12.5 to 13.5 wt% chromium, one would expect that the 13 wt% data correlations shown in Figures 17(c) and 18(c) would be optimum. Another possibility is that the high end of the critical chromium range better indicates the maximum value for attack. In order to test this point, depletion profiles were again examined to give estimated widths at 13.5 wt% (Figure 19). A very slight improvement in the VP versus EPR-DOS fit was determined by regression analysis over the 14 wt% data. Although this improvement is not significant by itself, it agrees with the overall data base. The equation obtained from regression analysis for the 13.5 wt% data is:

$$\text{EPR-DOS} = 1.1\ VP - 6.1 \times 10^{-3}\ VP^3 + 1.3 \times 10^{-5}\ VP^3 \qquad (26)$$

In summary, EPR-DOS was found to depend on the width and depth of the chromium depleted zone. Direct measurements of depletion indicated that only regions below about 12.5 to 13.5 wt% were attacked in the EPR test. A correlation and functional relationship was determined which best fit the data base using a critical chromium concentration of 13.5 wt%. This correlation will be discussed further as part of the evolution and evaluation of a model to quantitatively predict DOS in Section 5.0.

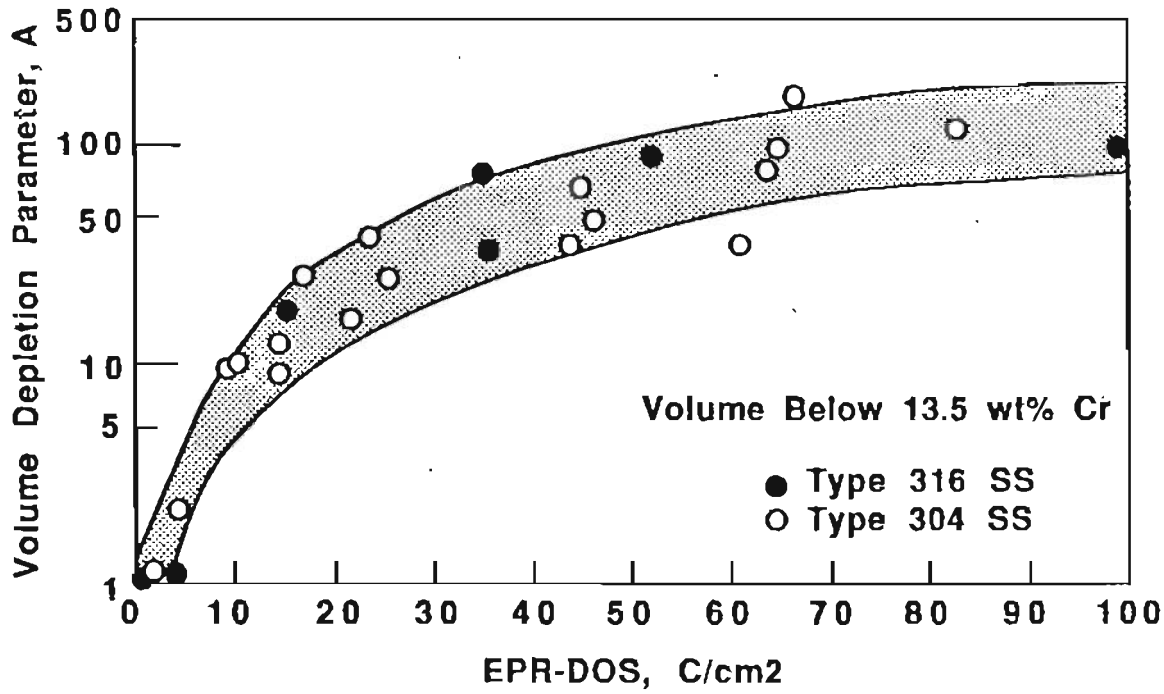

FIGURE 19. Correlation Between Volume Depletion and EPR-DOS for Depletion at 13.5 wt% Chromium

Although the EPR test does quantitatively indicate chromium depletion, it must be pointed out that the EPR-DOS value does not specify a unique depletion profile. In fact, significantly different widths and minimums can produce the same EPR-DOS. Another reality concerning EPR quantification is that charge transfer during the test is normalized by a grain boundary area term which has no relation to chromium depletion or actual grain boundary attack. Clarke[114] made several simplifying assumptions: (1) Width of intergranular attack is constant at 1 μm and (2) All boundaries are attacked uniformly.

Neither of these assumptions are quantitatively correct and, in many cases, not even qualitatively correct. For example, at low levels of sensitization (<10 C/cm^2) attack is rarely continuous along grain boundaries. Thus, EPR-DOS is underestimated when attack is not continuous, at least in how it relates to maximum chromium depletion.

The importance of recognizing the limitations of EPR to measure DOS is critical to the concept and application of any indirect technique. It is essential to understand what is and what is not being measured. EPR does not inherently specify a material's resistance to IG corrosion or SCC in service. The test does give information that can be used quantitatively to assess DOS. If a material's susceptibility to degradation directly depends on chromium depletion, EPR is an effective method of evaluating this susceptibility. However, since EPR-DOS is not specific to the profile characteristics, problems can still arise. Was and Rajan[138] documented such a situation using EPR to determine IGSCC susceptibility of Alloy 600 in an aggressive acidic sulfate environment. SCC was found to depend primarily on the minimum grain boundary concentration and not on the depletion width. As a result, EPR which strongly depends on the width was shown to misrepresent IGSCC susceptibility. This reiterates that the mechanism of degradation in service must correspond to the mechanism of attack in the indirect test. Relationships amoung EPR-DOS, chromium depletion and IGSCC in aerated, high temperature water will be examined in the following section.

3.3 STRESS CORROSION CRACKING SUSCEPTIBILITY

Evidence for relationships between grain boundary composition and IGSCC has been reported for many alloy systems including iron and nickel alloys. Because of this significant interest, it is somewhat surprising that detailed comparisons between grain boundary chromium depletion and IGSCC have not been conducted. While several researchers have documented that chromium depletion controls IGSCC, tests have been isolated and have not clearly defined critical characteristics of the depletion profile. As noted, Was and Rajan[137] performed a series of room-temperature tests on a nickel-base alloy to illustrate EPR limitations. The present work was performed to assess depletion effects on IGSCC in more pertinent, high-temperature water environments.

3.3.1 Experimental Procedure

The high-carbon, Type 304 stainless steel heat C6 was selected for SCC tests. In particular, the dual heat treatment series, where chromium minimum concentrations were modified with significant changes to the depletion width were examined. Data on these specimens are listed in Table 4 and was discussed in Sections 3.1.2 and 3.2.3. Examples of typical chromium depletion profiles were presented in Figure 11. The purpose of these treatments was to keep microstructural and microchemical aspects as constant as possible except for the minimum chromium level.

Flat tensile specimens were machined to 6.3 cm in length and 0.32 cm thick with gage length of 2.54 cm. Specimens were mounted in

TABLE 4. Grain Boundary Chromium Depletion, EPR and Slow Strain Rate Test Results

Heat Treatment °C/h	Interpolated[a] Cr Minimum, wt%	Depletion Width, nm Below 15 wt% Cr	EPR-DOS C/Cm^2	Strain to Failure, %	Reduction of Area, %	% IG Fracture
600/9 + 5% c/h[b]	8.3	60	45	10	13	100
600/57	10.3	50	43	12	9	100
600/57 + 800/0.03	12.1	70	21	15	17	90
600/57 + 825/0.03	12.5	60	14	20	22	90
600/57 + 850/0.03	13.3	70	4	25	22	70
600/57 + 900/0.03	13.7	80	0.5	26	25	35

(a) Interpolated concentration determined from profile characteristics using Equation 23.
(b) Specimen deformed at a strain rate of $1 \times 10^{-4} s^{-1}$ during isothermal anneal.

a slow-strain-rate tensile machine with grips and specimen situated within a high-temperature, stainless steel autoclave. Tests were conducted in 300°C, non-deaerated water at a constant extension rate corresponding to an initial strain rate of 10^{-6} per second. Specimens were exposed to the high-temperature water for about 0.5 h before straining was begun.

All tests were run until specimen fracture, and elongation to failure was recorded. Specimens were removed, dried and measured to determine reduction of area. Several measurements of the fracture crossection dimensions were averaged to estimate the final area. Fracture surfaces were examined using scanning electron microscopy and the amount of IG fracture determined by a line intercept method. Because of fracture surface topography, this measurement is only accurate within about 5%.

3.3.2 Chromium Depletion Effects on IGSCC

Grain boundary chromium concentration was found to control observed ductility and the percent IG fracture during slow strain rate tests. Intergranular cracking was initiated when local chromium

levels dropped to about 14 wt% or less. Cracking severity and ductility loss increased as the boundary chromium content decreased. The effects of minimum chromium levels on test results is summarized in Table 4. Ductility changes with grain boundary chromium concentration are illustrated in Figure 20 for reduction of area measurements.

The fracture mode changed from 100% IG for specimens heat treated only at 600°C to a combination of IG and ductile rupture for specimens given the short high-temperature second anneal. This corresponds to 100% IG fracture when minimum chromium levels are consistently below about 11 wt%. Apparently, within the conditions of these tests, a critical chromium content exists of about 14 wt%. Chromium concentrations in the 600 + 900°C specimen were never observed below ~13.7 wt% (interpolated value) and still exhibited considerable IG cracking. Even considering limitations in STEM-EDS measurements discussed earlier, it appears reasonable to conclude that chromium depletion levels below 13 wt% are not required to promote IGSCC. This critical concentration will depend on both material and environmental test conditions and is only valid for the experimental characteristics of this study.

Unfortunately, dual heat treatment conditions did not produce a specimen that failed by 100% ductile rupture. All specimens showed a large fraction of IG cracking as illustrated in Figure 21. Solution annealed material exhibited no IG cracks, but then it did not contain the same distribution of IG carbides and chromium depletion. From the

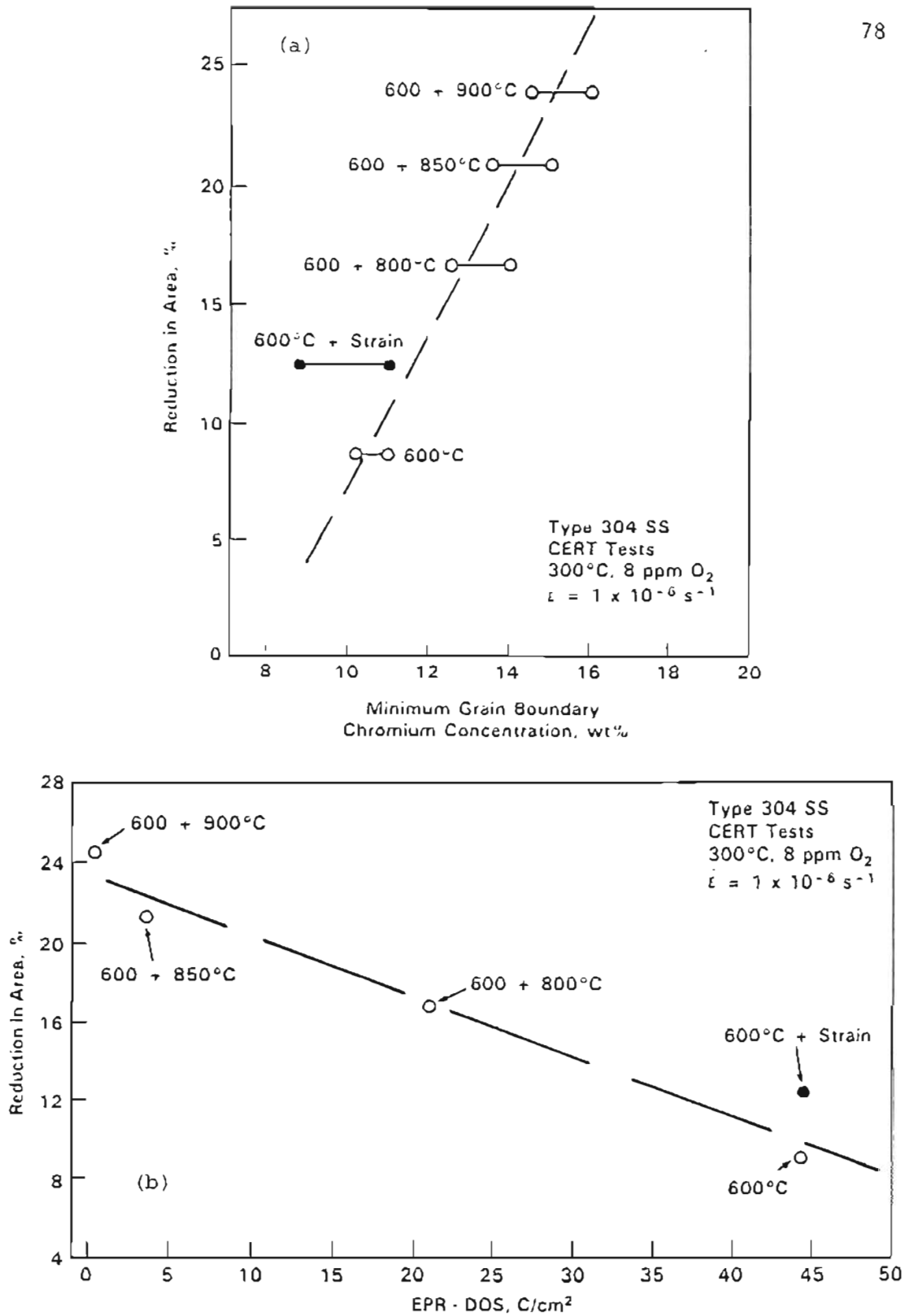

FIGURE 20. Correlations Between Direct Measurements of Chromium Depletion by STEM-EDS (a) or Indirect Measurements of DOS by EPR (b) versus Ductility in Slow-Strain-Rate SCC Tests

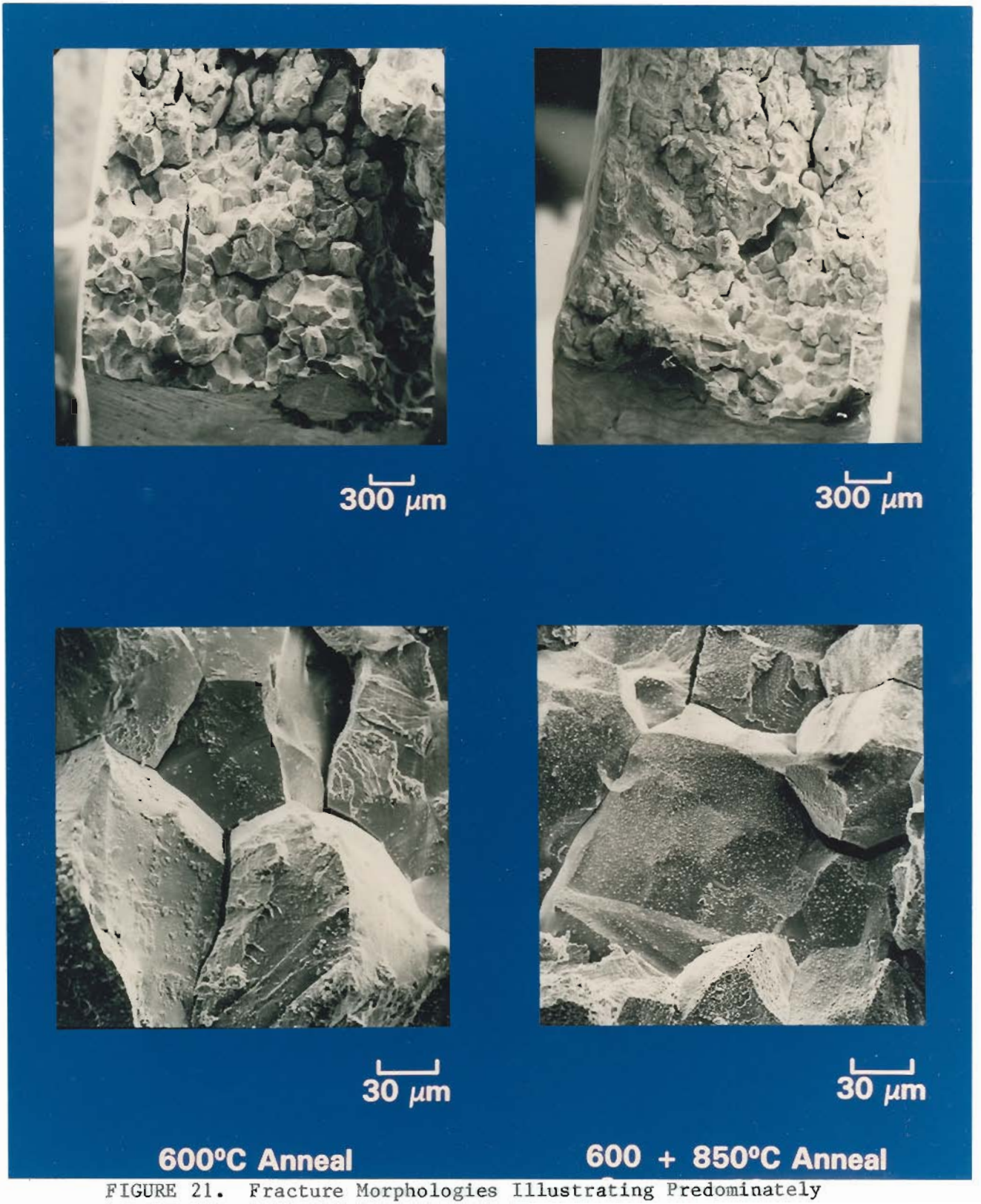

FIGURE 21. Fracture Morphologies Illustrating Predominately Intergranular Cracking During Slow-Strain-Rate SCC Tests in High-Temperature Water

trend in ductility and IG fracture with minimum chromium concentration, the above estimate of a critical content of near 14 wt% was made. However, without additional tests on specimens with higher grain boundary chromium levels, a critical concentration cannot be accurately substantiated.

A good correlation was also documented between EPR-DOS and specimen ductility (Figure 20b). The sensitivity of EPR to minimum chromium levels and volume depletion, described in the previous section, is similar to that revealed in the IGSCC tests. Reduction in area increases from about 10% when EPR-DOS is near 45 C/cm^2 to 25% when EPR-DOS drops to 0.5 C/cm^2. This correlation breaks down if the solution annealed specimen is added. EPR-DOS drops slightly to zero, but reduction in area increases by a factor of two. As mentioned above, the best comparison would require additional tests with other microstructural and microchemical components besides chromium depletion kept constant.

It is interesting to note that considerable IGSCC was observed for the 600 + 900°C specimen where EPR-DOS was very low (0.5 C/cm^2). Values much higher than that, i.e., 5 C/cm^2, have been reported to be necessary to promote IGSCC in BWR-type environments similar to that used in this study. The present results suggest that the minimum grain boundary chromium at which cracking occurs is slightly greater than that to promote attack in the EPR test. From the previous discussions, these values appear to be about 14 wt% for IGSCC and 13.5 wt% or less for EPR. This work puts the acceptance criteria of 5

or even 2 C/cm^2, as proposed by Clarke and others[114-116], somewhat in doubt. However, one must remember that present work has examined rather unique chromium depletion characteristics. In most normal circumstances, low EPR-DOS values reflect discontinuous carbide precipitation and depletion. As a result, IGSCC may not occur until a much higher EPR-DOS. Again interpretation of indirect test results must be performed with care, keeping in mind capabilities and limitations of the technique.

4.0 QUANTITATIVE DATA BASE DEVELOPMENT

4.1 MATERIALS

A primary objective of the overall program was to evolve a data base and modeling capability which had general application for unstabilized, austenitic stainless steels. To accomplish this, more than 30 heats of 300 series stainless steel were obtained with most being either Type 304 or 316. More than half of these heats were 10-cm-diameter piping either schedule 40 or 80, while the remainder were in plate form from 0.9 to 2.5 cm in thickness. Since bulk carbon concentration is the primary element controlling sensitization response, heats were selected to cover a wide range of possible carbon contents. Chemical analysis was performed on all heats to confirm reported compositions from heat specifications. Discrepancies (e.g., >0.01 wt% C) were found between reported and analyzed compositions for several heats. In these cases, samples were sent out for a third independent analysis which tended to discredit mill analyses. Measured bulk compositions are listed for all heats in Table 5.

The most extensive evaluations of sensitization response were conducted on the pipe heats labeled heats SS-1 through SS-17. An exception to this would be the already discussed work (Section 3.0) on plate heats C-6 and C-10. Low carbon, Type 316L stainless steel heats were obtained as a function of nitrogen concentration. Many of these

TABLE 5. Bulk Compositions and Grain Sizes for Program Heats

Heat[a]	Type	Composition, wt%										Grain[b] Size, μm
		C	Cr	Ni	Mo	Mn	Si	P	S	N	B	
SS-1	304L	0.013	18.21	10.34	0.07	1.54	0.58	0.012	0.008	0.039	0.001	70
SS-2	304L	0.013	18.20	10.54	0.25	1.82	0.45	0.009	0.022	0.046	0.002	55
SS-3	304L	0.019	18.30	10.33	0.20	1.51	0.45	0.012	0.001	0.018	0.001	55
SS-4	304	0.044	18.35	9.18	0.31	1.63	0.36	0.012	0.001	0.049	0.002	30
SS-5	304	0.054	18.42	8.47	0.08	1.01	0.53	0.012	0.011	0.062	0.001	40
SS-6	304	0.050	18.67	8.78	0.16	1.89	0.38	0.012	0.002	0.059	0.001	35
SS-7	304	0.060	19.17	9.54	0.12	1.31	0.42	0.013	0.015	0.041	0.001	70
SS-11	316L	0.015	17.93	12.73	2.11	0.89	0.65	0.014	0.001	0.020	0.001	40
SS-12	316L	0.014	17.77	12.64	2.18	0.89	0.60	0.014	0.005	0.023	0.001	40
SS-13	316L	0.013	17.53	12.70	2.10	1.39	0.59	0.014	0.001	0.027	0.001	40
SS-14	316L	0.020	16.92	12.90	2.30	1.66	0.38	0.014	0.002	0.011	0.001	40
SS-15	316	0.035	17.32	10.91	2.15	1.71	0.63	0.013	0.012	0.062	0.002	80
SS-16	316	0.058	17.11	11.43	2.26	1.77	0.41	0.014	0.005	0.008	0.002	35
SS-17	316	0.067	16.81	11.21	2.20	1.46	0.28	0.016	0.020	0.071	0.003	80
C-1	304L	0.016	18.55	8.91	0.14	1.81	0.46	0.019	0.004	0.083	--	70
C-2	304L	0.020	18.38	9.03	0.23	1.65	0.51	0.033	0.009	0.067	--	40
C-3	304	0.034	18.25	8.77	0.29	1.70	0.59	0.024	0.009	0.075	--	50
C-4	304	0.052	18.16	8.26	0.19	1.72	0.77	0.018	0.006	0.088	--	80
C-5	304	0.050	18.64	8.92	0.17	1.80	0.61	0.022	0.007	0.098	--	40
C-6	304	0.062	18.48	8.75	0.20	1.72	0.39	0.013	0.013	0.065	--	70
C-7	304	0.072	18.53	9.33	0.43	1.74	0.46	0.046	0.017	0.036	--	55
C-8	302	0.052	18.43	8.42	--	1.81	0.36	0.125	0.007	--	--	35
C-9	303	0.086	17.71	9.30	0.40	1.70	0.40	0.017	0.195	0.066	--	35
C-10	316	0.050	17.40	12.50	2.17	1.30	0.66	0.032	0.018	--	--	90
C-11	317L	0.025	18.42	13.25	3.58	1.71	0.20	0.035	0.009	0.056	--	40
C-12	317	0.060	18.80	12.75	3.40	1.78	0.58	0.033	0.018	--	--	55
N-1	316L	0.011	16.50	10.18	2.06	1.67	0.62	0.030	0.013	0.086	--	80
N-2	316L	0.019	16.20	10.35	2.15	1.70	0.42	0.030	0.013	0.087	--	80
N-3	316LN	0.023	17.00	10.48	2.16	1.84	0.61	0.025	0.003	0.154	--	50
N-4	316LN	0.014	16.80	10.34	2.16	1.63	0.59	0.026	0.009	0.145	--	80
N-5	316LN	0.024	16.75	10.49	2.10	1.62	0.54	0.023	0.018	0.163	--	50
N-6	316LN	0.012	16.63	10.60	2.10	1.69	0.52	0.022	0.006	0.190	--	55
N-7	316LN	0.015	16.70	10.60	2.15	1.66	0.55	0.030	0.006	0.110	--	40

(a) SS designation indicates pipe material (seamless), C and N designations indicate plate material.

(b) Grain sizes are for as-received, mill-annealed material.

heats fit (composition-wise) within the nuclear-grade Type 316 specifications. Others are LN grades with nitrogen levels up to 0.19 wt%.

Grain sizes for the stainless steel heats were measured in accordance with ASTM Practice E 112. The ASTM grain size number is listed in Table 5 for heats in the as-received, mill-annealed condition. Both pipe and plate heats exhibited grain sizes between 30 and 80 μm (ASTM No. 7 and 4). Final mill-anneal temperatures appeared to be from 1050 to 1100°C for many of the heats. Unfortunately, only a few of the heat specifications included such information. All solution-annealed specimens examined in this study were heat treated at 1100°C for 1 hour. Grain size tended to stabilize at about average grain diameters of 110 to 150 μm, i.e., ASTM No. 3 to 2.

Time-temperature-DOS measurements have also been compiled from the literature. Data was limited to Types 304 and 316 heats evaluated using either the modified Strauss or an EPR-type test to document DOS. As discussed in Section 2.5, both of these tests directly depend on chromium depletion. Information on more than one-hundred heats has been examined to determine various parameters such as time-to-sensitize and maximum temperature for measurable sensitization. Some of these data are presented and analyzed here or for modeling assessments in Section 5.2. A summary of sensitization data obtained from program heats and that extracted from the literature is listed in Appendix B.

4.2 ISOTHERMAL SENSITIZATION

A standard heat treatment matrix was selected for all heats at temperatures from 500 to 800°C as outlined in Table 6. Certain of these exposures were omitted for the low-carbon heats where sensitization was unlikely (e.g., short times at 500°C). Heat treatments were added for some heats to better map sensitization response. Exposure times were extended to 500 h on several of the low-carbon heats for this purpose. However, no attempt was made to document time-temperature-DOS in detail for all the stainless steels. Time-temperature-DOS trends can be determined from the heat data bases. More importantly, quantitative DOS changes are measured over a large temperature and time matrix enabling a proper assessment of modeling predictive capability and the evolution of a quantitative model (Section 5.2). Specific aspects of the sensitization response for the

TABLE 6. Heat Treatment Matrix for Isothermal Studies

	Temperature, °C				
Time, h	500	600	650	800	800
0.1				X	X
1.0		X	S	X	X
10	X	X	S	X	X
25		S	S	S	S
100	X	X	S	X	
500	S	S			

X = Baseline heat treatments for most heats
S = Selected heat treatments for certain heats

Type 304 and 316 heats will be discussed in the following sections. The data base itself is summarized in Appendix B which includes DOS results for all of the heats.

4.2.1 Carbon Series Alloys - Type 304SS

All of the heats examined exhibited sensitization as a result of heat treatment. However, temperature and time range over which it was observed was dependent on heat composition. High-carbon heats reached measurable EPR-DOS values during thermal treatment over the full range of temperatures, 500 to 800°C. Examples of this behavior are presented in Figure 22 for pipe heats SS-5 and SS-7 and was previously described for heat C-6 in Section 3.2.2. At short exposure times, EPR-DOS scaled with heat treatment temperature. Sensitization was observed after the 0.1 h treatments only at 800 or 700°C. Carbide nucleation and growth kinetics are too slow at lower temperatures to promote sufficient depletion in this time frame.

Temperature effects become more complex as heat treatment times are increased due to desensitization. Specimens heat treated at 800°C did not exhibit increasing EPR-DOS with time. On the contrary, the 0.1 h treatment typically represented the highest DOS and EPR-DOS approaches zero for exposures of ~10 h (Figures 14a and 22). DOS at 700°C sharply increased as time is extended from 0.1 to 10 h. Levels rose from below 10 C/cm^2 at 0.1 h to more than 60 C/cm^2 after 10 h. Maximum DOS at 700°C was achieved in about 50 to 100 h for the high-carbon heats (i.e., carbon > 0.05 wt%). Heat treatment times greater

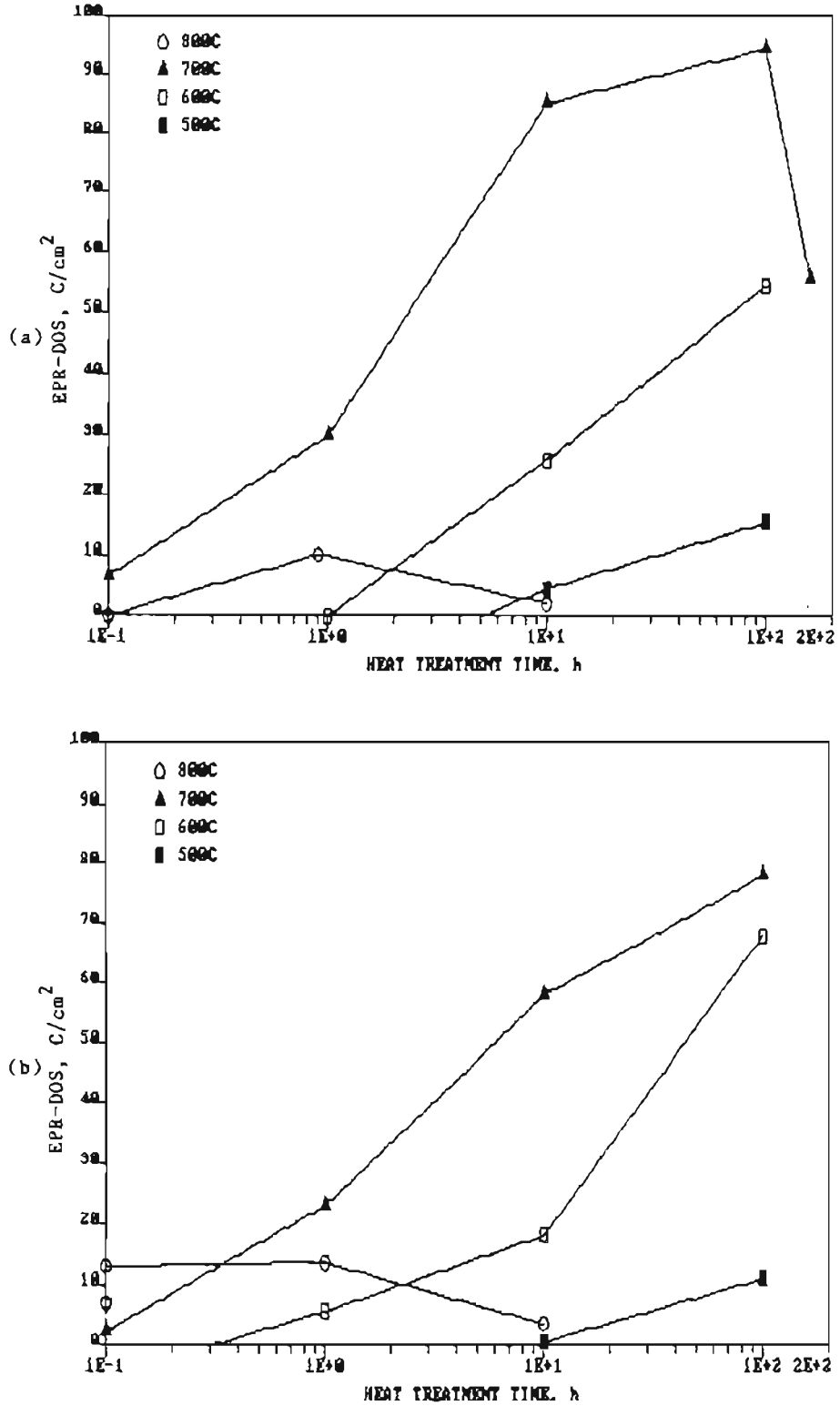

FIGURE 22. Sensitization Development in High-Carbon, Type 304 Stainless Steel Heats: (a) SS-5, 0.054 wt% C and (b) SS-7, 0.060 wt% C.

than 100 h at 700°C indicate that EPR-DOS is decreasing with exposure time as shown for heat SS-5 in Figure 22a. Time to reach maximum DOS depends on the carbon content remaining in solution, thus should track with the bulk carbon content. Although there is insufficient data to document this effect, comparisons to lower carbon heats suggest this is the case, as illustrated in the 700°C results for heat SS-4 (0.044 wt% C) in Figure 23a. A maximum in EPR-DOS occurred after an anneal of about 10+ h and dropped to nearly zero after 100 h. This compares to much longer times recorded for higher carbon heats such as C-4 (Figure 23b) and those noted above.

A better comparison of the sensitization behavior of these heats at 700°C is depicted in Figure 24. Sensitization development for the heats up to 10 h is remarkably consistent. Only slight differences in measurements can be seen for data at 0.1, 1 and 10 h. Such differences are within the probable data scatter for the most part. As exposure time is increased past 10 h, desensitization becomes an important factor and the lower carbon heat (SS-4) response deviates from the other heats. The similarity in sensitization kinetics at 700°C indicates the limitation in assessing potential sensitization behavior on bulk carbon content alone. Additional factors including composition of other alloying elements and material condition must be considered.

Sensitization increased with heat treatment time (out to 500 h) at 500 and 600°C. This behavior is again consistent with the kinetics

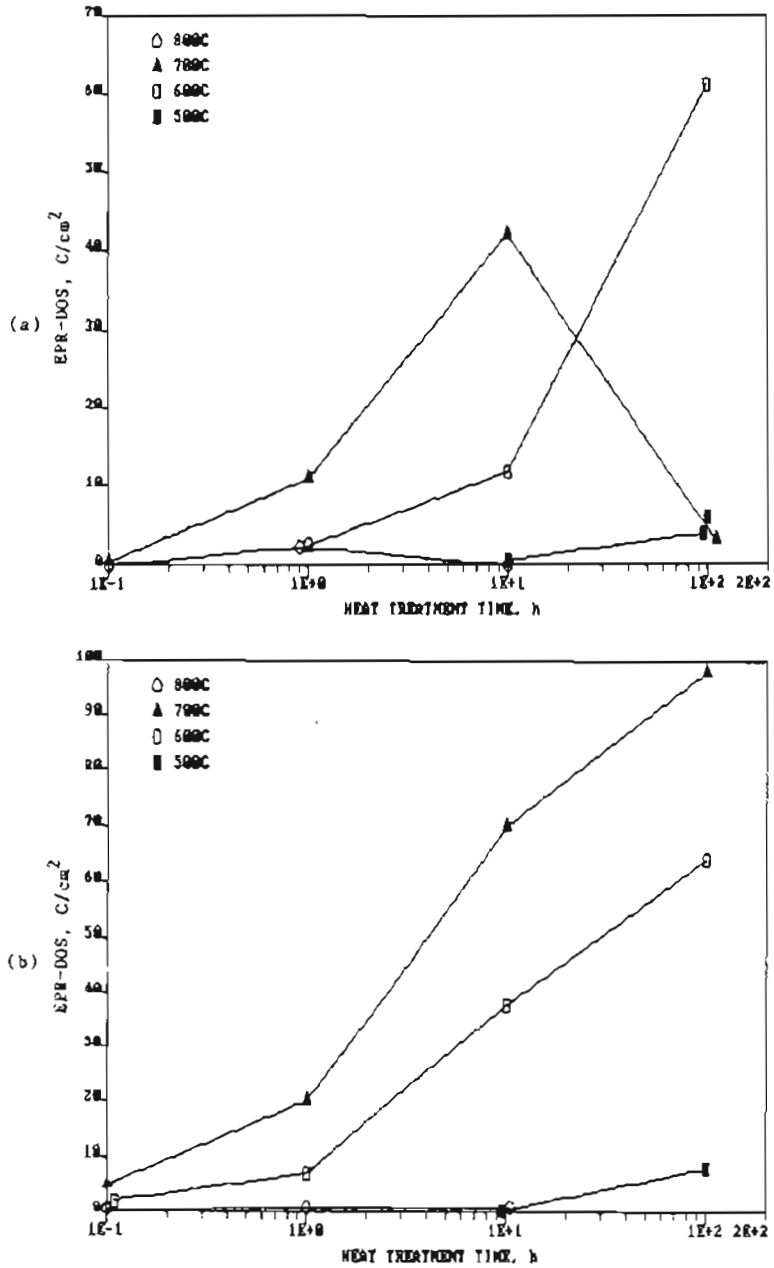

FIGURE 23. Sensitization Development in Moderate- to High-Carbon Type 304 Heats: (a) SS-4, 0.044 wt% C and (b) C-4, 0.052 wt% C.

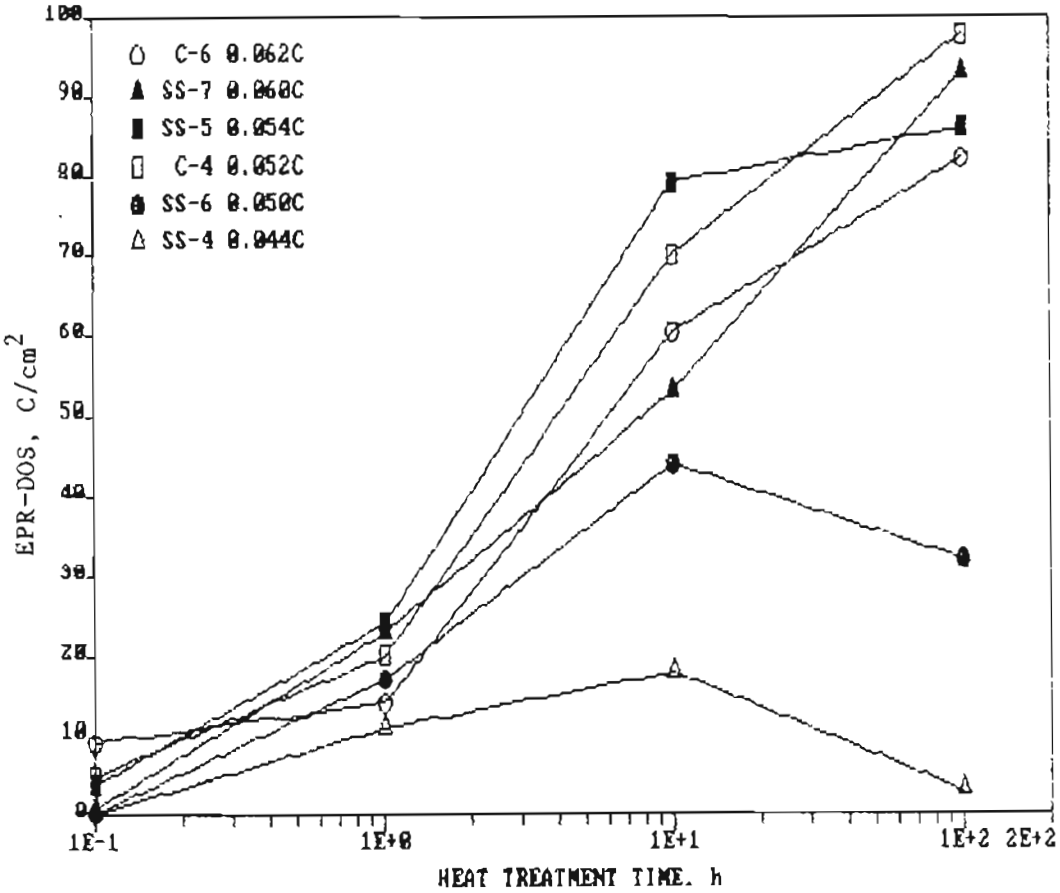

FIGURE 24. Comparison of Sensitization Response at 700°C Among Various Moderate- to High-Carbon, Type 304 Stainless Steel Heats.

of the process. Carbide nucleation and sensitization development is relatively slow at 500°C even in high-carbon heats. Times on the order of 10 h were required for DOS to be measured. EPR-DOS values only reached about 10 C/cm^2 after 100 h, which was less than that developed after 1 h at 700°C or 0.1 h at 800°C. Chromium diffusion kinetics (Equation 10, Section 2.3.3) explain these differences since chromium migration distances are similar after each treatment at about 10^{-12} cm^2.

The most consistent sensitization development with time is observed at 600°C. Carbide nucleation and initial DOS occurred for

exposure times less than 1 h and did not exhibit desensitization for times out to 500 h. EPR-DOS reached values of about 60 C/cm^2 in the high-carbon heats after 100 h and approached DOS levels for 700°C exposures as desensitization becomes significant at the higher temperature. If heat treatments are extended past 100 h (e.g., SS-5 in Figure 22a) or lower carbon heats (e.g., SS-4 in Figure 23a) are examined, DOS at 600°C exceeds that measured at 700°C due to desensitization effects.

The consistency in sensitization response among the high-carbon heats can again be noted comparing the 600°C data (Figure 25). DOS versus heat treatment time at 600°C is summarized in several of Type 304 heats. Data for the individual heats show considerable overlap. Some differences in EPR-DOS can be seen at early times indicating differences in carbide nucleation kinetics. Heat SS-5 was one of the few moderate- to high-carbon heats which had no measurable DOS after 1 h at 600°C. Although more variability is present among the 600°C data in Figure 25, trends are similar for most heats. This behavior points out the limitation in assessing potential sensitization response by bulk composition (e.g., carbon content) alone.

Bulk carbon content does directly impact a stainless steel's sensitization behavior. This can be illustrated by examining sensitization development in the low-carbon, Type 304 heats. Results for two heats are shown in Figure 26. No measurable DOS was found after heat treatments at 800°C and only slight sensitization observed at 700 or

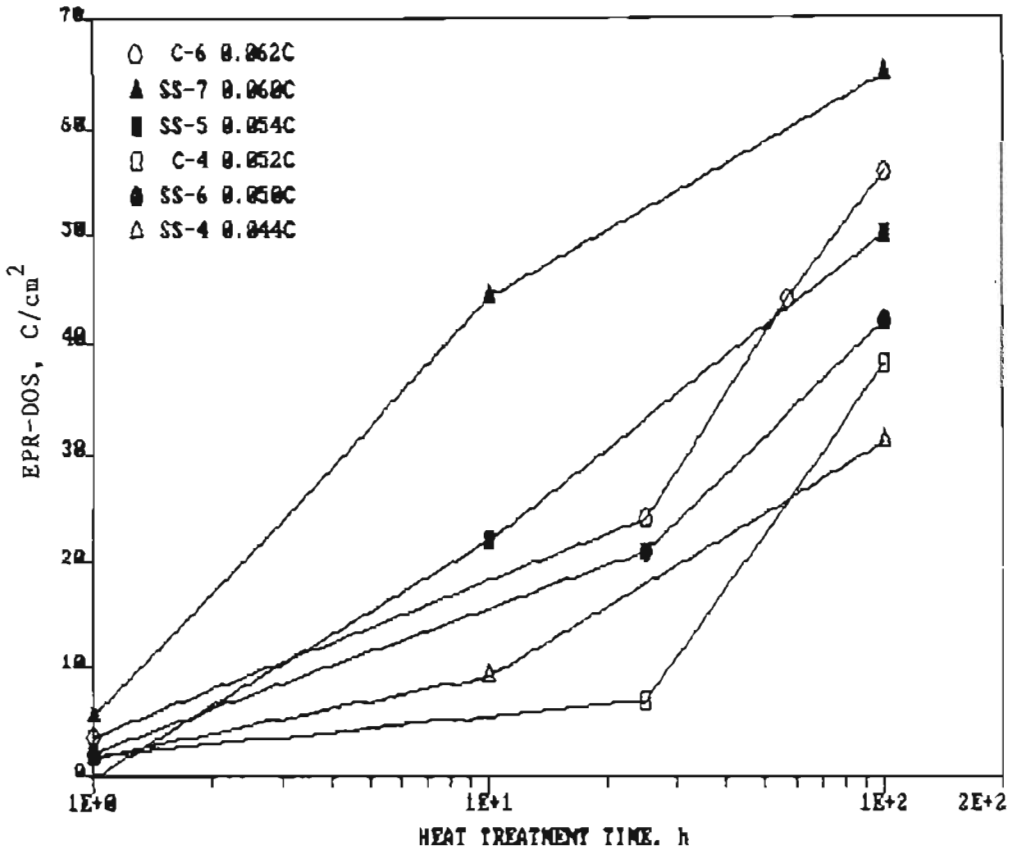

FIGURE 25. Sensitization Development at 600°C for Various Moderate- to High-Carbon Type 304 Heats.

500°C. Thermodynamics prompt the 800 and 700°C behavior (precipitation occurs, but chromium minimum concentrations are too high to promote significant attack in the EPR test) and kinetics (carbide nucleation and growth) limit DOS at 500°C.

Sensitization behavior for the Type 304L heats illustrated in Figure 26 and documented in Appendix B shows that the 600°C data is best suited for data comparisons. Each of the heats exhibits attack in the EPR test within 10 h and increase in DOS as heat treatment time is extended to 100 h. Sensitization development as a function of

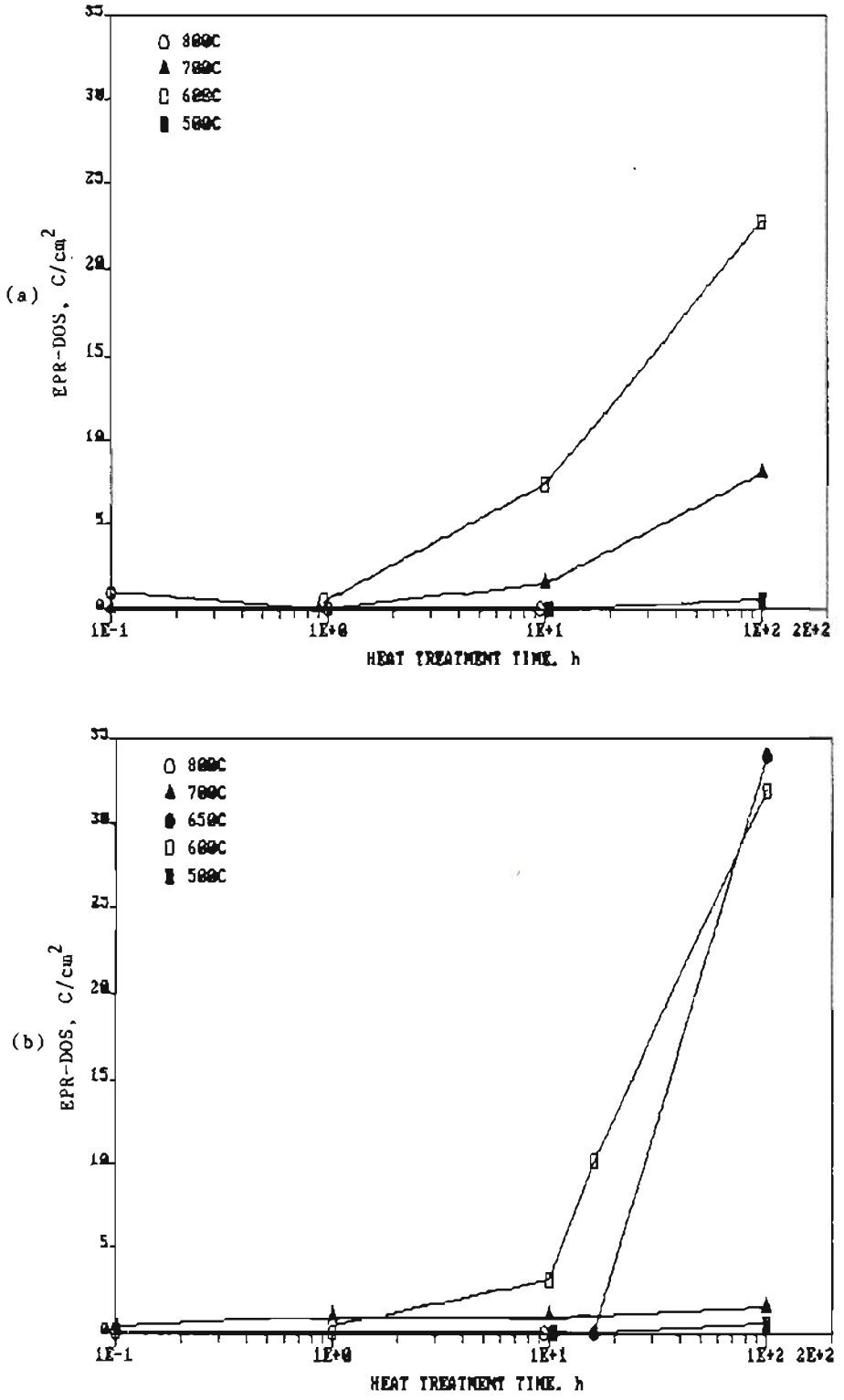

FIGURE 26. Sensitization Development in Two Low-Carbon, Type 304L Stainless Steels: (a) SS-3, 0.019 wt% C and (b) C-2, 0.02 wt% C.

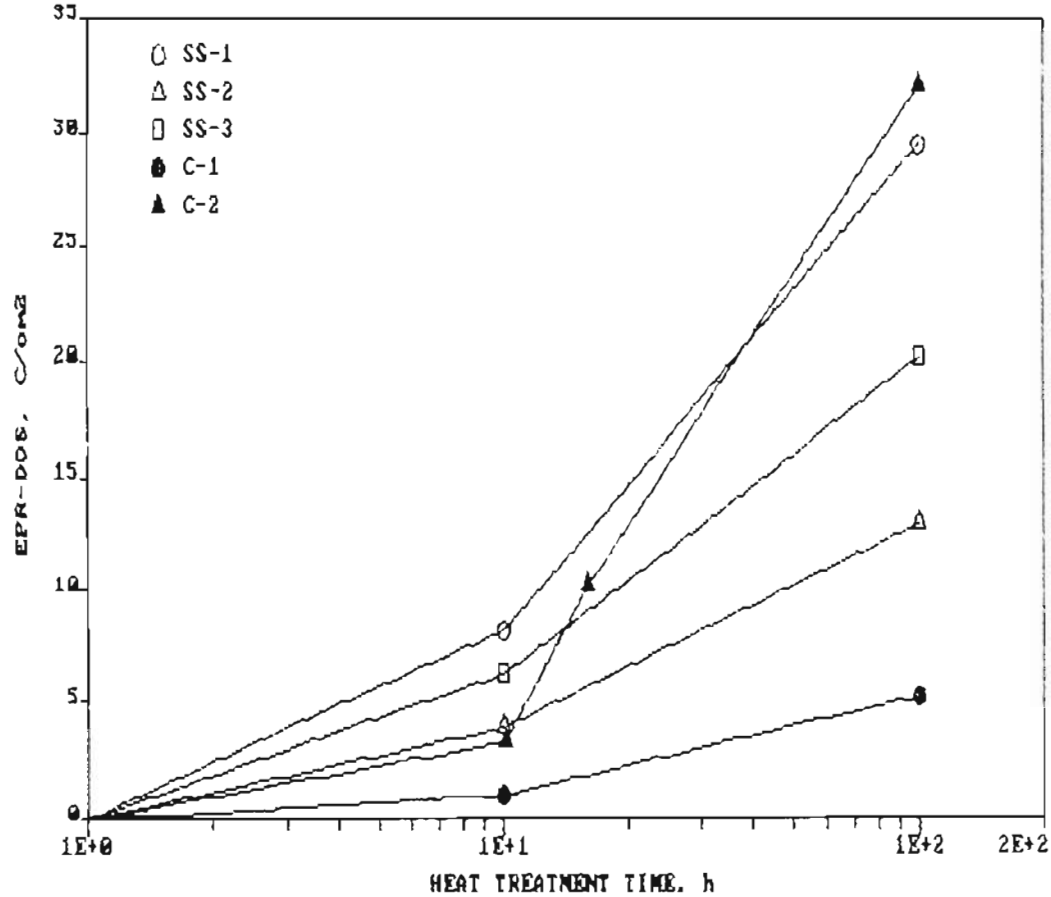

FIGURE 27. Sensitization Development at 600°C for Five Low-Carbon (<0.02 wt%), Type 304L Heats.

annealing time at 600°C is presented in Figure 27 for all five low-carbon heats. Maximum EPR-DOS values are now less than about 30 C/cm^2, much lower than recorded for the higher carbon specimens. Heats C-2 and SS-3, both having a bulk carbon content of ~0.02 wt%, reach higher DOS levels at 600°C and are the only heats to exhibit EPR-DOS values greater than 2 C/cm^2 at 700°C.

The five low-carbon, Type 304L stainless steels examined can become "sensitized" even though these heats have carbon contents of 0.02 wt% or less. A maximum limit of 0.02 wt% has been specified for the nuclear grade stainless steels to resist sensitization. However,

it is important to note that such heats are not immune to sensitization if exposed to severe thermal treatments. Heats with carbon contents near the maximum can become severely sensitized (EPR-DOS > ~20 C/cm^2). Stress-relief heat treatments at temperatures between 600 and 700°C still could promote sensitization and IGSCC.

The dominant effect of bulk carbon content can now be demonstrated by combining data for low- and high-carbon heats. Sensitization development at 600°C is compared in Figure 28 for five pipe heats ranging from 0.013 to 0.060 wt% C. EPR-DOS measurements agree with what would be expected, the larger the bulk carbon content, the larger the resultant DOS. This trend is even more dramatic at higher temperatures where significant DOS is only observed in the high-carbon heats.

4.2.2 Carbon Series Alloys - Type 316

Sensitization behavior in the Type 316 stainless steels was documented over the same temperature range (500 to 800°C) as for Type 304 heats. Major differences were observed in sensitization and desensitization kinetics and in the maximum temperature for sensitization. These differences between Type 304 and 316 are consistent with molybdenum effects on chromium diffusivity (Section 2.3.3) and carbide precipitation thermodynamics (Section 2.3.2). No sensitization was determined at 500°C due to the slower kinetics, while large EPR-DOS values were measured at 800°C due to the reduced carbon activity in the molybdenum-containing alloy.

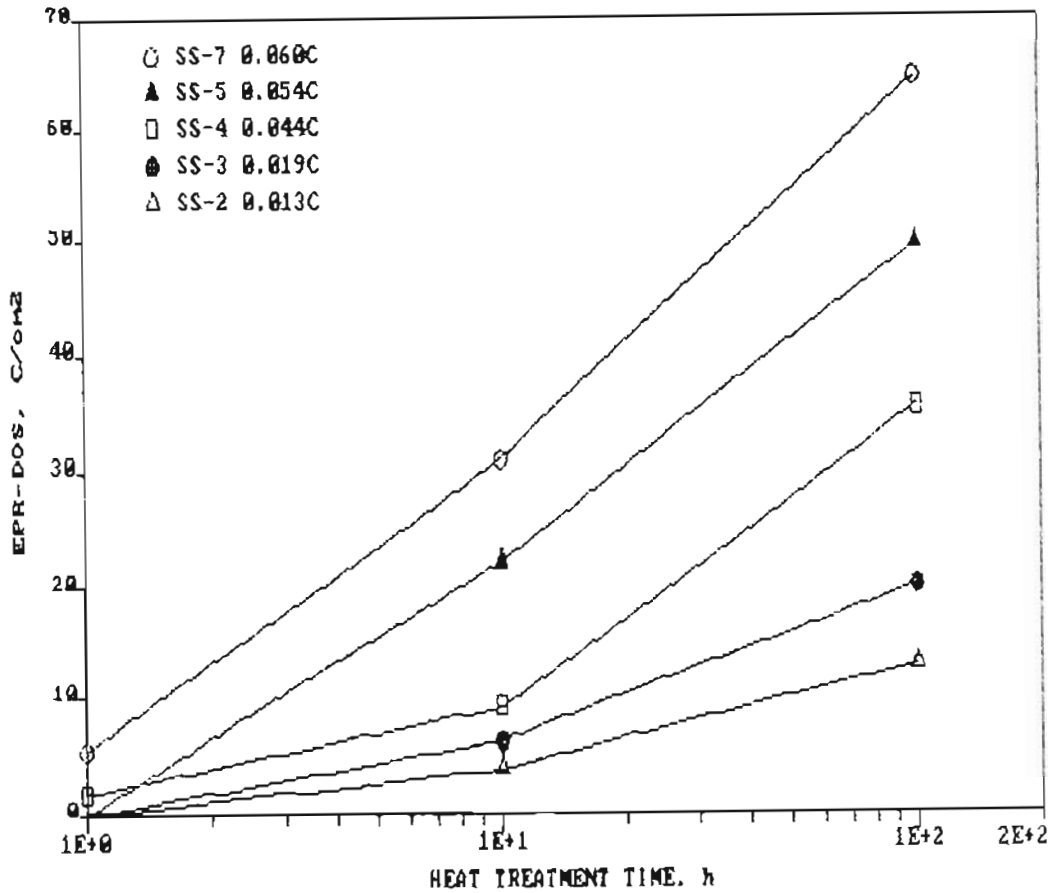

FIGURE 28. Effect of Bulk Carbon Content on Sensitization Development at 600°C in Type 304 Heats.

Examples of typical sensitization behavior for Type 316 is presented in Figure 29. A high-carbon (SS-17, 0.067 wt% C) and a moderate-carbon (SS-15, 0.035 wt% C) heat is shown in parts (a) and (b), respectively. EPR-DOS values of about 80, 180 and 60 C/cm^2 are reached during heat treatment of SS-17 at 800, 700 and 600°C. The 180 C/cm^2 EPR-DOS was the largest recorded for any heat or heat treatment. Typically, EPR-DOS was limited to about 100 C/cm^2 for Type 304 with Type 316 showing slightly larger values (see Appendix B). However, no attempt was made to maximize DOS. Extended heat treatments (>500 h) at lower temperatures (600 to 650°C) would probably promote

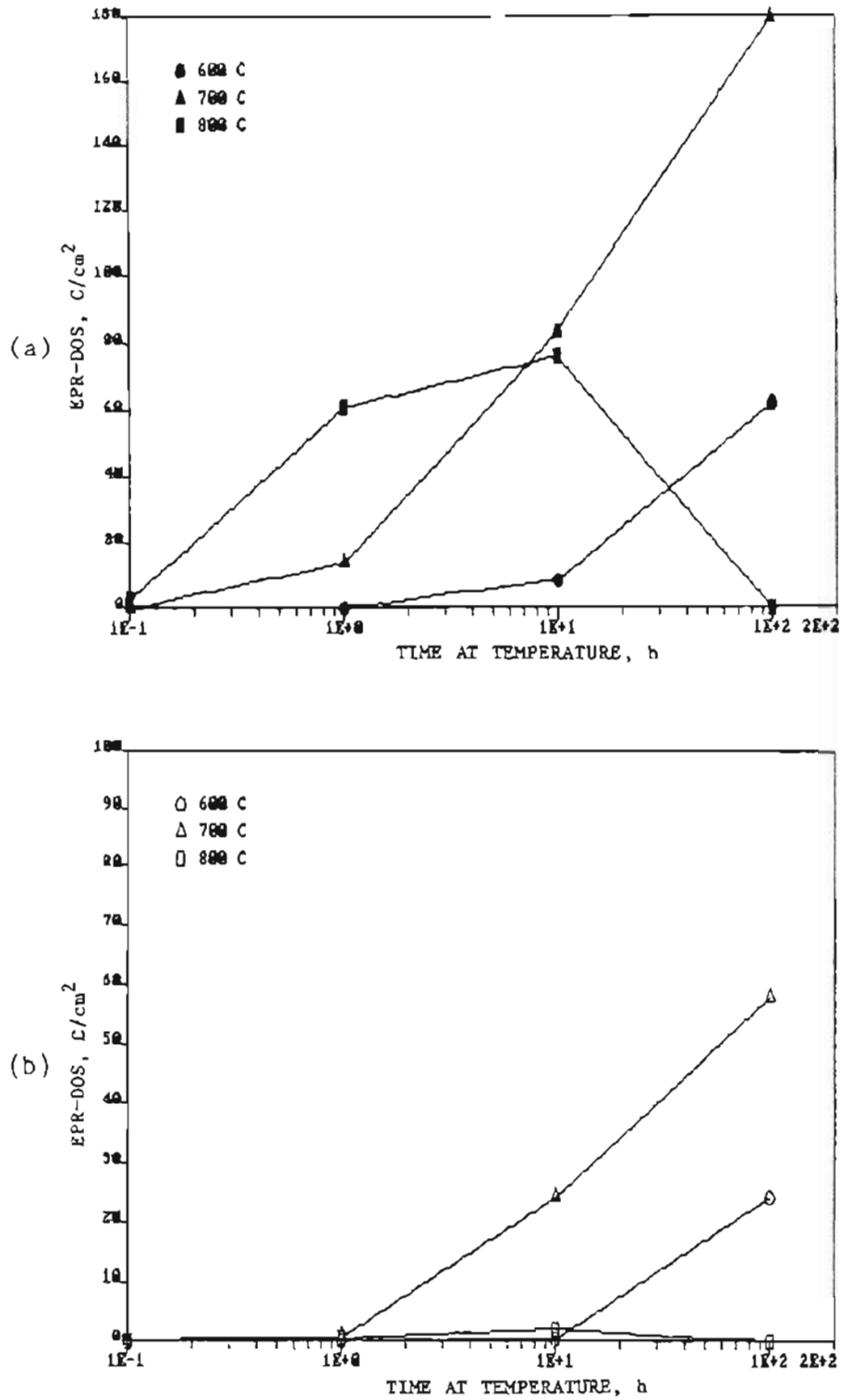

FIGURE 29. Sensitization Development in a High-Carbon (a) and a Moderate-Carbon (b) Type 316 Stainless Steel.

even larger DOS since more carbon is available to precipitate and desensitization effects are delayed.

The lower-carbon heat reaches much smaller DOS values at each temperature. EPR-DOS was very small at 800°C similar to the response for the high-carbon Type 304 heats. This again indicates molybdenum effects on precipitation thermodynamics. A 0.035 wt% C, Type 316 heat tends to behave like a 0.06 wt% C, Type 304 heat as to the maximum temperature where sensitization is observed. Therefore, at high temperatures (e.g., 800°C), Type 316 stainless steel is much more prone to sensitization than Type 304 stainless steel.

The main benefit of the molybdenum addition from a sensitization point of view is the reduced sensitization kinetics at lower temperatures. Differences in kinetics are illustrated in Figure 30 comparing data for Type 304 (SS-7) and 316 (SS-16) heats with approximately the same bulk carbon content. Initial sensitization occurs in less than 1 h at 600°C and about 0.1 h at 700°C for SS-7, while times of several hours at 600°C and about 0.5 h at 700°C are required for SS-16. Such differences in kinetics can be extremely important for brief, low-temperature or continuous-cooling thermal exposures. They have led to the general perception that Type 316 stainless steel is less prone to sensitization than Type 304. This conclusion can be erroneous depending on the specific thermal treatment. As illustrated at 800°C, Type 316 can be much more susceptible than Type 304.

The compositional variable controlling sensitization behavior among the Type 316 stainless steels is carbon as it was for Type 304.

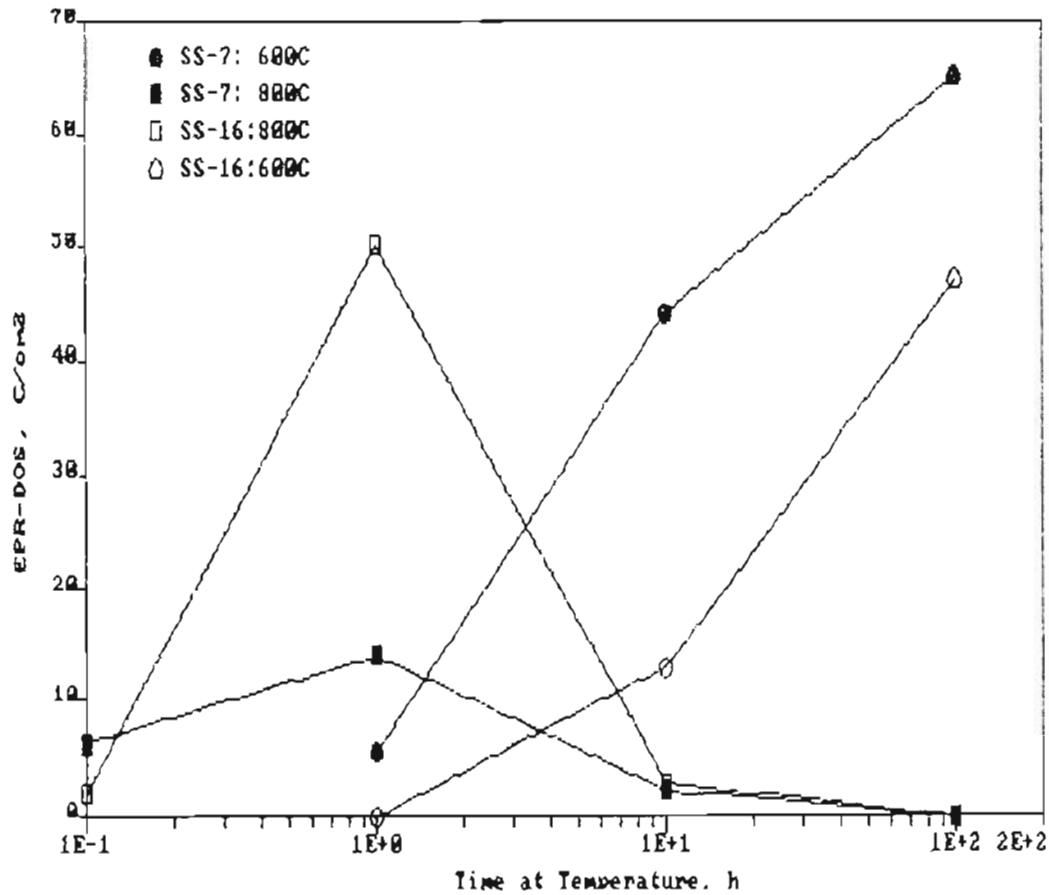

FIGURE 30. Comparison of Sensitization Response Between a Type 304 (SS-7) and a Type 316 (SS-16) Heat with Similar Bulk Carbon Contents (~0.06 wt%).

Reducing the bulk carbon concentration reduces the temperature range over which sensitization is observed and increases the time required for measurable sensitization to develop. An example of these effects can be seen by comparing Figures 29a and b. More detailed comparisons of bulk carbon effects on kinetics are presented in Figure 31 for sensitization development at 600 (a) and 700°C (b).

Times to reach a significant DOS increase by more than an order of magnitude as carbon level drops from about 0.06 to 0.02 wt%. Maximum EPR-DOS values are much less for the low-carbon heats due to both thermodynamic and kinetic effects. Minimum interfacial chromium

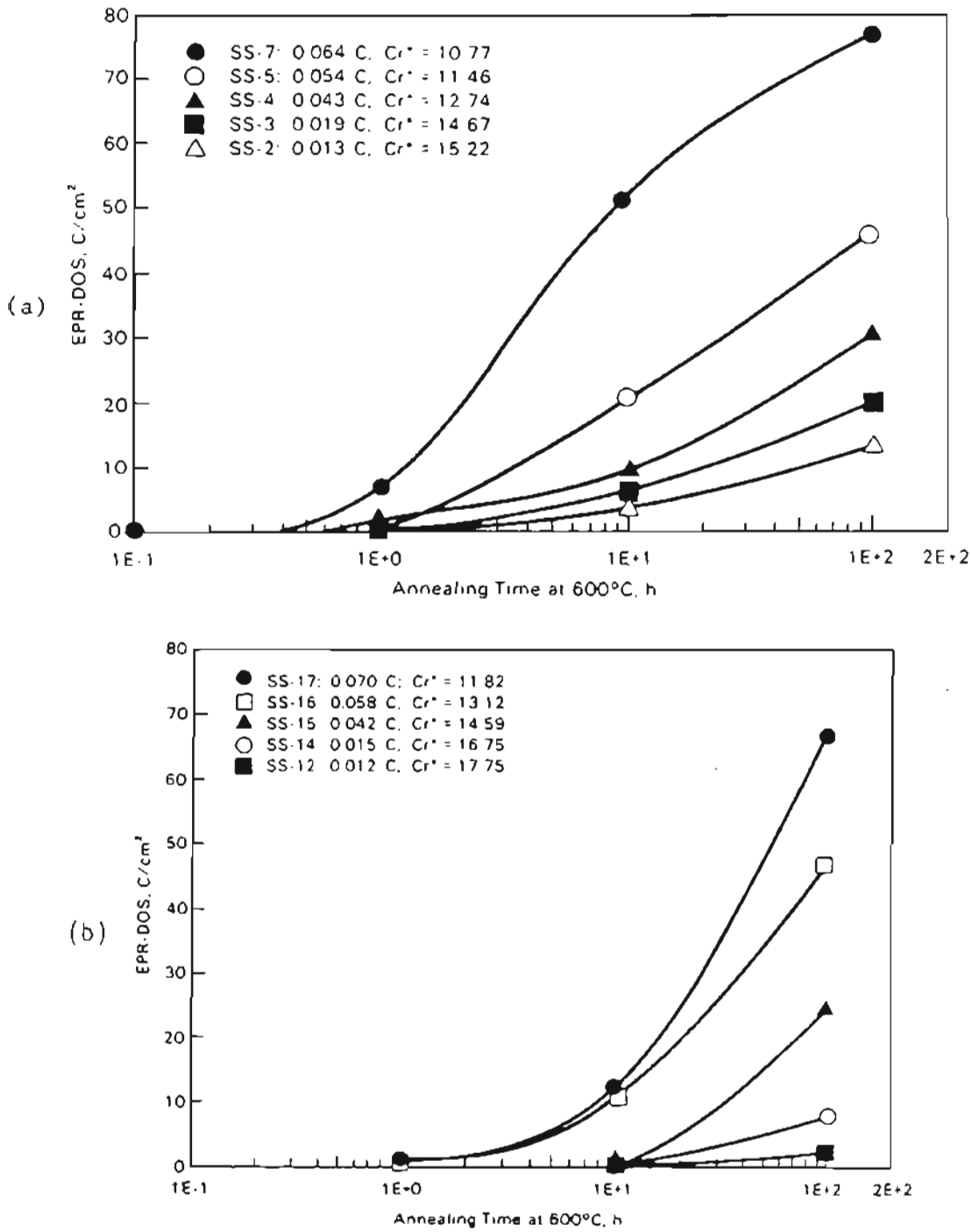

FIGURE 31. Effect of Carbon Content on Sensitization Development in Type 316 Stainless Steel at Heat Treatment Temperatures of 600 (a) and 700°C (b).

concentrations will increase as bulk carbon levels (and carbon activities) drop, prompting a reduced depletion volume and EPR-DOS for the same kinetically produced depletion width. Limited direct measurements of chromium depletion in low-carbon heats indicate that minimum chromium concentrations are approximately 12 wt% after anneals at 600 to 700°C. This compares to measured minimums of 10 wt% for high-carbon, Type 316 (Table 2).

Because of the current interest in and application of extra-low carbon, Type NG316 stainless steel, nine different heats meeting its carbon specification (< 0.02 wt%) have been examined. Several of these contain significant nitrogen levels and will be discussed in the following section. The importance in understanding sensitization response of the extra-low carbon heats is to quantify the benefit obtained by reducing carbon to very low concentrations. Some of this benefit was documented in Figure 31 and discussed above, but it is worthwhile to make a closer examination of sensitization behavior in these heats.

Sensitization development was consistently more rapid and reached larger EPR-DOS values in the 0.02 wt% C heat (SS-14) than in the three lower-carbon heats (SS-11, SS-12 and SS-13). Data for thermal exposures at 700 and 600°C are summarized in Figure 32. Appreciable DOS was only observed for heat SS-14 at 700°C. This gives some insight into bulk carbon effects on the maximum temperature for sensitization. It appears that a carbon level between 0.015 and 0.02 wt% is required for sensitization (as measured by the EPR test) to occur

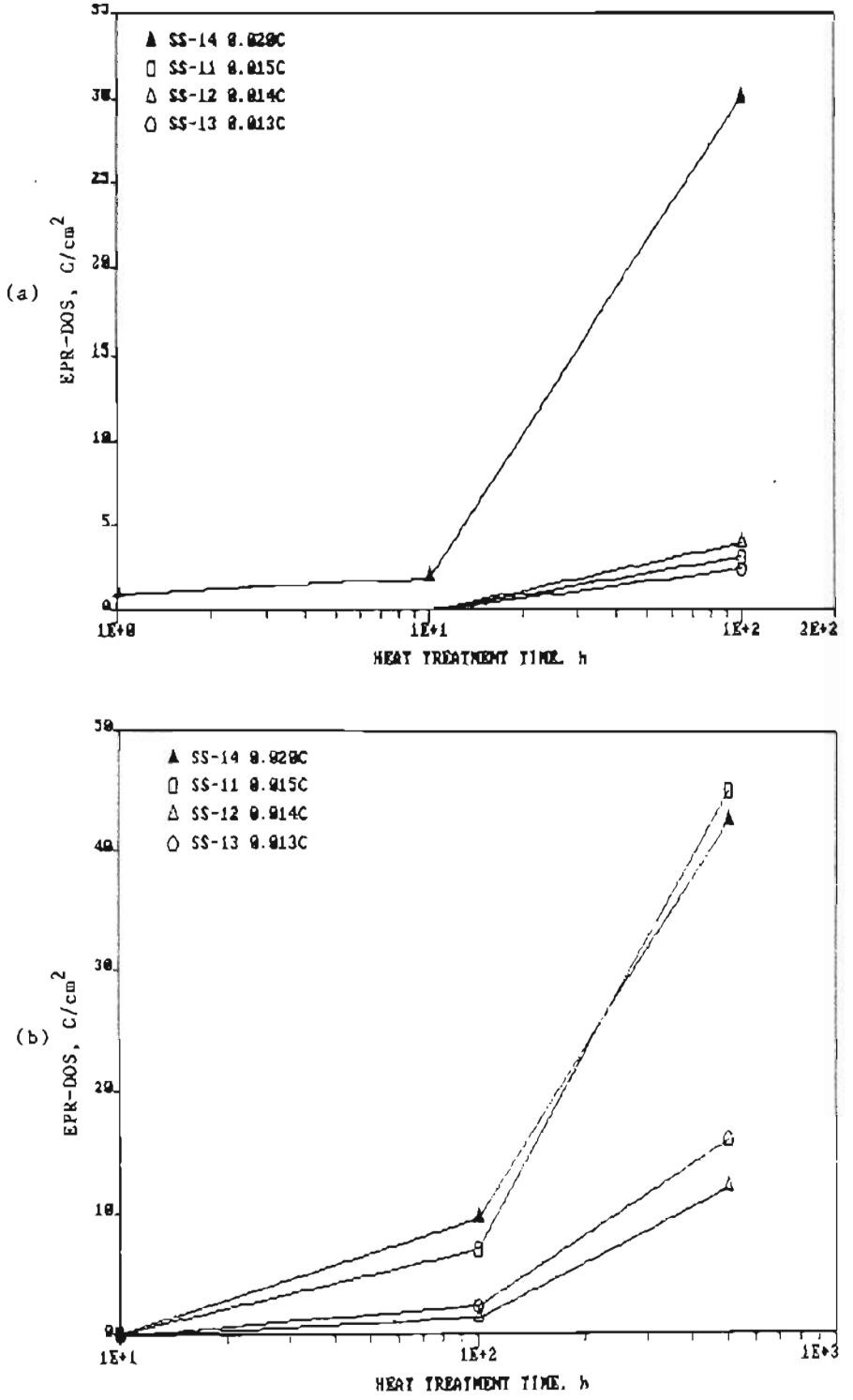

FIGURE 32. Sensitization Development in Extra-Low-Carbon, Type 316L Stainless Steels at 700 (a) and 600°C (b).

at 700°C. In other terms, the interfacial chromium concentration for a 0.02 wt% specimen must be slightly below 13 wt% and above about 13 wt% for a 0.015 wt% specimen. Bulk compositions of other alloying elements (e.g., chromium, molybdenum and nickel) will also impact this relationship.

Appreciable sensitization levels were measured for each of the heats after 500 h at 600°C. This severe heat treatment demonstrates that reducing bulk carbon contents to 0.02 wt% or even to 0.013 wt% will not produce a stainless steel which is "immune" from sensitization. EPR-DOS approaches values commonly considered severely sensitized and susceptible to IGSCC. However, it is important to point out that these extra-low carbon, Type 316 stainless steels are extremely resistant to sensitization development, requiring relatively long exposure times within a narrow temperature range. Data at 650°C (Appendix B) also agrees with this assessment. EPR-DOS is about 1 to 6 C/cm^2 after 20 h, but rises to very large values after 500 h for most heats.

Heat treatments necessary to promote sensitization in the extra-low carbon heats can be estimated based on this data. Carbon content remains important even at these levels with 0.02 wt% being more prone to sensitize than 0.013 to 0.015 wt% heats. The temperature range where sensitization can occur is between about 550 and 700°C. Significant sensitization requires times in the tens of hours at 600 to 700°C and times increase to hundreds of hours below 600°C. Carbide nucleation kinetics become extremely slow as temperatures drop below

600°C (Section 2.3.3). It is not known if a dual heat treatment, for example, a short time at higher temperature for nucleation plus a second treatment at lower temperature to promote depletion, would accelerate sensitization development. Many hours are necessary to produce a reasonable density of intergranular precipitates at 700°C with few carbides forming at higher temperatures.

4.2.3 Nitrogen Series Alloys

The role of nitrogen on sensitization and IGSCC is of considerable interest since nitrogen is a critical alloying element (for strengthening) in Type NG316 stainless steel. Additions are typically about 0.07 to 0.1 wt% to achieve strength levels in the 0.02 wt% C alloy comparable to high-carbon stainless steel (i.e., that for Type 304 or 316). Extra-low carbon heats of Type 316L without nitrogen additions have already been discussed. High-nitrogen Type 316L (N-1 and N-2) and 316LN (N-3 through N-7) have also been examined to assess nitrogen effects. Compositions of these heats are listed in Table 5. Heats N-1, N-2 and N-7 have bulk compositions within specifications for Type NG316 stainless steel.

Nitrogen concentrations do not have a controlling influence on sensitization development in the extra-low carbon heats. Once again carbon content was the determining variable in most cases. Sensitization response was mapped at 600, 650 and 700°C for heats N-1 through N-6. Changes in carbon from 0.014 to 0.019 wt% had a larger effect

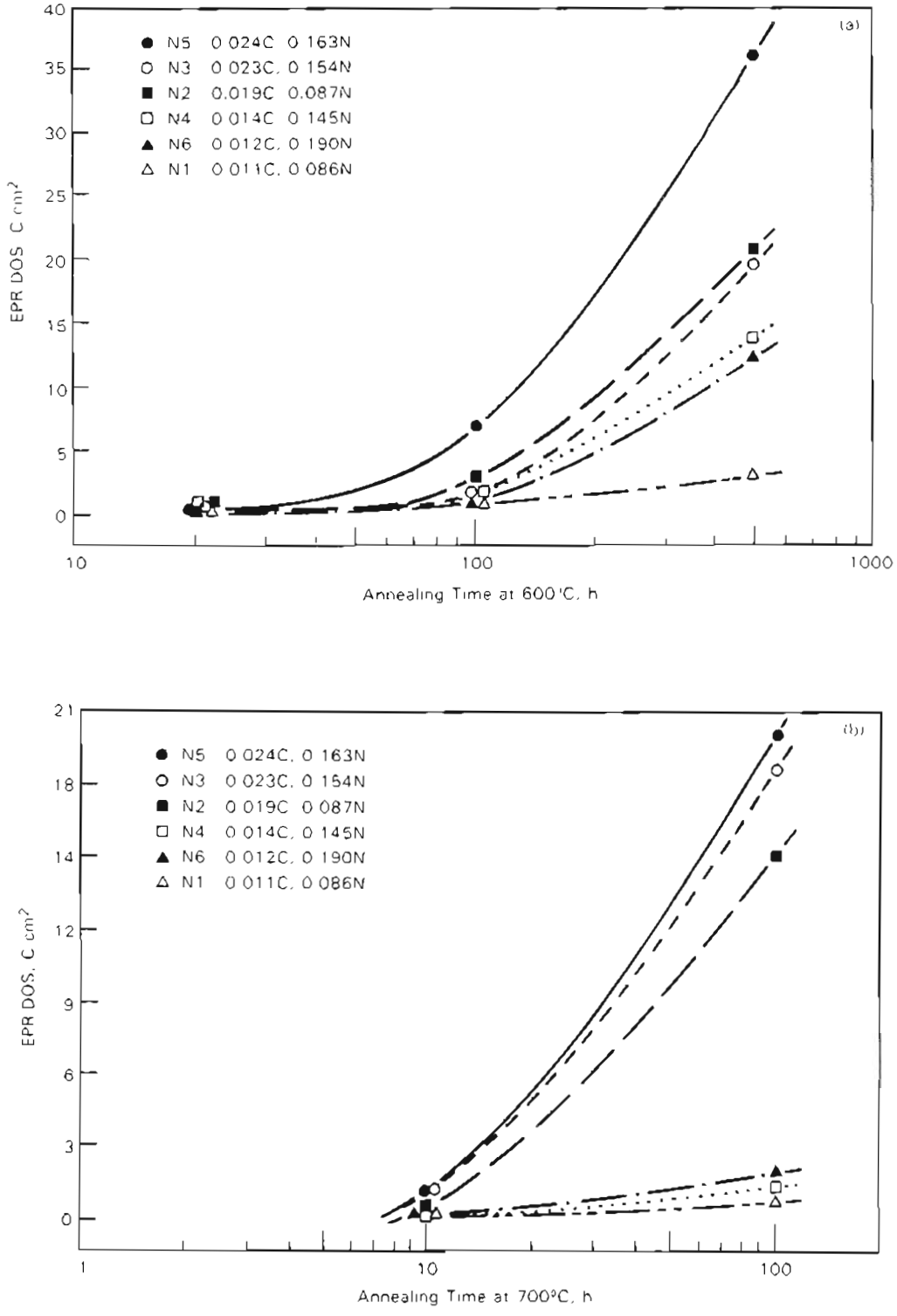

FIGURE 33. Sensitization Development in Nitrogen Series Heats at 600 (a) and 700°C (b).

than changing nitrogen levels from 0.086 to 0.19 wt%. EPR-DOS measurements at 600 and 700°C are summarized in Figure 33 for the nitrogen series heats.

Heats with higher carbon concentrations (0.019 to 0.024 wt%) exhibit consistently larger DOS, reaching values greater than 15 C/cm^2 after 100 h at 700°C or 500 h at 600°C. EPR-DOS increases to more than 50 C/cm^2 after 500 h at 650°C (Appendix B) for heats N-2, N-3 and N-5. For heats N-1, N-4 and N-6 with carbon contents less than 0.015 wt%, EPR-DOS remains near zero after 700°C heat treatments (Figure 33b), but attains values on the order of 10 C/cm^2 after 500 h at 600 or 650°C. This behavior is in agreement with the Type 316L heats (SS-11 to SS-14) where carbon levels between 0.015 and 0.02 wt% were necessary to promote sensitization at 700°C, but where significant DOS could still develop after long times at lower temperatures. The presence of nitrogen does not change these conclusions. Extra-low carbon (< 0.015 wt%) with or without nitrogen can become severely sensitized by extreme thermal treatments (e.g., 500 h at 600 or 650°C).

Although nitrogen does not appear to have a dominant effect on sensitization behavior, detailed comparisons were made isolating the influence of nitrogen from that of carbon. Comparable carbon heats can be examined by integrating the Type 316L and 316LN data. Sensitization response of six heats with bulk carbon concentrations between 0.011 and 0.015 wt% is compared in Figure 34 for heat treatments at 600°C. Four of these heats (SS-12, SS-13, N-4 and N-6) show remarkably similar behavior. This suggests that the addition of 0.145

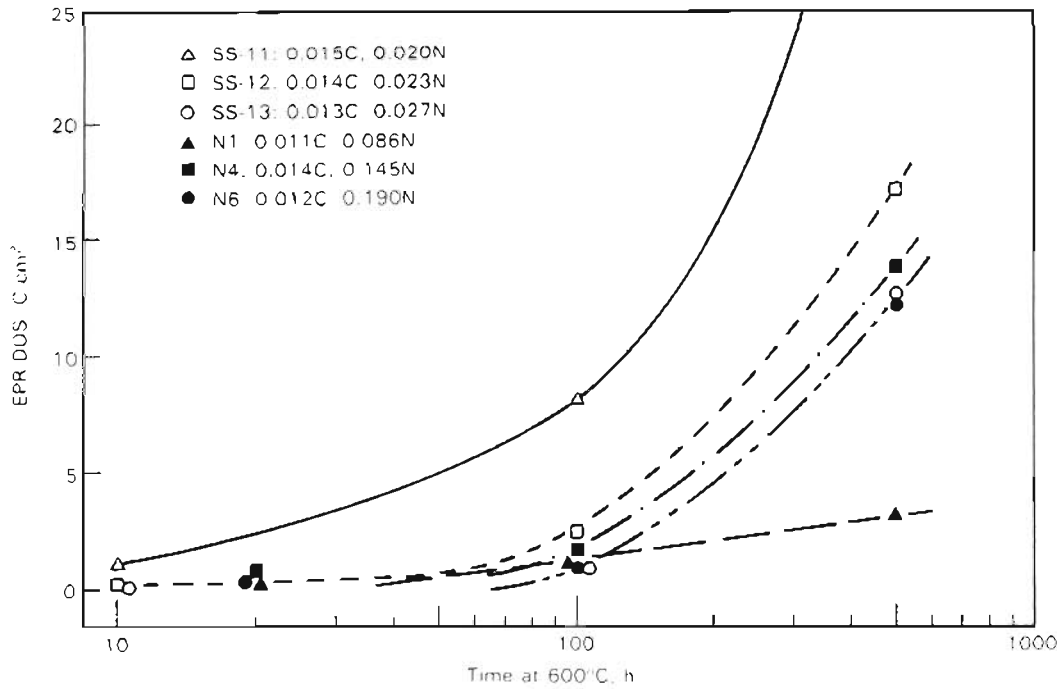

FIGURE 34. Nitrogen Effects on Sensitization Behavior at 600°C for Extra-Low-Carbon Type 316L and 316LN Stainless Steels.

to 0.19 wt% nitrogen has no detrimental or beneficial influence on resultant DOS. EPR-DOS data at 650 and 700°C also supports this conclusion. For example, SS-12 and N-4 both reach EPR-DOS values of approximately 15 C/cm^2 after 500 h at 650°C and 2 C/cm^2 after 100 h at 700°C.

The observation that significant additions of nitrogen did not influence EPR-DOS is somewhat surprising. Nitrogen at these levels would be expected to promote chromium nitride precipitation as reviewed in Section 2.3.1. Such precipitates should in turn impact EPR-DOS. However, EPR is an indirect technique to indicate chromium depletion and cannot determine whether nitrides are present. In order

to better assess nitrogen effects, selected specimens from the Type 316L and 316LN heat treatment matrix were examined by analytical electron microscopy (AEM).

Chromium nitrides (Cr_2N) were found along grain boundaries in the high nitrogen heats. Nitrides appeared to be regularly spaced among $M_{23}C_6$ carbides in the highly sensitized specimens. A typical distribution of intergranular precipitates is shown in Figure 35 along with energy dispersive X-ray spectra from second phases. Identification of these precipitates was determined using microdiffraction techniques. Nitrides were found to be much more chromium-rich than the mixed $M_{23}C_6$ carbide as indicated by the spectra in Figure 33. Carbides incorporate iron, molybdenum, nickel and silicon along with chromium.

The presence of multiple second phases along grain boundaries in Type 316LN stainless steel is consistent with the work of Hall et al.[94,138] where heats with about 0.03 wt% carbon and up to 0.16 wt% nitrogen were examined. Besides $M_{23}C_6$ and Cr_2N precipitates, Laves, Z- and X-phases were identified in high nitrogen heats. No attempt was made in the present study to assess various second phases or quantitatively analyze compositions of specific precipitates. A primary result from the limited AEM examinations was to identify the presence of a relatively high density of Cr_2N precipitates along with $M_{23}C_6$ carbides in the nitrogen heats. This compared to finding only $M_{23}C_6$ carbides in the Type 316L heats after identical heat treatments and with similar measured EPR-DOS values.

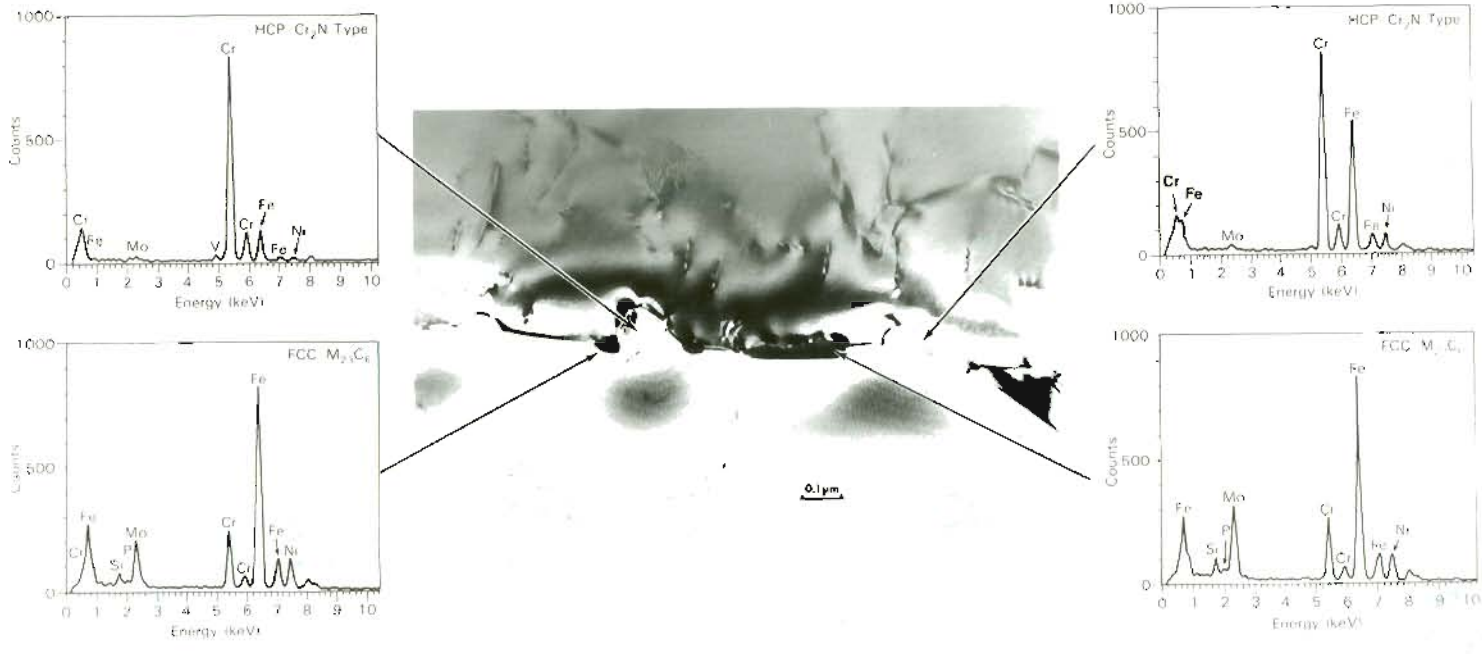

FIGURE 35. Grain Boundary Second Phase Precipitates in a Type 316LN Heat (N-5) After a Heat Treatment of 700°C for 100 h.

Chromium depletion was also documented by AEM in the N-5 specimen heat treated to 700°C for 100 h. Minimum chromium concentrations at grain boundaries were about 12 wt% with depletion widths (below 15 wt%) extending out to nearly 80 nm. Thus, direct measurements of depletion agree with the EPR-DOS level of 20 C/cm^2. A typical depletion profile is presented in Figure 36. Large differences in depletion profile characteristics were not observed across or along grain boundaries; i.e., a location near Cr_2N precipitates exhibited a chromium minimum concentration and depletion width similar to that measured between $M_{23}C_6$ carbides.

The AEM results put a different perspective on the comparable sensitization behavior between extra-low carbon heats with low nitrogen (SS-12 and SS-13) and those with high nitrogen (N-4 and N-6) displayed in Figure 34. Chromium depletion is similar in both cases, but grain boundary precipitates are quite different. Nitrogen has been shown to improve sensitization resistance at bulk levels up to 0.12 to 0.16 wt%.[16,37-42] It is possible that the present results represent a balance between nitrogen's beneficial effect to retard carbide formation and the detrimental effect of nitride precipitation. Heat N-1 with 0.086 wt% N is the most resistant alloy in respect to sensitization development consistent with its low carbon content and moderate nitrogen content.

Additional insight into nitrogen effects can be assessed by comparing the higher-carbon Type 316L and 316LN heats. Sensitization increases more slowly in Type 316LN heats N-2 and N-3 than the

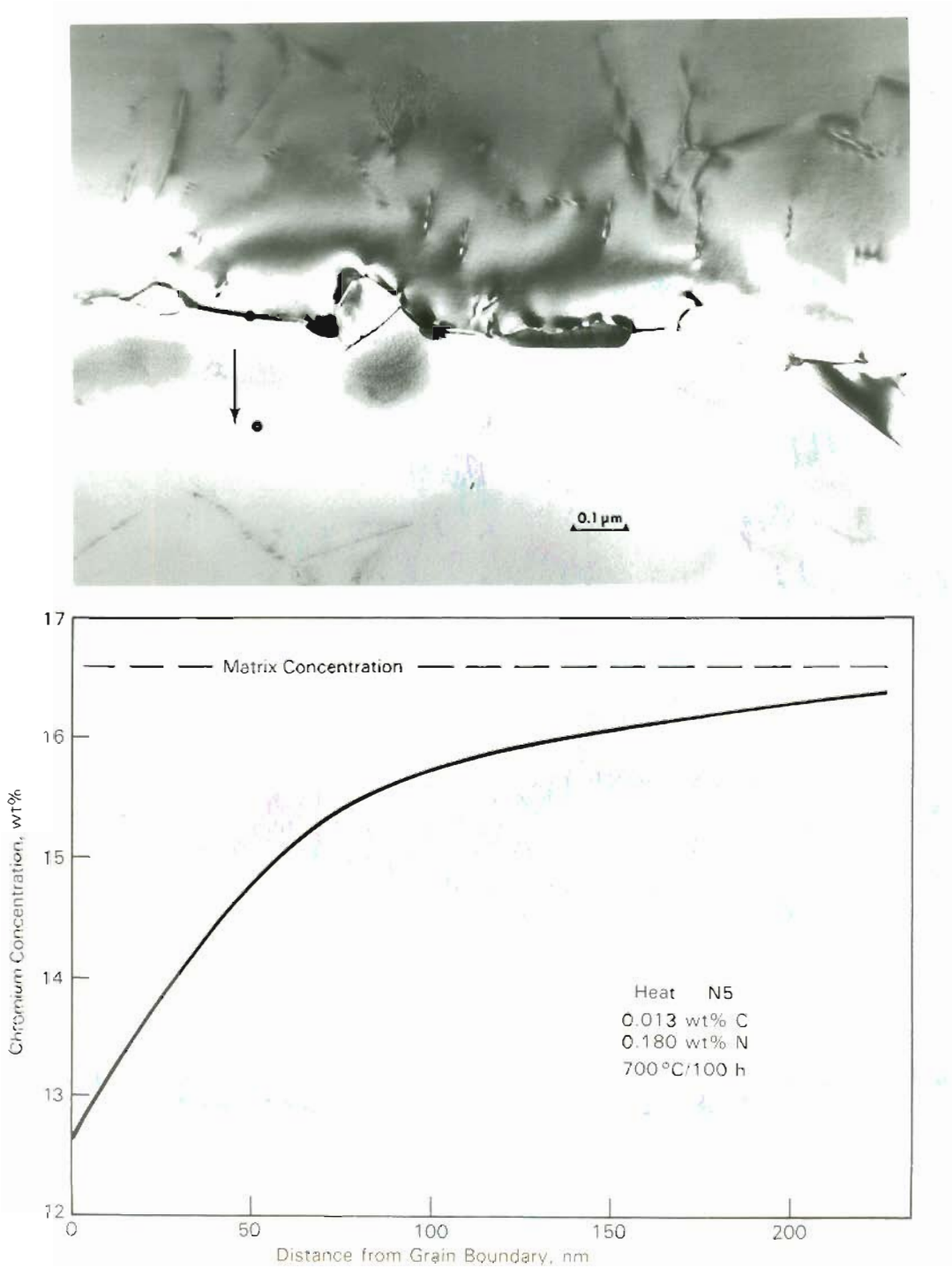

FIGURE 36. Typical Chromium Depletion Profile Determined AEM in Type 316LN, Heat N-5 After a 100 h Anneal at 700°C. Location along the grain where composition profile was measured is indicated in the TEM micrograph.

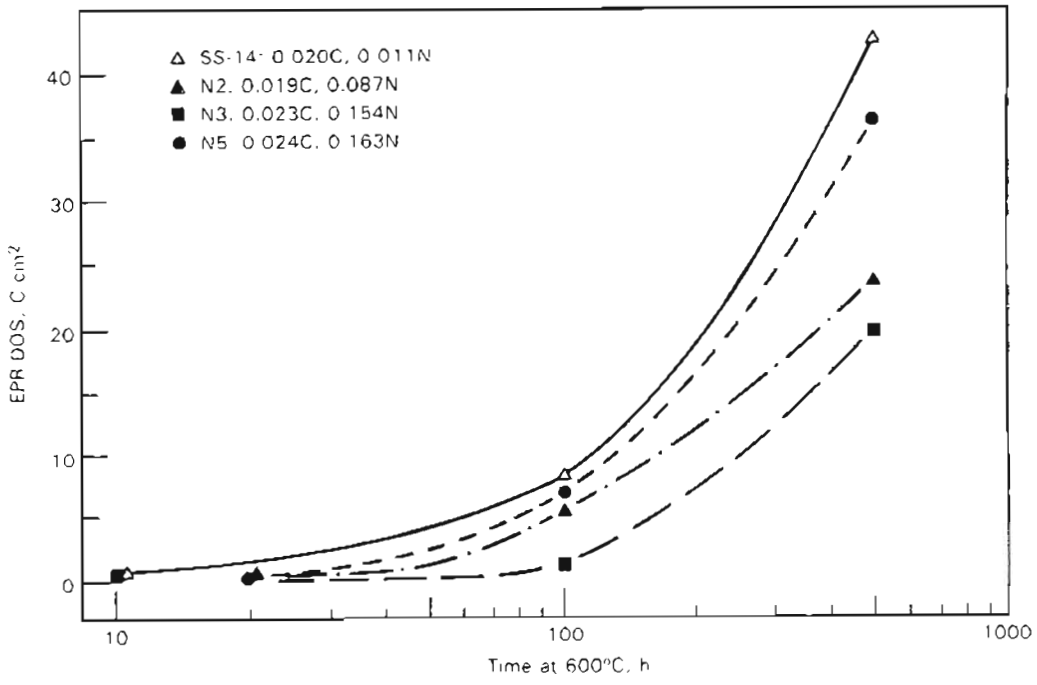

FIGURE 37. Comparison of Sensitization Response in a Low-Nitrogen (SS-14) and Three High-Nitrogen (N-2, N-3 and N-5) Heats at 600°C.

Type 316L heat SS-14 even though each heat contains about 0.02 wt% C. This behavior is illustrated in Figure 37 which maps EPR-DOS changes with time at 600°C. Although heat N-3 exhibits the best response at 600°C, it reaches higher EPR-DOS values at 650 and 700°C than heat N-2 which has lower carbon and nitrogen contents. If all the EPR data is considered for the higher carbon L and LN heats (Appendix B), a slight increase can be seen in time-to-sensitize and a decrease in EPR-DOS at most heat treatment times.

The role of nitrogen on the sensitization behavior of austenitic stainless steels has been studied by a number of investigators.[20,37-42,128,138] From this research, nitrogen appears to

reduce sensitization kinetics and may influence carbide precipitation thermodynamics. Experiments described above which were limited to low-carbon, Type 316L alloys do not show a large effect of bulk nitrogen content on sensitization behavior. Small changes in bulk carbon far outweighed the effects of nitrogen additions. Sensitization results can be interpreted in line with other investigators,[20,37-42] but the main conclusion is that nitrogen has only a small effect on sensitization in these low-carbon heats. The critical step in reducing susceptibility to sensitization is dropping the bulk carbon concentration.

4.2.4 Additional Stainless Steels

Most of the isothermal sensitization experiments were performed on 304 or 316-type alloys described in the previous three sections. However, data was also obtained on several other stainless steels including Types 317, 302 and 303. Compositions of these materials are listed in Table 5 and all EPR-DOS data is compiled in Appendix B. Certain aspects of the sensitization behavior will be presented and discussed to indicate effects of particular alloying (molybdenum) or impurity (sulfur) elements.

The effect of molybdenum on sensitization was illustrated in Sections 3.1.2, 3.2.2 and 4.2.2 through the comparison of Type 316 and 304 behavior. Molybdenum additions of about 2 wt% reduce sensitization kinetics and shift the nose of the TTS curve to higher temperatures. Examination of the Type 317 (C-12) heat which contains

3.4 wt% Mo adds further evidence demonstrating molybdenum's influence on sensitization kinetics.

No measurable sensitization was observed after heat treatments of 100 h at 600°C or 10 h at 700°C. EPR-DOS reached only about 15 C/cm^2 after 100 h at 700°C. These values document a much slower kinetics for the high-molybdenum Type 317 than for Type 316. Sensitization development in Type 304, 316 and 317 heats with similar carbon contents is displayed in Figure 38. Differences in times-to-sensitize and EPR-DOS magnitude at any time are large among the heats. It is interesting that the Type 317 heat shows such a significant improvement in sensitization resistance at 600 and 700°C. Times-to-sensitize increased more between the 316 and 317 heats (molybdenum from 2.3 to 3.4 wt%) than between 304 and 316 heats (molybdenum from 0.2 to 2.3 wt%).

Quantifying comparisons of this type to elucidate molybdenum effects is not possible, since chromium and nickel bulk concentrations also change among the alloys. However, the influence of molybdenum on sensitization kinetics, probably through its effect on chromium diffusivity, is demonstrated by the comparison in Figure 38. The improved resistance of the high-molybdenum Type 317 is consistent with the chromium equivalence concepts discussed in Section 2.6.1. Predictions using this approach to account for molybdenum effects will be evaluated in the following section.

Sensitization response was also mapped for a free-machining stainless steel, Type 303 - Heat C-9. This heat contains very high

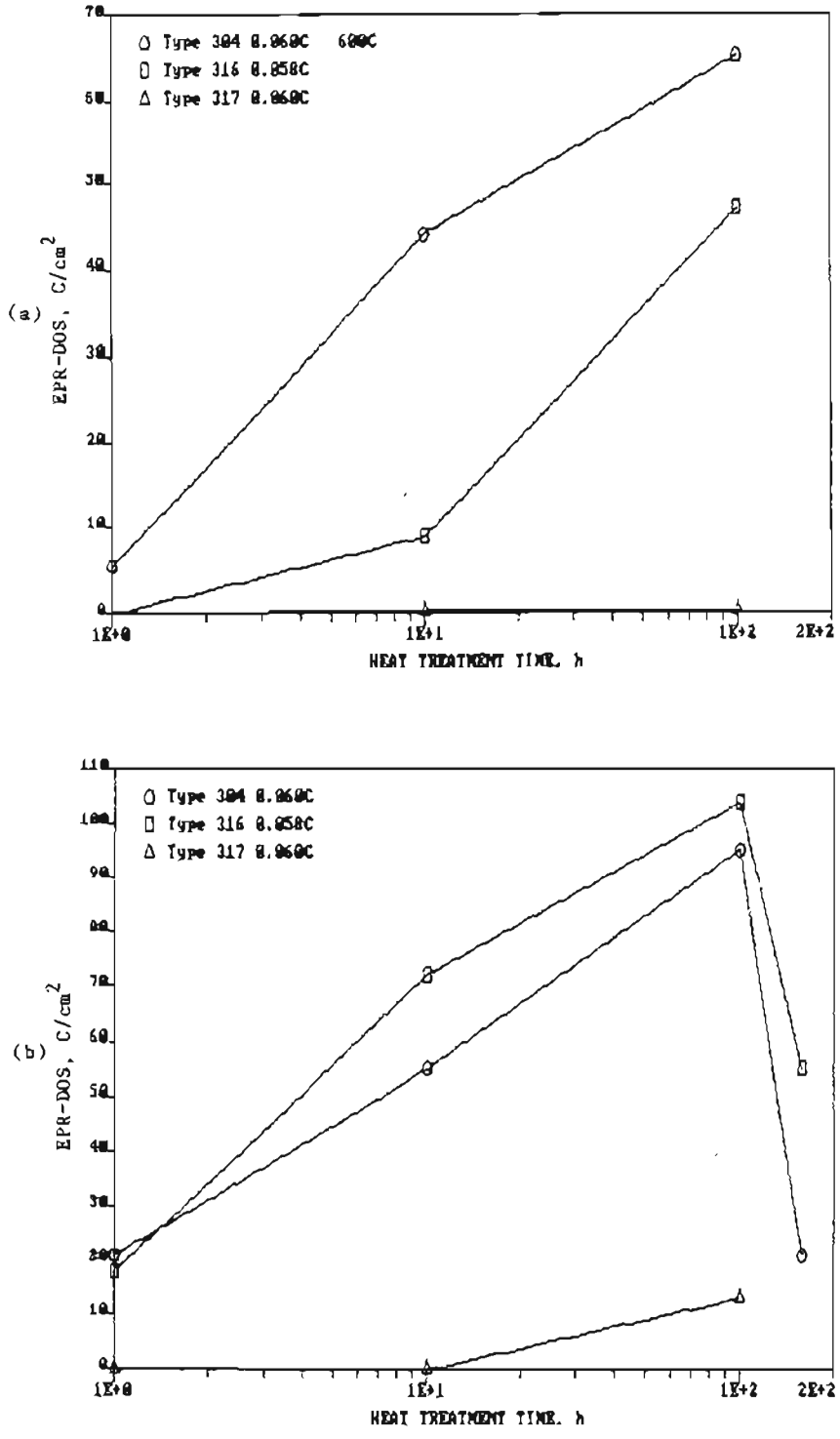

FIGURE 38. Comparison in Sensitization Behavior Among Types 304 (SS-7), 316 (SS-16) and 317 (C-12) with Similar Bulk Carbon Concentrations: (a) 600°C and (b) 700°C Data.

sulfur additions (0.195 wt%) and the highest carbon level (0.086 wt%) of any stainless steel tested. Sulfur would not be expected to directly influence sensitization development since its solubility is extremely small. Heat C-9 is compared to the highest-carbon Type 304 (Heat C-7, 0.072 wt%) in Figure 39. Results at 600 and 700°C do not reflect the increased carbon level in the Type 303 heat (0.086 wt%). This heat also shows a sharp decrease in EPR-DOS after 100 h at 700°C. Significant desensitization effects are not expected in such short times due to its high carbon content. For the Type 304 heats, EPR-DOS

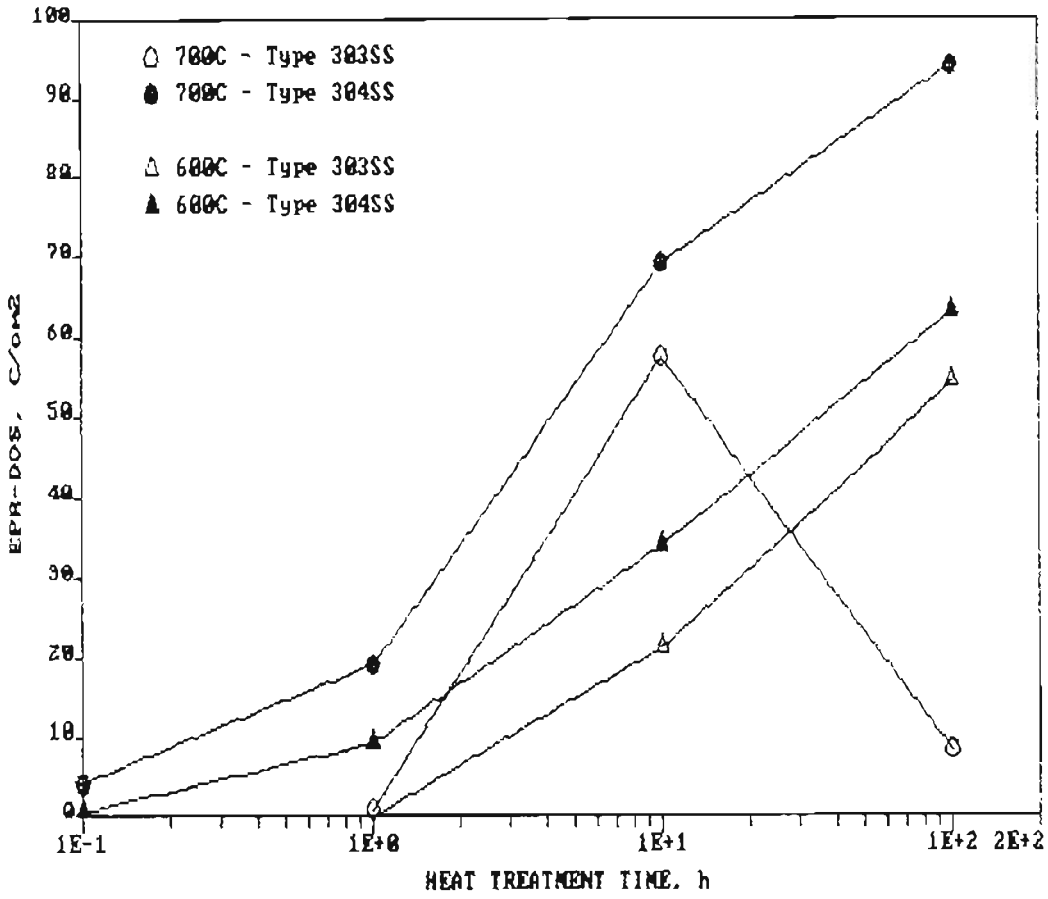

FIGURE 39. Sensitization Development in High-Carbon Type 304 and Free-Machining Type 303 Stainless Steels.

continued to show an increase from 10 to 100 h if bulk carbon contents were greater than 0.06 wt%. However, DOS probably goes through a maximum at times less than 100 h.

The high sulfur concentration in the free-machining steel did not prompt the accelerated desensitization behavior. Inter- and intragranular carbides were present in the initial microstructure of this high-carbon heat. If the carbon in solution before heat treatment is about 0.05 wt%, then desensitization would be expected within the observed time frame. Type 304 heat SS-6 (0.05 wt% C) exhibited comparable behavior with heat treatment time at 700°C. Large EPR-DOS values at short times may also have been caused by the pre-existing intergranular carbide microstructure.

4.2.5 Composition Equivalence Modeling

The ability to normalize composition effects on sensitization through chromium equivalence modeling was briefly reviewed in Section 2.6.1. A simple equation (No. 22) defines a composite chromium concentration in terms of the primary alloying element compositions and was found by Bruemmer[6] to predict times-to-sensitize for a large data base from the literature. The scatter in the correlation shown in Figure 5 was partly blamed on the diverse experimental procedures used among the many different laboratories. Sensitization behavior on 32 stainless steel heats has been determined in the isothermal matrix

using a consistent and reproducible methodology. Composition equivalence modeling will be evaluated versus the controlled data base of this study.

Excellent agreement was observed between chromium composite calculations and experimentally determined times-to-sensitize for the heats in Table 5. Correlations are shown in Figure 40 for data at 600 and 700°C. Heat treatment times to produce an EPR-DOS value of 5 C/cm^2 were estimated from the data compiled in Appendix B. In most cases, data was plotted versus time and extrapolations made between

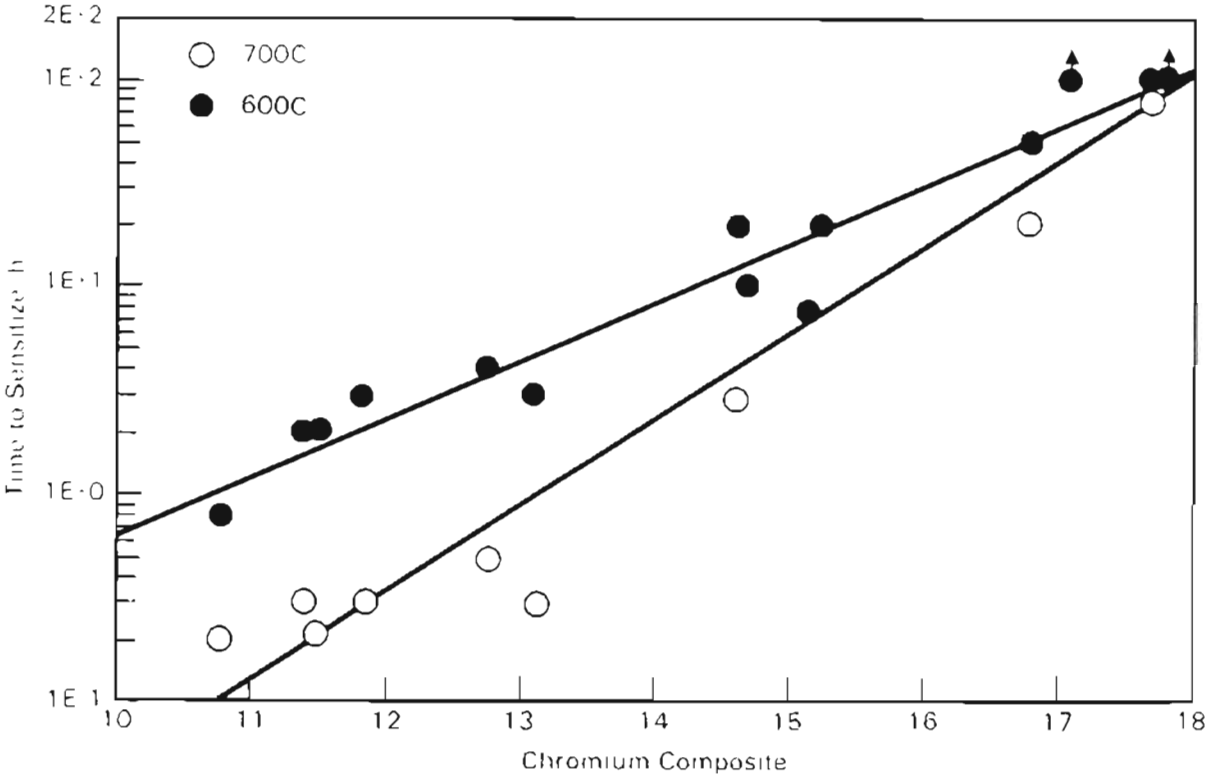

FIGURE 40. Correlations Between Calculated Chromium Composite Concentrations (Equation 22) and Times-to-Sensitize at 600 and 700°C.

existing EPR-DOS points to identify approximate times. Times-to-sensitize for the heats reported here along with an extensive list of data from the literature is also summarized in Appendix B.

Chromium composite-composition normalization appears to be an effective method to qualitatively account for heat-to-heat composition differences. Relative sensitization resistance can be compared among Type 304 and 316 stainless steels. Other austenitic stainless steels such as Type 302, 303 and 317 also fall close to this correlation. Overall variance determined by a linear regression fit to the correlation in Figure 40 is more than an order of magnitude better than that shown in Figure 5 for the literature data base. Thus, this approach represents a useful first step to compare expected sensitization tendencies of austenitic stainless steel heats. However, it must be kept in mind that composition equivalent equations cannot predict whether or not a component is sensitized or susceptible to cracking.

4.2.6 Material Condition Effects

Sensitization development depends on not only a material's composition, but also its initial condition. Most of the experimental work in this study was conducted on materials in the as-received, mill-annealed condition before low-temperature (sensitization) heat treatment. Selected heats were solution-annealed before subsequent testing for sensitization response to assess potential material condition effects.

Type 304 and 316 heats, SS-7 and SS-16, were picked because of their high carbon content. Carbides will remain stable for longer times and at higher temperatures in high-carbon steels. A second relatively high-carbon, Type 304 heat (SS-5) was examined because it exhibited larger than expected EPR-DOS values for its composition. This behavior might be due to initial material condition, making it a good choice for analysis. The final heat was a moderate-carbon, Type 316 (SS-15) for which desensitization behavior was well documented at 700°C.

Solution-annealing increased the grain size for each heat, in general, from about 50 μm (ASTM 6) to about 100 μm (ASTM 3). Heat SS-7 exhibited the least change in grain size, increasing from approximately 70 to 100 μm, while heat SS-16 showed the largest change from 35 to 110 μm. In each case a definite increase in grain size was noted indicating a modification of material condition. Sensitization behavior was then examined at 600 and 700°C.

The change in initial material condition did not induce a large change in subsequent sensitization response. Sensitization development for mill-annealed and solution-annealed heats is compared in Figures 41 (304 heats) and 42 (316 heats). Overall, data for the two material conditions was remarkably similar. This suggests that final mill-anneal temperatures were apparently high enough and cooling rates fast enough to keep most of the carbon in solution. The few heat specifications which supplied final anneal temperatures listed

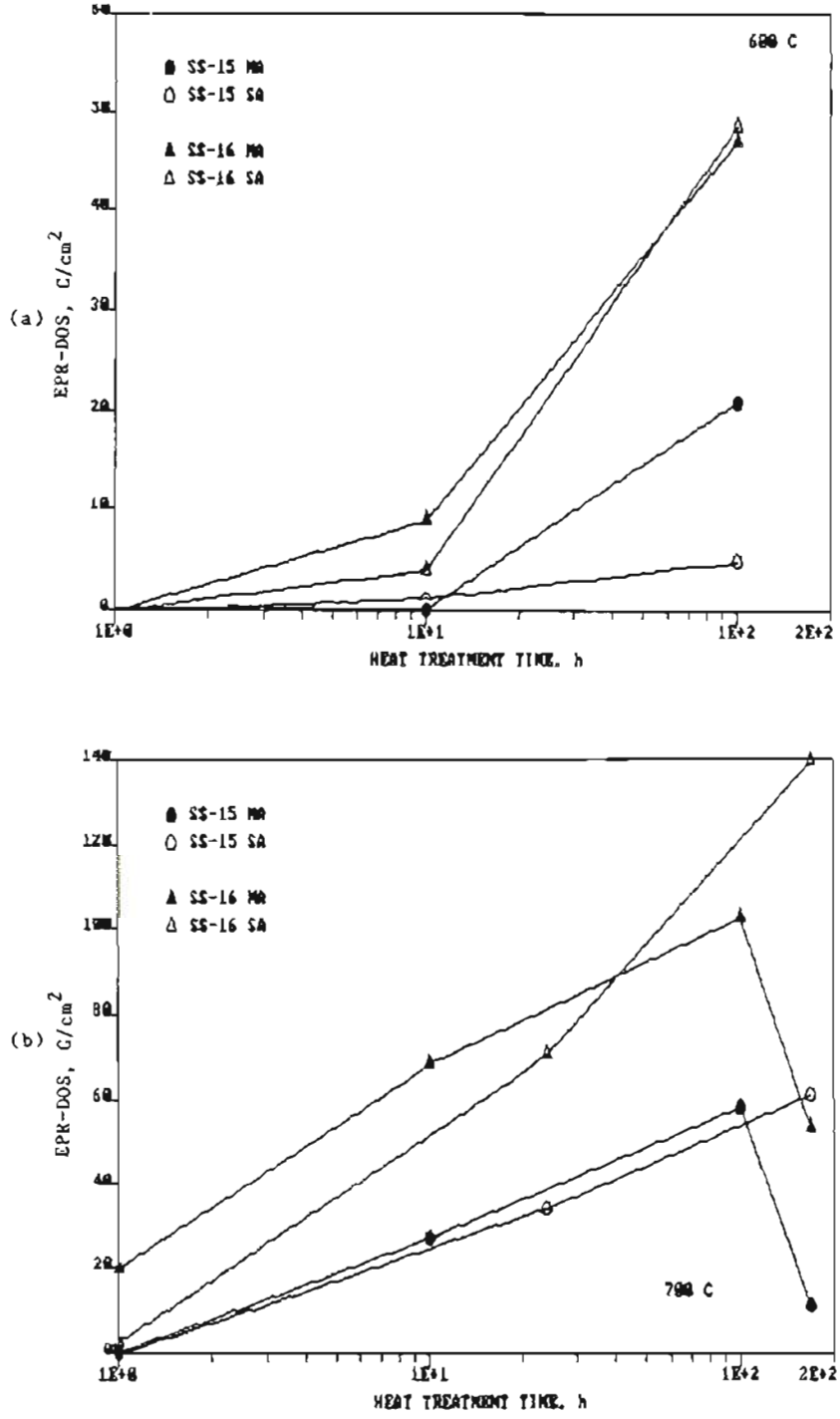

FIGURE 42. Comparison of Sensitization Development at 600 (a) and 700°C (b) for Type 316 Heats Initially in the Mill-Annealed (MA) or Solution-Annealed (SA) Condition.

temperatures between 1050 and 1100°C. Such temperatures could put carbon back into solution if the time at temperature was sufficient.

Although large differences in sensitization were not observed, several specific differences can be identified. For example, the SS-5 heat was selected to determine if the mill-anneal condition was accelerating sensitization development. Solution-annealing did nothing to reduce EPR-DOS values. If anything, DOS is larger for the solution-annealed material. Desensitization behavior mapped in the SS-15 heat at 700°C for the mill-annealed material was quite different in the solution-annealed condition. No decrease in EPR-DOS is found after 168 h, while such a decrease was obvious within 150 h for the mill-annealed material. This difference may simply reflect the change in grain size. As grain size increases, the grain boundary length for precipitation decreases. Thus, the time-to-desensitize will tend to increase with increasing grain size.

4.3 CONTINUOUS COOLING SENSITIZATION

Eleven heats were selected for continuous-cooling thermal treatments based on the isothermal sensitization behavior. Three Type 304 (SS-7, SS-5 and SS-4), two 304L (SS-3 and SS-2), two 316 (SS-16 and SS-15), two 316L (SS-14 and SS-13) and two 316LN (N-2 and N-5) were examined. The experimental matrix included five maximum temperatures (800, 900, 950, 1000 and 1050) and four cooling rates (approximately 0.02, 0.1, 0.5 and 2°C/s). Cooling rates were determined from time-temperature plots. A linear fit to the temperature decrease with time

from 800 to 550°C was used to specify cooling rates for comparison. Cooling rates varied somewhat depending on the maximum temperature.

Sensitization development was found to be a function of heat composition (carbon content in particular), cooling rate and maximum temperature. Low-carbon heats (SS-3, SS-13, SS-14, N-2 and N-5) did not reveal measurable EPR-DOS as a result of continuous cooling heat treatments. Only heats SS-3 and SS-14 were exposed to the complete temperature-cooling rate matrix, while the other heats saw isolated treatments. Low-carbon, Type 304 heat SS-2 exhibited slight DOS after certain exposures. This lack of sensitivity for the low-carbon stainless steels reiterates the dominant effect of carbon content. The remaining discussion will concentrate on moderate-to-high carbon heats where other variables can be studied.

The composition equivalence calculations and comparisons in Section 4.2.5 demonstrated the importance of additional alloying elements (besides carbon) on relative sensitization resistance. A similar comparison can be made using the continuous cooling data as was done for the isothermal data. Time-to-sensitize can be replaced by a similar variable, cooling-rate-to-sensitize. Once again extrapolation to an EPR-DOS value of 5 C/cm^2 was made to specify times of interest. In order to integrate Type 304 and 316 sensitization behavior, data for a maximum temperature of 900°C was analyzed and is plotted in Figure 43 versus chromium composite concentrations calculated using equation 22.

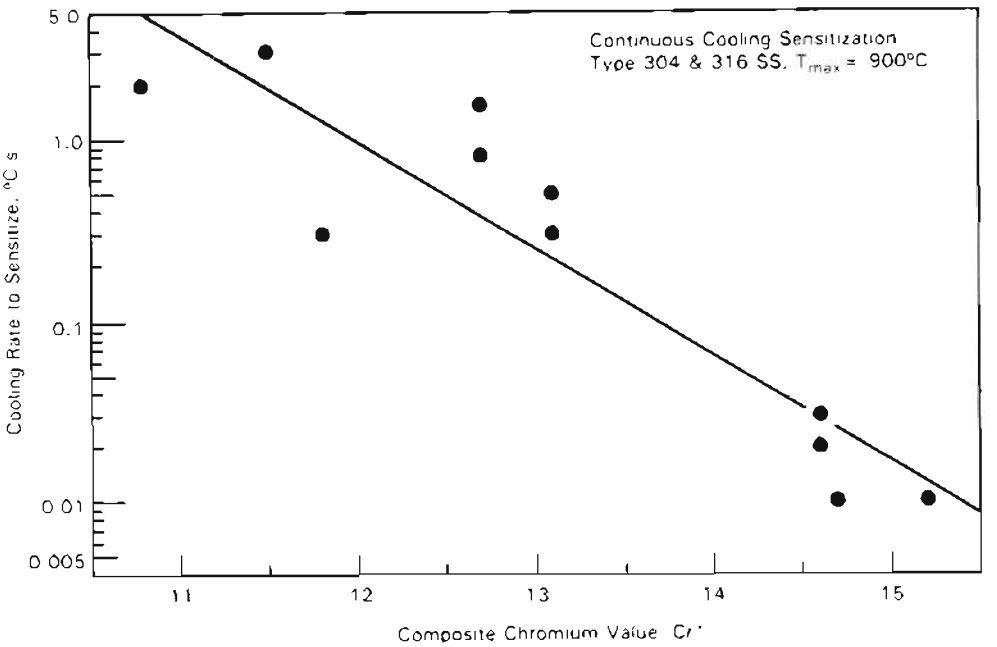

FIGURE 43. Comparison Between Cooling-Rate-to-Sensitize from EPR Tests and Chromium Composite Concentrations Calculated Using Equation 22.

Cooling rate-to-sensitize is inversely related to the chromium composite concentration. In other words, faster cooling rates promote sensitization in more susceptible (lower Cr*) stainless steels.

Although the correlation depicted in Figure 43 shows reasonable agreement, a better fit was demonstrated for isothermal data at 600 and 700°C (Figure 40). This agreement for the continuous cooling sensitization response also breaks down when comparing data at other maximum temperatures. Such observations illustrate increased complexity in thermal treatment between isothermal and continuous cooling. Because of the short times at temperature during continuous cooling, carbide nucleation can become much more important than it is at a constant temperature of 700°C, for example. Initial material condition

may exert a stronger role due to differences in grain boundary characteristics including preexisting carbides, nucleation sites and solute segregation.

The complexity inherent in the continuous cooling heat treatment is best illustrated by the effect of maximum temperature on sensitization development. An example of this behavior is presented in Figure 44 for high-carbon Type 304 (SS-7) and Type 316 (SS-16). EPR-DOS which evolves during cooling from a maximum temperature of 1050°C is much smaller than that from other maximum temperatures. No obvious grain growth can be detected during the 1050°C thermal treatment, but the initial material condition is probably affected. This high temperature exposure may be the only one with enough time at high enough temperatures to put preexisting carbides and carbides formed during the heat-up cycle back into solution.

The exact mechanism prompting the change in sensitization behavior after reaching the 1050°C maximum temperature is not known at this time. There is clear evidence that sensitization (and probably precipitate nucleation) kinetics are reduced. While it is likely that some aspect of material condition is changing at or near 1050°C, solution annealing treatments in the same temperature range did not influence subsequent isothermal sensitization kinetics. Therefore, changes in initial grain boundary microstructure (ledges, etc.) or in bulk dislocation densities cannot explain these differences. This suggests that behavior may depend on microstructural and microchemical changes

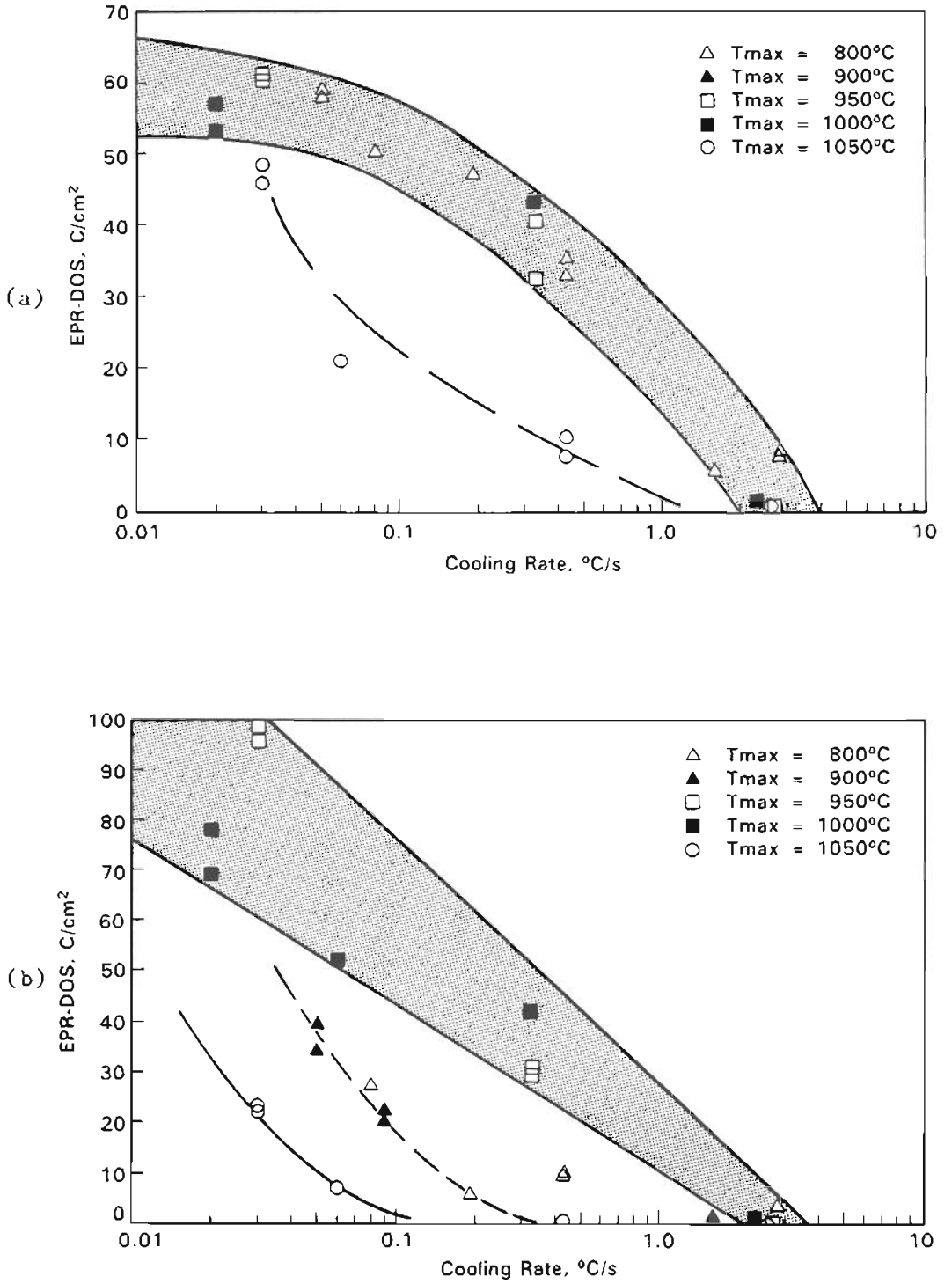

FIGURE 44. Comparison of Maximum Temperature Effects on Continuous Cooling Sensitization Behavior for a Type 304, Heat SS-7 (a) and a Type 316, Heat SS-16 (b) Stainless Steel.

which occur during specimen heat-up to the maximum temperature. No measurable EPR-DOS is observed due to the heat-up step for any maximum temperature, but grain boundary enrichment of carbon and chromium may occur along with the formation of carbide nuclei. Such a local microchemistry might develop at temperatures up to 900 or 950°C and be stable, or dissolve slowly, until temperature reaches much higher, i.e., 1050°C. Additional research is required to understand the basis for the observed sensitization behavior.

The continuous cooling response for the Type 304 heat in Figure 44(a) is similar for maximum temperatures of 800, 900, 950 and 1000°C, while this is not the case for the 316 heat in Figure 44(b). EPR-DOS data at 800 and 900°C for the 316 heat follows a different trend with cooling rate. Sensitization kinetics appear to be slower than for maximum temperatures at 950 and 1000°C, but not quite as slow as for a maximum temperature of 1050°C. A possible explanation is that precipitation nucleation and growth remain important at temperatures greater than 900°C. Thus, resultant DOS will increase with maximum temperatures about 900°C. Similar behavior would be expected for the Type 304 heat at lower temperatures than for Type 316 due to differences in the time-temperature-precipitation response. More detailed comparisons of the actual data points for the three high-carbon Type 304 heats do not indicate any significant differences between the 800°C maximum temperature sensitization data and the 900°C data as shown in Figure 45(a) for heat SS-5.

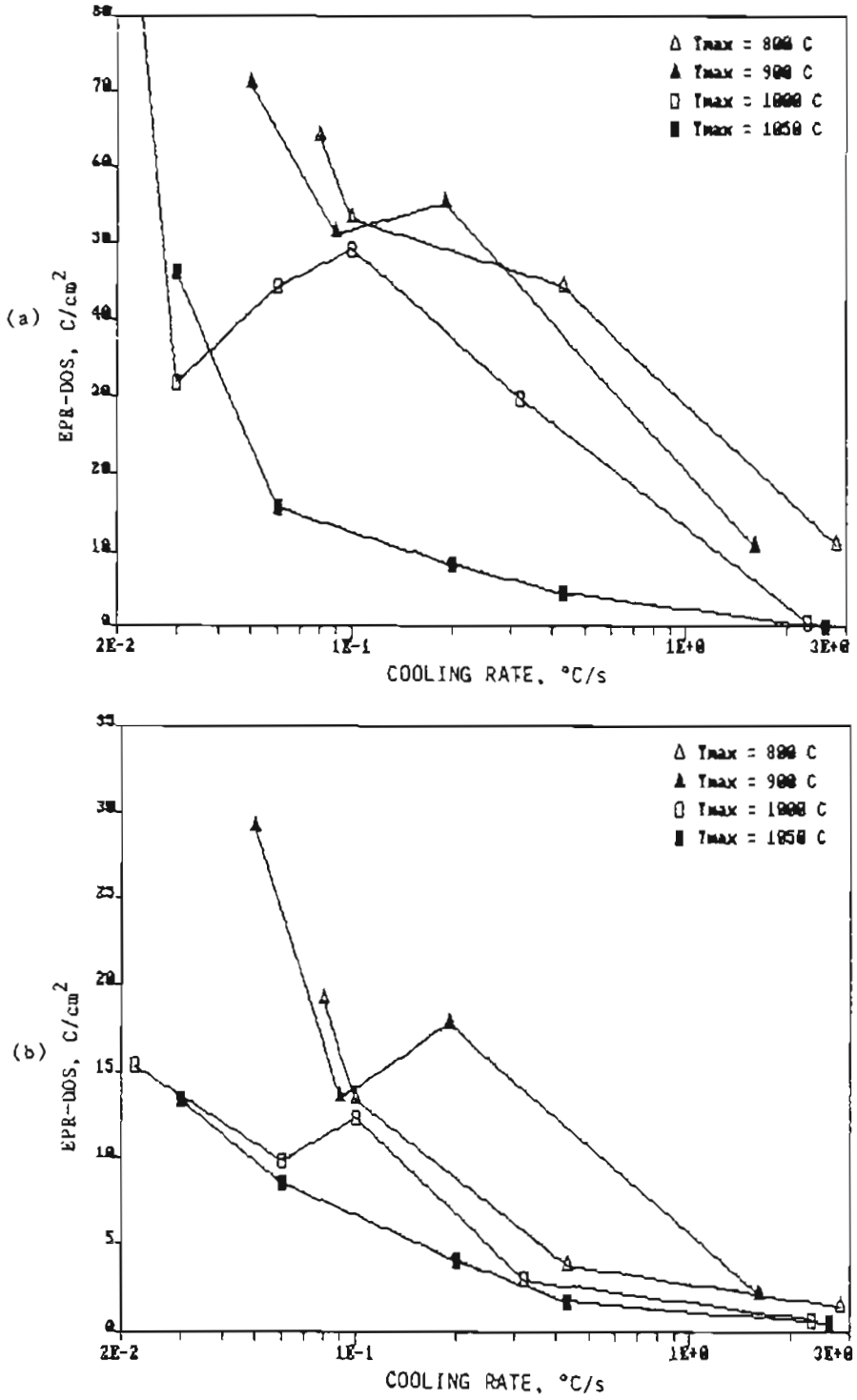

FIGURE 45. Maximum Temperature Effects on Continuous Cooling Sensitization for High-Carbon (a) and a Moderate-Carbon (b) Type 304 Heat.

The addition of continuous cooling sensitization data for other stainless steels in the evaluation of maximum temperature effects shows that these effects also depend on carbon content. Moderate-carbon heats, SS-4 and SS-15, exhibit a decrease in sensitization kinetics as maximum temperatures reach 1000°C, not 1050°C as for the higher carbon steels. Sensitization behavior for heat SS-4 is mapped at various maximum temperatures in Figure 45(b). EPR-DOS evolved at 800 and 900°C are similar and consistently greater than that at 1000 and 1050°C.

Measurable sensitization is not observed in heat SS-15 if the maximum temperature is greater than 950°C, while small EPR-DOS values are recorded at lower maximum temperatures. EPR-DOS is on the order of 1 to 5 C/cm^2 at the slowest cooling rates with maximum temperatures of 800, 900 or 950°C. This behavior agrees with carbon effects on carbide precipitation and dissolution temperatures. The higher the carbon content, the higher the temperature will be where the solubility limit is exceeded and precipitation will occur. Carbide dissolution temperature will follow a similar dependence. All of this gives supporting information concerning maximum temperature effects on continuous cooling sensitization development and suggests that differences result from material condition changes at higher temperatures.

The last aspect of the continuous cooling heat treatment that must be considered is cooling rate. As noted in Figure 43, cooling rate can be considered to have a comparable effect on sensitization development as isothermal heat treatment time. It does determine the

time the specimen is exposed to temperatures where precipitation and depletion are thermodynamically and kinetically favored. Thus, decreasing cooling rates will increase time in this precipitation/sensitization range and promote larger EPR-DOS values. This general behavior has already been illustrated in Figures 44 and 45.

Cooling rate effects on continuous cooling sensitization response are summarized for Type 304 and 316 stainless steels in Figures 46 and 47. EPR-DOS in almost all cases increases with decreasing cooling rate as expected. Cooling rates to promote measurable sensitization are on the order of 1 to 3°C/s. Additional tests at these rates would be required to document exact differences among the heats and maximum temperatures. EPR-DOS reached maximum values for the 900°C data set with the SS-5 and SS-7 heats recording levels of 60 to 70 C/cm^2 at a cooling rate of 0.03°C/s. It is interesting to note that the SS-5 heat exhibited larger EPR-DOS than the higher-carbon SS-7 heat. This is consistent with isothermal sensitization results in that the DOS developed was larger than expected based on carbon content.

Slower sensitization kinetics for the high-carbon Type 316 heats can be seen in Figure 46. At maximum temperatures below 950°C, cooling rates to sensitize are much less than the Type 304 heats (<0.5 vs ~3.0°C/s). However, as maximum temperatures are increased, Type 316 response becomes similar to that for Type 304. This reflects a balance between the higher-temperature precipitation tendencies with molybdenum present which accelerates sensitization development and the

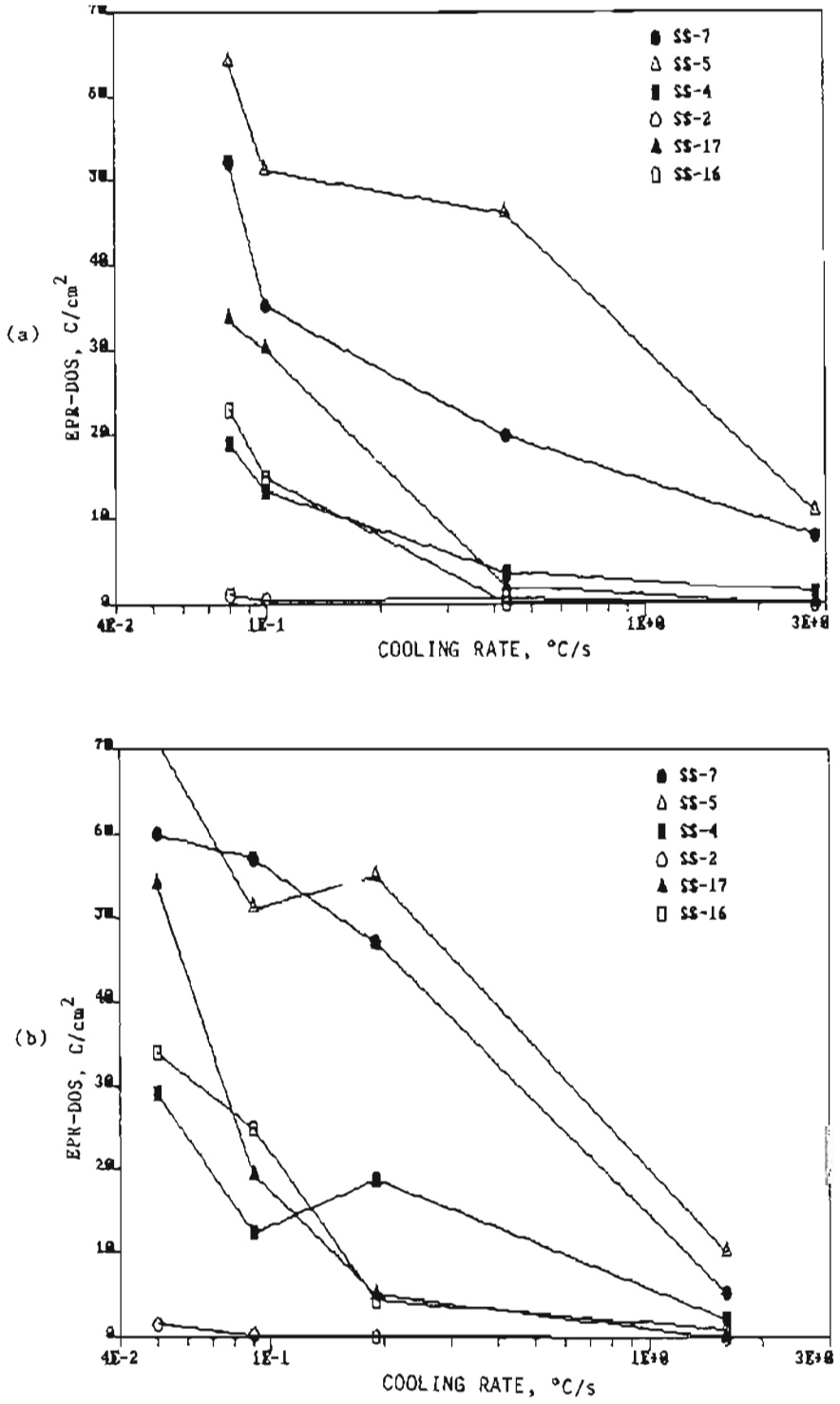

FIGURE 46. Continuous Cooling Sensitization Development from Maximum Temperatures of 800 (a) and 900°C (b).

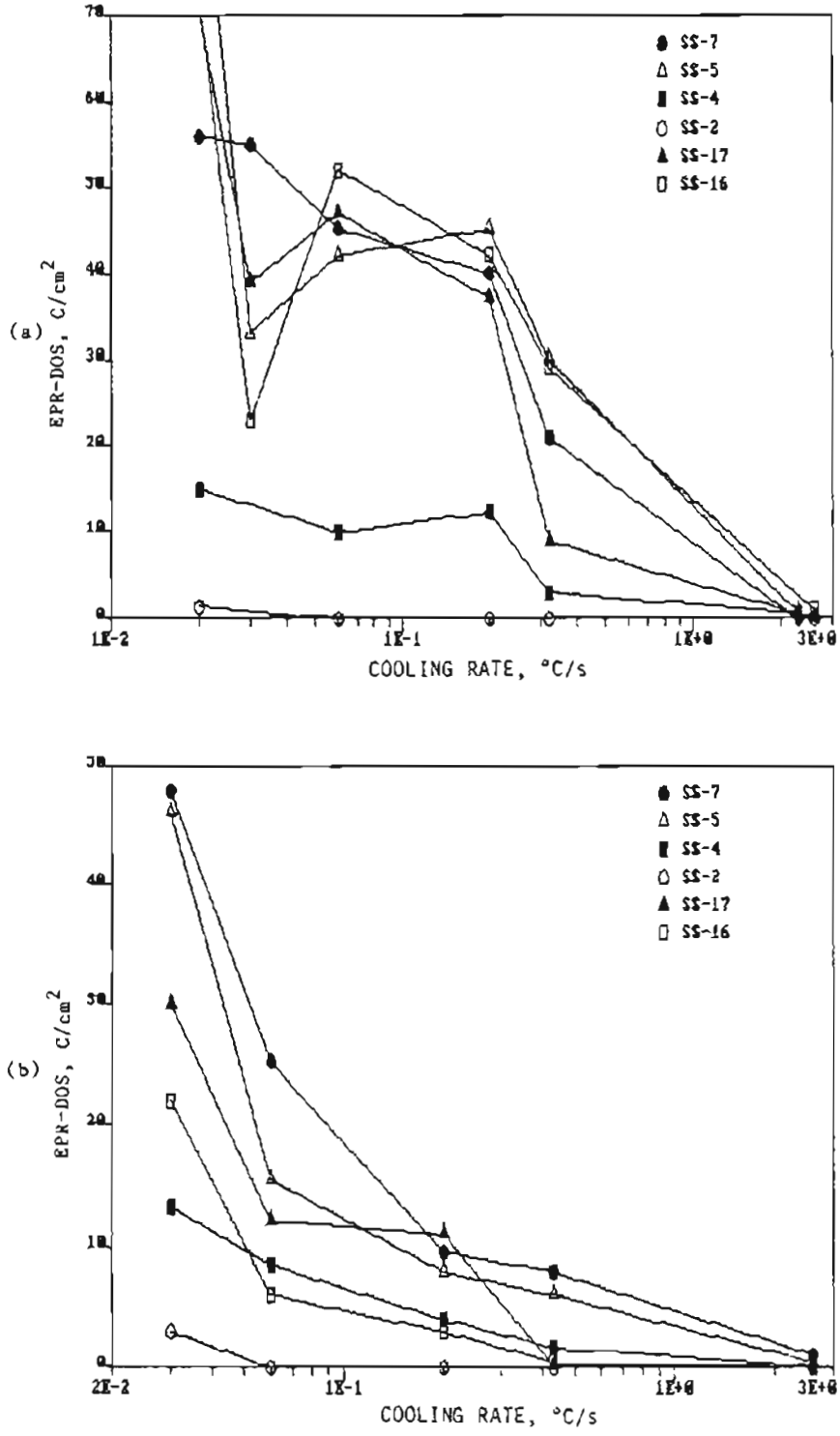

FIGURE 47. Continuous Cooling Sensitization Development for Maximum Temperatures of 1000 (a) and 1050°C (b).

reduced kinetics at lower temperatures. Such complex behavior makes it extremely difficult to assess expected sensitization response for a heat without detailed knowledge of thermal history.

Cooling rate effects on sensitization development do not show a relatively simple inverse dependence for data at 1000°C. While not linear on the semi-log plots in Figures 46 and 47(b), EPR-DOS does decrease with increasing cooling rate at other maximum temperatures. However, EPR-DOS appears to be smaller at slow cooling rates (0.03 to 0.06°C/s) than at faster cooling rates (0.1 to 0.3°C/s) for heats at a 1000°C maximum temperature. Additional cooling rates were examined and tend to corroborate this change in response with cooling rate as shown in Figure 46(a).

A possible explanation for this reversal refers back to the discussion concerning the 1050°C data. As cooling rates are reduced, the time specimens are exposed to potential solution-annealing temperatures increases. Microstructures and microchemistries which are not dissipated during a short time at 1000°C (i.e., cooling rates > 0.1°C/s) may be significantly affected as cooling rates decrease and time near 1000°C increases. More work is necessary to understand these effects, including examination of time at maximum temperature, quenching from intermediate temperatures and heating rate effects on precipitation and sensitization.

4.4 THERMOMECHANICAL HISTORY EFFECTS

Continuous cooling thermal treatments were shown in the previous section to increase the complexity of the sensitization process. Understanding continuous cooling sensitization development is an important step toward the practical cases of interest, such as processing or fabrication-induced phenomena. The best known and perhaps most complex example is heat-affected-zone (HAZ) sensitization developed during welding. Another factor is superimposed on the microstructural/microchemical evolution with thermal treatment, i.e., deformation. Stainless steels are exposed to a thermomechanical history which can greatly influence sensitization behavior.

4.4.1 Experimental Procedure

Three high-carbon stainless steel heats (C-6, C-7 and SS-16) were selected for thermomechanical history experiments because of their respective isothermal data bases. Sensitization behavior for the Type 304, C-6 heat had been extensively characterized by both EPR and STEM-EDS methods. Because of these direct measurements of chromium depletion, much of the work concentrated on heat C-6. Both steels were solution annealed at 1100°C for 1 h and water quenched before machining.

Uniaxial deformation effects were investigated on flat, dogbone-shaped tensile specimens. Specimens were deformed at variable constant extension rates from 1% to 10% strain per hour. Isothermal heating was attained using a clamshell furnace surrounding the tensile

specimen. Temperatures were measured across the gage section during heat treatment and were found to be within 5°C of the specified 600°C for these tests. Thermal exposures were all conducted in air.

Simultaneous-deformation specimens were dynamically loaded at 600°C, while prior-deformation specimens were strained at room temperature then heat treated. In each case, 1-2 hour steps were taken between documentation of DOS. Field-cell EPR tests were conducted on two locations near the center of the gage length. Thus, a series of experimental data points was obtained from each test which was made up of 5 to 10 additive isothermal exposures. Control samples to document isothermal response were attached to the gage region to ensure an identical thermal history for comparison.

4.4.2 Simultaneous Deformation Effects

Simultaneous straining dramatically accelerated sensitization development. Measurable DOS is observed in shorter times, and EPR-DOS reached higher values during additive 600°C anneals in strained versus unstrained specimens. Sensitization response as a function of heat treatment time is documented in Figure 48 for the two Type 304 stainless steels. Large EPR-DOS values (>10 C/cm^2) can be noted after only 1 h at 600°C in the deformed specimen, whereas more than 9 h was required to approach a comparable EPR-DOS in the control specimens. EPR-DOS values of more than 35 C/cm^2 are observed after 9 h for the C-6 strained specimen versus only about 5 C/cm^2 for the unstrained specimen.

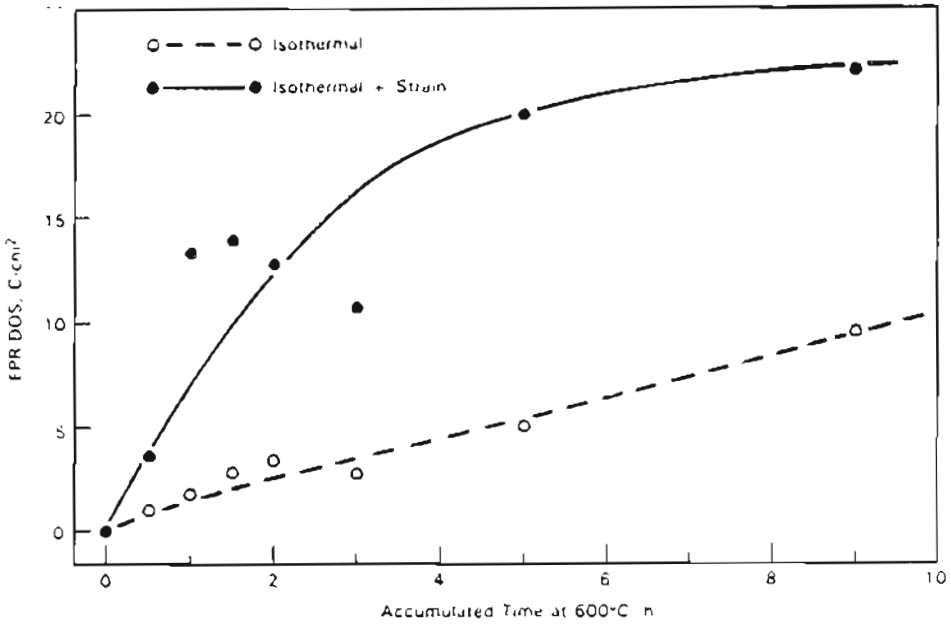

(a)

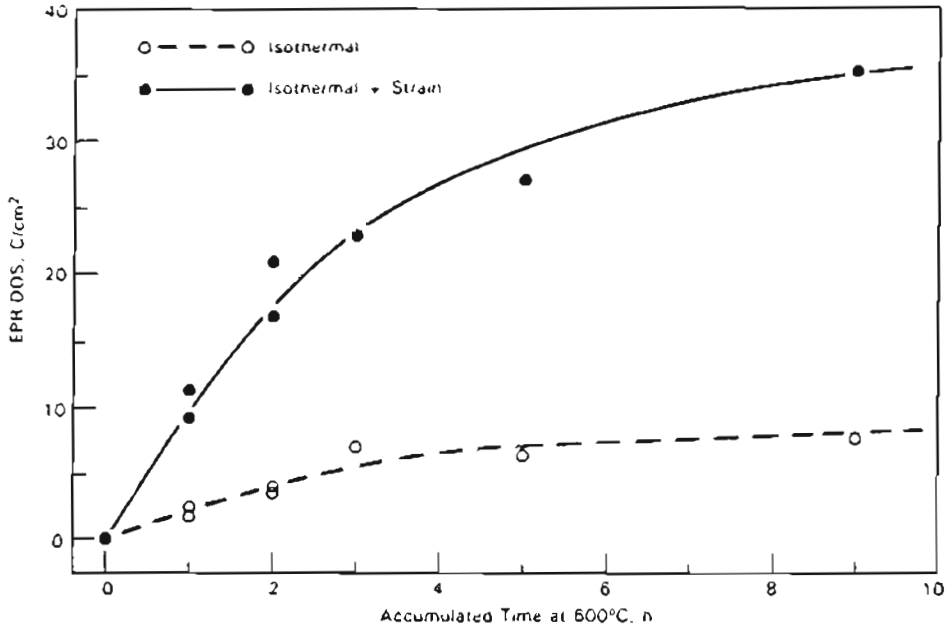

(b)

FIGURE 48. Simultaneous Deformation Effects on Sensitization Development in Type 304 Stainless Steels: (a) Heat C-7 and (b) Heat C-6. Specimens were deformed at a rate of 6%/h.

Differences of this magnitude illustrate the critical importance of thermomechanical, not just thermal, effects on sensitization development. Simple isothermal heat treatments of many hours did not result in significant IG corrosion in the EPR test, only isolated regions along some grain boundaries were attacked. On the other hand, strained specimens showed almost continuous grain boundary attack after only one hour. This suggests that deformation can promote a much more uniform development of chromium depletion along boundaries in much shorter thermal exposure times. Continuous depletion along grain boundaries is often referred to as a prerequisite for IGSCC.

Grain boundary carbide precipitation and chromium depletion characteristics were examined on strained and unstrained specimens after the additive cycles were complete. Bright and dark field TEM micrographs are shown in Figure 49 for the C-7 specimen after 9 h at 600°C. EPR results for this specimen were presented in Figure 48(a). A deformation rate of 6% strain per hour produces an accumulated strain of more than 50%. This damage is reflected in the high dislocation density which can be seen in the bright-field image (upper right, Figure 49). Dislocations are continually created with time during the simultaneous deformations leading to an increasing dislocation density. Although some fraction of the dislocations are annealed out at 600°C, apparently at this deformation rate more are created than annihilated.

Grain boundary carbide morphologies are also quite different when comparing strained to unstrained specimens in Figure 49.

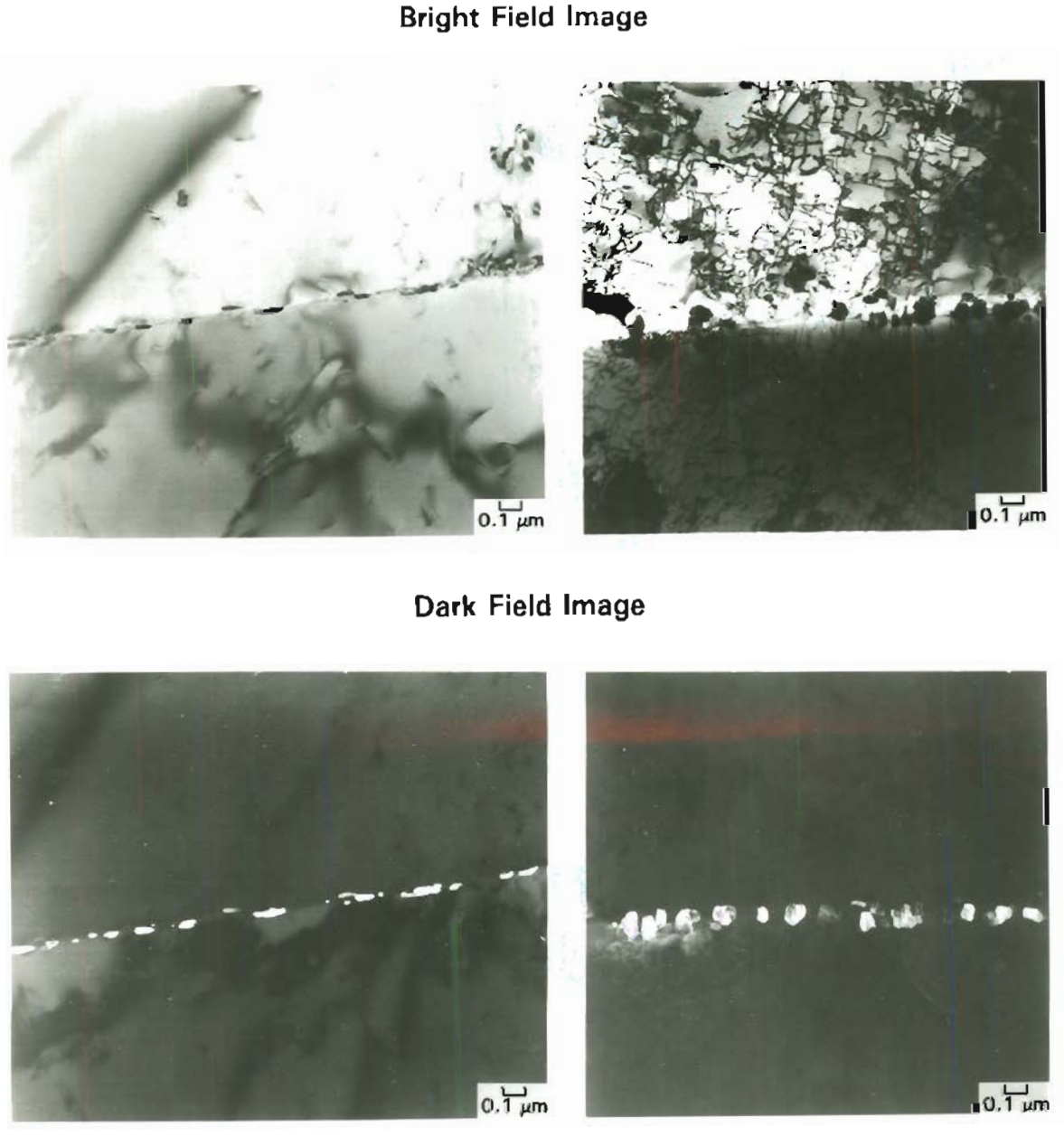

FIGURE 49. Transmission Electron Micrographs Illustrating Grain Boundary Carbide Precipitate Morphologies in Strained and Unstrained C-7 Specimens.

Carbides are elongated along the boundary in the isothermal case, but extend preferentially into one grain with deformation. Not all boundaries in the strained material exhibit this appearance. It is possible that only interfaces which are properly oriented with the applied uniaxial stress are influenced. Deformation may promote discontinuous carbide growth due to short-circuit diffusion paths created by the influx of dislocations. Discontinuous or cellular precipitation involves grain boundary diffusion and migration. Betrabet et al.[41] have documented discontinuous precipitation of $Cr_{23}C_6$ carbides in Type 304 after isothermal heat treatments.

Discontinuous carbide precipitation mechanisms whether interface-energy driven[139] or chemically driven[140] will lead to the formation of asymmetric depletion profiles. Precipitation resulting from volume diffusion where grain boundary migration does not occur will create nearly symmetric profiles as was documented in Section 3.1. Chromium depletion was mapped for both strained and unstrained specimens. Consistent with its much larger EPR-DOS, the strained specimens exhibited lower chromium minimums and wider depletion widths. Depletion profile characteristics for the two C-7 specimens are illustrated in Figure 50.

Differences in symmetry between the two profiles can be noted with the strained specimen's profile skewed to one side of the interface. Depletion extends preferentially into the same grain as noted for carbide growth. Chromium minimums were measured at about 8 wt%

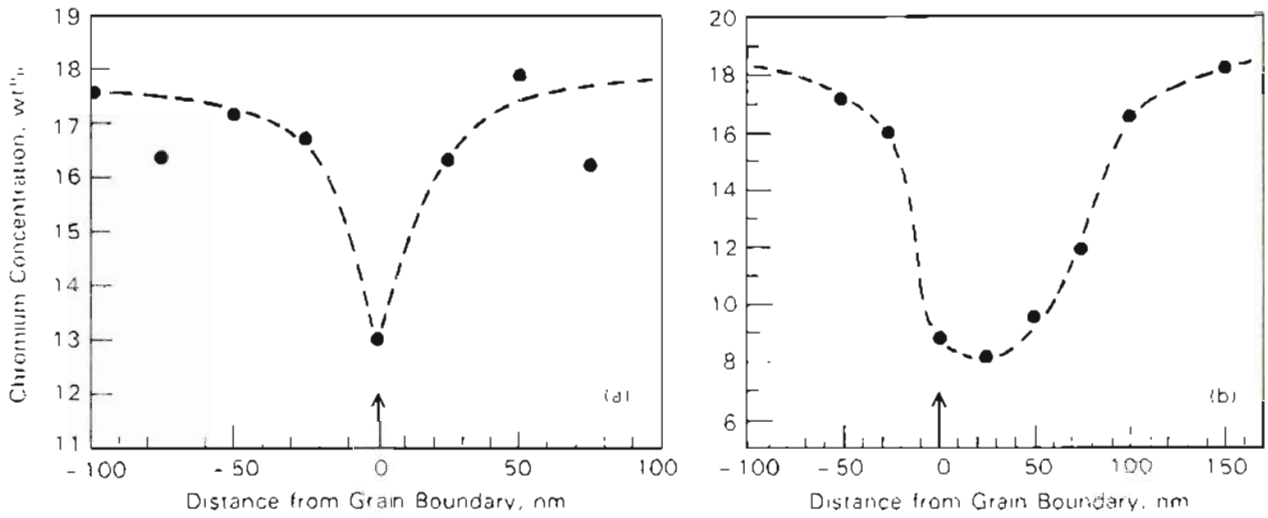

FIGURE 50. Grain Boundary Chromium Depletion Profiles in Unstrained (a) and Strained (b) C-7 Specimens After Cumulative Heat Treatment of 9 h at 600°C.

for the strained versus 13 wt% for the unstrained specimen. The measured minimum for the deformed stainless steel at 600°C is the lowest value found regardless of heat treatment. It is 2 wt% lower than ever observed for an isothermally heat treated specimen at 600°C and is even lower than that found in specimens heat treated at 480°C (see Table 2, Section 3.1).

The asymmetry in depletion profiles of strained specimens typically results in the minimum chromium concentration being measured some distance from the grain boundary. Minimum chromium was found about 20 to 30 μm from the interface as demonstrated for the C-7 specimen in Figure 50. Grain boundary migration appears to be a key in the accelerated sensitization kinetics. Deformation promotes migration at lower temperatures and directly influences chromium depletion width and DOS. The effect on chromium minimum concentration

due to deformation may be caused by changes in grain boundary or carbide interface thermodynamics. Research is needed to determine specific understanding of simultaneous deformation effects.

Additional simultaneous strain experiments were conducted on the C-6 stainless steel to determine the effect of deformation rate on sensitization development. Specimens were deformed at a rate of 1 and 3% strain per hour and compared to the 6% results. Sensitization kinetics scaled consistently with increasing deformation rate as shown in Figure 51. Data for all four isothermal control (unstrained) specimens are also plotted which gives some indication of data scatter for these measurements. After 9 h, EPR-DOS is about 7, 15, 23 and 35 for deformation rates of 0, 1, 3 and 6%/h. These differences in kinetics

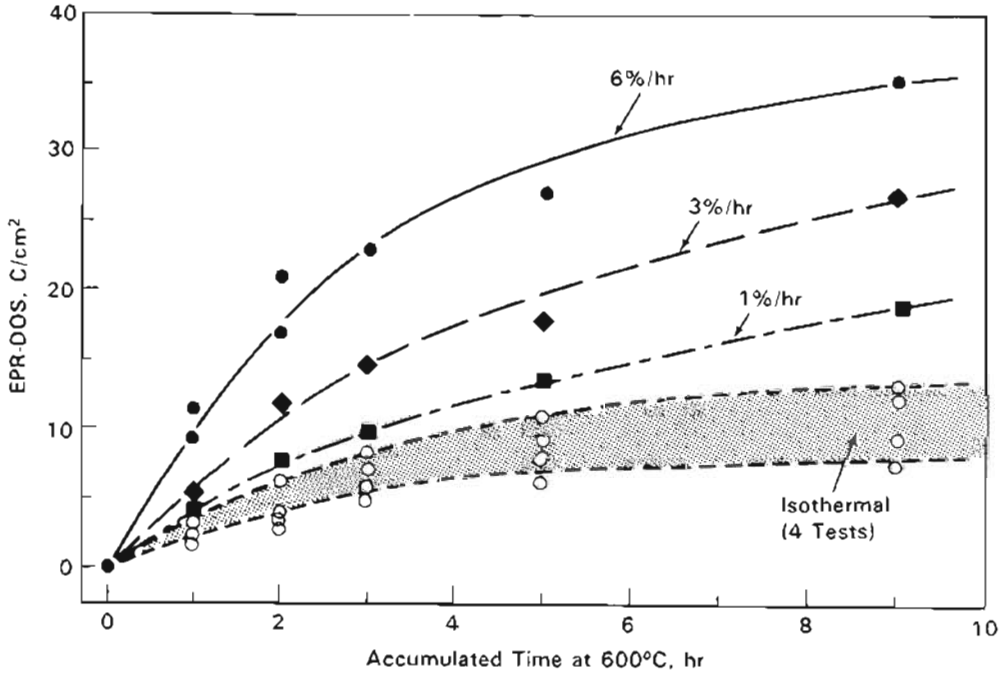

FIGURE 51. Simultaneous Deformation Rate Effects on Sensitization Development in Heat C-6 at 600°C.

with increasing deformation can be explained by dislocation pipe diffusion of chromium. If the effective chromium diffusivity is a function of the mobile dislocation density, then the rate that dislocations are created will control chromium diffusion which in turn controls carbide growth, depletion width and DOS. Modeling of deformation and dislocation pipe diffusion on sensitization development will be discussed in Section 5.2.5.

Deformation also accelerated sensitization development in Type 316 (Heat SS-16) stainless steel. Carbide nucleation and subsequent sensitization are slow at 600°C for the molybdenum containing heats. Simple isothermal heat treatments of 10 h or greater are needed before significant DOS is evolved as discussed in Section 4.2.2. Data for unstrained and strained specimens are presented in Figure 52(a) for the SS-16 heat. Without deformation, measurable EPR-DOS is not detected until an exposure of 30 h and only reaches a value slightly more than 5 C/cm^2 after 50 h at 600°C. These values are less than the isothermal response documented previously (Section 4.2.2, Figures 30 and 31) where EPR-DOS reached about 8 C/cm^2 after 10 h at 600°C. The simultaneously deformed specimen shows a measurable DOS at short times (~2 h) and increases to about 10 C/cm^2 after 5 h, 20 C/cm^2 after 10 h and 30 C/cm^2 after 13 h. These values are significantly larger than the control specimen reached in 50 h. Thus, simultaneous deformation has a similar effect in both Type 304 and 316 stainless steels.

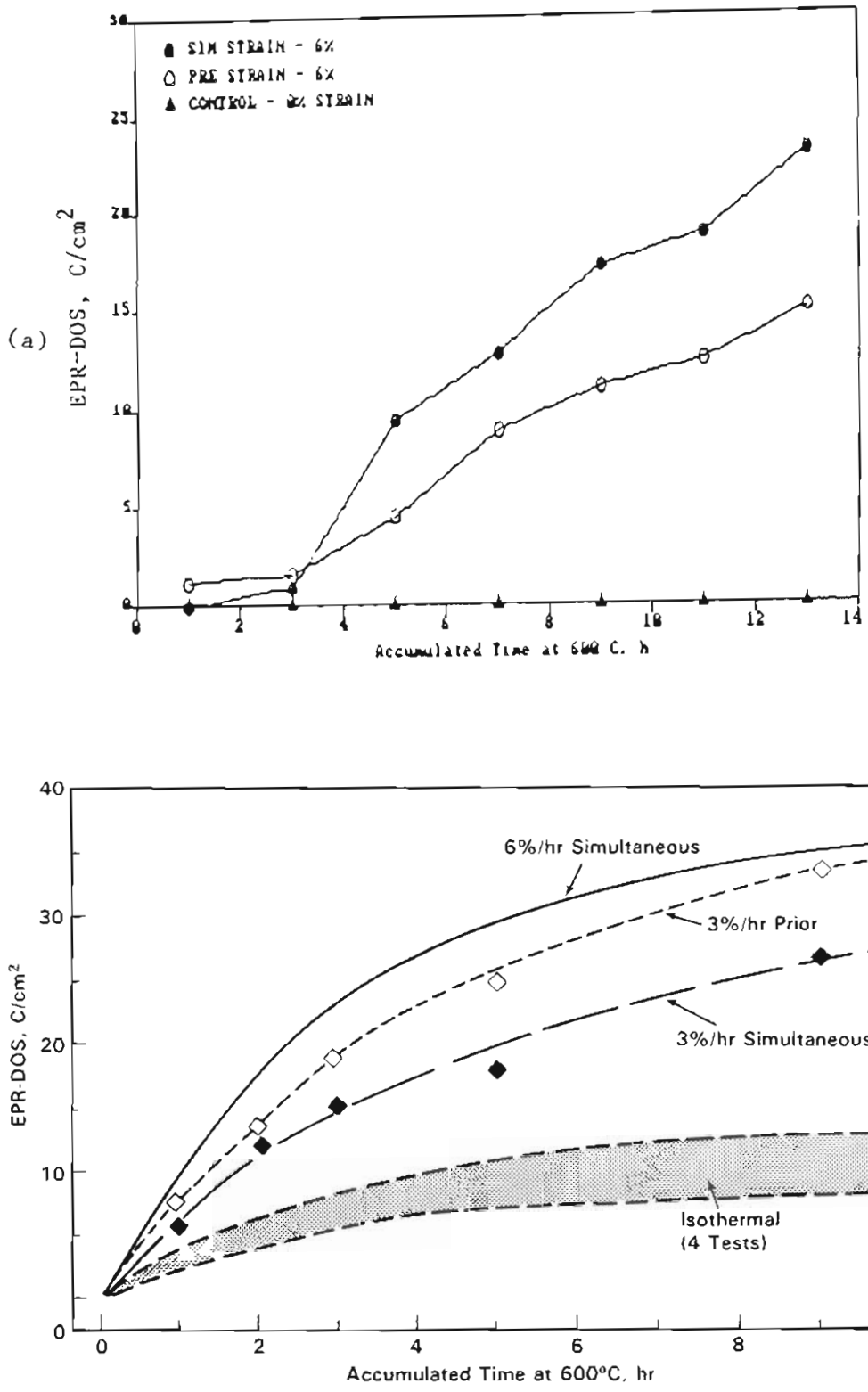

FIGURE 52. Comparison of Prior and Simultaneous Deformation Effects on Sensitization Development in Type 316 Heat SS-15 (a) and Type 304 Heat C-6 (b).

4.4.3 Prior Deformation Effects

To gain further insight into deformation effects on sensitization development, a few prior deformation experiments were performed. These tests followed the same pattern of cumulative isothermal heat treatments, but deformation was applied at room temperature before thermal treatment. Thus, dislocations are not being produced dynamically during aging, but are present before aging.

Prior deformation has a large effect on sensitization in both Type 316 and 304 heats as shown in Figures 52(a) and (b). EPR-DOS tracks quite well with simultaneous strain data exhibiting reduced times-to-sensitize and much larger DOS values with annealing time at 600°C. For the Type 316 case, the prior deformation specimen shows measurable DOS after only 1 h versus 3 h for the simultaneous specimen and about 30 h for the unstrained specimen. The simultaneously strained specimen does tend to promote slightly larger EPR-DOS as time at temperature is increased. This difference is not thought to be significant. The opposite behavior is demonstrated in Figure 50(b), comparing prior and simultaneous strain, for heat C-6. Prior deformation rates of 3% strain per hour resulted in larger EPR-DOS at all times.

Detailed conclusions cannot be made from these few comparisons, but do indicate that prior or simultaneous deformation promotes similar acceleration of sensitization kinetics. Chromium depletion characteristics were also examined for the Type 304 heat after 9 h at 600°C. Minimums were again lower than found for unstrained isothermal

exposures. However, minimums were still higher than for the simultaneously deformed specimens. Chromium concentrations were measured down to about 9.2 wt% for the prior deformation specimen versus 8 wt% for the simultaneous specimens. Profiles again were found to be slightly asymmetric after the cumulative prior deformation and heat treatment sequence. Total depletion zone widths were comparable for the two deformation conditions. It is not known whether differences in some profile characteristics are significant, thereby implying mechanistic differences in the effects of prior and simultaneous deformation on sensitization.

4.5 HEAT AFFECTED ZONE SENSITIZATION

Up to this point, controlled thermal and thermomechanical histories have been examined and sensitization development evaluated. The final data set which will be presented is for 61-cm-diameter, Schedule 80, Type 304 pipe weld. Welding was performed using mechanized gas tungsten arc system. Heat input ranged from 7 to 28 kJ/cm, but did not exceed 12 kJ/cm during the first 12 passes (35 total) where all sensitization development was observed.

The inside diameter of the pipe was instrumented with thermocouple and strain gages to monitor HAZ temperatures and deformations. Thermomechanical history measurements, analysis techniques and pass-by-pass data are reported in detail elsewhere.[7,141,142] Some of the temperature and strain histories measured in the HAZ for several of the early weld passes are used to model sensitization

development in Section 5.3.4. Because of this unique thermomechanical history characterization, EPR-DOS was mapped on the inner diameter surface as a function of distance from the weld centerline after each weld pass as long as DOS was changing.

The field-cell EPR technique with two different analysis areas was used to map HAZ DOS. Better spatial resolution was obtained employing a 0.1-cm by 0.6-cm rectangular mask. This enabled EPR-DOS to be measured in 0.1-cm steps across the HAZ. A second series of EPR measurement was also taken using a larger mask, 0.4 cm in diameter, to corroborate the small-area results. Preliminary measurements indicate that edge effects (due to the mask) could lead to higher EPR-DOS. Care was exercised with the small mask to ensure that preferential attack did not occur near or under edges of the mask. Repetitive measurements were within 30% for the small mask and 10-15% for the larger mask. Three tests were conducted at each location and averaged.

EPR-DOS measurements versus HAZ location is displayed in Figure 53 for both the mask sizes. Measurements were consistently larger for the small mask results reaching EPR-DOS values of about 28 C/cm^2, while the large mask results peaked at about 8 C/cm^2. A significant part of this difference is due to the better spatial resolution of the fine probe since it appears that DOS exhibits a maximum in the region 0.5 to 0.6 cm from the weld centerline. Such a localized maximum would not be reflected in the large probe which averages over a 4-cm dimension. Both probes document measurable sensitization after pass

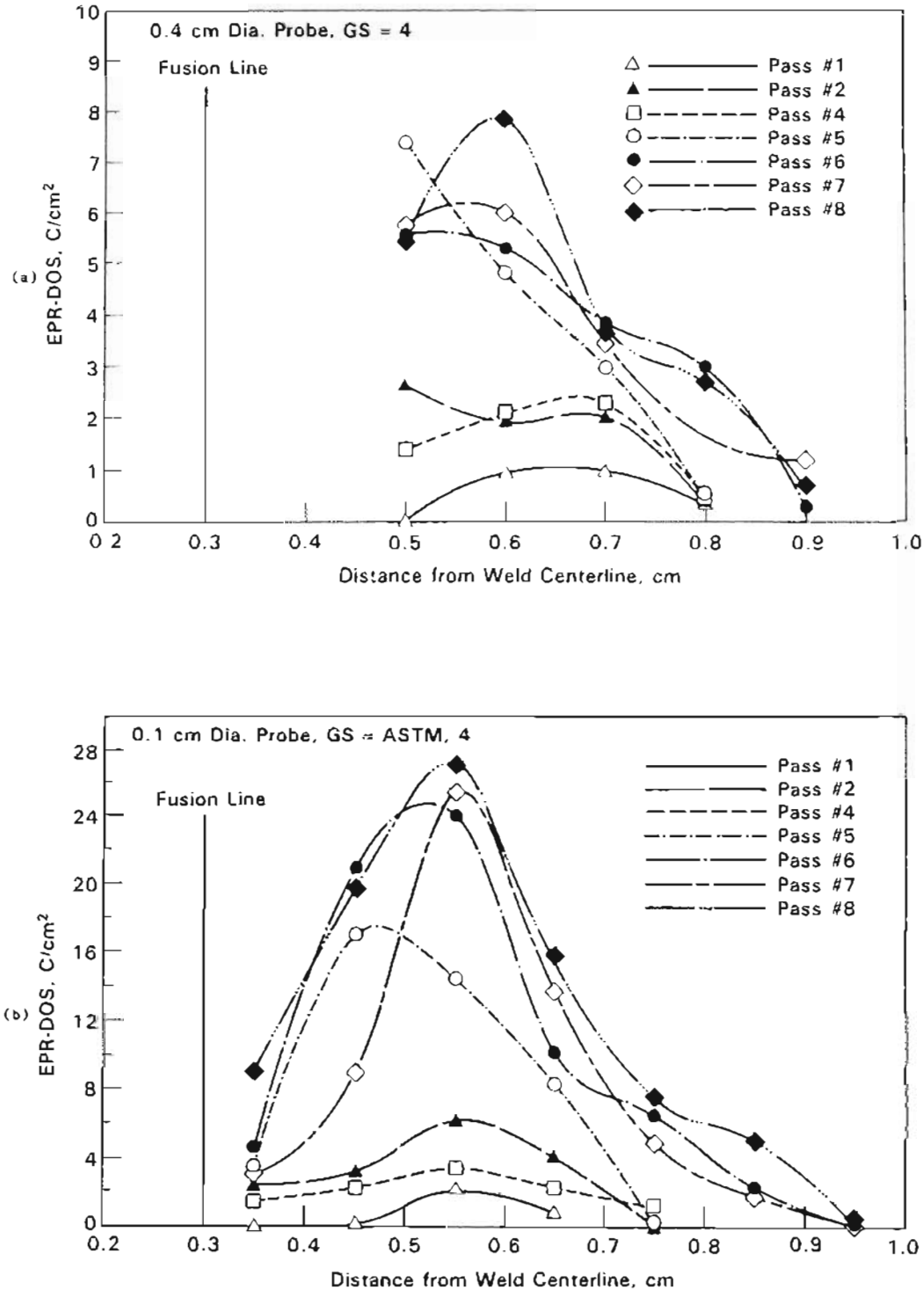

FIGURE 53. Measured HAZ Sensitization Development for a 24-in.-dia, Type 304 Pipe Weldment Using Either a Large-Area (a) or Small-Area (b) Mask and the Field-Cell EPR Test Technique.

one, small changes in EPR-DOS through pass four, a sharp increase after pass five and some additional increase in maximum DOS and width of the HAZ sensitized up to pass eight. No further increase in EPR-DOS was found after passes 9, 10, 12 and 35.

The consistency between the small and large probe measurements gives a high degree of confidence in the qualitative and some quantitative aspects of the HAZ sensitization data. Sensitization is confined to a region extending from the fusion line out about 0.6 cm. Within this 0.6-cm region, a much more localized area about 0.1 to 0.2 cm in width is highly sensitized as measured by the EPR test. This distribution in DOS across a HAZ agrees with other weldment sensitization[114,121,143,144] and typical location of IGSCC cracks in BWR piping.

Sensitization development only during the initial eight passes was consistent with HAZ temperatures which reach high levels (>800°C) during passes 1-5, moderate levels (>600°C) during passes 6-8, but drop below 500°C after pass 8. Thus, no increase in DOS would be expected after pass 8 with most developing during the first 5 passes. The EPR-DOS data suggests that carbide nucleation and early growth (with low DOS) occur through pass 4 which converts to significant DOS levels during the thermomechanical exposures in passes 5 and 6. Correlations between measured thermomechanical histories and EPR-DOS in the HAZ will be discussed in greater detail in Section 5.3.4.

5.0 QUANTITATIVE MODELING OF SENSITIZATION

A model for the prediction of material DOS as a function of bulk composition, initial condition and thermomechanical history has been developed. Detailed aspects of the model, SSDOS, will be presented and quantitatively evaluated in this section by comparison to the data base documented in Section 4.0 and Appendix B. Basic methodology of SSDOS is shown in Figure 54. Components include determination of the chromium concentration at the carbide-matrix interface based on the thermodynamics of carbide formation, depletion characteristics based on the effective chromium diffusivity, and an empirical correlation

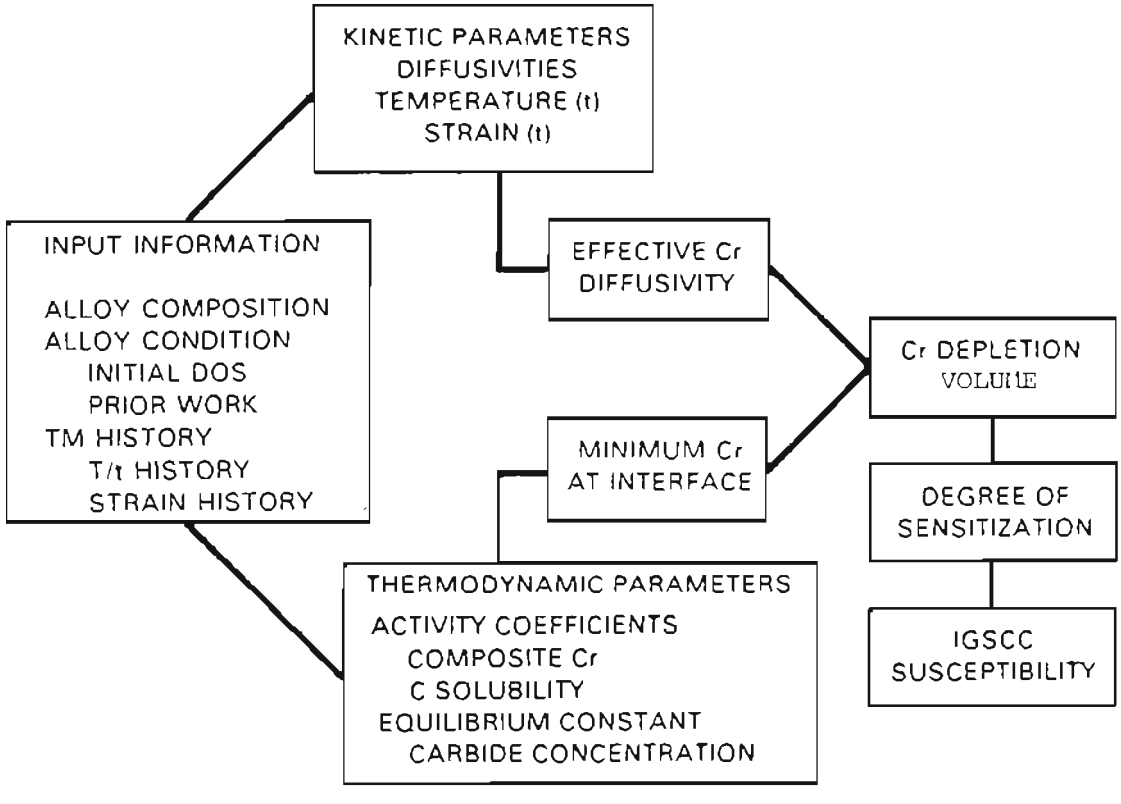

FIGURE 54. Flow Diagram Illustrating DOS Prediction Approach.

between chromium depletion and DOS as measured by the EPR test. Empirically based modifications are present in several facets of the model and will be discussed in the following sections.

The DOS predictive model is written in BASIC to run on a personal computer. SSDOS requires input of material composition (C, Cr, Ni, Mo, and N) and condition (mill-annealed, solution-annealed or cold-worked), details of which are obtained by an interactive questioning sequence. Information concerning the thermal or thermomechanical exposure to be evaluated is also set up in this format. Predictions are output in tabular form listing both chromium depletion characteristics and EPR-DOS.

5.1 DESCRIPTION OF MODEL COMPONENTS

As indicated in Figure 54, sensitization prediction deals with the thermodynamics and kinetics of chromium carbide precipitation and growth. Thermodynamics primarily depends on temperature and material composition, while kinetics is governed by temperature, composition and condition. Kinetic effects tend to be more complex since carbide nucleation, depletion zone formation and desensitization must be considered. Theoretical basis for several of the most important model components will be described in this section along with modifications evolved from data base comparisons. Critical equations used in the SSDOS program will be identified and empirical modifications justified.

The SSDOS predictive model has been developed and validated for Type 304 and 316 alloys. As a result, there are specific assumptions and limitations that are inherent in its make-up and application. Several aspects worth noting for the model are:

1. Only second phase that forms is $M_{23}C_6$ carbide,
2. Carbides precipitate only at grain boundaries,
3. Local equilibrium conditions exist at carbide-matrix interfaces and at grain boundaries due to rapid grain boundary diffusion,
4. Carbon activity is effectively uniform through the grain due to its rapid diffusivity,
5. Alloy composition is within certain limits comparable to that for Types 304 and 316 stainless steel, i.e., carbon - 0.01 to 0.08 wt%, chromium - 16 to 20 wt%, nickel - 8 to 14 wt% and molybdenum - 0 to 3 wt%.

5.1.1 Carbide Thermodynamics - Interfacial Depletion

General aspects of $M_{23}C_6$ carbide precipitation thermodynamics were reviewed in Section 2.3.2, equations 7, 8 and 9. Interfacial chromium concentration in equilibrium with the carbide was shown to be equal to:

$$X_{Cr} = (1/K)^{1/23} \ (\gamma_{Cr}) \ (\gamma_C \ X_C)^{6/23} \qquad (9)$$

Derivation of this equation required the assumption that $M_{23}C_6$ carbides are essentially $Cr_{23}C_6$. For the Type 304 alloys this simplification is justified, but leads to problems in Type 316 alloys due to the presence of molybdenum. Complex analysis is required to theoretically model the 5-element system which prompts the creation of a number of unknown interaction parameters. While interpolations of many of these parameters can be made, a much simpler approach has been adopted in SSDOS.

Molybdenum effects sensitization development in stainless steels in a manner similar to chromium. Both incorporate into the $M_{23}C_6$ carbide, become depleted during carbide growth and increase the passive nature of the corrosion product film. It is therefore proposed that an effective bulk chromium concentration can be used which integrates molybdenum and chromium effects. Fullman[51] calculated such an equivalency based on an equal carbide-matrix interfacial chromium concentration. This enables an effective chromium concentration ($Cr^{\bullet}$) to be defined as

$$Cr^{\bullet} = Cr + 0.35\ Mo \qquad (27)$$

where Cr and Mo represent the bulk molybdenum and chromium concentration. Incorporating molybdenum into $Cr^{\bullet}$ greatly simplifies evaluation of Type 316 alloys. $Cr^{\bullet}$ directly influences carbon and chromium activities and the interfacial chromium level.

Composition effects on sensitization stem (for the most part) from their effects on carbon activity and therefore on the interfacial

chromium concentration. This was illustrated in Figure 2 (Section 2.3.2) from the predictions of Tedmon.[50] The carbon activity coefficient (γ_c) embodies these effects and can be determined using the approach of Wagner[49] and of Natesan and Kassner.[25] Simplifying and plugging in the appropriate constants allows γ_c to be determined in terms of temperature (T) and bulk composition (C, Cr*, and Ni):

$$\ln \gamma_c = -1.845 + 5100/T + \left(C * (11.92 - 6330/T)\right) - \left(Ni * (2.2 - 7600/T)\right) + \left(Cr^* * (24.4 - 38400/T)\right) - \left(Cr^{*2} - (96.8 - 84800/T)\right) \quad (28)$$

Since the interfacial carbon content (X_c) is assumed equal to C, only the equilibrium constant K and γ_{cr} need to be determined to find X_{cr}. K can be calculated from equation 7 by setting the free energy of formation for the carbide (172) as:

$$\Delta G = -98280 - 9.2 * T \quad (29)$$

The final parameter that must be defined is γ_{cr}. Empirical and theoretical approaches have been used to determine this term without a great deal of proven success. Predictions of Tedmon,[50] Stawstrom and Hillert[57] and Fullman[51] are plotted in Figure 55 versus the measured chromium minimums on high-carbon Type 304 stainless steel. Measurements obtained by analytical techniques represent maximum

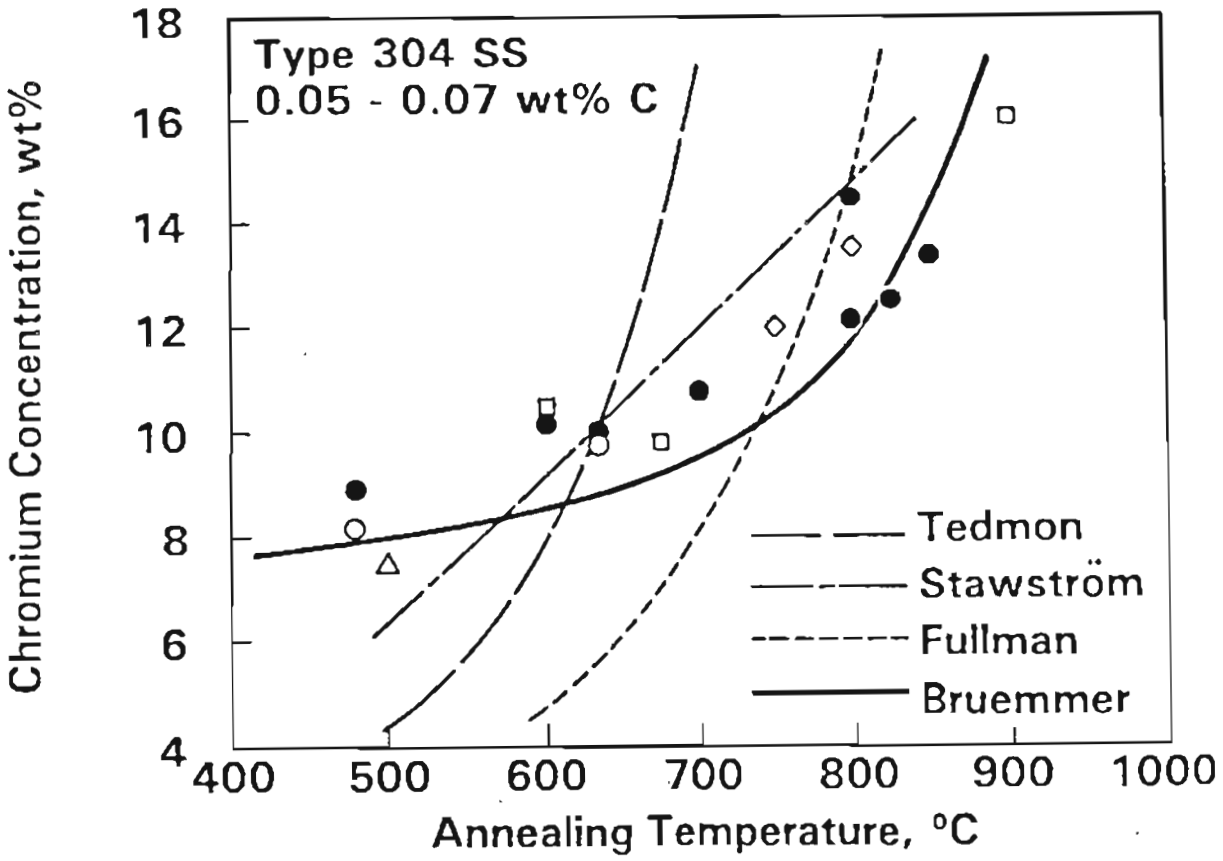

FIGURE 55. Comparison of Measured and Predicted Minimum Interfacial Chromium Concentrations as a Function of Heat Treatment Temperature.

values due to technique limitations and to the fact that desensitization is occurring, thereby raising X_{Cr}. Thus, predictions should consistently be less than measurements at all temperatures. Filled data points are from the STEM-EDS work presented in Section 3.1 and open points are from the literature. Each of the three approaches shown by the dashed lines overpredicts measurements at high temperatures (>700°C) and underpredicts at low temperatures (<600°C). Agreement is

obtained between measurement and prediction only over a very narrow temperature range. Therefore, it is not surprising that overall predictive capabilities have been poor.

To overcome this significant limitation, an empirical correlation was developed between interfacial chromium concentration and chromium activity. This relationship defines the activity coefficient from direct measurements of chromium depletion. As might be expected from the mismatch between measurement and prediction in Figure 55, γ_{Cr} is a complex function of temperature. An indication of this complexity is illustrated in Figure 56 for a high-carbon Type 304 stainless steel. The magnitude of γ_{Cr} goes through a maximum at about 750°C and sharply decreases as temperatures increase above 800°C. Below 700°C, γ_{Cr} drops more gradually reaching a value of about 50% of the maximum at 450°C.

Defining γ_{Cr} by direct measurement of chromium depletion gives a good correlation between predicted and measured interfacial chromium concentrations in Figure 55. Agreement can be seen even at the high and low temperatures due to the functional relationship demonstrated in Figure 56. The equation obtained by polynomial regression for γ_{Cr} is:

$$\gamma_{Cr} = 10.55 - (94.84 * T') + (282.9 * T'^{2}) - (242.8 * T'^{3}) \quad (30)$$

where T' = T/2000 for Type 304 and T' = (T-30)/2000 for Type 316 stainless steel and T is temperature in °K. This equation holds over the practical sensitization temperature range, 500 to 850°C, and

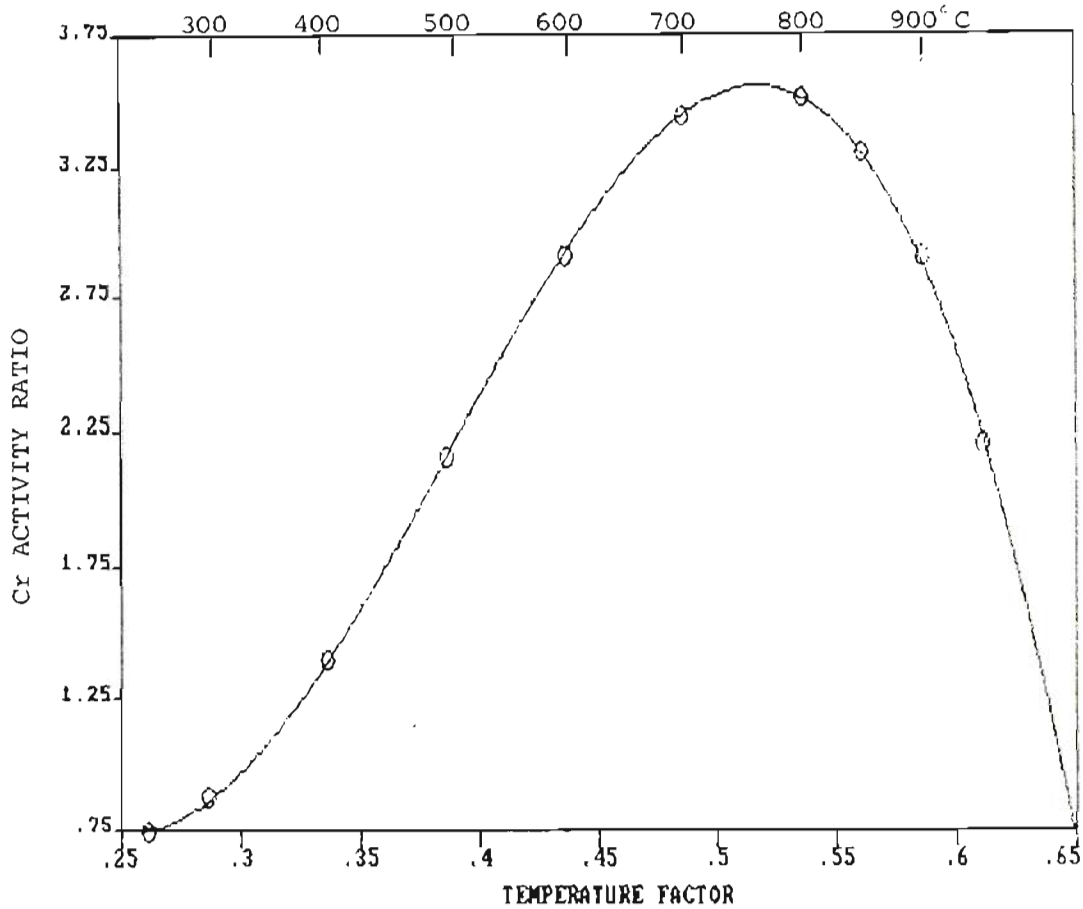

FIGURE 56. Functional Relationship Between Chromium Activity Coefficient and Temperature Based on Direct Measurements of Chromium Depletion.

appears to give reasonable predictions at temperatures as low as 300°C and as high as 950°C. However, data is not available to validate such an extrapolation.

Agreement between prediction and measurement in Figure 55 does not indicate any general applicability of equation 31. In order to assess predictive capability, interfacial chromium minimum measurements from many additional heats including Type 304, 316, 304N, 316L and 316LN were compared to SSDOS prediction. This data is summarized

in Figure 57(a). The line in the figure represents a one-to-one fit between prediction and measurement. Data points should consistently be at or below this line due to measurement limitations noted earlier. Data for the Type 304 heats follow this trend, but several Type 316 heats show predicted values greater than that measured. Several of these points are for Type 316LN heats examined in the current work and elsewhere.[36]

From a practical point of view, interfacial concentration of both chromium and molybdenum are important to corrosion and SCC resistance. Therefore, it is the combined concentration that is needed to predict environmental response. Molybdenum effects have been factored into chromium depletion prediction through the use of $Cr^{\bullet}$, but no attempt is made to predict molybdenum depletion. Such depletion does occur in a similar fashion as that for chromium with concentrations often dropping to about 1 wt%. Unfortunately, few measurements of molybdenum depletion have been documented. If a fractional depletion of molybdenum is assumed to be equal to that for chromium, data in Figure 57(a) can be replotted in 57(b) comparing predictions to the combined interfacial chromium plus molybdenum concentration. All points now fall on or below the one-to-one fit in agreement with the Type 304 data.

Another way to assess the capability of SSDOS to predict interfacial minimums is by comparison to the EPR data base. It was found in Section 3.2.3 and demonstrated in Figure 16 that as the interfacial chromium concentration increases above about 13 wt%, EPR-DOS drops to

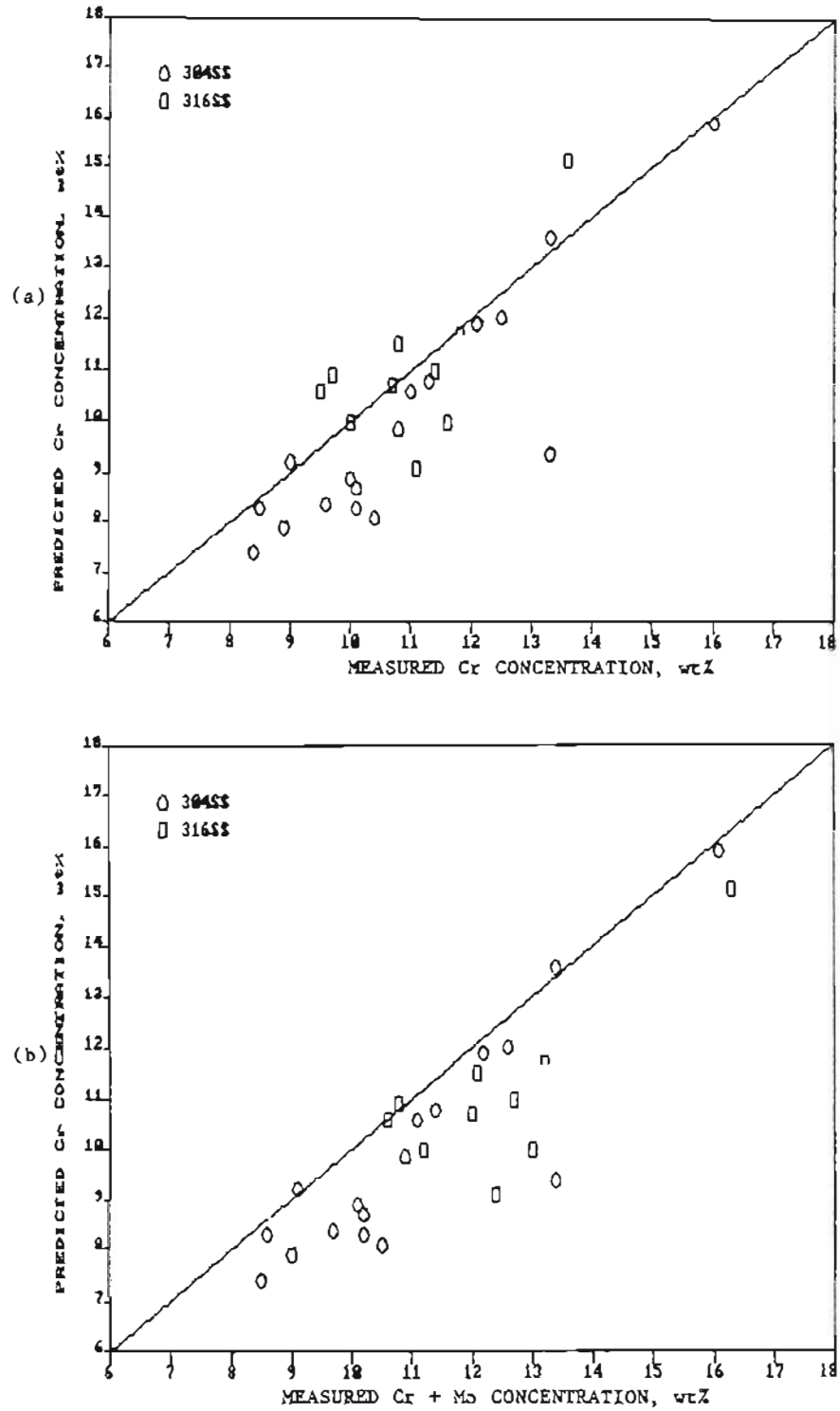

FIGURE 57. Comparison of Measured and Predicted Interfacial Chromium (a) and Chromium Plus Molybdenum (b) Minimum Concentrations in Stainless Steels.

zero. This behavior allows EPR data to be used to estimate the critical temperature where minimums become greater than 13 wt% since it is the maximum temperature where EPR-DOS is observed. For many of the heats discussed in Section 4.2, this critical temperature could be determined within 25°C and is shown in Figure 58 as a function of bulk carbon content. Critical temperatures increase with bulk carbon reflecting carbon solubility for both the Type 304 (58a) and 316 (58b) heats. SSDOS model predictions for an interfacial chromium minimum of 13 and 14 wt% are also presented. The 13 wt% prediction is in excellent agreement with the EPR data. Type 316LN heats show some scatter at the low end of the data in Figure 58(b) due to the high bulk nitrogen levels. Nitrogen additions were not considered for SSDOS predictions.

Comparisons in Figures 55, 57 and 58 indicate SSDOS predictions of interfacial chromium concentrations are a marked improvement over prior capabilities. More importantly, they quantitatively approach actual chromium levels. Minimums are accurately predicted for heats with variable composition and over a wide range of heat treatment temperatures. This capability is an essential first step to develop the overall quantitative sensitization (and IGSCC) prediction model.

Bulk composition changes within the typical stainless steel specifications are taken into account by their influence on carbon and/or chromium activities. Therefore, varying a primary alloying element impacts the resultant interfacial chromium concentration and DOS. Carbon has the most significant effect on depletion with

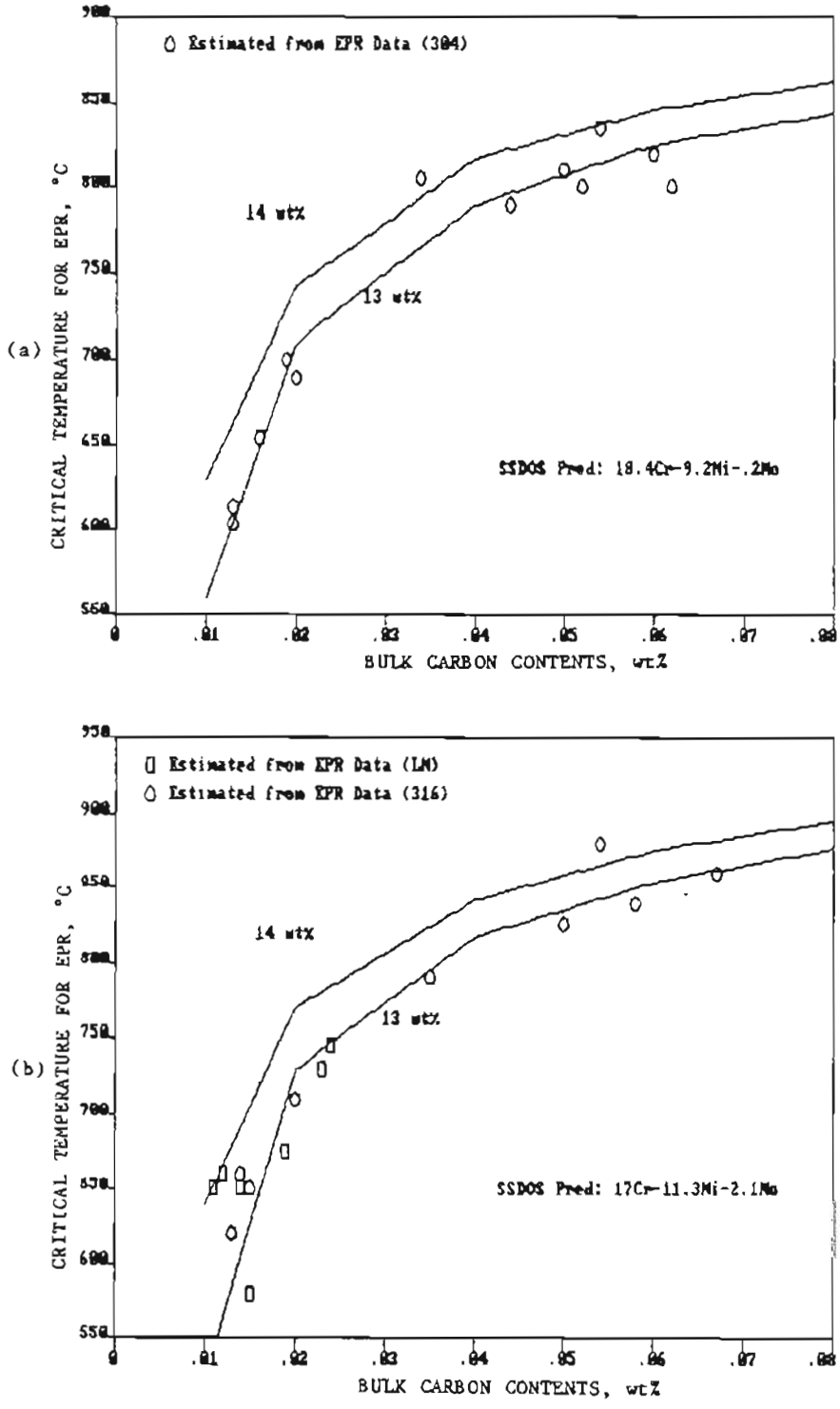

FIGURE 58. Maximum Temperature for Sensitization as a Function of Bulk Carbon Content for Type 304 (a) and 316 (b) Heats. SSDOS model predictions are shown for chromium minimums of 13 and 14 wt%.

interfacial minimums dropping sharply with increasing carbon concentration. This behavior was indicated by the data and predictions in Figure 58 and is better illustrated in Figure 59. SSDOS predictions show minimum chromium levels decreasing with increasing carbon or nickel content, while the converse occurs with increasing bulk chromium or molybdenum. Interfacial chromium concentrations can vary

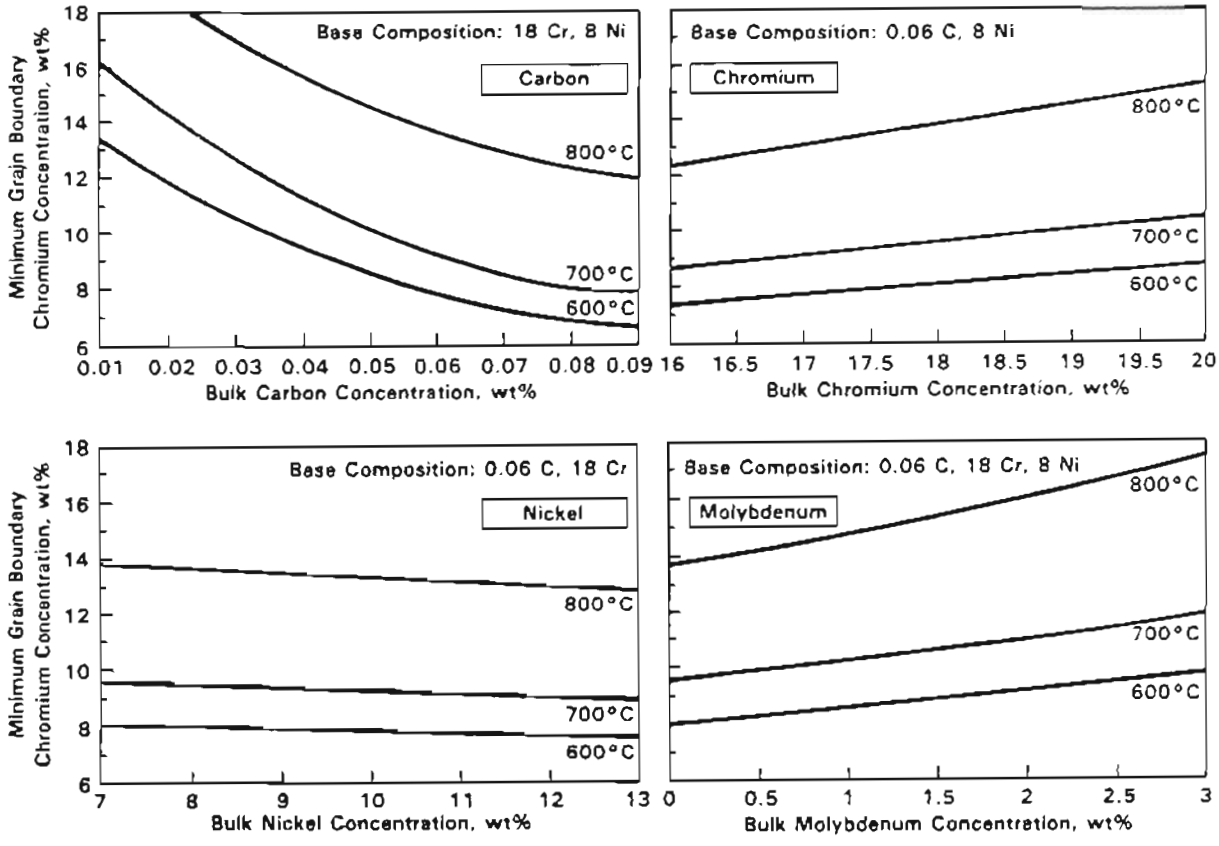

FIGURE 59. SSDOS Model Predictions Illustrating Bulk Composition Effects on Interfacial Chromium Concentrations in a Stainless Steel.

from 16 to 8% at 700°C when comparing an extra-low- to a high-carbon Type 304. Other alloying elements have a much smaller effect, changing the interfacial chromium by only 1 or 2% over the possible bulk composition range.

One additional element modifies interfacial chromium predictions, i.e., nitrogen. Nitrogen has been shown by many researchers to retard sensitization development when present in moderate (0.06 to 0.16 wt%) amounts.[16,36-38] This appears to be potentially important for the Type 316NG material with extra-low carbon contents. In order to account for these effects, nitrogen additions greater than 0.04 wt% modify the carbon content used to determine the carbon activity coefficient in equation 28. The effective carbon content (C^*) decreases slightly with bulk nitrogen up to about 0.12 wt%, then increases. Nitrogen additions greater than about 0.2 wt% result in $C^* > C$ and predicted sensitization increases with increasing bulk nitrogen. SSDOS predictions of nitrogen effects will be demonstrated and compared to experimental data in Section 5.2.

5.1.2 Carbide Nucleation Kinetics

The approach of Grobner[61] as adapted by Logan[60] has been used to predict $M_{23}C_6$ precipitation kinetics in SSDOS. Nucleation time (t_N) is calculated by taking the inverse of the rate equation described in Section 2.3.3 (Equation #14):

$$t_N = \frac{1}{C} \exp\left(\frac{Q_D + F}{RT}\right) \qquad (31)$$

Critical terms in this equation are Q_D, the activation energy for diffusion of the rate limiting element, and F, the energy necessary to form a stable nucleus. Logan assigned Q_D based on the shape of the time-temperature-nucleation curve, which turned out to be much greater than the activation energy for carbon diffusion and less than that for chromium diffusion. It seems likely that chromium diffusivity either along grain boundaries or through the matrix will be rate limiting. Therefore, since the self-calibration approach of Logan is not practical for a general model, both diffusivities were evaluated by comparison to the literature data base. Lattice diffusivities were found to give the most consistent results if the appropriate relationships for the free energy terms are used as described below.

Two energy components make up the second critical term in equation 31. The magnitude of F depends on the free energy change due to the carbide formation (F_c) and the energy needed to create the new surface area (F_s). Following Logan, stable growth occurs when the nucleus reaches a size where:

$$F = \frac{4}{27}\frac{F_s^3}{F_c} \qquad (32)$$

For $M_{23}C_6$ precipitation in Types 304 and 316, it has been assumed that F_s is constant and F_c is a function of temperature and material composition (i.e., C, Cr and Mo).

The parameters described have been optimized by comparison to literature data on nucleation kinetics for Type 304 and 316 stainless

steels. Nine sets of nucleation or at least early precipitation data were found for $M_{23}C_6$ carbides. Examples of measured versus predicted time-temperature nucleation curves are presented in Figure 60. Careful examination of the experimental data shows a significant scatter in most cases. Predicted curves agree quite well with measured nucleation times. Largest differences are near the nose of the curve where nucleation times are extremely small (minutes or less).

Overall predictive capability is assessed by summarizing all experimental data and predictions in Figure 61. Most points relating predicted and measured nucleation times fall close to the line representing a one-to-one fit. About 100 nucleation times are compared from more than 20 heats including Type 304, 304L, 304N, 304LN, 316 and 316LN. The agreement demonstrated in Figure 61 gives confidence that reasonable estimates for nucleation times are being predicted by SSDOS.

Bulk composition has a significant effect on $M_{23}C_6$ nucleation kinetics. Carbon again has the dominant effect, shifting the nose of the time-temperature-nucleation curve to lower temperatures and to longer times with decreasing carbon content. This behavior is illustrated in Figure 62 for Type 304 and 316 stainless steel. Nucleation times become increasingly important for sensitization prediction as heat treatment temperatures drop below about 600°C. Differences between Type 304 and 316 can be seen by comparing Figures 62(a) and (b). Note that time scales for the two plots are not the same.

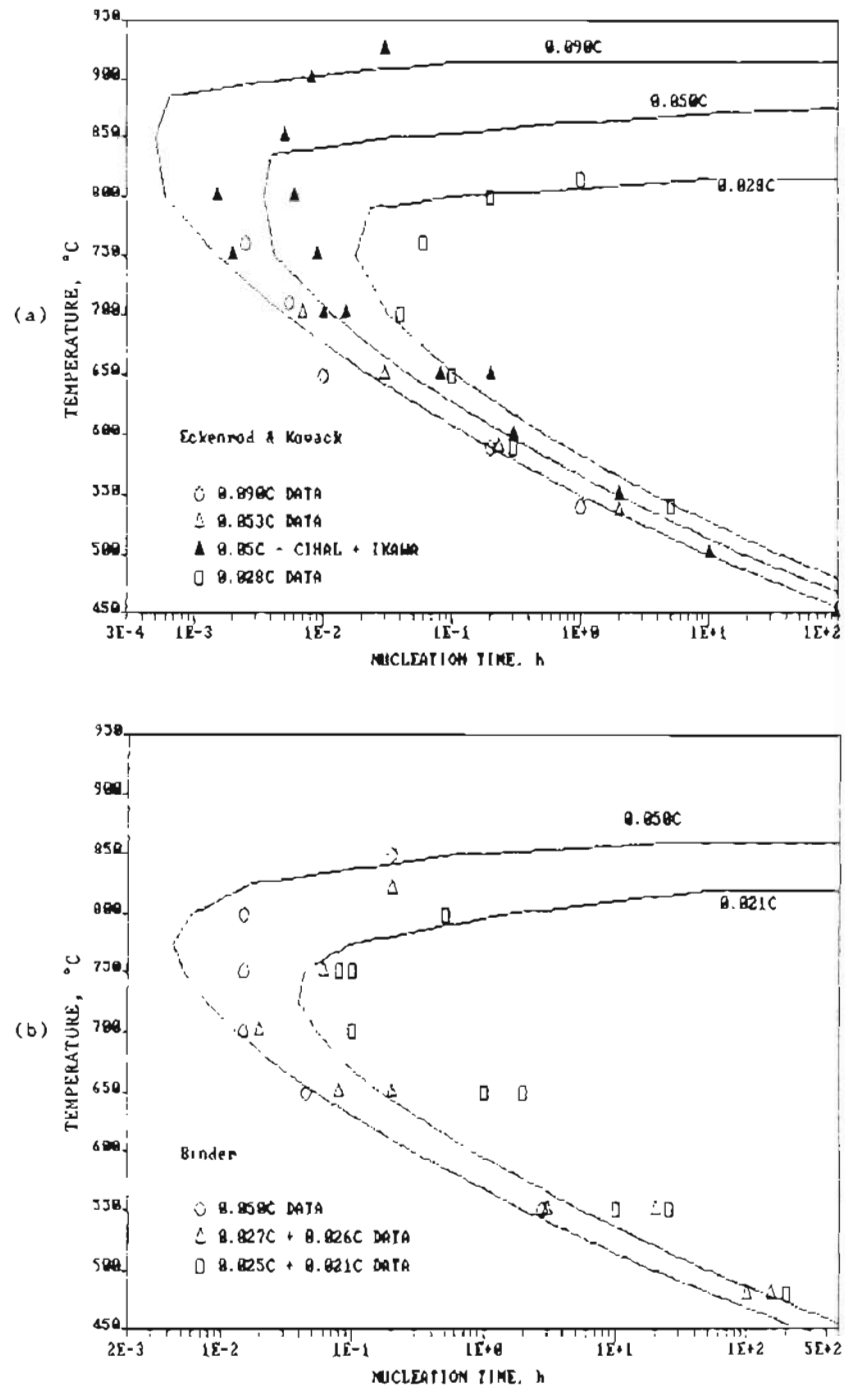

FIGURE 60. Comparison of Measured and Predicted Nucleation Times for Type 304 (a, b and c) and 316 (d) Stainless Steels.

(c)

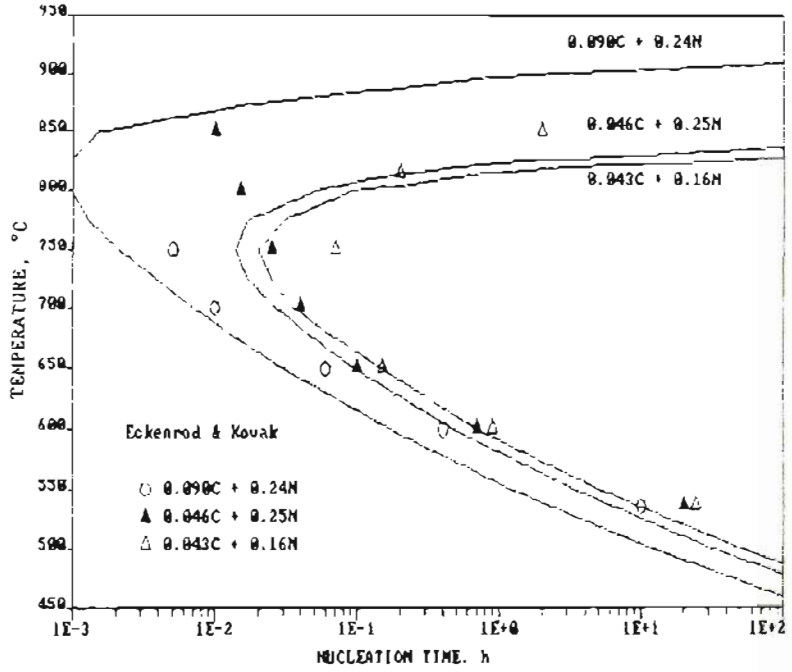

(d)

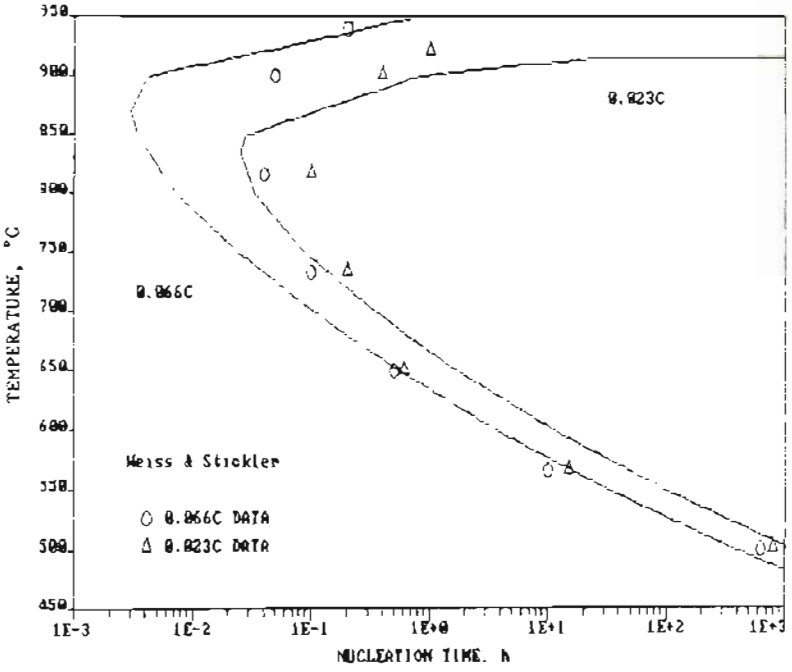

FIGURE 60. (contd)

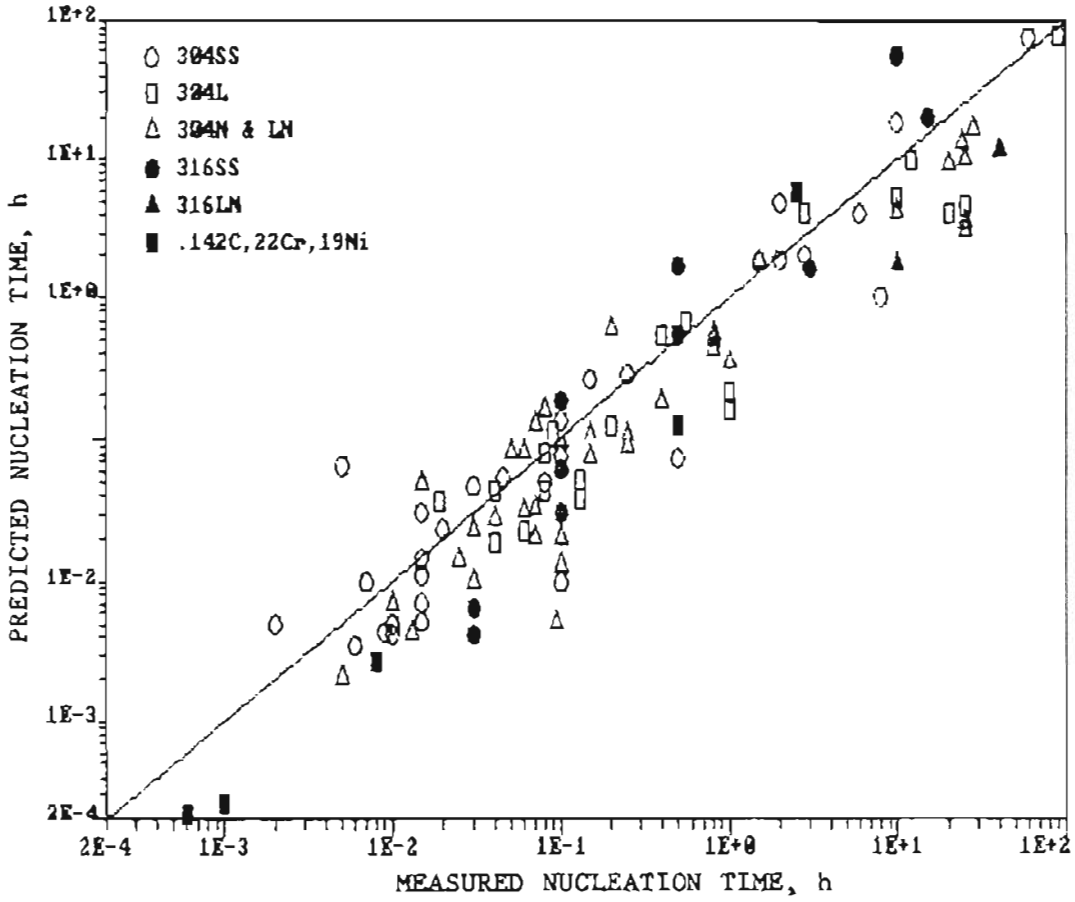

FIGURE 61. Summary of Measured and Predicted Nucleation Times for Various Type 304 and 316 Heats.

Molybdenum addition in the Type 316 pushes the nose of the curve to higher temperatures and to longer times. Nucleation times can be much longer for Type 316 (e.g., about 100 versus 1 h at 550°C) primarily due to the slower chromium diffusivity and more negative activation energy for diffusion.

5.1.3 Chromium Depletion Kinetics

Once carbide nucleation has occurred and the grain boundary has equilibrated itself with the carbide-matrix interface, depletion of

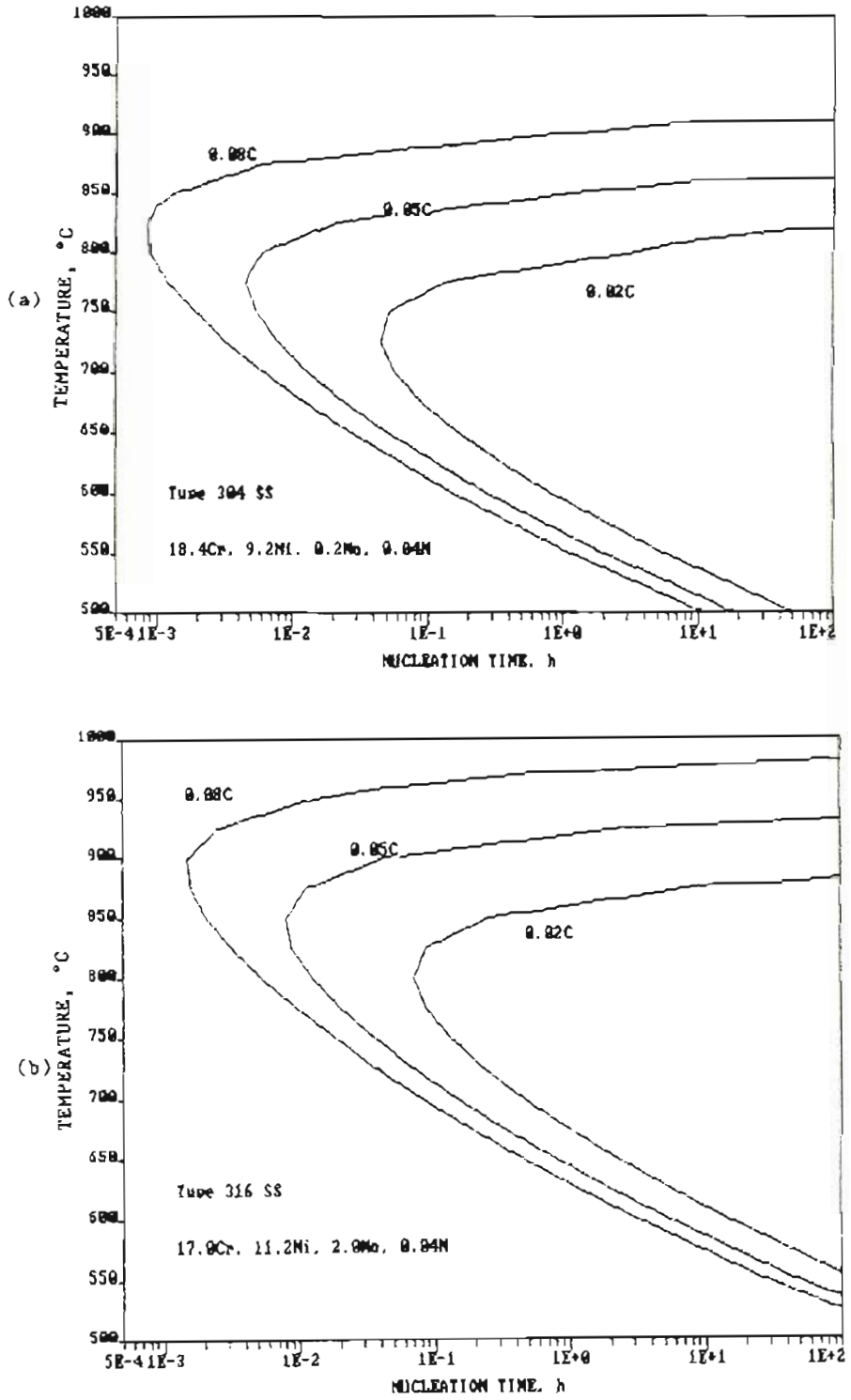

FIGURE 62. Carbon Effects on $M_{23}C_6$ Nucleation Kinetics for Type 304 (a) and 316 (b) Stainless Steel.

the adjoining matrix begins. Kinetics of this process were modeled by Stawstrom and Hillert[66] considering a one-dimensional diffusion problem. The basic equation for the development of the chromium depleted zone was described in Section 2.3.3. Depletion width (W'_{Cr}) was shown to depend on both the interfacial chromium concentration in equilibrium with the growing carbide (X'_{Cr} and the chromium diffusivity (D_{Cr}):

$$W'_{Cr} = 2\sqrt{D_{Cr}\, t}\ \frac{X'_{Cr} - X_{Cr}}{Cr - X_{Cr}} \qquad (16)$$

Direct measurements of chromium depletion reported in Section 3.1.2 can be compared to SSDOS predictions. Depletion widths as a function of heat treatment for heats C-6 (Type 304) and C-10 (Type 316) were listed in Table 2. Although the data is limited, comparisons can be made relative to SSDOS predictions for several temperatures as shown in Figure 63. SSDOS tends to slightly overpredict depletion widths for the Type 304 heat, but is very close for the Type 316 heat. Considering the many problems determining statistically relevant information from the STEM-EDS measurements, this agreement is quite good. Temperatures from 600 to 900°C are included in Figure 63 and demonstrate that predictions are representative at each temperature.

The correlation between predicted and measured depletion widths is summarized in Figure 64. Additional Type 304 and 316 heats and heat treatments are plotted to lend credibility to the comparison. A

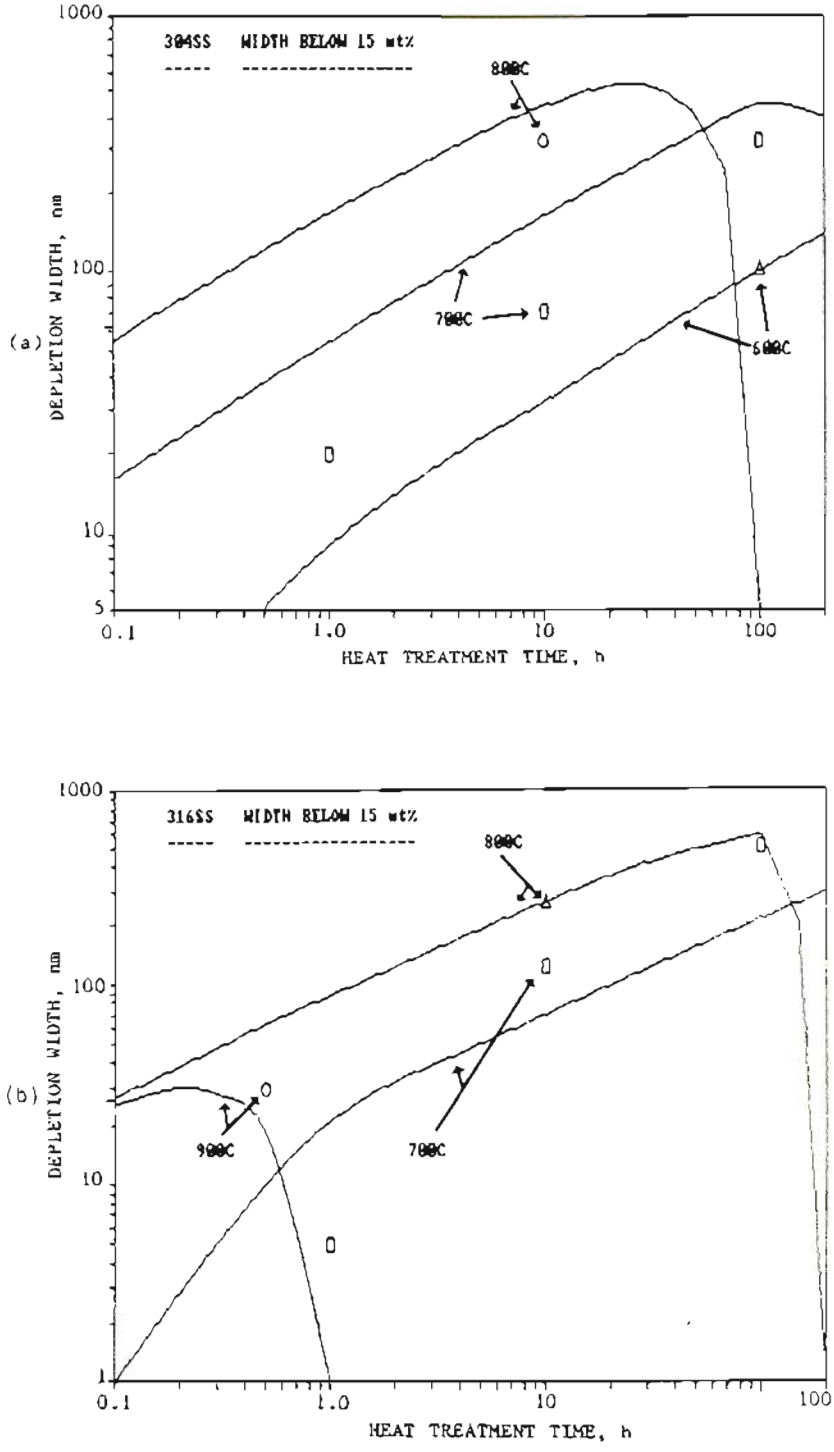

FIGURE 63. Comparisons of Measured and Predicted Chromium Depletion Widths for Type 304 - Heat C-6 (a) and for Type 316 - Heat C-10 (b).

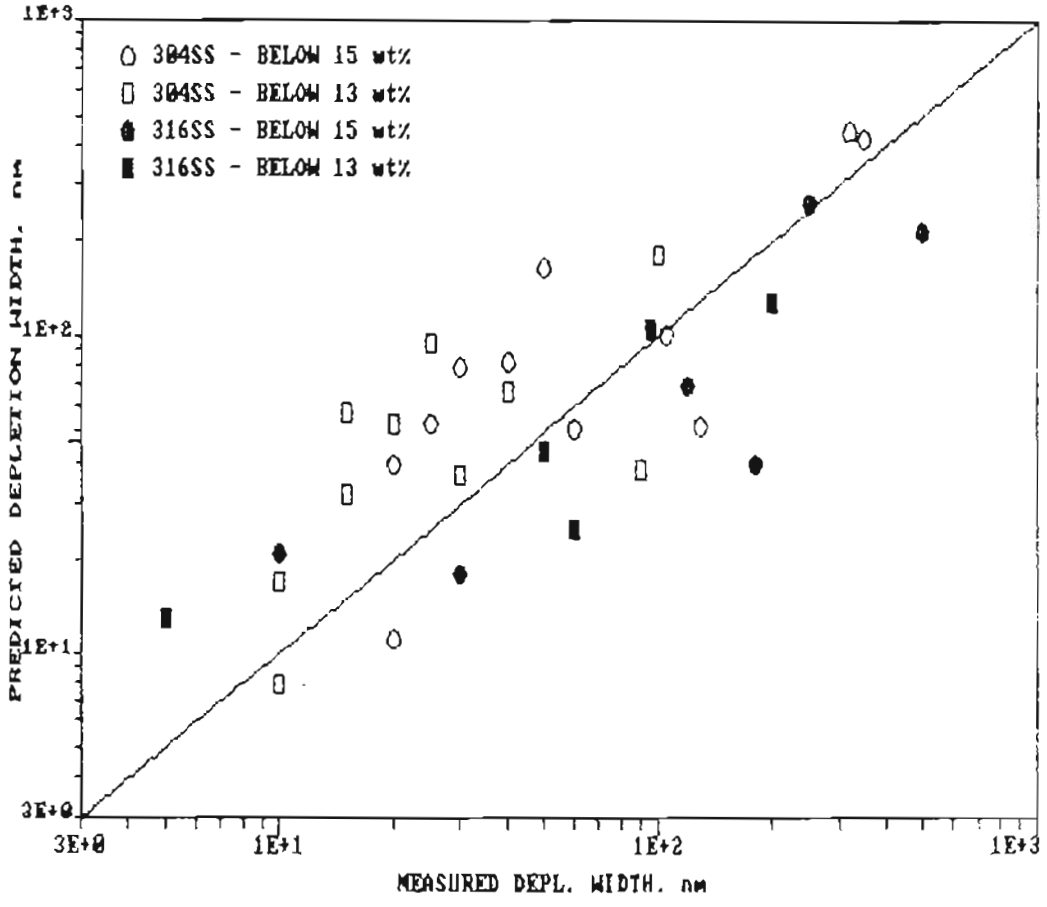

FIGURE 64. Summary of Measured Versus Predicted Data for Chromium Depletion Widths Below 13 and 15 wt%.

significant scatter exists around the one-to-one fit line drawn on the graph, but indicates a reasonable correlation between prediction and measurement. It does appear that the Type 304 data is slightly over-predicted and the Type 316, slightly underpredicted. However, it is not possible to make definite conclusions based on the depletion width data due to its basic nature. Limitations and variability in the width measurements were discussed in Sections 3.1.2 and 3.2.3.

Primary assessments of SSDOS capabilities to predict sensitization kinetics were conducted using the extensive EPR data base

presented in Section 4.0. SSDOS predictions of chromium depletion are converted into EPR-DOS values by equations 24 and 26. Thus, model capabilities can be examined versus a large data base. Predictions of sensitization development after various thermal and thermomechanical treatments will be compared to the EPR data base in Section 5.2.

5.1.4 Desensitization Kinetics

A critical aspect of sensitization development is the change in grain boundary chromium minimum concentration with heat treatment time. As carbide growth and depletion proceeds, carbon is removed from the bulk, thereby decreasing carbon activity and increasing interfacial chromium. This process, called desensitization or self-healing, begins during the early stages of precipitate growth and eventually eliminates the region of chromium depletion. Many examples of desensitization were observed during high-temperature isothermal sensitization experiments described in Section 4.1.

Stawstrom and Hillert[57] proposed a simple relationship to estimate the time-to-desensitize (t_{DS}):

$$t_{DS} = \left(\frac{GS \cdot C}{Cr - \bar{X}'_{Cr}}\right)^2 / D_{Cr} \qquad (33)$$

where GS is the grain size and all other variables have been defined previously. This approach often approximates the shape of the time-temperature-desensitization curve, but rarely predicts the right magnitude. Examples of the predictive capability of equation 33 are

shown for literature data on Type 304 and 316 stainless steel in Figures 65(a) and (b), respectively. Although some scatter in the experimental data for desensitization time exists, it is obvious that predictions sharply underpredict times.

Two major changes were made in order to improve predictions in SSDOS. The large effect of grain size on desensitization time in equation 33 was reduced by normalizing this term relative to an average grain diameter of 60 μm. This significantly improved prediction variability and, along with appropriate constants, brought t_{DS} predictions quite close to experimental measurements. The excellent agreement between measurement and prediction is demonstrated in Figures 65(c) and (d). Constants were picked to optimize the predictive capability.

In order to corroborate these changes to equation 33, predictive capability was assessed by comparison to several additional Type 304 and 316 heats. Unfortunately, the amount of experimental data documenting desensitization times is limited. Only isolated points were available for certain heats. Most sensitization studies are not extended to long enough times for complete desensitization to occur. The isothermal heat treatments in this work had this same shortcoming in most cases. Desensitization times for about 25 heats were found in the literature or extrapolated from the EPR data in Appendix B and compared to SSDOS predictions in Figure 66. Except for a few points the match between measurements and predictions is very good. It is important to note that large variations in grain size were not

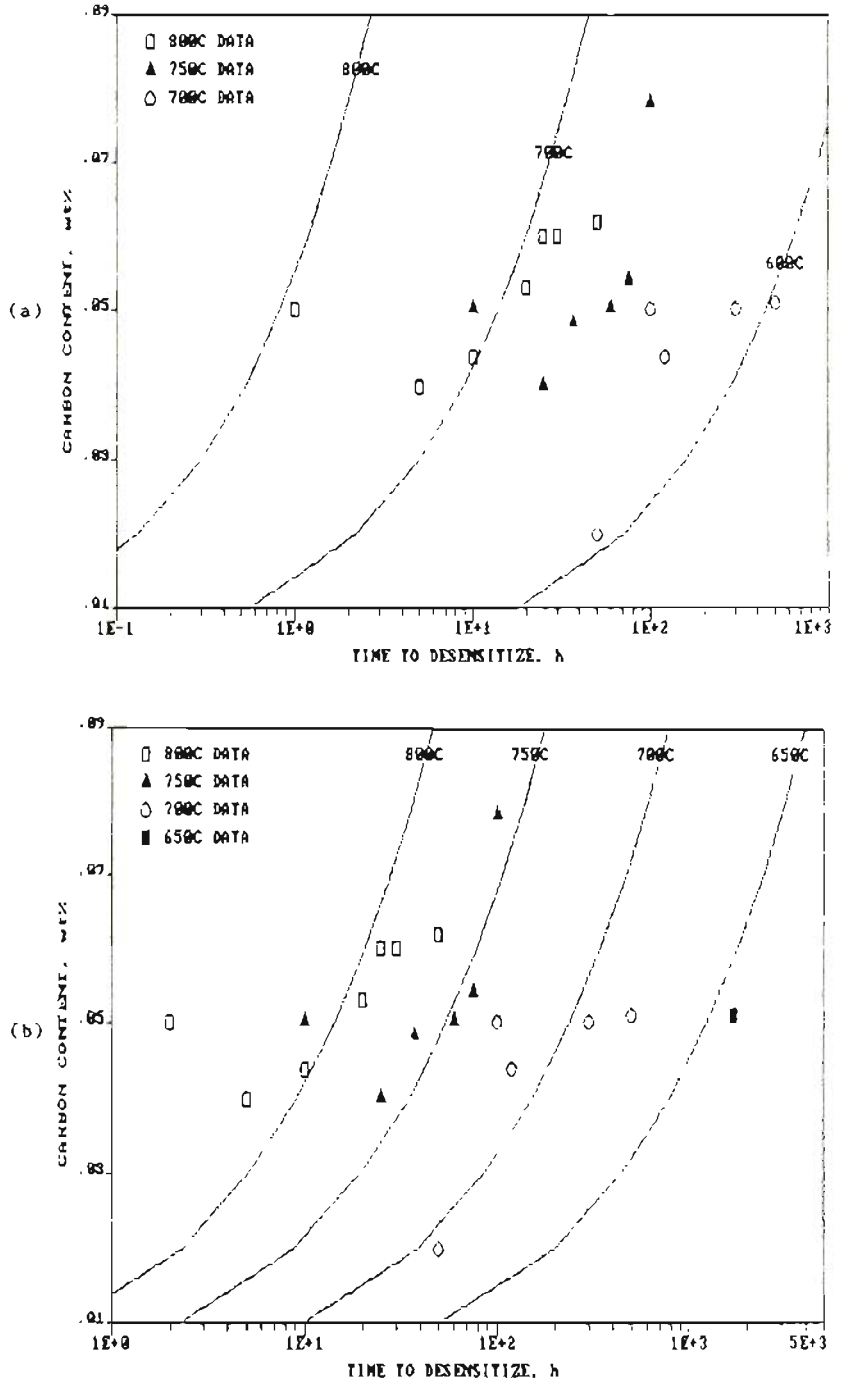

FIGURE 65. Comparison Between Measured and Predicted Times-to-Desensitize for Type 304 (a and b) and 316 (c and d). Predictions using equation 33 are shown in (a) and (c), SSDOS in (b) and (d).

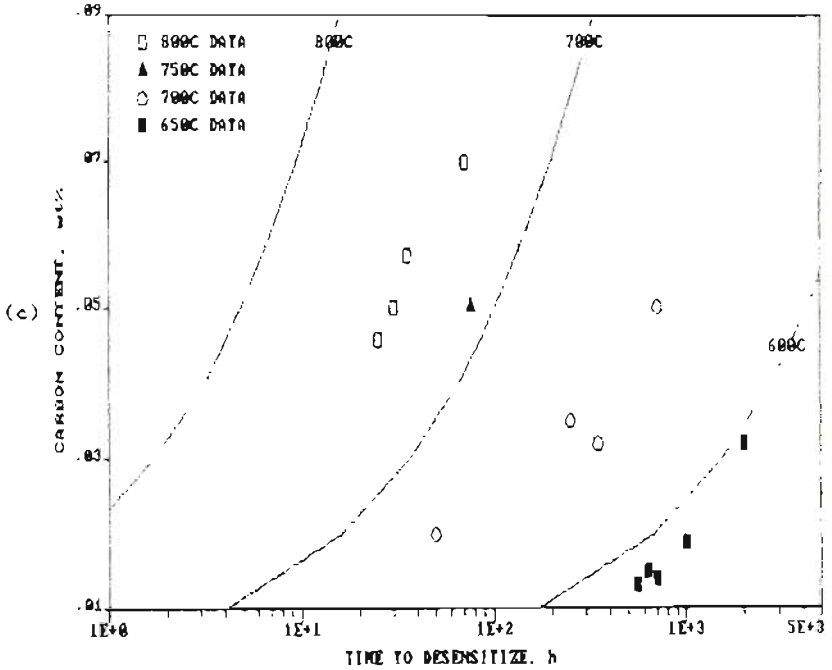

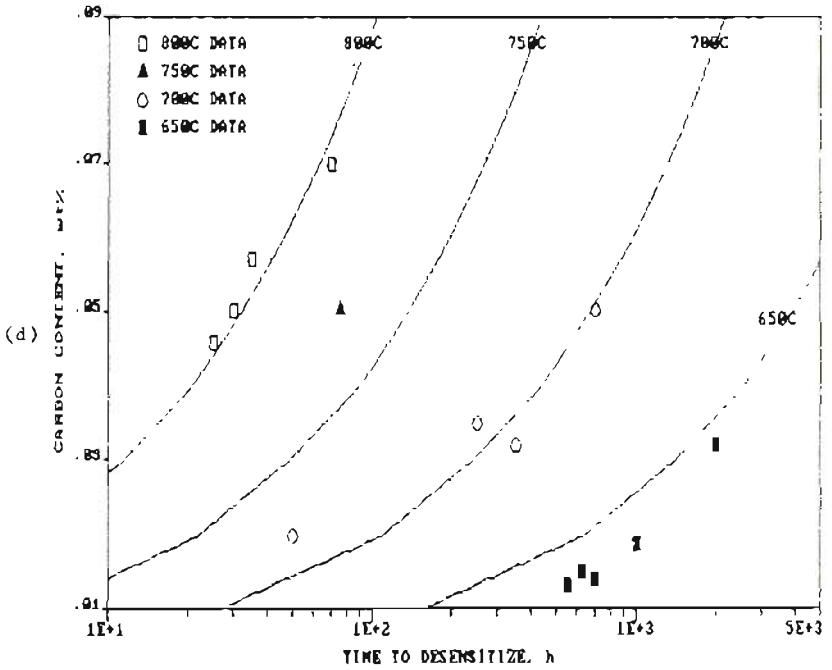

FIGURE 65. (contd)

evaluated in these heats and may lead to a different conclusion. Heats included in Figure 66 had average grain diameters from about 40 to 110 μm.

5.1.5 Material Condition and Thermomechanical Effects

Initial material condition can significantly affect subsequent sensitization response. Certainly, a material with preexisting carbides will behave differently than one properly solution annealed. Preliminary experiments that compared mill-annealed to solution-annealed specimens did not demonstrate differences as discussed in Section 4.2.6. These results were somewhat surprising and suggest that material condition may not be an important concern for many stainless steel product forms if processing temperatures are high enough.

SSDOS requires the input of material condition and, if available, detailed mill-anneal or solution-anneal thermal history to assess initial condition. Since for many practical situations processing thermal history is not known, calculations are made without special consideration to initial condition. It is important to note that the primary data base used to quantify SSDOS predictions was developed for sensitization response of stainless steels in the mill-annealed condition. These conclusions concerning material condition are based on isothermal results; continuous-cooling exposures will be examined in the next section.

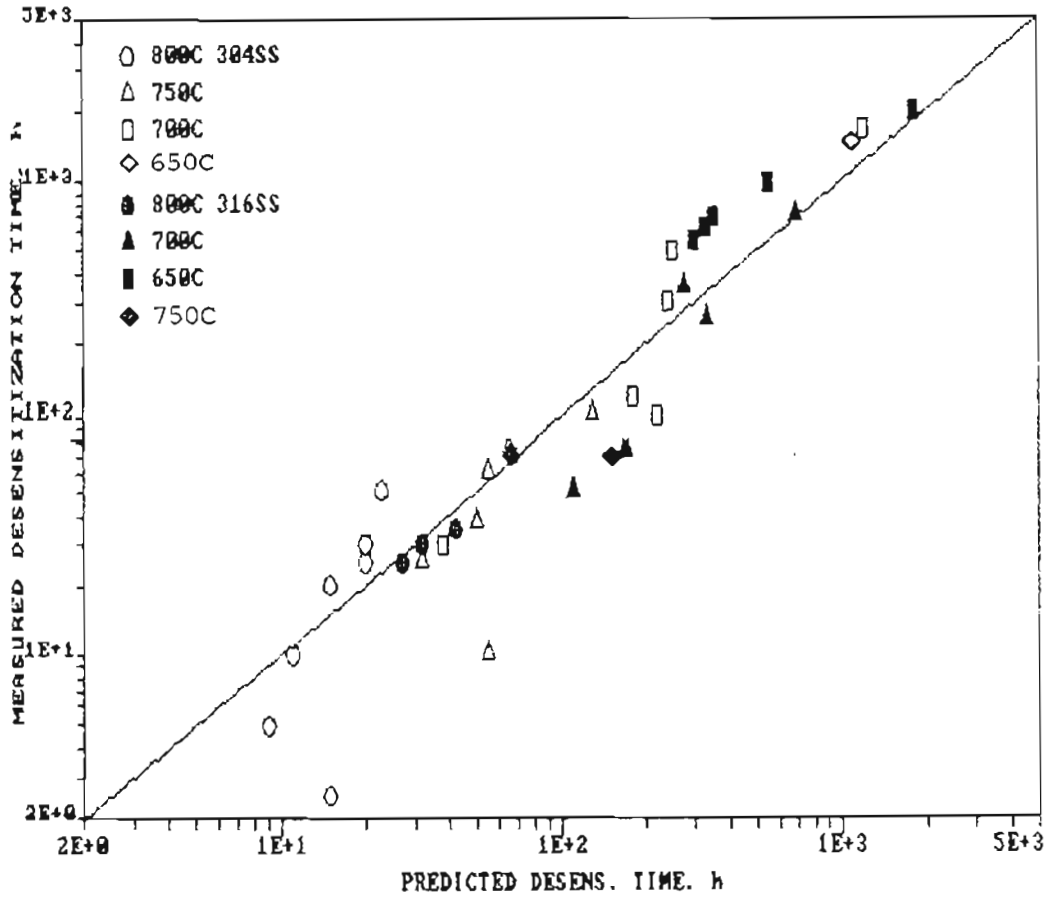

FIGURE 66. Correlation Between Measured and Predicted Desensitization Times for Type 304 and 316 Stainless Steels.

One aspect of material condition that is factored into model calculations is prior deformation. Preliminary experiments documented the detrimental effects of prior and simultaneous deformation on sensitization development and were described in Sections 4.4.2 and 4.4.3. SSDOS accounts for deformation through its influence on chromium diffusivity. Deformation, or more appropriately dislocation density resulting from deformation, promotes enhanced chromium migration to growing carbides via pipe diffusion. Although it seems more likely

that small solutes like carbon will migrate along dislocations than a relatively large solute like chromium, sensitization kinetics are accelerated with increasing deformation. Because of the limited quantitative data available, an effective chromium diffusivity is defined and used in SSDOS. Diffusivity coefficients are increased by a nonlinear function that varies from 1 at 0.5% strain (prior or simultaneous) to approximately 10 times at 10% strain.

Predictions using this effective diffusivity in SSDOS are presented in Figure 67 for the simultaneous strain results. This data is selected because it is the most complete series of tests that have been performed. Prior deformation is predicted using the same empirical correlation. Deformation effects are predicted to level off from about 10 to 20% strain and decrease as deformation is increased to higher amounts.

Model capabilities in this area are limited and can only be justified under the same experimental conditions employed for the tests reported. There is no intent that the correlations in SSDOS will accurately predict effects during thermal treatments at higher or lower isothermal temperatures or after continuous cooling exposures. The current correlation is the first step toward understanding and modeling complex thermomechanical history effects on sensitization development. Its use should improve predictive capability for many thermomechanical treatments.

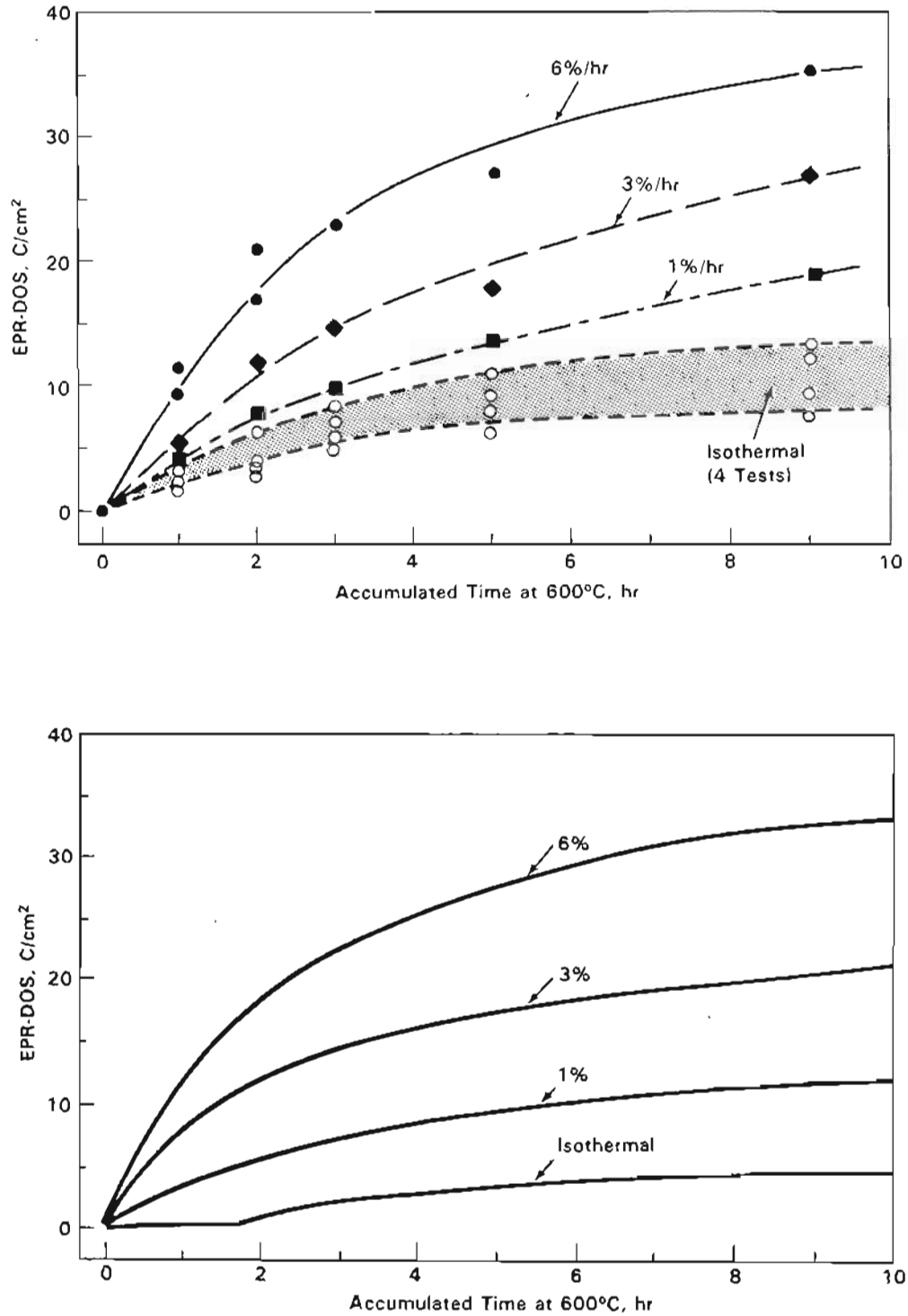

FIGURE 67. Comparison of Measured (a) and Predicted (b) Sensitization Development as a Function of Deformation Rate and Time at 600°C.

5.1.6 Continuous Cooling Thermal Simulation

The continuous-cooling thermal history is approximated by dividing the cooling curve into small isothermal segments. DOS analysis is conducted every five degrees, and the time increment at each temperature determined from the specified cooling rate. Chromium depletion characteristics are accumulated as the temperature is reduced. Minimum temperatures evaluated during a continuous-cooling exposure are determined from the cooling rate. The faster the cooling rate, the higher the minimum temperature evaluated. This results in larger predicted interfacial chromium minimums and agrees with STEM-EDS measurements. A certain time at temperature is required to establish realistic thermodynamic minimums. Therefore, even though a specimen is exposed to very low temperatures during cooling (e.g., <500°C), the time at temperature is not sufficient to impact depletion characteristics and DOS.

Continuous cooling sensitization behavior was discussed in detail in Section 4.3 and will be compared to prediction in Section 5.2.2. One aspect of this data which prompted a change in predictive approach will be considered here. Maximum temperatures above about 1000°C were found to sharply reduce subsequent sensitization kinetics during continuous cooling. Specimens exposed to a maximum temperature of 1050°C exhibited smaller EPR-DOS values for most cooling rates. Initially, this difference was assumed to result from a change in specimen condition, i.e., mill-annealed to solution-annealed. However, as discussed in Section 4.3, such a conclusion is

not consistent with the isothermal material condition studies. Other possible explanations for this behavior were presented earlier.

To model this change in sensitization response, the effective chromium diffusivity was modified when maximum temperatures were greater than a critical temperature. Critical temperature was a function of cooling rate and material composition. Maximum temperature and cooling rate effects on model predictions are illustrated in Figure 68. EPR-DOS increases for all three cooling rates as the maximum temperature increases up to about 800°C. Predictions remain constant as maximum temperatures rise above the region for carbide growth and then fall when the critical temperature is exceeded. Critical temperatures are as low as about 950°C for slow (0.1°C/s) cooling rates and increase to above 1050°C for fast (10°C/s) cooling rates.

The basis for this change in diffusivity when a critical maximum is exceeded is not well founded. It may be that the isothermal material condition experiments cannot be used to indicate effects on continuous cooling sensitization. If this is the case, then the two plateaus in each curve shown in Figure 68 represent predictions for mill-annealed (upper) and solution-annealed (lower) material conditions. When high temperatures (>~950°C) are reached for a sufficient length of time, material condition changes. Grain boundary migration may occur along with the removal of localized grain boundary enrichments during mill processing or during specimen heat-up in the

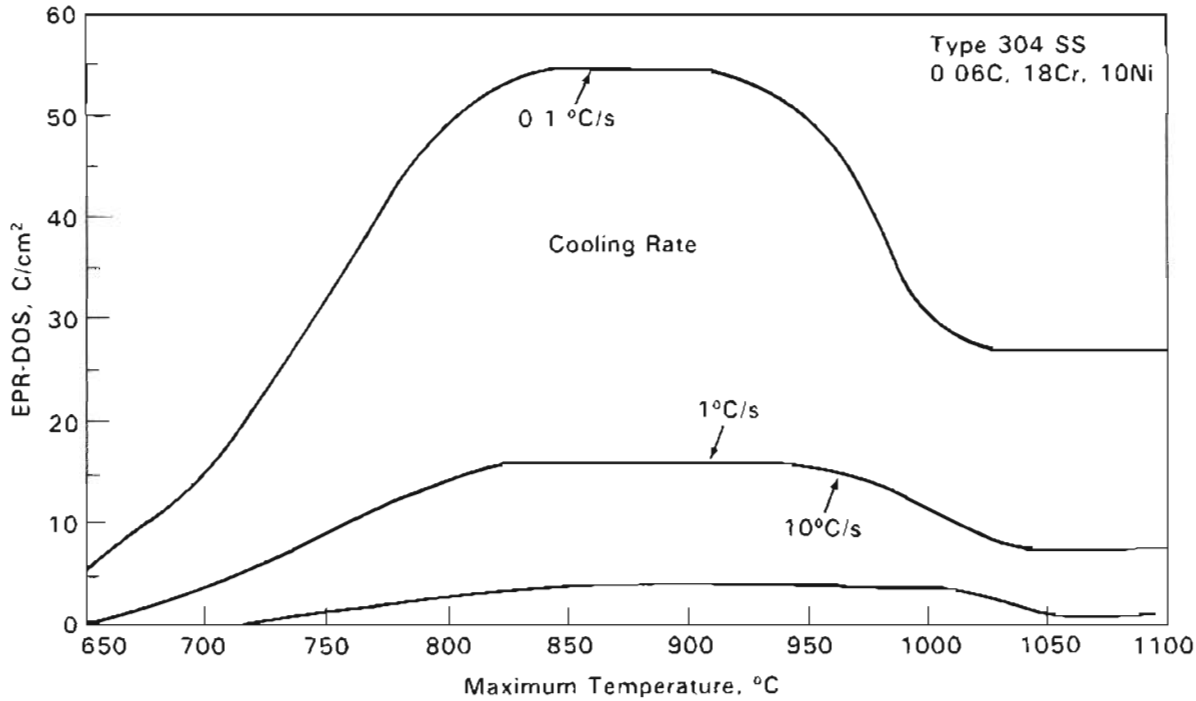

FIGURE 68. SSDOS Model Predictions of Continuous Cooling Sensitization Development as a Function of Maximum Temperature and Cooling Rate.

continuous cooling experiment itself. Regardless, the effective chromium diffusivity drops and the resultant EPR-DOS evolved is smaller at the same cooling rate.

Support for the importance of material condition on continuous cooling sensitization can be indicated by results of other researchers on mill-annealed and solution-annealed stainless steels. Data from several sources have been compared to model predictions in Figure 68. Curves represent a predicted EPR-DOS value of about 5 C/cm^2, while data points specify attack (filled point) or no attack (open point) in the modified Strauss test solution. Good qualitative agreement can be observed over a wide range of carbon contents for both Type 304

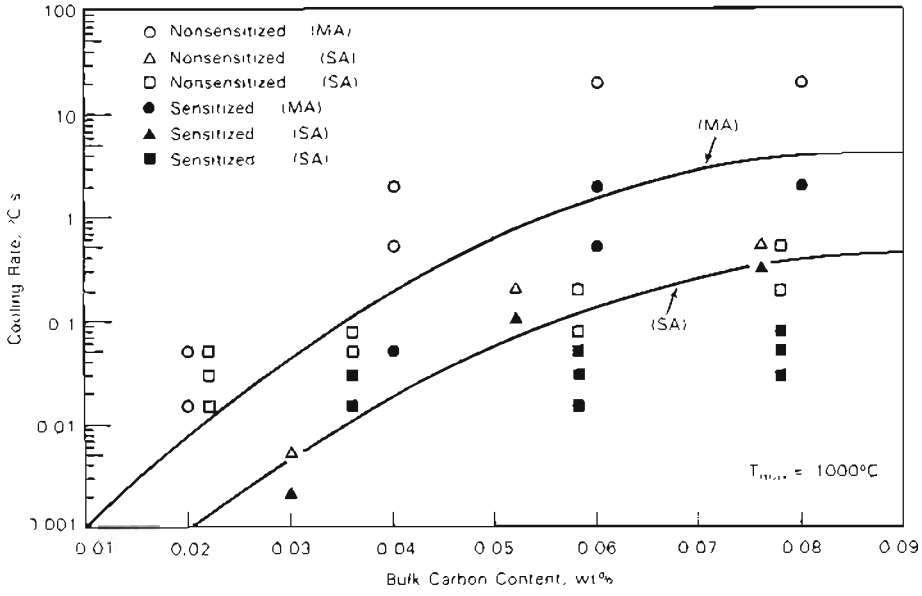

FIGURE 69. Comparison of SSDOS Model Predictions for Several Type 304 Stainless Steel Heats in the Mill-Annealed (MA) or Solution-Annealed (SA) Condition.

stainless steel in the mill-annealed or solution-annealed condition. Differences between predictive curves disappear at low carbon contents and slow cooling rates because the critical temperature for condition change is exceeded below about 0.05 wt% carbon. As carbon levels are reduced to very low levels, model predictions show steels becoming solution-annealed during the continuous cooling exposure at a maximum temperature of 1000°C.

Detailed comparisons between measurements and predictions for the program heats will be made in Section 5.2.2. One example corroborating maximum temperature effects discussed above is presented in Figure 70. Although some scatter exists when attempting to quantitatively compare measured and predicted EPR-DOS values, the general match is quite good. In particular, the modification of effective

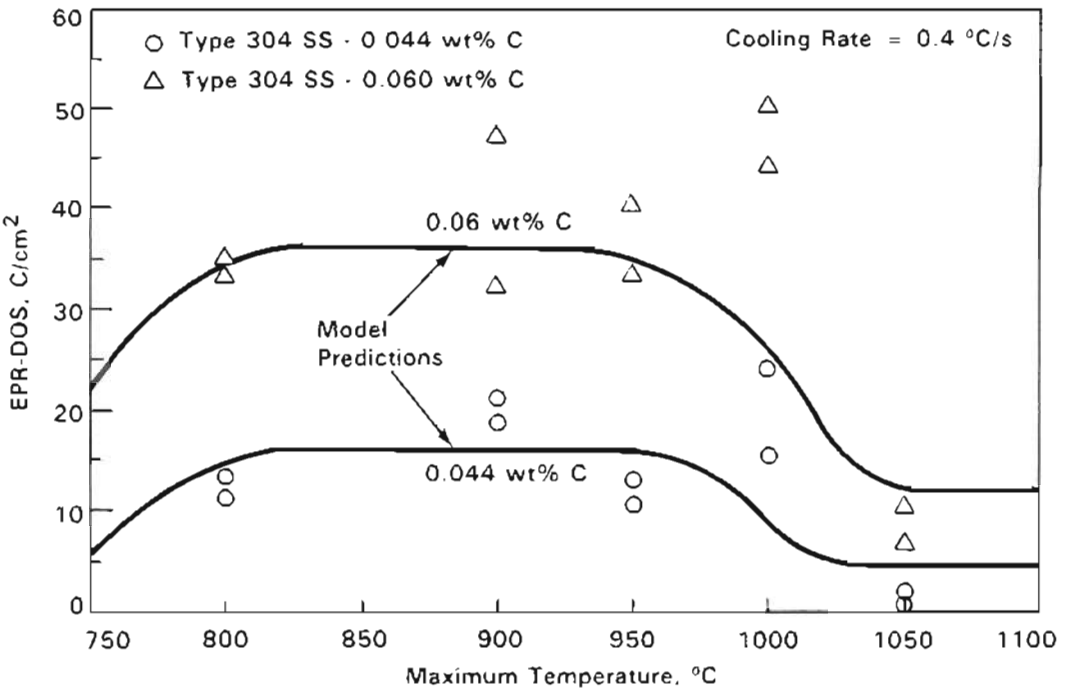

FIGURE 70. Maximum Temperature Effects on Measured and Predicted Continuous Cooling Sensitization.

chromium diffusivity for high maximum temperatures (1050°C) prompts an accurate prediction of the reduced sensitization response.

5.2 QUANTITATIVE MODEL ASSESSMENT

The basic components, theoretical and empirical, of the SSDOS sensitization prediction model were presented and discussed in Section 5.1. Key aspects of SSDOS center on its empirical correlations to help quantify thermodynamic and kinetic predictions. Evolution of these empirical correlations stemmed in large part from the isothermal and continuous-cooling data base of this study. Quantitative prediction capabilities will be demonstrated and evaluated by direct comparisons to sensitization response. Detailed comparisons will be made versus available EPR-DOS data from the program heats and appropriate data from the literature.

5.2.1 Isothermal Sensitization

Program Heats

Carbon has been identified as the critical compositional variable controlling sensitization. This behavior is reiterated by SSDOS predictions for several of the Type 304 and 316 stainless steel pipe heats in Figure 71. Time-temperature-sensitization curves for heats ranging in carbon concentrations from 0.013 (SS-2) to 0.06 (SS-7) wt% are shown in Figure 71(a) and from 0.015 (SS-11) to 0.058 wt% (SS-16) in Figure 71(b). SSDOS predictions are made for an EPR-DOS value of 5 C/cm^2 to establish these curves. Carbon content effects on the shape, size and location of the C-curves for each heat can be seen. The sensitization range decreases and moves to lower temperatures as bulk carbon levels decrease.

The qualitative prediction of carbon effects in Figure 71 is similar to previous sensitization modeling efforts. Comparisons to experimental data have been made by adjustment of minimum chromium levels of depletion width necessary for attack in the indirect test solution. A first step in quantifying such a comparison is illustrated in Figure 72 for a high-carbon Type 304 and 316 heat. Curves are predicted for two EPR-DOS values, either slightly (5 C/cm^2) or severely (40-50 C/cm^2) sensitized. Measured and predicted EPR-DOS agree reasonably well for both heats. Position and shape of the curves match measurements for the low and high EPR-DOS values.

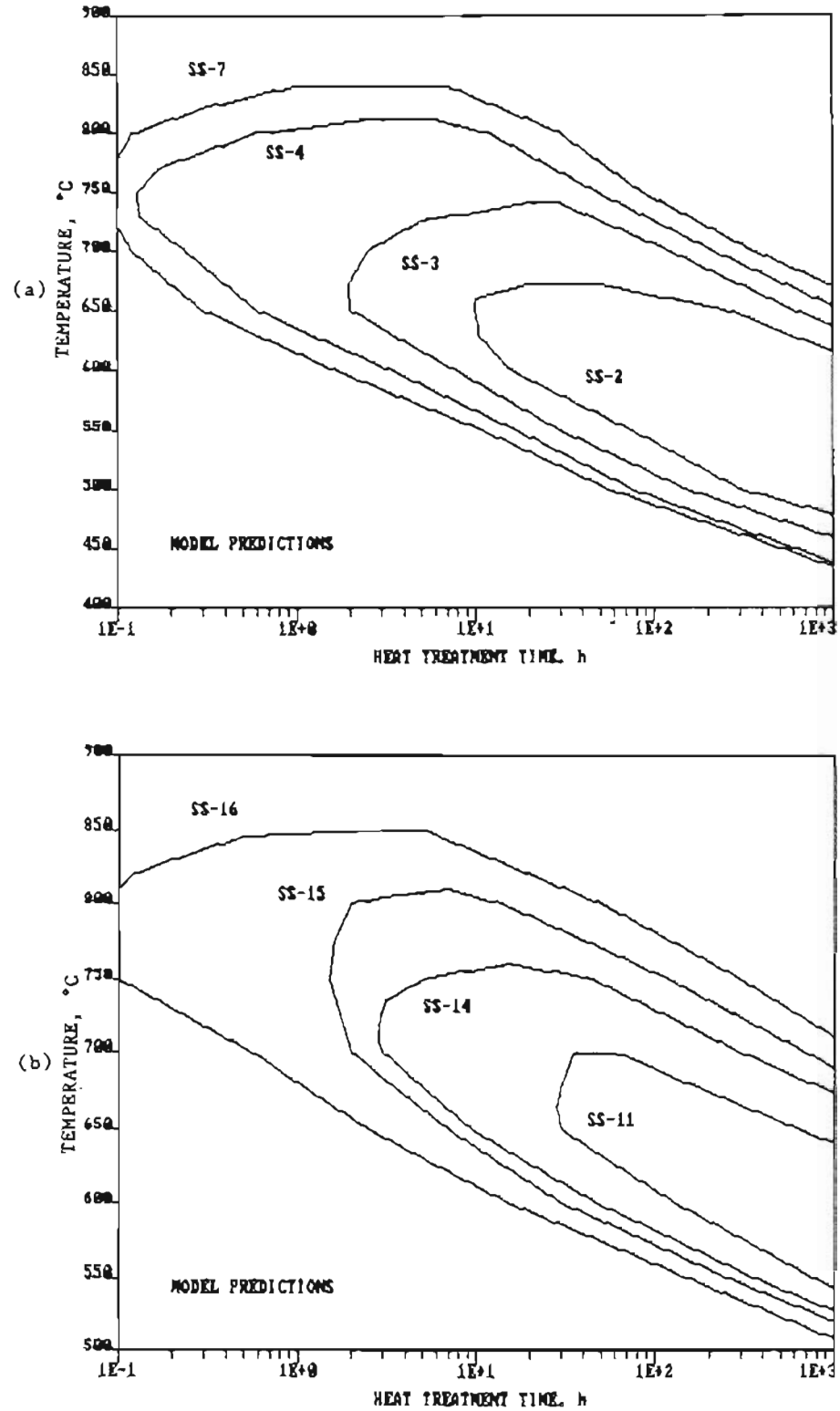

FIGURE 71. Predicted Time-Temperature-Sensitization Behavior for Type 304 (a) and 316 (b) Heats with Variable Carbon Concentration.

Time-temperature sensitization predictions like those presented in Figure 72 allow some indication of the general model predictive capability, but much more specific comparisons of quantitative sensitization response are needed. From a practical viewpoint, SSDOS will not give exact predictions of DOS. However, it will do more than simply indicate trends. In order to assess how quantitative SSDOS predictions of EPR-DOS are, detailed mapping of sensitization development has been made at each of the heat treatment temperatures, for each of the program heats. Therefore, quantitative comparisons can be extracted indicating the model's flexibility to adjust to different thermal histories and material compositions.

Examples of these detailed comparisons are documented in Figures 73, 74 and 75 for Type 304/304L, 316/316L and 316LN, respectively. Data for twenty heats are summarized in these figures and sensitization kinetics at various temperatures examined. Duplicate specimens were tested for several heats and heat treatments. Average EPR-DOS values are plotted for these specimens to better represent the data base. Even though a relatively large time-temperature matrix was evaluated, many additional times would be useful. Some differences that exist between measured and predicted EPR-DOS are difficult to assess. A more continuous sequence of tests at certain temperatures with smaller time intervals between tests is needed. For example, times between 1 and 10 h at 700 and 800°C and between 10 and 100 h at 600 and 700°C would help quantitate times-to-sensitize and desensitization effects for many heats.

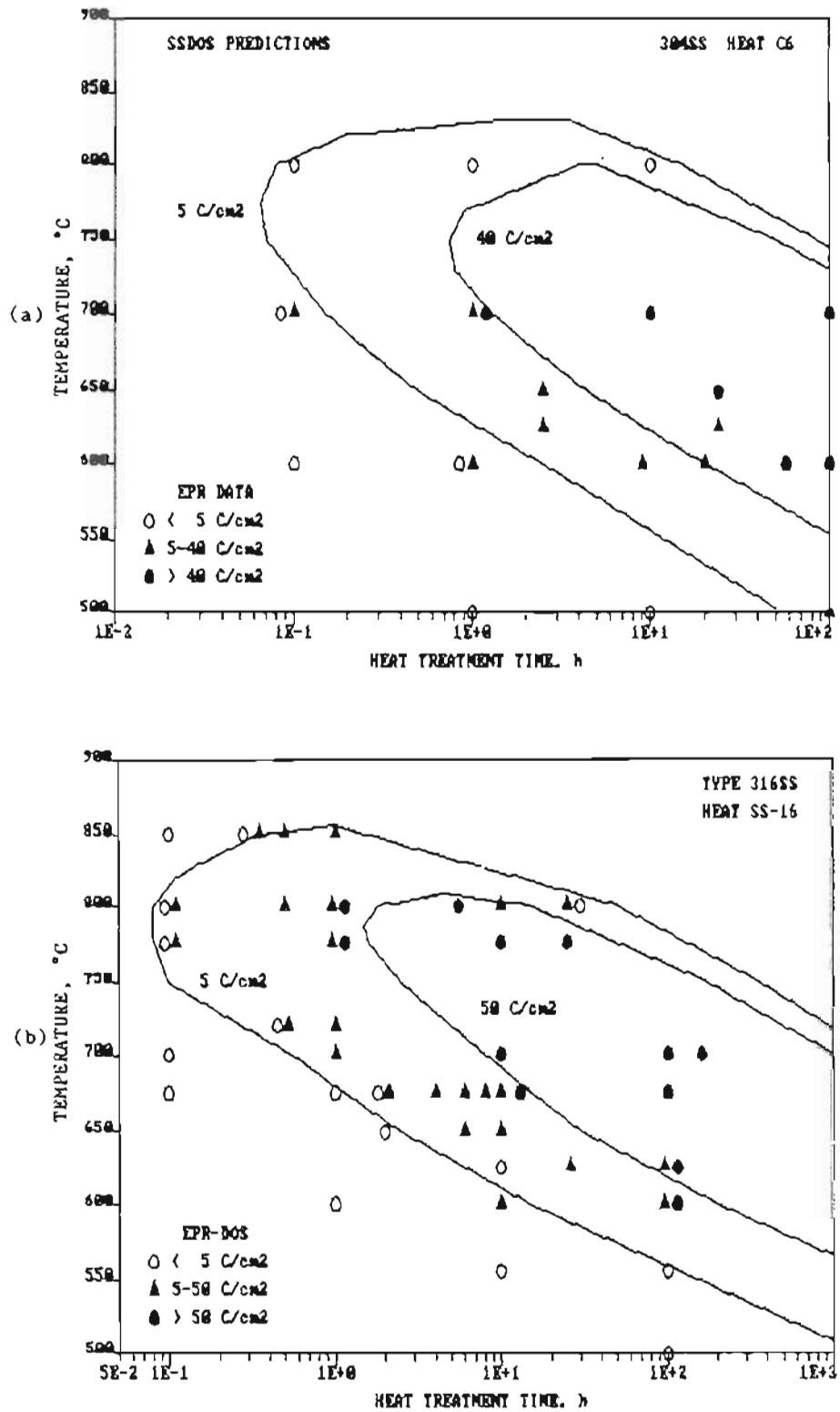

FIGURE 72. Comparison of Measured and Predicted Time-Temperature-Sensitization Behavior for a High Carbon Type 304 (a) and 316 (b) Stainless Steel.

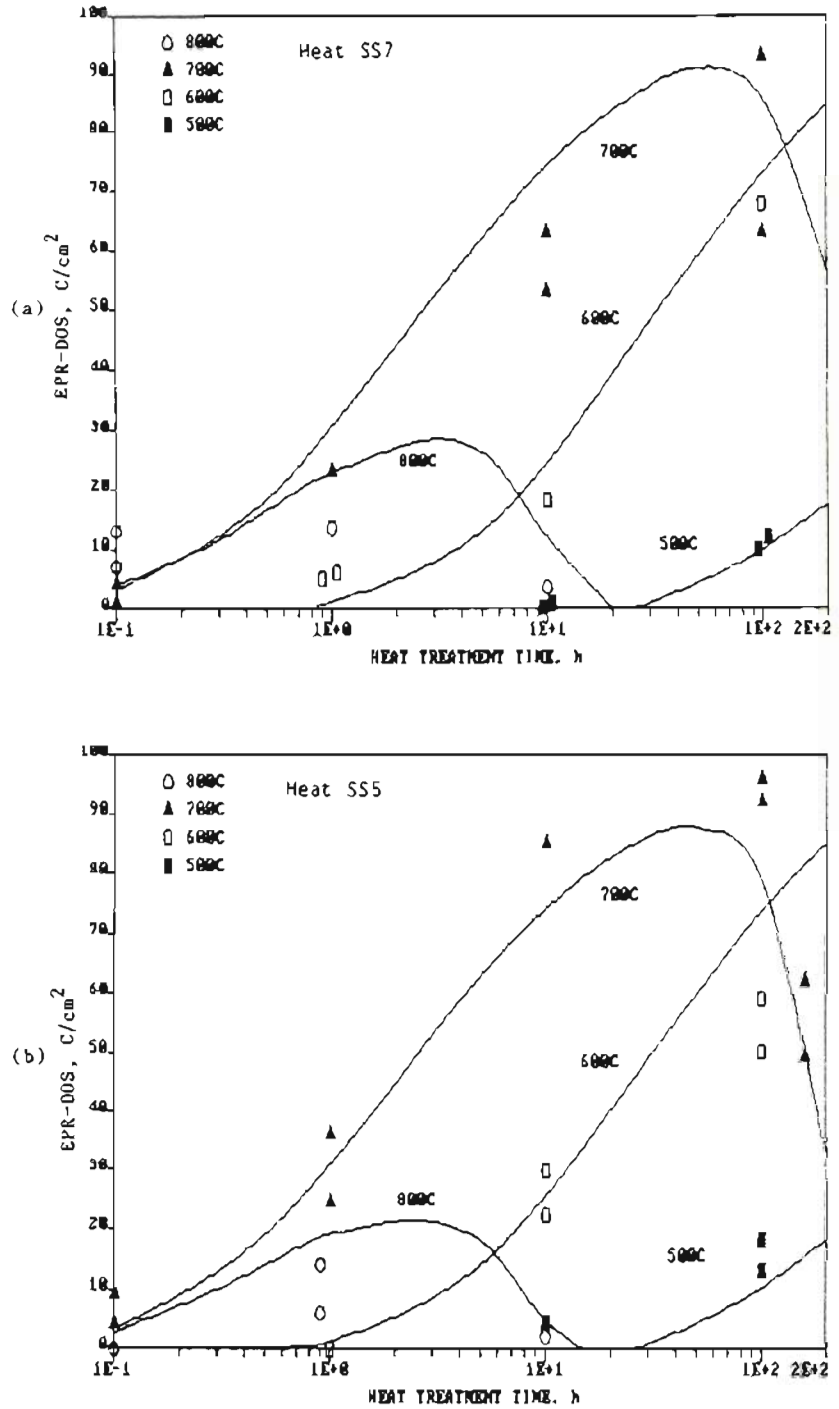

FIGURE 73. Detailed Comparisons Between Measured and Predicted EPR-DOS for Type 304 (a, b, c) and 304L (d) Heats.

(c)

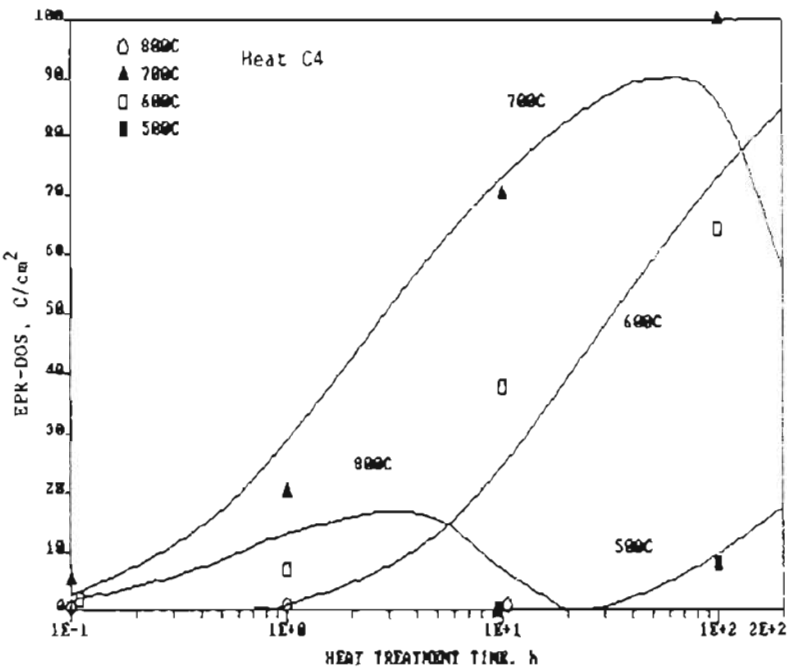

(d)

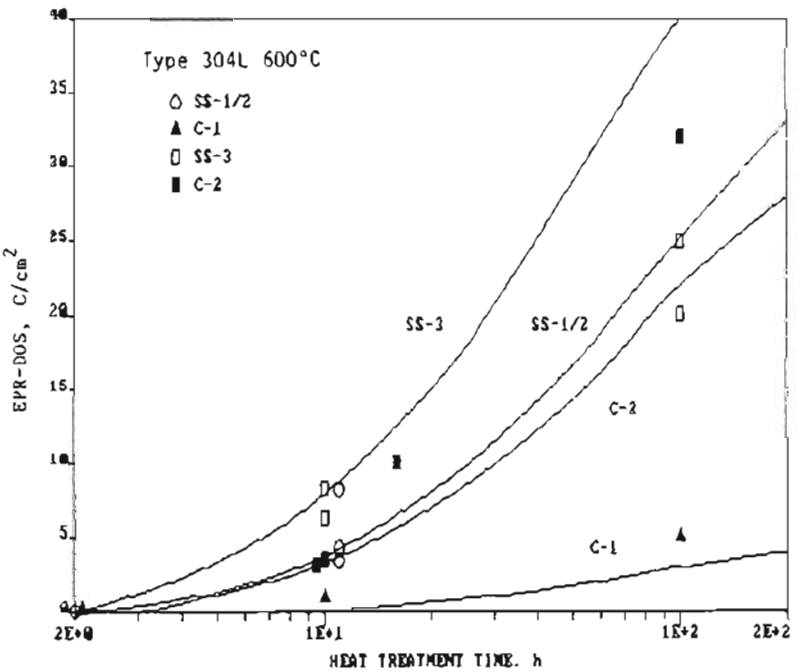

FIGURE 73. (contd)

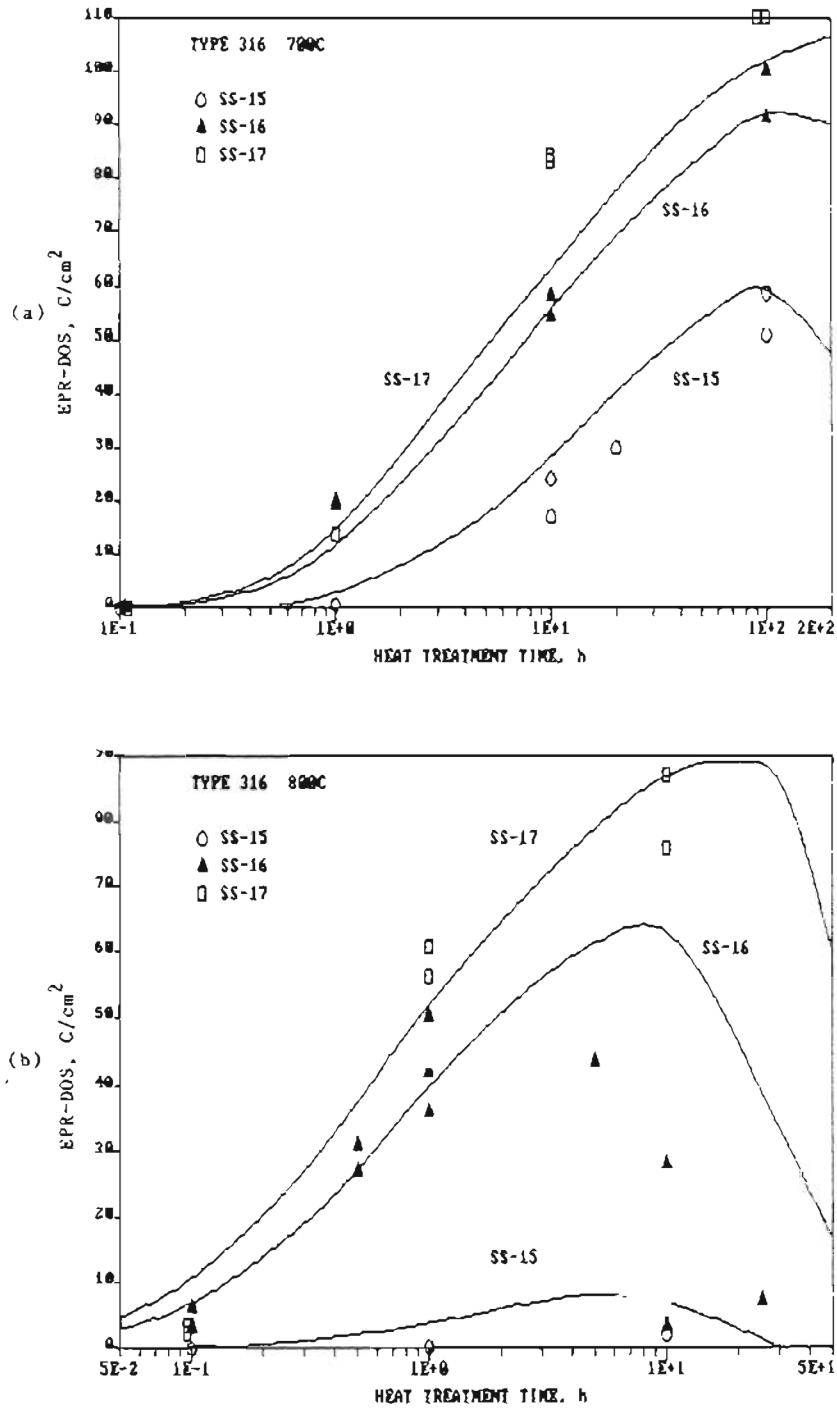

FIGURE 74. Detailed Comparison Between Measured and Predicted EPR-DOS for Type 316 (a, b) and 316L (c, d).

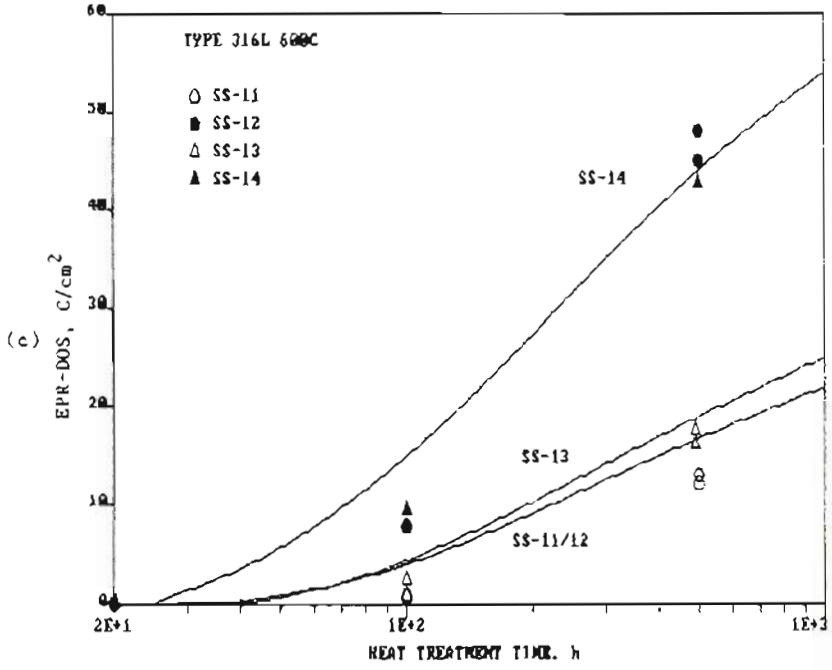

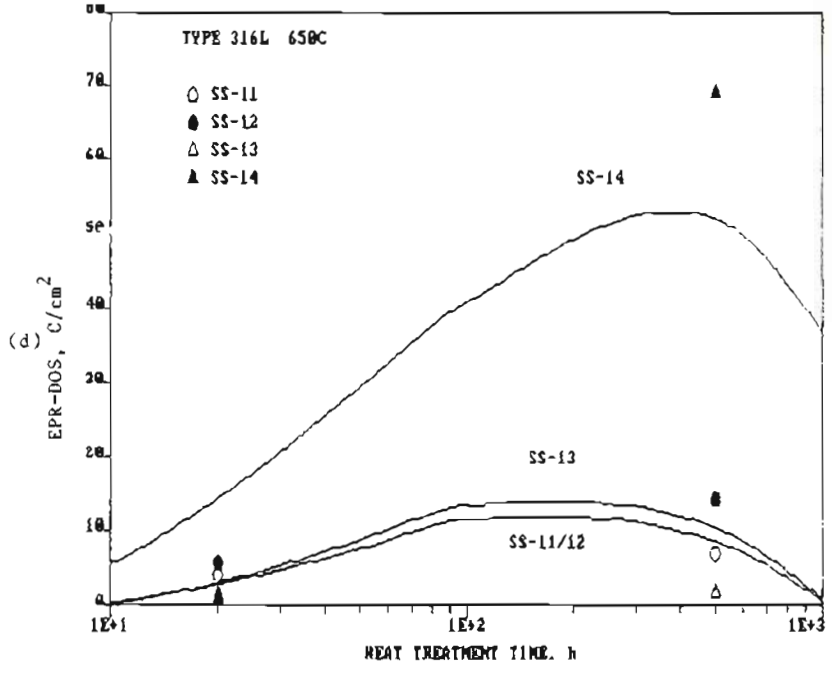

FIGURE 74. (contd)

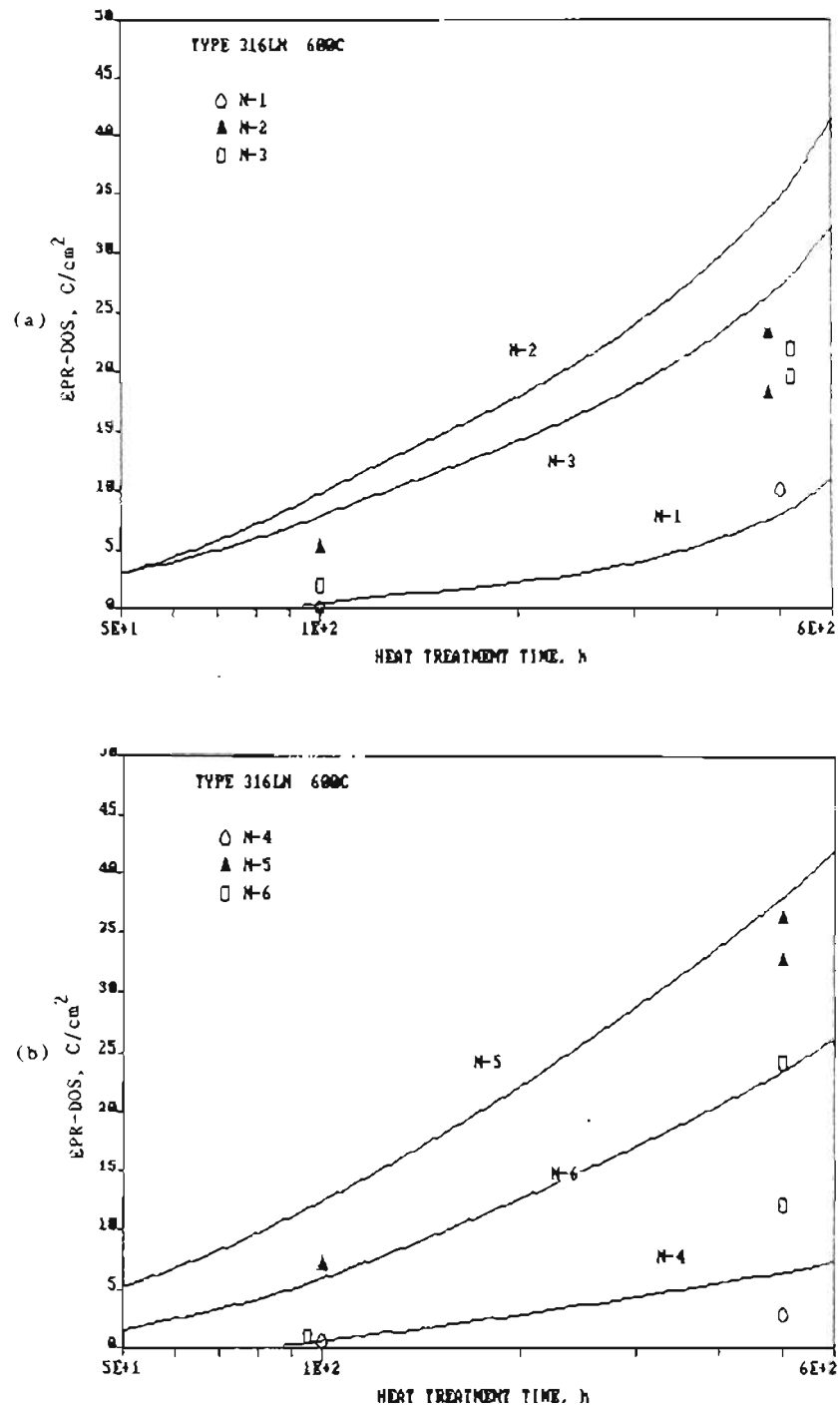

FIGURE 75. Detailed Comparison Between Measured and Predicted EPR-DOS for Type 316LN Heats at 600 (a, b) and 650°C (c, d).

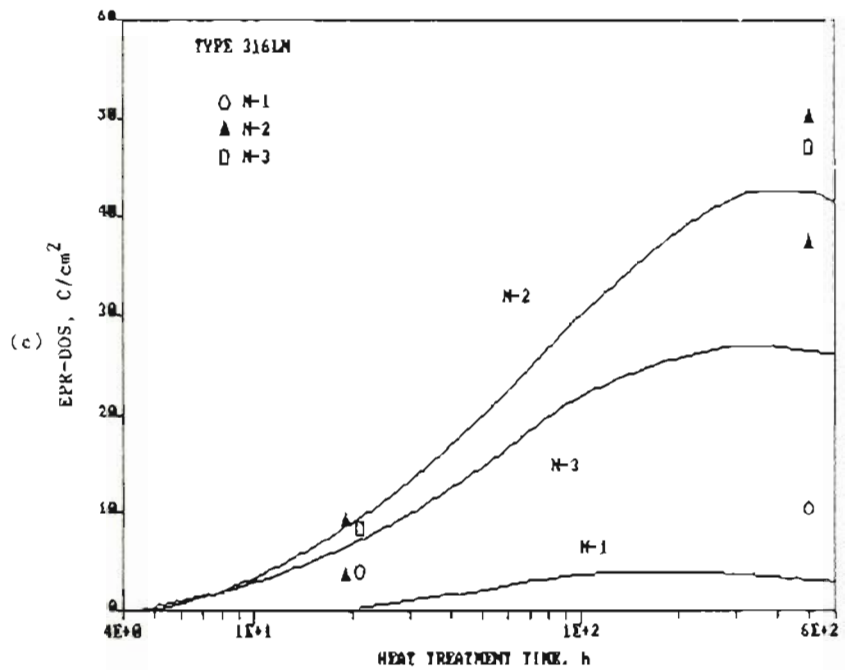

(c)

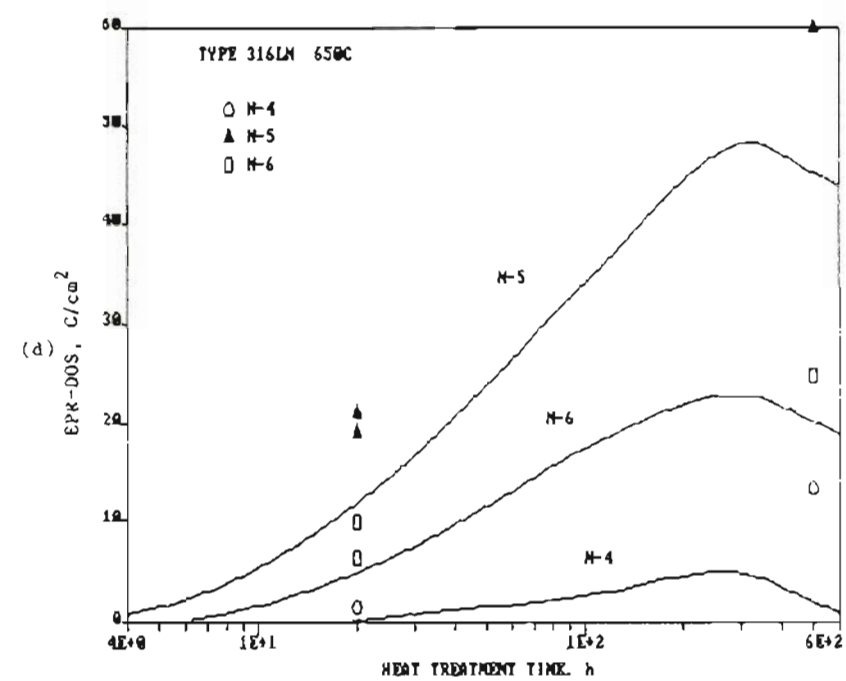

(d)

FIGURE 75. (contd)

SSDOS predictions of sensitization kinetics are in good agreement with the isothermal data base. Plotting measurements versus predictions quantitatively as in Figures 73 through 75 illustrates that SSDOS provides not only the qualitative data trends, but reasonably estimates the magnitude of DOS at any temperature and time. Desensitization effects shown in the moderate- to high-carbon Type 304 (Figure 73a, b and c) and Type 316 (Figure 74a and b) are accurately predicted, even though the data base is insufficient to adequately validate behavior. The timing of desensitization is critical since it controls the maximum DOS that can be achieved. Comparisons for the higher-carbon heats show that the value of the DOS maximum and time to reach the maximum are consistent between measurement and prediction.

Several specific aspects of the predictive capability can be determined from this type of detailed comparison. The 800°C data for high-carbon Type 304 stainless steels are slightly overpredicted. Kinetics of desensitization appear to be predicted well, but the predicted maximum achieved between 1 and 10 h is somewhat high (Figures 73a, b and c). EPR-DOS depends on the interfacial chromium minimum as discussed in Section 3.2.3. The 800°C predictions are very sensitive to this factor since minimums are near 13.5%. If the volume depletion parameter is based on a critical chromium concentration of 13% instead of 13.5%, predicted EPR-DOS values decrease and improve the data fit. However, overall predictive capabilities are not improved.

The quantitative nature of SSDOS predictions also extends to the low-carbon heats. Predictions and measurements show little or no sensitization at temperatures greater than 700°C. Sensitization development in these heats was best evaluated at 600 or 650°C. Some problems can be seen for the Type 304L comparison in Figure 73(d). EPR-DOS appears to be overpredicted for heat SS-3 and underpredicted for heat C-2. In both cases, predictions agree at times up to about 10 h and only disagree with the data after the 100 h heat treatment. This comparison reflects the limitations in the data base. It is also important to point out that the scales for the low-carbon heats have been reduced and differences appear larger than indicated for the higher-carbon heats.

A better correlation is observed for the Type 316L heats in Figure 74(c) and (d). Measured and predicted sensitization development is quite consistent at 600 and 650°C. The same is not true for certain aspects of the Type 316LN comparisons in Figure 75. Some of these differences may be due to the precipitation of Cr_2N, but for the most part, it is the inconsistent effects of nitrogen additions on sensitization response that is the cause. This data set was described and discussed in Section 4.2.3 and did not always follow expected trends for nitrogen effects. Again it must be recognized that differences are not very large in the worst case (Figure 75a) and are relatively good agreement is observed in other cases (Figure 75c).

Individual comparisons for many of the program heats have indicated the quantitative predictive capability of the SSDOS model. The

isothermal sensitization is summarized in Figure 76 directly correlating measured and predicted EPR-DOS values. A solid line is drawn representing a one-to-one fit for the data set. As suggested by the individual heat assessments above, an excellent agreement is demonstrated. Many of the points falling farthest from the line are due to uncertainties in predicting desensitization effects for several of the lower-carbon heats.

Literature Data

A large isothermal sensitization data base incorporating more than 100 heats has been assembled from the literature. This data had

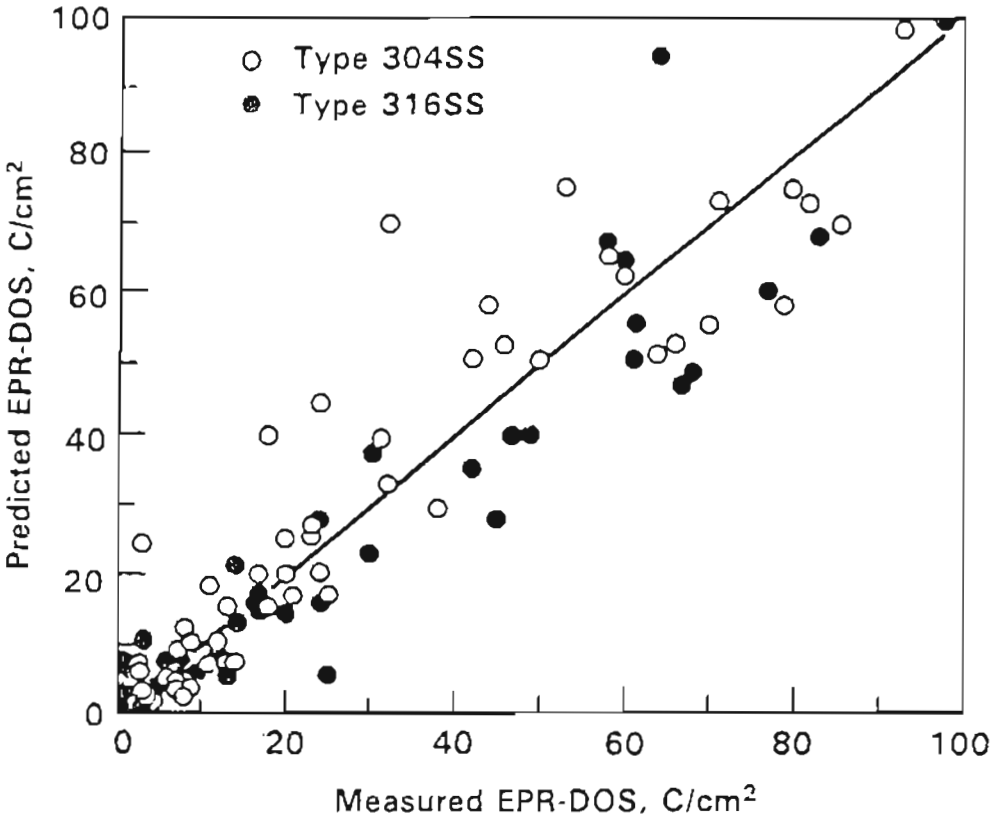

FIGURE 76. Comparison Between Measured and Predicted EPR-DOS for the Type 304 and 316 Heats.

been used previously to assess composition equivalency models as reviewed in Section 2.6.1. Some of the literature data is reported in sufficient detail to allow quantitative comparisons to be made. Of particular interest to the present work is EPR data which enables a direct comparison to model predictions.

Umemura and Kawamoto[145] mapped time-temperature-sensitization development in a high-carbon Type 304 stainless steel using the EPR technique. A comparison between SSDOS predicted iso-DOS curves and their data is presented in Figure 77. Although more detailed EPR-DOS values were not available, the general agreement between measured and predicted EPR-DOS is demonstrated. Similar examples were found by examining EPR results from many other sources.[40,41,114-116,120,121,145]

Detailed isothermal sensitization response has also been determined using the ASTM standard corrosion tests described in Section 2.5.1. As mentioned, the modified Strauss test is an effective method to assess chromium depletion and DOS. One interesting data set will be examined because of its implications on material condition effects discussed in Section 4.2.6 and 5.1.5.

Solomon[146] found a significant difference between the isothermal sensitization response for a mill-annealed versus a solution-annealed high-carbon Type 304 stainless steel. Modified Strauss test results for the onset of sensitization are shown in Figure 78. The

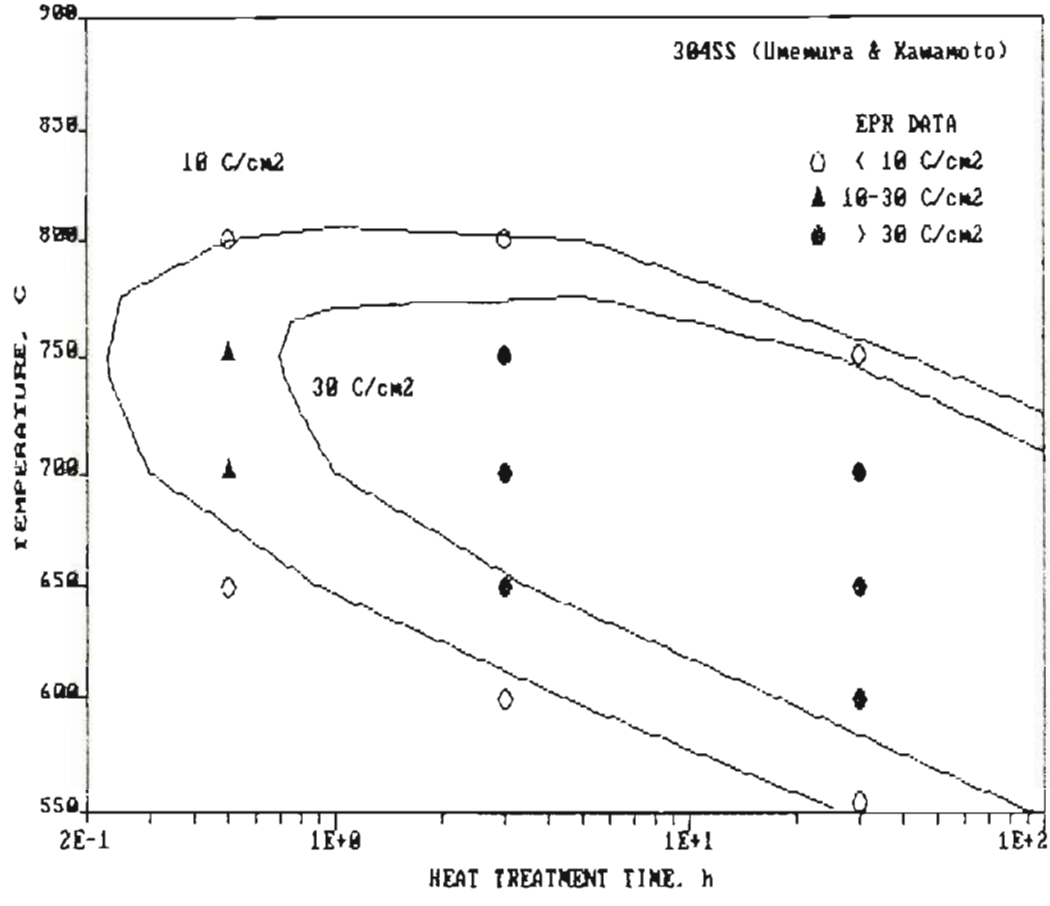

FIGURE 77. Example of SSDOS Prediction for Time-Temperature-EPR Data of Umemura and Kamamoto.[146]

mill-annealed material sensitized much more rapidly and desensitizes at shorter times. This sharp difference in behavior with material condition is in contrast to the current experiments (Section 4.2.6). SSDOS predictions for an EPR-DOS value of 5 C/cm^2 (dashed line) agree reasonably well with the solution-annealed data, thereby overpredicting times-to-sensitize at most temperatures. To approximate the mill-annealed data, preexisting carbides and chromium depletion must be input into SSDOS as a starting condition. Picking initial

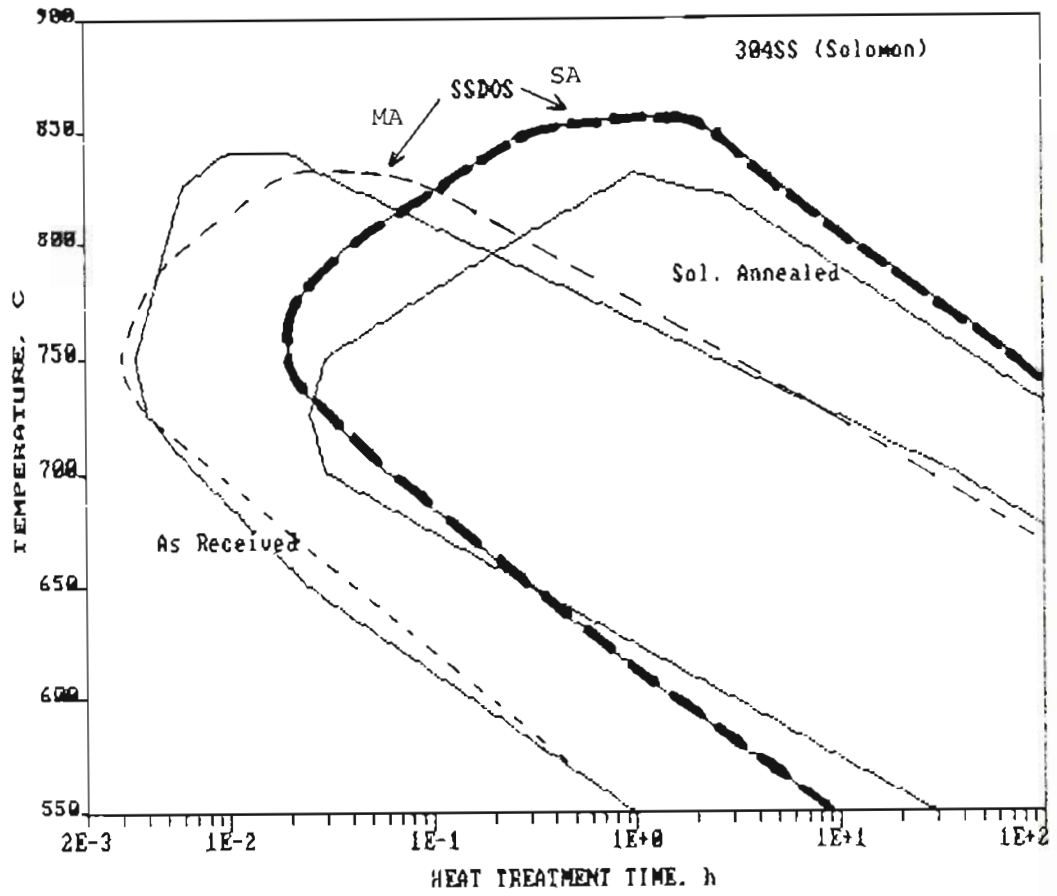

FIGURE 78. Measured and Predicted Time-Temperature-Sensitization for a Mill-Annealed and Solution-Annealed High-Carbon Type 304 Stainless Steel.

depletion conditions appropriately, SSDOS can predict the mill-annealed data as well. Predictions are plotted in Figure 78 as a dotted line.

Many additional correlations have been made between measured and predicted DOS to assess general SSDOS capabilities. Detailed comparisons illustrating these results will not be presented. The comparisons documented in the previous figures have demonstrated the quantitative nature of SSDOS predictions. However, one last assessment can

be made relative to the large isothermal data base from the literature and that is predictions of times-to-sensitize. Heats where adequate composition and material condition data were reported are plotted in Figure 79 for heat treatments at 600, 650 and 700°C. The scatter around the one-to-one fit indicates some of the realities in predicting a diverse, multi-laboratory data base. It is important to note that much of this scatter is inherent in the data itself and that SSDOS prediction groups the results around the one-to-one correlation fit.

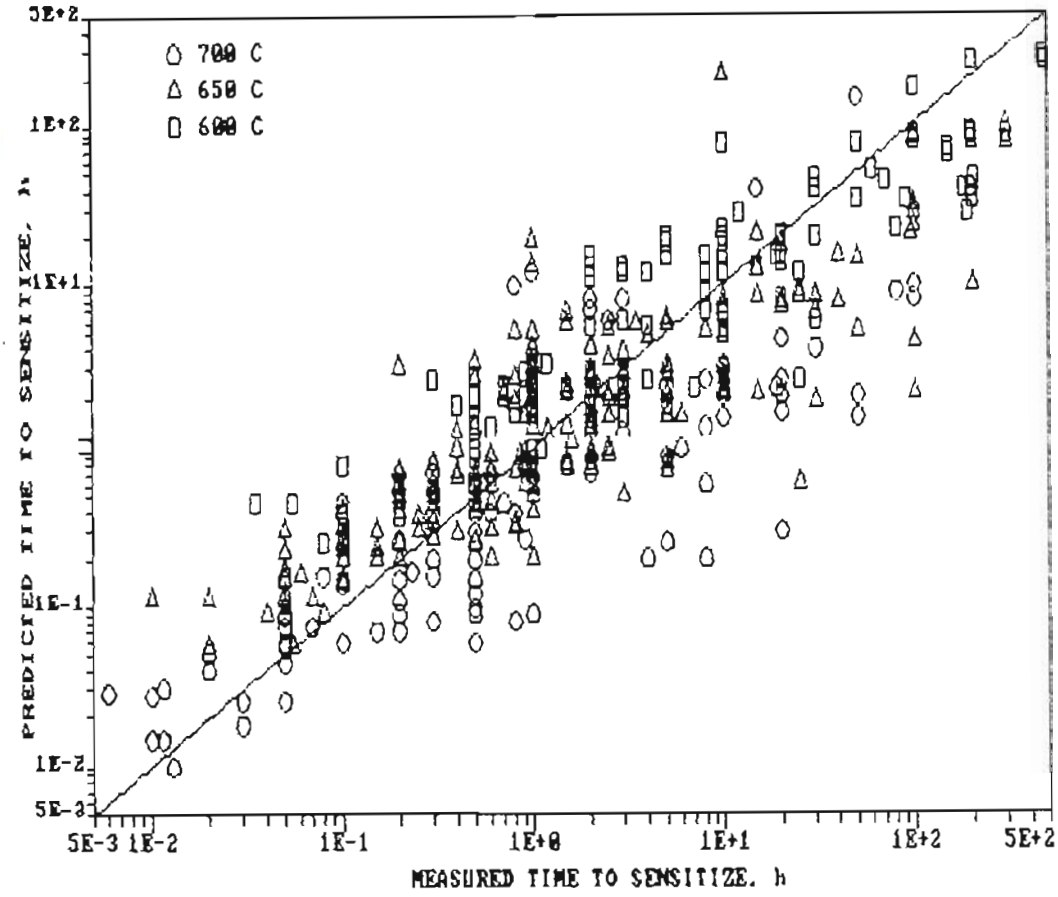

FIGURE 79. Summary of Measured and Predicted Times-to-Sensitize for Type 304 and 316 Stainless Steels Based on EPR and Modified Strauss Test Results.

5.2.2 Continuous Cooling Sensitization

SSDOS predictions of continuous cooling sensitization will not be examined in the same detail as was done for isothermal sensitization. The primary reason for this reduced analysis stems from the limited data base for continuous cooling heat treatments and quantitative measurements. Some initial correlations related to maximum temperature effects were presented in Section 5.1.6. Specific examples of SSDOS predictive capabilities will be shown here and analyzed to determine if the model's quantitative nature can be extended to more complex thermal treatments.

The effect of maximum temperature and cooling rate on measured and predicted EPR-DOS values is demonstrated for high-carbon Type 304 and 316 stainless steels in Figures 80 and 81, respectively. Predictions match the general shape of the curves, the magnitude of EPR-DOS and the position of individual curves with respect to the specimen's maximum temperature. For both heats, identical curves are predicted for maximum temperatures between 900 and 950°C. This behavior was explained in Section 5.1.6 and shown in Figure 68. Material condition changes at high temperatures prompt the slight reduction in predicted EPR-DOS for a maximum temperature of 1000°C and the large decrease observed in Figures 80(b) and 81(b).

Several differences can be recognized between measured and predicted EPR-DOS in these figures. The SS-7 data shows a convex shape as a function of cooling rate versus the slightly concave shape predicted by SSDOS. In other words, measured EPR-DOS is larger than

(a)

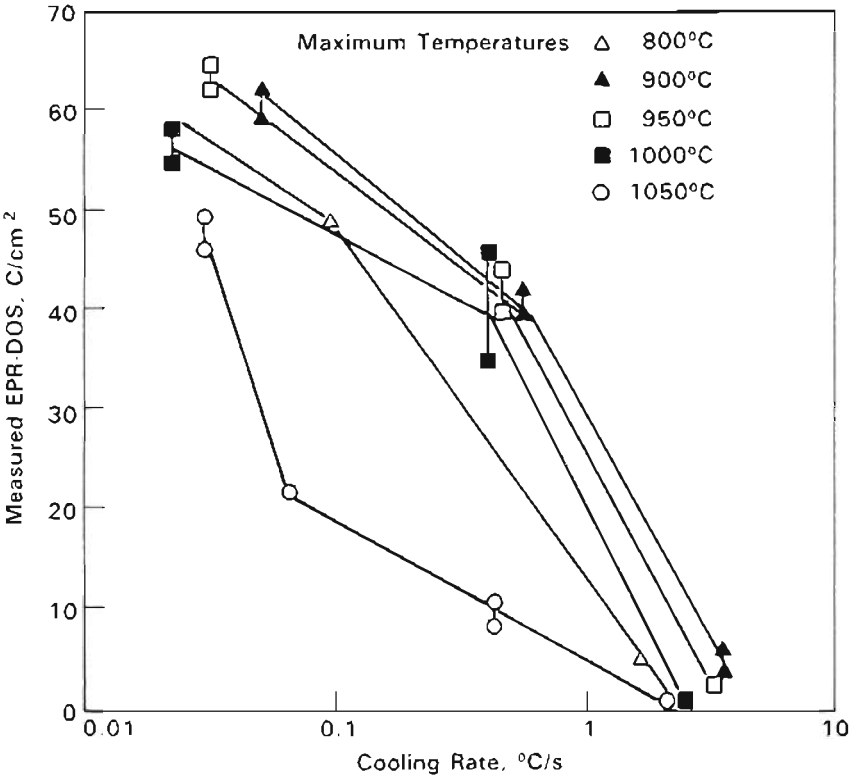

(b)

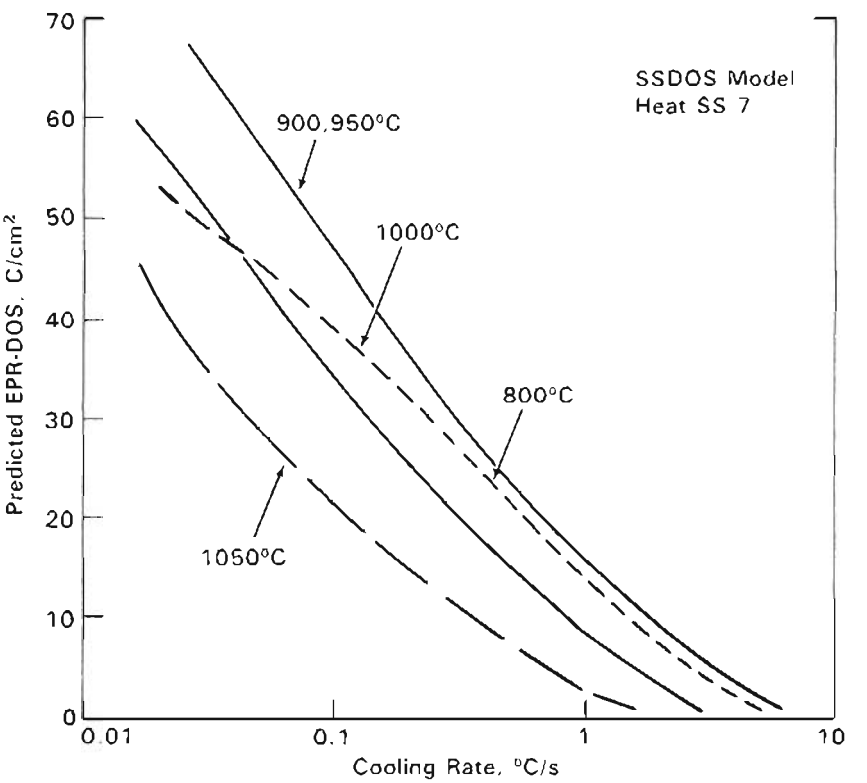

FIGURE 80. Measured (a) and Predicted (b) Continuous Cooling Sensitization Development for a High-Carbon Type 304 Stainless Steel as a Function of Cooling Rate from Several Maximum Temperatures.

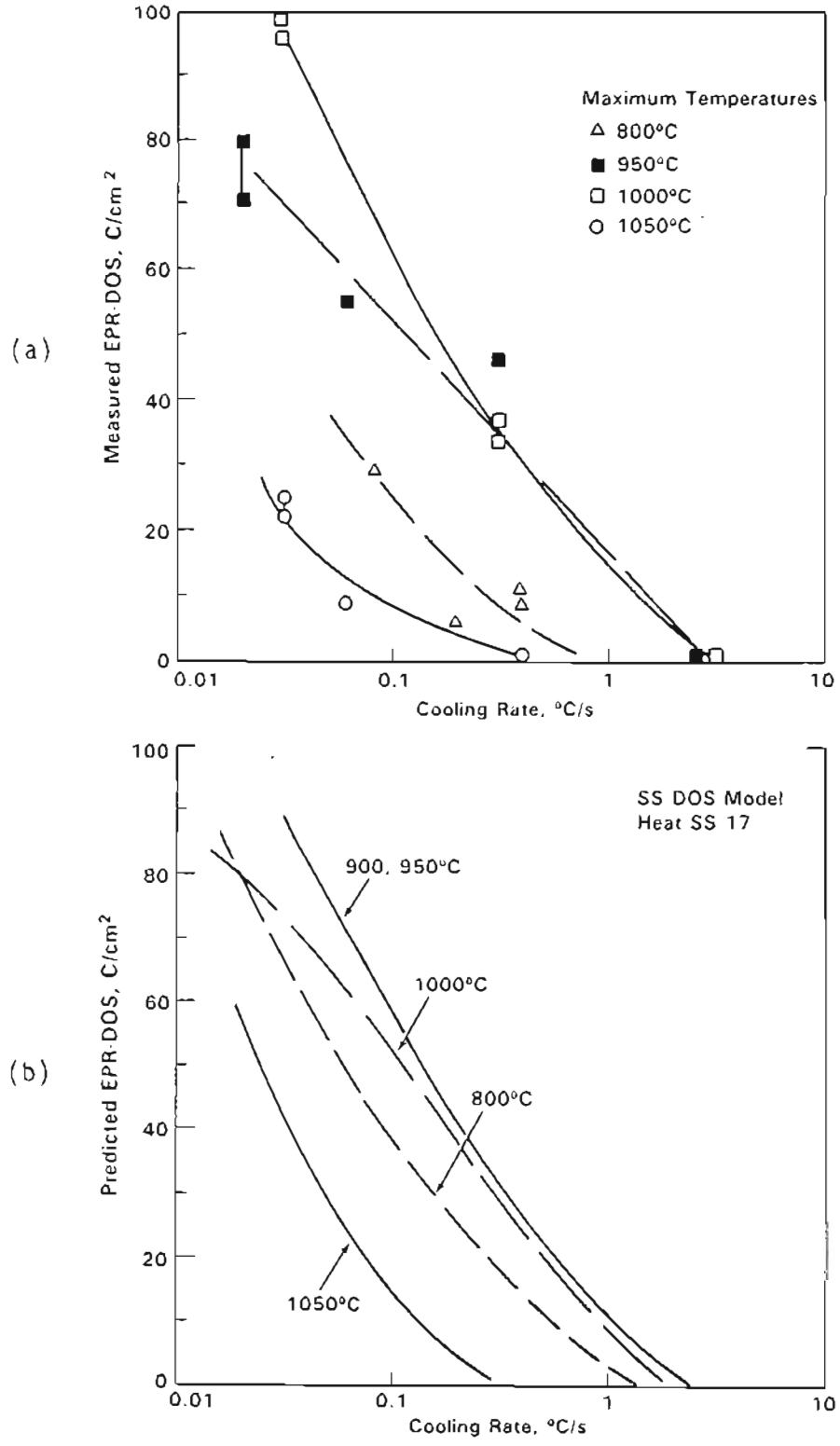

FIGURE 81. Comparison Between Measured (a) and Predicted (b) Continuous Cooling Sensitization for a High-Carbon Type 316 Stainless Steel.

predicted for the moderate cooling rates (~0.5°C/s). This is not the case for the 1050°C maximum temperature where measured and predicted EPR-DOS values are quite similar for the SS-17 data set. Predictions overestimate EPR-DOS at 800°C for the Type 316 heat as indicated in Figure 81. Such a difference may result from ignoring carbide nucleation kinetics in the continuous cooling predictions.

Aside from the inconsistencies noted above, a good match between measured and predicted continuous cooling sensitization can be seen. The overall predictive capability of SSDOS can be assessed by integrating the EPR-DOS measurements and predictions into a single diagram. This data is summarized in Figure 82 relative to a one-to-one fit. Quantitative continuous cooling sensitization data shows a larger scatter than that for the isothermal results (Figure 76). In addition, it appears that Type 316 data tends to be overpredicted (primarily due to 800°C maximum temperature tests), while Type 304 appears to be overpredicted at moderate EPR-DOS and perhaps underpredicted at large EPR-DOS. However, these differences must be kept in context considering the data base available. With this in mind, good agreement is demonstrated in Figure 82 and suggests that SSDOS can be quantitatively used to predict continuous cooling sensitization.

5.2.3 Weldment Heat Affected Zone Sensitization

A final example of SSDOS predictive capability will be demonstrated by analysis of EPR-DOS measurements on, and predictions for,

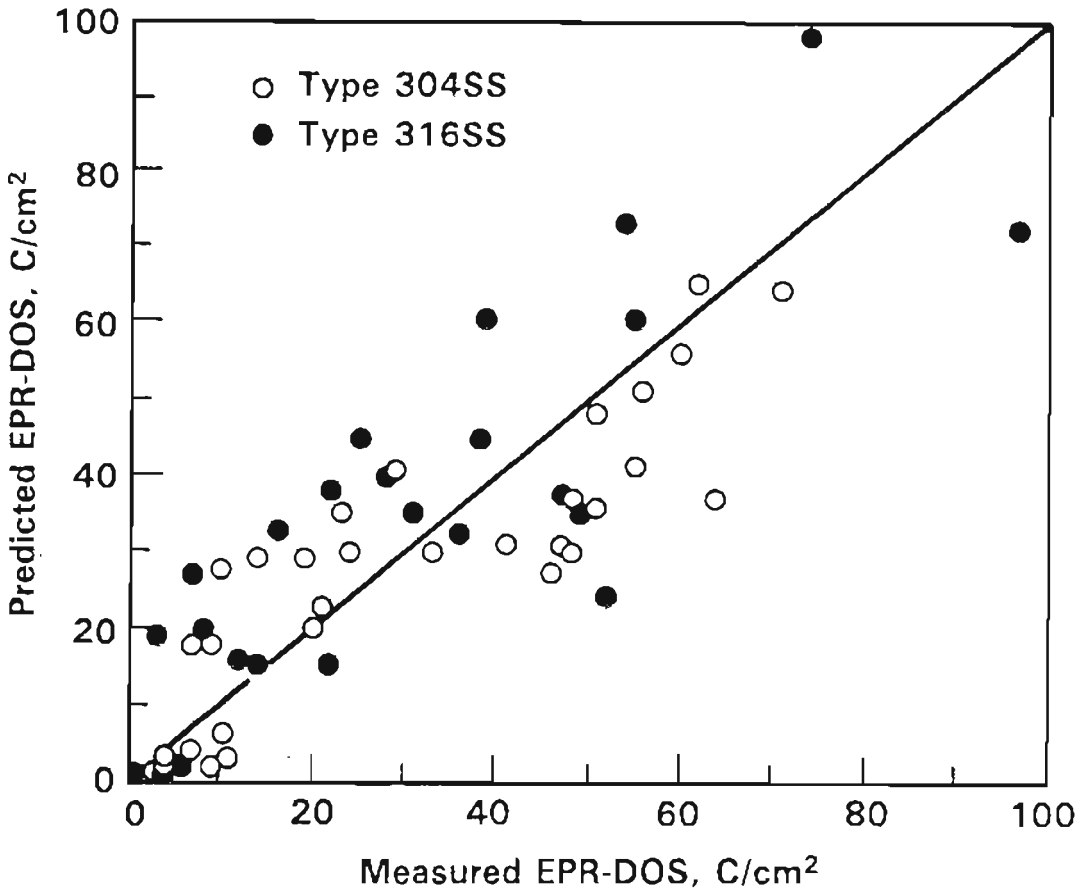

FIGURE 82. Summary of Measured and Predicted EPR-DOS Values for Continuous Cooling Thermal Treatments.

an instrumented, 61-cm-dia. pipe weld. Details of the HAZ measurements performed on a pass-by-pass basis were described in Section 4.6. Sensitization development as a function of distance through the HAZ was presented in Figure 53.

HAZ thermomechanical history was collected using a computer-based data retrieval and analysis system. Temperature and displacement information was obtained from a series of sensors placed at selected locations in the HAZ. Information was collected dynamically

allowing detailed thermomechanical histories to be recorded on a pass-by-pass basis. Additional specifics concerning the HAZ measurement techniques have been reported elsewhere.[7,142,143]

Thermal history from HAZ thermocouples was compiled during heating and cooling for each sensor location and input for model predictions. Separate heat-up and cool-down cycles were included for each pass along with a short isothermal hold-time near the maximum temperature. This hold-time was important to account for the transition region of the temperature-time curves going from heat-up to cool-down. Heating and cooling rates input into SSDOS were estimated from measured rates between 800 and 600°C. As the maximum temperatures dropped below 800°C, rates were determined from the maximum temperature to 600°C.

Predicted sensitization on a pass-by-pass basis is shown in Figure 83(a), and is calculated from the inputted HAZ thermal history. EPR-DOS gradually increases during the first five passes and then effectively saturates. The HAZ location that shows the largest DOS is initially about 0.6 cm from the weld centerline and moves slightly closer in as additional passes are predicted. Final location appears to be between 0.5 and 0.6 cm from the centerline. Data points in Figure 83(a) refer to the thermocouple locations where thermal history was measured.

Pass-by-pass sensitization data can be directly compared to the measured EPR-DOS data from Figure 53. The small-probe data is reproduced in Figure 83(b) to facilitate this assessment. Good agreement

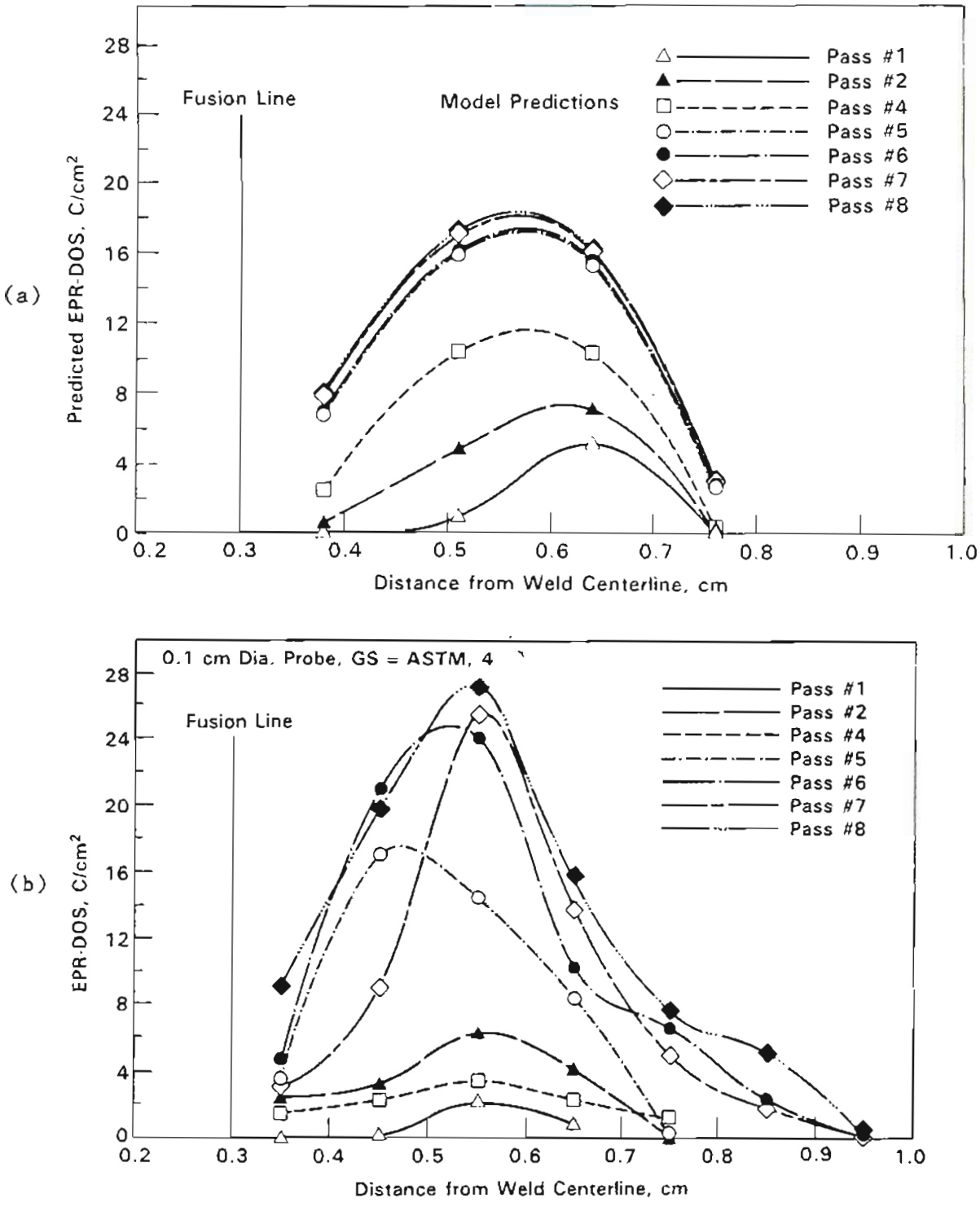

FIGURE 83. Sensitization Development in the HAZ of a Type 304 Stainless Steel Pipe Weldment: (a) SSDOS Predictions Based on Measured Thermal History and (b) Measured EPR-DOS.

is found for the location of the maximum EPR-DOS and in the shape of the DOS versus HAZ location curves. However, significant differences are observed when comparing the magnitude of the EPR-DOS values. Final EPR-DOS is measured at about 26 C/cm^2 versus a predicted value of less than 15 C/cm^2. This difference would be even greater if the model did not overpredict sensitization during the initial passes.

Overprediction of sensitization during the first passes may reflect the need for carbide nucleation to be considered in the continuous cooling prediction. The final underprediction of EPR-DOS is to be expected since deformation effects have been neglected for the calculations in Figure 83(a). Strain gage measurements[7,143] documented a complex plastic deformation history within the HAZ. Plastic strains up to 9% were produced in the HAZ during the first eight weldment passes. As a result, HAZ will experience simultaneous deformation during each pass and will accumulate prior deformation from previous passes.

The empirical correlations developed for deformation effects described in Section 5.1.5 are used to approximate the HAZ situation. If a prestrain or simultaneous strain of 3% per pass is input into SSDOS during the first six passes, final EPR-DOS levels reach values comparable to those measured. Predictions and maximum EPR-DOS measurements are presented in Figure 84. The intent here is not to

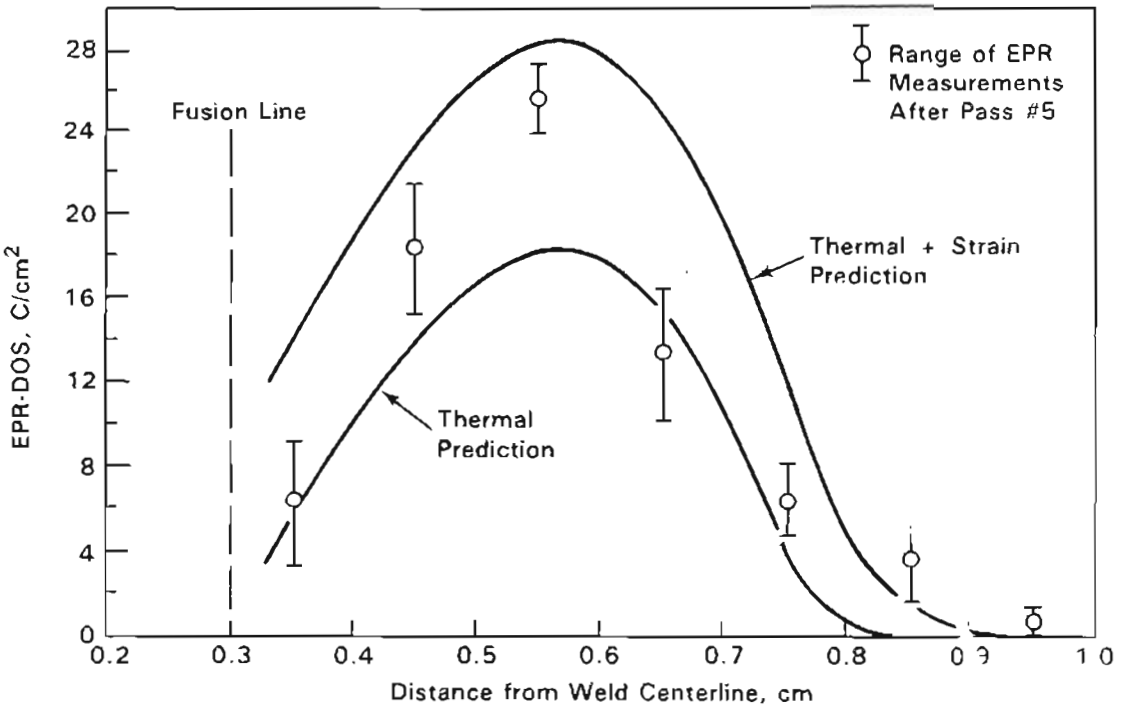

FIGURE 84. Comparison of Measured and Predicted HAZ Sensitization in the 61-cm-dia., Schedule 80, Pipe Weldment.

indicate that the present model can quantitatively predict HAZ sensitization. However, good predictions of stainless steel sensitization can be made even after complex thermomechanical treatments if accurate input information is available.

5.3 FUTURE RESEARCH REQUIREMENTS

The current work addresses a critical aspect concerning structural reliability of stainless steels, i.e., sensitization. An ability to quantitatively measure and model sensitization development after simple thermal treatments has been documented. In addition, preliminary results show promise that more complex, thermomechanical treatments can be predicted. Future research requirements center on

the understanding and modeling of these more complex (and practical) treatments on sensitization and a need to expand measurement and modeling into other areas of microstructural development.

Although sensitization phenomena have been studied extensively over the last 50 years, effects of complex thermal and thermomechanical treatments are not understood. Examples of this are reflected in the current work, for example, maximum temperature effects on continuous cooling sensitization and deformation effects on isothermal sensitization. Deformation appears to be a critical aspect which requires detailed examination. It was shown to induce grain boundary migration, a change in carbide morphology and a dramatic increase in chromium depletion. Direct experiments using analytical techniques are needed to isolate deformation effects on both kinetic and thermodynamic phenomena related to sensitization development.

Sensitization is not the only microstructural/microchemical feature which impacts structural reliability of stainless steel, particularly as it pertains to welded components. Deformation itself induces a significant change in microstructure through the matrix and grain boundary dislocation density. Dislocation density and structure can influence susceptibility to environmental degradation, e.g., SCC. This aspect may be more important in the extra-low-carbon, nuclear-grade stainless steels where sensitization is extremely unlikely under practical circumstances.

Another microchemical characteristic that can impact stainless steel structural reliability is grain boundary impurity segregation.

Very little quantitative information has been documented in this area. Impurities such as phosphorus and sulfur have received the most attention, but few direct links between segregation and cracking or between thermal or thermomechanical history and the extent of segregation have been made. Impurity segregation appears to be primarily responsible for irradiation-assisted SCC and may be a critical factor in determining environmental degradation resistance of the nuclear-grade stainless steels.

Each of the aspects identified above plays an essential role in structural reliability assessment of stainless steels and their weldments. Mechanistic studies are required to evolve the fundamental understanding necessary to model microstructural and microchemical development and resultant fracture resistance. Basic understanding must then be tested using a quantitative data base to properly develop, evaluate and verify the modeling capability.

6.0 SUMMARY AND CONCLUSIONS

Three interrelated areas were examined in this work dealing with the quantitative measurement and modeling of sensitization development in austenitic stainless steels. Significant results were obtained in each area leading up to the evolution of a unique model for DOS assessment. This work clarifies and quantifies many phenomenological and mechanistic aspects of sensitization. Several of the more important observations are summarized below.

Quantitative Measurement of Sensitization

- Chromium depletion characteristics were determined as a function of thermal and thermomechanical history by analytical electron microscopy.
- Grain boundary chromium minimums decreased with decreasing heat treatment temperature and increased with increasing time at any temperature.
- Attack in the EPR test depends on the extent of chromium depletion, i.e., width and depth of the depleted zone.
- Chromium must be depleted below about 13.5 wt% in Type 304 and 316 stainless steels for attack in the EPR test.
- A good correlation between the width or the volume of the depleted region (measured by AEM) and DOS (measured by EPR)

was documented. The best correlation was for volume depletion below 13.5 wt% versus EPR-DOS.

- The EPR test effectively determined stainless steel DOS over a full range of conditions including low and high levels of sensitization and desensitization.
- Chromium depletion controlled the susceptibility of Type 304 stainless steel to IGSCC in high-temperature water environments. Crack growth rate, percent IG fracture and overall ductility all could be directly related to the grain boundary chromium concentration. EPR measurements also accurately reflected cracking susceptibility.

Quantitative Data Base Development

- Sensitization development was mapped as a function of isothermal heat treatment for more than 30 stainless steel heats.
- Carbon content was the primary compositional variable controlling sensitization response. Molybdenum was also shown to have a significant effect by decreasing sensitization kinetics and increasing temperatures where sensitization will occur.
- Extended heat treatments at 600 or 650°C can promote severe sensitization even in extra-low carbon materials such as Type 316NG.

- Nitrogen additions to Type 316L heats are beneficial or have little effect at levels up to about 0.15 wt%. Additions above about 0.20 wt% appear to accelerate sensitization due to the presence of Cr_2N precipitates at grain boundaries.
- Sensitization development during a continuous cooling heat treatment depend on maximum temperature and cooling rate.
- Cooling rates above about 3°C/s did not produce a measurable EPR-DOS after a single thermal cycle even in high-carbon Type 304 heats.
- A large decrease in sensitization was observed in high-carbon Type 304 and 316 heats after continuous cooling for a maximum temperature of 1050°C versus lower maximum temperatures (800 to 1000°C).
- Prior or simultaneous deformation greatly accelerates sensitization development at 600°C. The rate of acceleration scaled with deformation rate at 1, 3, and 6% strain/h.
- Deformation influences carbide growth processes and promotes grain boundary migration which produces asymmetric chromium depletion profiles.
- Sensitization development in the inside surface of a 61-cm-dia., Schedule 80, Type 304 pipe weld HAZ was mapped on a pass-by-pass basis. EPR-DOS increased rapidly through pass Number 6 and did not significantly change as a result of the remaining 29 passes.

- Maximum DOS was found at a distance 0.5 to 0.6 cm from the weld centerline and 0.2 to 0.3 cm from the fusion line. The maximum EPR-DOS value measured was about 28 C/cm^2.
- Sensitization measurements reported in the literature were reviewed and organized. Quantitative data for more than 100 stainless steel heats were extracted including times-to-sensitize to enable proper evaluation of model predictions.

Quantitative Modeling of Sensitization Development

- A theoretically-based, empirically-modified model, SSDOS, has been developed which allows prediction of DOS as a function of material composition, initial condition and thermomechanical history.
- Individual parts of the model were evolved by direct assessment of available experimental data. For example, relationships to determine interfacial chromium concentrations were based on the thermodynamics of $M_{23}C_6$ carbide formation, but modified to fit chromium minimum measurements. Similar approaches were taken to account for carbide nucleation kinetics and desensitization.
- The integration of theoretical and empirical components enables a quantitative prediction of DOS. Excellent correlations were documented between measured and predicted DOS after isothermal and continuous cooling heat treatments.

- Good agreement was also observed when predicting thermomechanical history effects on sensitization development. Preliminary results suggest that prior and simultaneous deformation effects can be estimated through the use of an effective chromium diffusivity.
- Initial attempts demonstrated that HAZ sensitization can be predicted if the detailed thermomechanical history is known.

The present work represents a departure from the traditional approaches to study sensitization phenomena. Sensitization is examined, analyzed and modeled in a quantitative manner which significantly improves the current state-of-the-art understanding. This is a first step toward a viable assessment of microstructural development and structural reliability in stainless steel weldments.

7.0 REFERENCES

1. E.C. Bain, R.H. Aborn and J.J.B. Rutherford, Trans. Amer. Soc, Steel Treating, 21, 481 (1933).
2. NRC Pipe Crack Study Group, "Investigation and Evaluation of Stress Corrosion Cracking in Piping of BWR Plants," U.S. Nuclear Regulatory Commission Reports: NUREG-75/067 (1975), NUREG-0531 (1979), and NUREG-1061 (1984).
3. J.C. Danko, CORROSION/84, Paper No. 162, National Association of Corrosion Engineers, 1984.
4. M.E. Taylor, Nucl. Eng. Des., 69, 223 (1982).
5. Proc. Seminar on Countermeasures for Pipe Cracking in BWRs, ed. J.C. Danko, Electric Power Research Institute Reports: WS-79-174 (198) and NP-3684-S4 (1984).
6. S.M. Bruemmer, L.A. Charlot and D.G. Atteridge, "Compositional Effects on the Sensitization of Austenitic Stainless Steels," NUREG/CR-3918, U.S. Nuclear Regulatory Commission, 1984.
7. D.G. Atteridge and S.M. Bruemmer, "Evaluation of Welded and Repair-Welded Stainless Steel for LWR Service," U.S. Nuclear Regulatory Commission Reports: NUREG/CR-3806, Vol. 1 (1984), Vol. 2 (1985) and Vol. 3 (1986).
8. W.J. Shack, "Environmentally-Assisted Cracking in Light Water Reactors," U.S. Nuclear Regulatory Commission Reports: NUREG/CR-3806 (1984) and NUREG/CR-4287 (1985).
9. M. Fox, J. Mat. Energy Syst., 1, 3 (1979).

10. F.A. Nichols, "Mechanistic Aspects of Stress Corrosion Cracking of Type 304 Stainless Steel in LWR Service," NUREG/CR-3220, U.S. Nuclear Regulatory Commission, 1983.

11. NRC Inspection and Enforcement Bulletin 82-03, "Stress Corrosion Cracking in Large Diameter Stainless Steel Recirculation System Piping at BWR Plants," U.S. Nuclear Regulatory Commission, March 1983.

12. P.L. Andresen, H.F. Solomon and D.F. Taylor, "Basic Studies on the Variabilities of Fabrication-Relation Sensitization Phenomena in Stainless Steels," NP-1823, Electric Power Research Institute, 1981.

13. F.P. Ford, D.F. Taylor and M.E. Indig, "Mechanisms of Environmental Cracking in Systems Peculiar to the Power Generation Industry," NP-2587, Electric Power Research Institute, 1982.

14. R.L. Cowan and G.M. Gordon, in Proc. Conf. Stress Corrosion Cracking and Hydrogen Embrittlement, National Association of Corrosion Engineers, p. 1025, 1977.

15. S. Szklarska-Smialowska and G. Cragnolino, Corrosion, 36(12), 653 (1980).

16. H.E. Hanninen, Int. Metals Review, 3, 85 (1979).

17. Proc. Conf. Predictive Methods for Assessing Corrosion Damage to BWR Piping and PWR Steam Generators, ed. H. Okada and R.W. Staehle, National Association of Corrosion Engineers, 1982.

18. R.M. Latanision and R.W. Staehle, in Proc. Fundamental Aspects of Stress Corrosion Cracking, National Association of Corrosion Engineers, p. 214, 1969.

19. H.H. Klepfer, "Investigation of Cause of Cracking in Austenitic Stainless Steel Piping," NEDC 21000-1, General Electric Company, 1975.

20. V. Cihal, "Intergranular Corrosion of Steels and Alloys," Materials Science Monograph No. 18, Elsevier Publishing Co., New York, 1984.

21. J.K.L. Lai, Mat. Sci. Eng., 61,101 (1983).

22. R. Stickler and A. Vinckier, Trans. ASM, 54, 362 (1961).

23. B. Weiss and R. Stickler, Metall. Trans., 3, 851 (1972).

24. T.M. Divine, Trans. ASM, 11A, 791 (1980).

25. K. Natesan and T.F. Kassner, Nucl. Technol., 19, 46 (1973).

26. E.F. Petrova and I.A. Shvartsmen, Zh. Fiz. Khim., 46, 1980 (1972).

27. M. Deighton, J. Iron Steel Inst., London, 208, 1012 (1970).

28. V. Cihal and I. Kasova, Corr. Sci., 10, 875 (1969).

29. L.K. Singhal and J.W. Martin, Trans. AIME, 242, 814 (1968).

30. L.K. Singhal, Metall. Trans., 2, 1267 (1971).

31. S. Lartique and L. Priester, 31(11), 1809 (1983).

32. R.A. Varin, J. Mat. Sci., 14, 811 (1979).

33. R.B. Leonard, Corrosion, 25, 222 (1969).

34. V. Mararik and V. Cihal, Werkst. Korros., 25, 330 (1974).

35. C.B. Schmidt, R.D. Caligiuri, L.E. Eiselstein, S.S. Wing and D. Cubicciotti, Metall. Trans., 18A, 1483 (1987).

36. G. Grutzner, Stahl. Eisen., 93, 9 (1973).

37. J.J. Eckenrod and C.W. Kovach, in Proc. Properties of Austenitic Stainless Steels and Their Weld Metals, ASTM-STP 679, p. 7, 1979.

38. W.O. Binder, C.M. Brown and R. Franks, Trans. ASM, 41, 1301 (1949).

39. C.L. Briant, Corrosion 38(9), 468 (1982).

40. T.A. Mozhi, W.A.T. Clark, K. Nishiomoto, W.B. Johnson and D.D. Macdonald, Corrosion, 41(10), 555 (1985).

41. H.S. Betrabet, K. Nishiomoto, B.E. Wilde and W.A.T. Clark, Corrosion, 43(2), 77 (1987).

42. E.Z. Dullis, ISI Special, 86, 162 (1964).

43. C.L. Briant and A.M. Ritter, Metall. Trans., 11A, 2009 (1980).

44. C.L. Briant and A.M. Ritter, Metall. Trans., 12A, 910 (1981).

45. C.L. Briant, Corrosion, 38(11), 596 (1982).

46. M.G. Lackey, "Intergranular Stress Corrosion Cracking of Sensitized Austenitic Stainless Steel," Phd Dissertation, University of London, 1980.

47. M.G. Lackey and F.J. Humphreys, in Proc. Hydrogen Effects in Metals, ed. I.M. Bernstein and A.W. Thompson, TMS-AIME, p. 665, 1980.

48. H.E. Hanninen, T. Purra and J. Hakala, in Proc. 7th Int. Congr. on Metallic Corrosion, ABRACO, Rio de Janeiro, 1978.

49. C. Wagner, "Thermodynamics of Alloys," Addison-Wesley, Reading, Massachusetts, p. 51, 1952.

50. C.S. Tedmon, Jr., D.A. Vermilyea and J.H. Rosolowski, J. Electrochem. Soc., 118, 192 (1971).

51. R.L. Fullman, Acta Met., 30, 1407 (1982).

52. R.L. Fullman, ibid 5, Paper No. 6.

53. G.S. Was and R.M. Kruger, Acta Met., 33(5), 841 (1985).

54. F. Kohler, Monatsh. Chem., 91, 738 (1960).

55. L. Kaufman and H. Nesor, Z. Metallk., 64, 249 (1973).

56. M. Haseke and T. Nishizawa, in Proc. Appl. of Phase Diagrams in Metallurgy and Ceramics, ed. G.C. Carter, NBS Special Publ. 496, p. 911, 1978.

57. C. Stawstrom and M. Hillert, J. Iron Steel Inst., 77 (1969).

58. K. Arioka, M. Hourai, S. Nocuchi and K. Onimura, CORROSION/83, Paper No. 134, National Association of Corrosion Engineers, 1983.

59. R.B. Snyder, K. Nateson and T.F. Kassner, Argonne National Laboratory Report, ANL-8015, 1973.

60. R.W. Logan, "Computer Simulation of Sensitization in Stainless Steels," UCID-20000, Lawrence Livermore National Laboratory, 1983.

61. P.J. Grobner, Metall. Trans., 4, 251 (1973).

62. J.W. Christian, "The Theory of Transformations in Metals and Alloys," Pergamon Press, Oxford, pp. 178 and 620, 1965.

63. R. Becker, Ann. Phys., 32, 128 (1938).

64. R. Pascali, A. Benvenuti and D. Wenger, Corrosion, 40(1), 21 (1984).

65. R.J. Bendure, Trans. AIME, 221, 1032 (1961).

66. D. Sinigaglia, P. Fassina, D. Wenger and G. Re, Corrosion, 38(2), 92 (1982).

67. S. Shimodaira, in Proc. Passivity and Its Breakdown in Iron Base Alloys, National Association of Corrosion Engineers, p. 38, 1976.

68. Z. Szklarska-Smialowska and N. Lukonski, Corrosion, 34, 177 (1978).

69. K. Osozawa and H.J. Engell. Corr. Sci., 6, 389 (1966).

70. I. Aho-Mantila and H. Hanninen, in Proc. 9th Scand. Corr. Congr., Helsinki, p. 61, 1984.

71. M.E. Indig, B.M. Gordon, R.B. Davis and J.E. Weber, in Proc. 2nd Int. Sym. on Env. Deg. of Mat. in Nuclear Power Systems-Water Reactors, American Nuclear Society, p. 411, 1986.

72. B. Rosborg and A. Molander, ibid, p. 419.

73. D.D. Macdonald and G. Cragnolino, ibid, p. 426.

74. K. Osozawa, K. Bohnenkampf and M.J. Engell, Corr. Sci., 6, 421 (1966).

75. A. Desestret, "Contribution a' l' etude de la transpassivite des aciers inoxydables," PhD Dissertation, University of Paris, 1964.

76. J.S. Armijo, "Grain Boundary Studies of Austenitic Stainless Steels," GEAP-5503, General Electric Co., 1967.

77. B. Vyas and H. Isaacs, in Proc. Intergranular Corrosion of Stainless Steels, ed. R.F. Steigerwald, ASTM STP 656, American Society for Testing of Materials, p. 133, 1978.

78. I. Olefjord, Mat. Sci. Eng., 42, 161 (1980).

79. A.E. Yaniv, J.B. Lumsden and R.W. Staehle, J. Electrochem. Soc., 124(4), 490 (1979).

80. V. Cihal and M. Prazak, J. Iron Steel Inst., 193, 360 (1959).

81. A.R. Perrin and K.T. Aust, Mat. Sci. Eng., 51, 165 (1980).

82. W.J. Schwerdtfeger, Corrosion, 19(1), 17 (1963).

83. C.L. Briant, Metall. Trans., 18A, 691 (1987).

84. C.L. Briant, Scripta Met., 21, 71 (1987).

85. P.L. Andresen and C.L. Briant, in Proc. 3rd Int. Conf. Deg. of Mat. in Nuclear Power Ind., Traverse City, Mississippi, TMS-AIME, in press.

86. J.B. Lumsden and P.J. Stocker, Scripta Met., 15, 1295 (1981).

87. A. Joshi and D.F. Stein, Corrosion, 28, 321 (1972).

88. W. Losch and I. Andreoni, Scripta Met., 12, 227 (1978).

89. H. Hanninen and E. Minni, Metall. Trans., 13A, 2281 (1982).

90. S. Danyluk and J.Y. Park, Scripta Met., 16, 769 (1982).

91. C.L. White, R.A. Padgett and R.W. Swindeman, Scripta Met., 15, 777 (1981).

92. S.M. Bruemmer and C.H. Henager, Jr., ibid 71, p. 293.

93. S.M. Bruemmer, L.A. Charlot and C.H. Henager, Jr., "Microstructure, Microchemistry and Microdeformation of Alloy 600 Tubing," NP-4465, Electric Power Research Institute, 1986.

94. E.L. Hall and C.L. Briant, Metall. Trans., 16A, 1225 (1985).

95. M. Guttman, P.H. Dumunlin, N. Tan-Tai and P. Fontaine, Corrosion, 37, 416 (1981).

96. C.S. Was, H.H. Tischner and R.M. Latanision, Metall. Trans., 12A, 1937 (1981).

97. T.S.F. Lee, PhD Dissertation, Massachusetts Institute of Technology, 1982.

98. G.P. Airey, Metallography, 37, 21 (1980).

99. G.P. Airey, "Optimization of Metallurgical Variables to Improve Corrosion Resistance of Inconel Alloy 600," NP-3051, Electric Power Research Institute, 1983.

100. G.S. Was and J.R. Martin, Metall. Trans., 16A,349 (1985).

101. H. Okada, S. Abe, M. Kojima and Y. Hosai, ibid 48.

102. R.H. Jones, ibid 71, p. 173.

103. J.L. Brimhall, D.R. Baer and R.H. Jones, J. Nucl. Mat., 122/123, 196 (1984).

104. K. Nakata, I. Masaoka, Y. Katano and K. Shiraishi, Annual Meeting of Japan Inst. of Metals, Sept., 1984.

105. ASTM Book of Standards, Section 1, A262-81, American Society for Testing of Materials, Philadelphia, PA, p. 66, 1984.

106. ASTM Bulletins No. 188 (1953) and 195 (1954), American Society for Testing of Materials, Philadelphia, PA.

107. M.H. Brown, Corrosion, 30(1), 1 (1974).

108. L.A. Medvedeva, V.M. Knyzheva, Y.M. Kolotyrkin and S.G. Babich, Prot. Met., 12(7), 655 (1976).

109. L.A. Shapiro, V.M. Knyzheva, L.S. Saverina and A.B. Lamin, Prot. Met., 13(3), 229 (1977).

110. S. Pednekar and S. Smialowska, Corrosion, 36(10), 565 (1980).

111. P. Chung and S. Szklarska-Smialowska, Corrosion, 37(1), 39 (1981).

112. F. Duffaut, J.P. Pouzet and P. Lacombe, Corr. Sci., 6, 83 (1966).

113. P. Novak, R. Stefec and F. Franz, Corrosion, 31(10), 344 (1975).

114. W.L. Clarke, "The EPR Method for the Detection of Sensitization in Stainless Steels," NUREG-0251-1, U.S. Nuclear Regulatory Commission, 1976.

115. W.L. Clarke, V.M. Romero and J.C. Danko, CORROSION/77, Paper No. 180, National Association of Corrosion Engineers, 1977.

116. W.L. Clarke, R.L. Cowan and W.L. Walker, ibid 77, p. 99.

117. J. Backman and T. Purra, in Proc. 8th Scand. Corr. Congr., Helsinki, Vol. I, p. 1, 1978.

118. V. Cihal, Scand. J. Met., 9, 37 (1980).

119. V. Cihal, Corr. Sci., 20, 737 (1980).

120. M. Akaski, T. Kawamoto and F. Umemura, Corr. Eng. (Jpn), 29, 163 (1980).

121. F. Umemura, Y. Hanai and T. Kawamoto, IHI Eng. Review, 6(2), 1 (1983).

122. A.P. Majidi and M.A. Streicher, Corrosion, 40(8), 393 (1984).

123. A.P. Majidi and M.A. Streicher, Corrosion, 40(11), 585 (1984).

124. A.P. Majidi and M.A. Streicher, CORROSION/85, Paper No. 65, National Association of Corrosion Engineers, 1985.

125. S.M. Bruemmer, CORROSION/87, Paper No. 185, National Association of Corrosion Engineers, 1987.

126. V. Cihal, "Intergranular Corrosion of Cr-Ni Stainless Steel," Unieux Conference, May 1969.

127. S.M. Bruemmer, Corrosion, 42(1), 27 (1986).

128. R.A. Mulford, E.L. Hall and C.L. Briant, Corrosion, 39(4), 132 (1983).

129. T. Thorvaldsson and G.L. Dunlop, J. Mat. Sci., 18, 793 (1983).

130. A. Henjered, H. Norden, T. Thorvaldsson and H.O. Andren, Scripta Met., 17, 1275 (1983).

131. C.L. Briant and E.L. Hall, Corrosion, 42(9), 522 (1986).

132. C.L. Briant, C.S. O'Toole and E.L. Hall, Corrosion, 42(1), 15 (1986).

133. R.M. Kruger, S.F. Claeys and G.S. Was, Corrosion, 41(9), 504 (1985).

134. S.M. Bruemmer and L.A. Charlot, Scripta Met., 20, 1019 (1986).

135. S.M. Bruemmer, L.A. Charlot, M.T. Thomas and R.H. Jones, "Grain Boundary Composition and Intergranular Fracture of Steels," NP-3859, Vol. 1, Electric Power Research Institute, 1985.

136. G.S. Was and R.B. Ballinger, Semi-Annual Progress Report, NP-4613, Electric Power Research Institute, 1980.

137. G.S. Was and V.B. Rajan, Corrosion, 43, 576 (1987).

Welding Research, ed. S. David, Gatlinburg, TN, 1986.

143. W.L. Clarke and D.C. Carlson, Mat. Perform., March, 16 (1980).

144. C.D. Lundin, E.E. Stansbury, C.H. Lee and R. Menon, "HAZ Sensitization of Austenitic Stainless Steels," Welding Research Council, Dec. 1985.

145. F. Umemura and T. Kawamoto, ibid 17, p. 209.

146. H.D. Solomom, Corrosion, 36(7), 356 (1980).

APPENDIX A

SSDOS MODEL LISTING

SSDOS MODEL LISTING

```
10 PRINT:PRINT "                PROGRAM SSDOS  *  Version VB - September 1987"
20 PRINT:PRINT "                                Contact S.M.Bruemmer "
30 PRINT "                    Battelle Pacific Northwest Laboratory"
40 PRINT "                P.O.Box 999, Richland, WA      (509) 376-0636"
50 PRINT
60 PRINT "     This program enables the prediction of microstructural developmen
t"
70 PRINT "     and stress corrosion cracking resistance in an austenitic stainle
ss"
80 PRINT "     steel (Type 304 or 316) as a function of a 'user specified' therm
al or"
90 PRINT "     thermomechanical history. Information concerning material composi
tion,"
100 PRINT "     initial condition and time/temperature/deformation history must
be"
110 PRINT "     input. Time/temperature history in the heat affected zone can be
 calcu-"
120 PRINT "     lated and deformation history estimated from 'user specified' we
ld"
130 PRINT "     parameters in a separate program.  At present, microstructural d
evel-"
140 PRINT "     opment predictions are limited to quantitative degree of sensiti
zation"
150 PRINT "     (chromium depletion and EPR measured DOS) at this time.  Model"
160 PRINT "     development is part of a project sponsored by the Materials Engi
neering"
170 PRINT "     Technology Division of the Nuclear Regulatory Commission (Monito
r:  J."
180 PRINT "     Muscara).  This is a preliminary version of the microstructural
devel-"
190 PRINT "     opment prediction model and is not for general release.  Comment
s on"
200 PRINT "     its use and suggestions for improvements will be appreciated."
210 PRINT:PRINT
220 INPUT "          HIT RETURN FOR MICROSTRUCTURAL DEVELOPMENT PREDICTION MENU
 ",IIMENU
230 CRI=13.5:R=1.987:Z=1:DIM S(8),T(145),D(145),CRW(145),CRW1(145,8),WI(145,8),E
PRI(145,8)
240 DIM HT(20),TNUC(20),DST(145),HLC(145),A(2,5),B(8,2),DF(10,10)
250 CLS:GOTO 2980
260 PRINT:PRINT:PRINT:PRINT "INPUT INFORMATION FOR MODEL PREDICTION"
270 PRINT:INPUT "     Analysis Label (up to 6 characters)   =   ",A$
280 IF IREPET=1 THEN GOTO 980
290 PRINT:PRINT "Bulk Composition Information"
```

```
300 PRINT:PRINT "     Default Composition (wt%) = .05C,18.5Cr,9.0Ni,0.1Mo,.02N,.
01F"
310 PRINT:INPUT "     Enter 1 for default composition, RETURN to input composit
on  -  ",ICOMP
320 IF ICOMP=0 THEN GOTO 340
330 CW=.05:CRB=18.5:CRB1=18.5:NI=9!:NI1=9!:MO=.1:CW1=CW:ALLOY=304:NIT1=.02:P1=.0
1:CR1=13.5:GSNO=5:GOTO 480
340 PRINT:INPUT "              Carbon, Wt%                =  ", CW
350 IF CW<.001 OR CW>.1 THEN PRINT:PRINT "Input out of Range (.001-.1) - Please
Reset":GOTO 340
360 INPUT "              Chromium, Wt%              =  ", CRB:CRB1=CRB
370 IF CRB<15 OR CRB>21 THEN PRINT:PRINT "Input out of Range (15-21) - Please Re
set":GOTO 360
380 INPUT "              Nickel, Wt%                =  ", NI:NI1=NI
390 IF NI<7 OR NI>13 THEN PRINT:PRINT "Input out of Range (7-13) - Please Reset"
:GOTO 380
400 INPUT "              Molybdenum, Wt%            =  ", MO
410 IF MO>3.5 THEN PRINT:PRINT "Input out of Range (0-3.5) - Please Reset":GOTO
400
420 INPUT "              Nitrogen, Wt%              =  ",NIT:NITRO=NIT*.56/14
430 IF NIT>.2 THEN PRINT:PRINT "Input out of Range (0-.2) - Please Reset":GOTO 4
20
440 INPUT "              Phosphorus, Wt%            =  ",P1
450 IF P1>.1 THEN PRINT:PRINT "Input out of Range (0-.1) - Please Reset":GOTO 44
0
460 IF MO>1.5 THEN ALLOY=316 ELSE ALLOY=304
470 REM    ***  NITROGEN EFFECTS - ADJUSTS CARBON CONTENT   ***
480 NADJ = NIT - .12
490 IF NADJ<0 THEN NIT1=NIT ELSE NIT1=.12-NADJ
500 IF NIT1<0 THEN NIT1=0
510 IF NIT<.04 THEN NIT1=.04
520 CW1 = CW - (NIT1-.04)/6
530 IF CW1<.004 AND CW>.01 THEN CW1=.004
540 IF CW1<.0005 THEN CW1=.0005
550 REM    ***  NUCLEATION CONSTANTS  ***
560 FB = 172:COND = 2E-17/CW1:CONDJ = 3E-17/CW1
570 IF ICOMP=1 THEN GOTO 800
580 IF DDF>0 GOTO 6450
590 IF CONT>0 GOTO 920
600 PRINT:PRINT "Describe Initial Material Condition  "
610 PRINT:INPUT "    Enter 0 for Mill Annealed, 1 for Solution Annealed  -  ",IN
CON
620 IF INCON=0 THEN GOTO 670
630 INCON1=1:PRINT:INPUT "         ENTER ANNEALING TEMPERATURE IN DEG. C  - ",SA
TMP
640 INPUT "         ENTER ANNEALING TIME IN HOURS  - ",SATME
650 IF SATMP=1100 AND SATME>1 THEN INCON1=2:IF SATMP>1100 THEN INCON1=2
660 GOTO 720
```

```
670 PRINT:INPUT "       IF AVAILABLE ENTER ANNEALING TEMPERATURE IN DEG. C  - ",
MATMP
680 INPUT "       IF AVAILABLE ENTER ANNEALING TIME IN MINUTES  - ",MATME
690 INPUT "       IF AVAILABLE ENTER COOLING RATE IN DEG. C/SEC  - ",MACR
700 PRINT:INPUT "    If Available Enter Material Cold Work in Percent    - ",CL
DWK
710 IF CLDWK>60 THEN PRINT:PRINT "Input out of Range (0-60% - Please Reset":GOTO
 700
720 PRINT:INPUT "    If Available Enter Material Yield Strength (0.2% offset, in
 ksi)  -  ",YS
730 IF YS=0 THEN YS=30:GOTO 760
740 IF YS>80 OR YS<20 THEN PRINT:PRINT "Input out of Range (20-80 ksi - Please R
eset":GOTO 720
750 IF YS>45 AND CLDWK=0 THEN PRINT:PRINT "    Yield Strength Higher Than Expect
ed":PRINT "    for a Properly Annealed Stainless Steel"
760 PRINT:INPUT "    If Available Enter ASTM Grain Size Number -  ",GSNO
770 IF GSNO=0 THEN GSNO=5:GOTO 800
780 IF GSNO>10 OR GSNO<1 THEN PRINT:PRINT "Input out of Range (ASTM #1-10 - Plea
se Reset":GOTO 760
790 REM     ***   GRAIN SIZE NORMALIZATION   ***
800 GSNRM = (GSNO-5)/4 + 5
810 GSUM = 10000*EXP(-(3.47+GSNO/2.883))
820 GSCM = EXP(-(3.47+GSNRM/2.883))
830 IF DDF>0 THEN GOTO 920
840 IF ICOMP=1 THEN GOTO 920
850 PRINT:INPUT "    If Available Enter Initial Material EPR Value in C/cm2  -
",EPRIN
860 PRINT:PRINT:PRINT "                              ******************"
870 PRINT:PRINT:PRINT ">>> Two Approaches for Sensitization-Segregation Predicti
on can be Used:"
880 PRINT:PRINT "               > 1. Statistically Most Accurate (SMA) to Total
Data Base "
890 PRINT:PRINT "               > 2. Conservative which Better Predicts High End
 of Data Base"
900 PRINT:PRINT:INPUT "    Enter 1 for SMA Prediction or 2 for Conservative  -
",JPRED:CLS
910 IF JPRED=2 THEN CW1=CW+.01:CRB1=CR8-1:NI1=NI+1:JABC=1
920 CM=CW1*.56/12:C=CM:NIN=NI1*.56/58.7:CRN=((CRB1+.35*MO)*.56)/52
930 REM     ***   DESENSITIZATION CONSTANTS   ***
940 IF ALLOY=304 THEN HFAC=8 ELSE HFAC=16
950 CRN1=CRB1+.35*MO:CH=C+.001:IF ALLOY=316 THEN C=C+.0007 ELSE C=C+.0004
960 IF CONT>0 THEN GOTO 6450
970 IF KKK=5 THEN GOTO 1290
980 IF TMH=1 THEN GOTO 5890
990 IF ICCS=1 THEN GOTO 3510
1000 PRINT:PRINT:PRINT:PRINT "Isothermal Time/Temperature/Sensitization Setup "
1010 PRINT "-----------------------------------------------":PRINT
1020 IF KISOTT=1 THEN GOTO 1130
```

```
1030 INPUT "     Enter 1 for default T/t matrix, 0 to specify T/t matrix  -  ",J
ISO
1040 IF JISO=0 THEN GOTO 1060
1050 STEMP=800:KTEMP=500:ITEMP=100:GOTO 1190
1060 PRINT:INPUT "     Maximum Temperature, deg. C    -   ",STEMP
1070 IF STEMP<400 THEN PRINT:PRINT "          Improper Input - Please Reset ":PRI
NT:GOTO 1060
1080 INPUT "     Minimum Temperature, deg. C    -   ",KTEMP
1090 IF KTEMP<300 OR KTEMP>STEMP-.1 THEN PRINT:PRINT "          Improper Input -
Please Reset ":PRINT:GOTO 1080
1100 INPUT "     Temperature Increment, deg. C  -   ",ITEMP
1110 IF ITEMP<1 THEN PRINT:PRINT "          Improper Input - Please Reset ":PRINT
:GOTO 1100
1120 GOTO 1190
1130 INPUT "     Heat Treatment Temperature, deg. C  -  ",STEMP
1140 IF STEMP<250 OR STEMP>1100 THEN PRINT:PRINT "          Improper Input - Plea
se Reset ":PRINT:GOTO 1130
1150 INPUT "     Heat Treatment Time, hours          -   ",TTIME
1160 IF TTIME<.01 THEN PRINT:PRINT "          Improper Input - Please Reset ":PRI
NT:GOTO 1150
1170 JSCALE=0:S(1)=TTIME*3600:T(0)=273+STEMP
1180 IF ISTR=0 THEN GOTO 1440
1190 IF ISTR=0 THEN GOTO 1290
1200 PRINT:INPUT "     Enter simultaneous strain in percent  -  ",SIMSTR
1210 PRINT:INPUT "     Enter prior strain in percent         -  ",PRISTR
1220 IF SIMSTR>40 THEN SIMSTR=40
1230 IF PRISTR>40 THEN PRISTR=40
1240 SIMSTR = SIMSTR + PRISTR
1250 IF SIMSTR<.5 THEN SIMSTR=0
1260 IF SIMSTR>20 AND SIMSTR<40 THEN SIMSTR=40-SIMSTR
1270 IF KISOTT=1 THEN GOTO 1440
1280 REM   ***  Temperature and Time Matrices Setup  ***
1290 NTEMP=(STEMP-KTEMP)/ITEMP
1300 IF (STEMP-KTEMP)<ITEMP THEN NTEMP=0
1310 JTMP=ITEMP
1320 T(0)=273+STEMP
1330 JSCALE=INT(NTEMP)
1340 ISTEP=5
1350 IF NTEMP<1 THEN JSCALE=INT(NTEMP*25)
1360 IF NTEMP<1 THEN ISTEP=1
1370 IF KKK>1 THEN GOTO 1410
1380 FOR I=1 TO JSCALE:T(I)=T(I-1)-ISTEP:NEXT I
1390 S(1)=ISTEP/ITEMP
1400 GOTO 1440
1410 FOR I=1 TO JSCALE:T(I)=T(I-1)-ITEMP:NEXT I
1420 IF DDF>0 THEN S(0)=0:S(1)=3600:S(2)=36000':S(3)=360000'
1430 REM   ***  Chromium Diffusivity Determination  ***
1440 FOR J=0 TO JSCALE
1450 IF ALLOY=304 THEN D(J)=.08*EXP(-58500'/(R*T(J))) ELSE D(J)=.13*EXP(-63100!/
(R*T(J)))
```

```
1460 IF ICCS>0 OR IHAZ>0 THEN GOTO 1550
1470 REM   ***  CARBIDE NUCLEATION KINETICS  ***
1480 FA = .1*T(J) - (110 + CW1*150 +4*MO)
1490 FO = (4*F8*FB*FB)/(27*FA*FA)
1500 IF ALLOY=304 THEN TNUC(J)=COND*EXP((58500!+FO)/(R*T(J))) ELSE TNUC(J)=COND1
*EXP((63100!+FO)/(R*T(J)))
1510 IF EPRIN>0 THEN TNUC(J)=0
1520 IF T(J)<750 THEN TNUC(J)=TNUC(J)/4:GOTO 1550
1530 IF T(J)<900 THEN TNUC(J)=TNUC(J)*(1+((T(J)-900)/200))
1540 REM   ***  DEFORMATION EFFECTS ON Cr DIFFUSIVITY   ***
1550 IF INCON1=2 THEN D(J)=D(J)/1.2
1560 IF CLDWK>2 AND CLDWK<25 THEN D(J)=D(J)*(1+CLDWK/15)
1570 IF CLDWK>24.99 AND CLDWK<40.01 THEN D(J)=D(J)*(3.92-CLDWK/20)
1580 IF CLDWK>40 THEN D(J)=D(J)*(5!-CLDWK/13)
1590 IF IHAZ=1 THEN ISTR=1:SIMSTR=5
1600 IF ISTR=1 THEN D(J)=((SIMSTR*.4)+1)*D(J)
1610 IF ICCS>0 OR IHAZ>0 THEN GOTO 1660
1620 REM   ***  DESENSITIZATION TIME  ***
1630 HT = GSCM*CH/(CRN-.125)
1640 HT(J) = HT*HT/(D(J)*HFAC)
1650 HT(J) = HT(J) + 3600*TNUC(J)
1660 NEXT J
1670 FOR J=0 TO JSCALE
1680 REM   *** Carbon and Chromium Activities Determination  ***
1690 CA = C*EXP((11.92-6330/T(J))*C-1.845+5100/T(J)-(2.2-7600/T(J))*NIN+(24.4-38
400!/T(J))*CRN-(96.8-84800!/T(J))*CRN^2)
1700 ENERGY=(-98.28-.0092*T(J))*1000:EQUIL=EXP(-ENERGY/(R*T(J)))
1710 CRA = (1/(EQUIL*CA^6))^.044
1720 IF ALLOY=304 THEN XFAC = T(J)/2000 ELSE XFAC=(T(J)-30)/2000
1730 CRM = CRA/(10.55-(94.834*XFAC)+(282.9*XFAC*XFAC)-(242.8*XFAC*XFAC*XFAC))
1740 IF ICCS>0 THEN GOTO 1830
1750 IF KKK<7 THEN GOTO 1830
1760 REM   ***   TIME MATRICES FOR ISOTHERMAL   ***
1770 IF T(J)>1098 THEN S(0)=0:S(1)=360:S(2)=1080:S(3)=1800:S(4)=3600:S(5)=18000:
S(6)=36000!:S(7)=180000!
1780 IF T(J)<1098.1 AND T(J)>948 THEN S(0)=0:S(1)=360:S(2)=1800:S(3)=3600:S(4)=3
6000!:S(5)=180000!:S(6)=360000!:S(7)=900000!
1790 IF T(J)<948.1 AND T(J)>872.9 THEN S(0)=0:S(1)=1080:S(2)=3600:S(3)=36000!:S(
4)=180000!:S(5)=360000!:S(6)=900000!:S(7)=1800000!
1800 IF T(J)<873 AND T(J)>673 THEN S(0)=0:S(1)=3600:S(2)=36000!:S(3)=180000!:S(4
)=360000!:S(5)=900000!:S(6)=1800000!:S(7)=3600000!
1810 IF T(J)<673.1 THEN S(0)=0:S(1)=360000!:S(2)=1800000!:S(3)=3600000!:S(4)=1.8
E+07:S(5)=3.6E+07:S(6)=1.8E+08:S(7)=3.6E+08
1820 REM  ***  INTERFACIAL Cr MINIMUM DETERMINATION   ***
1830 CRW(J) = CRM*52/.56 + CRADJ:IF CRW(J)>CRI THEN RATIO=0
1840 IF CRW(J)>CRB THEN CRW(J)=CRB
1850 IF CRW(J)<CRI THEN RATIO=(CRI-CRW(J))/(CRB-CRW(J))
1860 IF EPRIN=0 THEN GOTO 1900
1870 WIDIN = EPRIN/24300000#
```

```
1880 IF J=0 THEN WIDIN1=WIDIN ELSE WIDIN1=0
1890 IF IWELD=0 THEN WIDIN1=WIDIN
1900 IF KISOTT=1 THEN KKJ=1 ELSE KKJ=KKK
1910 FOR I=1 TO KKJ
1920 CRW1(J,I) = CRW(J)
1930 IF ICCS>0 OR IHAZ>0 THEN ST=S(I):GOTO 2030
1940 IF T(J)<974 THEN ST = S(I) - 3600*TNUC(J) ELSE ST = S(I)
1950 IF ST<0 THEN ST=0
1960 IF CRW1(J,I)<13.5 THEN CRW1(J,I)=CRW1(J,I)+((13.5-CRW1(J,I))*SQR(ST/HT(J)))
1970 IF CRW1(J,I)<CRB1 AND CRW1(J,I)>13.5 THEN CRW1(J,I)=CRW1(J,I)+((CRB1-CRW1(J
,I))*SQR(ST/HT(J)))
1980 IF IWELD>0 THEN GOTO 2030
1990 IF CRW1(J,I)>CR8 THEN CRW1(J,I)=CR8
2000 IF CRW1(J,I)>CRI THEN RATIO=0:GOTO 2020
2010 RATIO = (CRI-CRW1(J,I))/(CRB-CRW1(J,I))
2020 IF IWELD=0 THEN GOTO 2060
2030 IF RATIO=0 THEN GOTO 2060
2040 TZERO = ((WICUM/(2*RATIO))^2)/D(J)
2050 REM  ***  INTERFACIAL Cr DEPLETION WIDTH DETERMINATION  ***
2060 WI(J,I) = WIDIN1 + (RATIO*2*((D(J)*(ST+TZERO))^.5))
2070 IF WI(J,I)<0 THEN WI(J,I)=0
2080 IF RATIO>0 THEN WICUM=WI(J,I)
2090 WID = WI(J,I) - 2.5E-07
2100 IF WID<0 THEN WID=0
2110 IF IWELD=0 THEN GOTO 2140
2120 WI(J,I) = WICUM
2130 REM  ***  INTERFACIAL Cr DEPLETION VOLUME DETERMINATION  ***
2140 VOLDEP = ((((CRI-CRW1(J,I))*WID)/(2*CRI))*400000!)-.005
2150 IF VOLDEP<0 THEN VOLDEP=0
2160 IF VOLDEP>2.5 THEN VOLDEP=2.5
2170 REM  ***  EPR-DOS DETERMINATION FROM DEPLETION VOLUME  ***
2180 IF VOLDEP>.934 THEN EPRI(J,I)=102.3+(VOLDEP-.934)*20:GOTO 2220
2190 IF VOLDEP>.25 OR T(J)<800 THEN EPRI(J,I)=(241.7*VOLDEP)-(217.1*VOLDEP*VOLDE
P)+(103.8*VOLDEP*VOLDEP*VOLDEP)-(24.45*VOLDEP*VOLDEP*VOLDEP*VOLDEP)
2200 IF T(J)<800 THEN GOTO 2220
2210 IF VOLDEP<.2501 THEN EPRI(J,I)=(9.32*VOLDEP)+(2060*VOLDEP*VOLDEP)-(7420*VOL
DEP*VOLDEP*VOLDEP)+(8348*VOLDEP*VOLDEP*VOLDEP*VOLDEP)
2220 IF EPRI(J,I)<.01 THEN EPRI(J,I)=0
2230 NEXT I
2240 VOLDEP = 0
2250 NEXT J
2260 IF KKK=7 THEN CNT=0
2270 CLS:PRINT:PRINT "                          ",A$
2280 IF DDF=1 THEN PRINT C$:PRINT G$
2290 IF DDF=2 THEN PRINT D$:PRINT H$
2300 IF IHAZ>0 THEN GOTO 2560
2310 IF JJJ>0 THEN PRINT:PRINT "Temp, C      Time, s          Min. Cr, wt%
Depl Wid, A          EPR, C/cm2"
```

```
2320 IF JJJ>0 THEN GOTO 2340
2330 PRINT:PRINT "Temp, C      Time, h          Min. Cr, wt%       Depl Wid, A
     EPR, C/cm2"
2340 PRINT "-------      -------          ------------       -----------        -
---------"
2350 IF DDF>0 THEN KKJ=3
2360 FOR J=0 TO JSCALE
2370 IF ICCS>0 OR DDF>0 THEN GOTO 2430
2380 IF T(J)>1098 THEN S(0)=0:S(1)=360:S(2)=1080:S(3)=1800:S(4)=3600:S(5)=18000:
S(6)=36000!:S(7)=180000!
2390 IF T(J)<1098.1 AND T(J)>948 THEN S(0)=0:S(1)=360:S(2)=1800:S(3)=3600:S(4)=3
6000!:S(5)=180000!:S(6)=360000!:S(7)=900000!
2400 IF T(J)<948.1 AND T(J)>872.9 THEN S(0)=0:S(1)=1080:S(2)=3600:S(3)=36000!:S(
4)=180000!:S(5)=360000!:S(6)=900000!:S(7)=1800000!
2410 IF T(J)<673.1 THEN S(0)=0:S(1)=360000!:S(2)=1800000!:S(3)=3600000!:S(4)=1.8
E+07:S(5)=3.6E+07:S(6)=1.8E+08:S(7)=3.6E+08
2420 IF T(J)<873 AND T(J)>673 THEN S(0)=0:S(1)=3600:S(2)=36000!:S(3)=180000!:S(4
)=360000!:S(5)=900000!:S(6)=1800000!:S(7)=3600000!
2430 FOR I=1 TO KKJ
2440 PRINT T(J)-273;
2450 IF JJJ>0 THEN PRINT USING "############.#";S(I);
2460 IF JJJ>0 THEN GOTO 2490
2470 PRINT USING "##############.#";S(I)/3600;
2480 IF CRW1(J,I)>CRW(J) THEN PRINT USING "##################.##";CRW1(J,I),WI(J,I
)*1E+08,EPRI(J,I):GOTO 2500
2490 PRINT USING "##################.##";CRW(J),WI(J,I)*1E+08,EPRI(J,I)
2500 NEXT I
2510 IF ICCS>0 OR DDF>0 THEN GOTO 2550
2520 IF IHAZ>0 THEN GOTO 2550
2530 PRINT:PRINT:PRINT:PRINT:PRINT:PRINT:INPUT "  * HIT RETURN TO CONTINUE * ",I
OUT
2540 PRINT:PRINT:PRINT:PRINT:PRINT:PRINT
2550 NEXT J
2560 IF KISOTT=1 THEN EPR1=EPRI(0,1):GOTO 2660
2570 IF KKK>1 THEN GOTO 2830
2580 WICUM1=WI(JSCALE,1):EPR1=EPRI(JSCALE,1)
2590 IF EPR1<0 THEN EPR1=0
2600 IF CNT>0 THEN PRINT:PRINT "Weld Pass Number:   ";JJJ
2610 IF KKK=1 THEN PRINT:PRINT "  *****  CUMULATIVE Cr DEPL. WIDTH, A     = ";
2620 PRINT USING "#####.#";WICUM1*1E+08
2630 IF KKK=1 THEN PRINT:PRINT "  *****  CUMULATIVE EPR-DOS VALUE, C/cm2  = ";
2640 PRINT USING "#####.#";EPR1
2650 IF IHAZ=1 THEN GOTO 2900
2660 IF IGSCC=0 THEN GOTO 2830
2670 PRINT:PRINT "EXPECTED IGSCC RESISTANCE"
2680 PRINT "-------------------------"
2690 IF EPR1>5 THEN PRINT:PRINT "  *  IGSCC may occur in BWR environments even w
ith good water chemistry  *"
```

```
2700 IF EPR1>40 THEN PRINT "  *  Highly susceptible, questionable even in low ox
ygen environments    *"
2710 IF EPR1>40 GOTO 2790
2720 IF EPR1>15 THEN PRINT "  * Moderate to High Susceptibility when oxygen leve
ls are greater than 50 ppb *"
2730 IF EPR1>15 THEN GOTO 2790
2740 IF EPR1>5 THEN PRINT "  * Low to Moderate Susceptibility when oxygen levels
 are greater than 100 ppb *"
2750 IF EPR1>5 THEN GOTO 2790
2760 IF EPR1>2 THEN PRINT:PRINT "  *  IGSCC may occur in BWR environments with p
oor water chemistry       *"
2770 IF EPR1<2 THEN PRINT:PRINT "  *  IGSCC is not expected to occur under norma
l operating conditions    *"
2780 IF EPR1>.5 THEN PRINT "  *  Slightly Sensitized -- May be affected by servi
ce exposure               *"
2790 IF ITBLE=1 AND IEXAMP=0 THEN GOTO 2950
2800 IF ITBLE=1 AND CONT=1 THEN PRINT:GOTO 6260
2810 IF ITBLE=1 AND CONT=2 THEN PRINT:GOTO 6260
2820 IF CONT>0 THEN GOTO 2860
2830 IF DDF=1 OR DDF=2 GOTO 6500
2840 IF IEXAMP=1 THEN PRINT:INPUT "            Hit RETURN to Continue   ",IEXMP:
GOTO 2860
2850 PRINT:INPUT "     Enter 1 to ouput results to printer, RETURN to continue
 ",K
2860 IF K=1 THEN GOTO 3960
2870 REM               *****      Printer Setup      *****
2880 IF K= 1 THEN GOTO 3960
2890 IF JJJ=0 THEN GOTO 2950
2900 DF(6,NDF)=EPR1:DF(5,NDF)=WICUM1
2910 NDF=NDF+1
2920 IF CNT>0 GOTO 5970
2930 PRINT:INPUT "     Enter 1 for Microstructural Development Menu, RETURN to C
ontinue  ",KJI
2940 IF KJI=0 THEN GOTO 3480
2950 PRINT:INPUT "     Hit Enter to Clear Screen and Return to OPTIONS",ICLS
2960 CLS
2970 JJJ=0
2980 PRINT "MENU 2"
2990 PRINT "======":PRINT:PRINT
3000 PRINT:PRINT "MICROSTRUCTURAL DEVELOPMENT PREDICTION FROM THERMOMECHANICAL H
ISTORY"
3010 PRINT "-----------------------------------------------------------------
":PRINT
3020 PRINT 1 "Background Information and Example Problems"
3030 PRINT 2 "Isothermal Time/Temperature/Sensitization Behavior  "
3040 PRINT 3 "Continuous Cooling Sensitization/Additive Thermal Cycles"
```

```
3050 PRINT 4 "Typical TM History Input for a 24-in dia. Weld/Sensitization Devel
opment"
3060 PRINT 5 "Deformation Effects on Sensitization Development Prediction"
3070 PRINT 6 "Impurity Segregation Prediction"
3080 PRINT 7 "Stress Corrosion Cracking Susceptibility Prediction"
3090 PRINT 8 "Restart Analysis - Same Material Conditions"
3100 PRINT 9 "Exit Analysis"
3110 WICUM=0:KXX=0:IEXAMP=0:DDF=0:CCNT=0:CNT=0:IHAZ=0:IT8LE=0:TMH=0:ICCS=0:KISOT
T=0:IJK=0:JJJ=0:IWELD=0:TZERO=0:NDF=0:WID=0:WI(0,1)=0
3120 IF INCON1=0 THEN INCON=0:ADJADD=0:ADJ2=1
3130 PRINT:PRINT:PRINT:INPUT "      Choice from Menu   -   ",CHOICE:CLS
3140 ON CHOICE GOTO 4560,3160,3320,5630,4430,5290,5470,6920,3150
3150 END
3160 PRINT:PRINT:PRINT "                    ***  ISOTHERMAL SENSITIZATION PREDICTION
  *** ":PRINT:PRINT
3170 PRINT "    Isothermal time/temperature/sensitization (TTS) behavior is mapp
ed"
3180 PRINT "    over a selected temperature range for heat treatment times rangi
ng"
3190 PRINT "    from 0.1 to 100000 hours. Default conditions can be specified wh
ich"
3200 PRINT "    sets the temperature range from 500 to 800 deg. C and evaluates
incre- "
3210 PRINT "    ments within this range.  Simultaneous deformation effects on is
othermal"
3220 PRINT "    sensitization development can be determined by selecting option
5 of the"
3230 PRINT "    Microstructural Development Menu before running the isothermal p
rediction."
3240 KKK=7:JABC=0:ISOTH=1
3250 PRINT:PRINT "    Prediction of sensitization development resulting from spe
cific"
3260 PRINT "    temperature/time (T/t) treatments can also be obtained.  Heat tr
eatment"
3270 PRINT "    temperature must be input in degrees C and time in hours.
3280 PRINT:PRINT "        Enter 0 for TTS prediction, 1 for single T/t predictio
n"
3290 INPUT "            or 2 for Microstructural Development Menu  -  ",KISOTT
3300 IF KISOTT=2 THEN GOTO 2960
3310 GOTO 260
3320 PRINT:PRINT:PRINT "           ***  CONTINUOUS COOLING SENSITIZATION PREDICT
ION  ***":PRINT:PRINT:PRINT
3330 PRINT "Linear cooling sensitization (LCS) - additive cycles; cumulative val
ues of"
3340 PRINT "GB Cr depletion and EPR-measured DOS are saved after each thermal or
"
3350 PRINT "thermomechanical cycle and resultant DOS reported.  Small isothermal
 T/t "
```

```
3360 PRINT "steps are used to approximate the selected cooling rate through the
temp-"
3370 PRINT "erature range of interest.  The minimum temperature considered in th
e "
3380 PRINT "calculations is 500 deg. C due to slow Cr diffusion kinetics at lowe
r"
3390 PRINT "temperatures.  Simultaneous deformation can be included by selecting
 option"
3400 PRINT "5 from the Microstructural Development Menu before running the conti
nuous"
3410 PRINT "cooling prediction.  Sensitization development at a particular locat
ion "
3420 PRINT "in the weld HAZ can be predicted if the per-pass TM history is known
.  A"
3430 PRINT "typical TM history for a 24 in. dia., Sch. 80 pipe weld HAZ is used
in"
3440 PRINT "option 4 from the Microstructural Development Menu."
3450 PRINT:PRINT:INPUT "   Enter 1 for Microstructural Development Menu, RETURN
to Set LCS Parameters",KCCS
3460 IF KCCS=1 THEN GOTO 2960
3470 WICUM=0:IJK=1:JABC=0:ICCS=1:KISOTT=0:WI(0,1)=0
3480 JJJ = JJJ + 1
3490 IWELD = 1
3500 IF JJJ=1 THEN GOTO 260
3510 PRINT:PRINT:PRINT:PRINT "            THERMAL CYCLE NO.       =",JJJ
3520 PRINT "         ------------------------------------------------"
3530 PRINT:INPUT "              Cooling Rate (CR), deg. C/s      =    ",ITEMP
3540 IF ITEMP=0 THEN PRINT:PRINT "Improper Cooling Rate Input "
3550 IF ITEMP=0 THEN INPUT "   Enter 1 for Microstructural Development Menu, RET
URN to reset Cooling Rate",KCCS
3560 IF ITEMP=0 AND KCCS=1 THEN GOTO 2960
3570 IF ITEMP=0 AND KCCS=0 THEN GOTO 3530
3580 PRINT:INPUT "              Maximum Temperature, deg. C      =   ",STEMP
3590 IF STEMP=0 THEN PRINT:PRINT "Improper Temperature Input ":GOTO 3550
3600 IF STEMP>1200 THEN STEMP=1200
3610 PRINT:PRINT "           Minimum Temp.:  Return to set"
3620 INPUT "          based on CR or input in deg. C      =   ",ETEMP
3630 IF STEMP=ETEMP THEN PRINT:PRINT "Improper Temperature Input ":GOTO 3550
3640 IF ETEMP>STEMP THEN PRINT:PRINT "Improper Temperature Input ":GOTO 3550
3650 IF STEMP<580 THEN PRINT:PRINT "          No sensitization will occur at the
se low temperatures.":INPUT "    Enter 1 for Microstructural Development Menu, R
ETURN to reset parameters  ",JCCS
3660 IF STEMP<500 AND JCCS=1 THEN GOTO 2960
3670 IF STEMP<500 AND JCCS=0 THEN GOTO 3530
3680 IF JJJ=2 THEN EPRIN=0:WIDIN1=0
3690 ADJ=0:ADJADD=0
3700 IF TMH>0 THEN GOTO 3790
```

```
3710 IF ISTR=1 THEN INPUT "Enter simultaneous strain in percent for this cycle
-  ",SIMSTR
3720 IF SIMSTR<.5 THEN SIMSTR=0
3730 IF SIMSTR>10 THEN SIMSTR=10
3740 REM   *****   TMAX FACTOR CONTROLS MAXIMUM TEMPERATURE EFFECTS   *****
3750 REM   *****  ON SUBSEQUENT CARBIDE NUCLEATION DURING COOLING BY  *****
3760 REM   *****   ADJUSTING MINIMUM GB Cr CONCENTRATION PREDICTION   *****
3770 IF ALLOY=316 THEN SOL1=870+(CW*1500) ELSE SOL1=800+(CW*2000)
3780 IF ALLOY=316 THEN TMAX=(STEMP-SOL1)/60 ELSE TMAX=(STEMP-SOL1)/100
3790 IF TMAX<0 THEN TMAX=0
3800 IF TMAX>1.5 THEN TMAX=1.5
3810 IF ETEMP>499 THEN GOTO 3840
3820 IF ALLOY=304 THEN ETEMP=650+LOG(ITEMP*5)*15 ELSE ETEMP=700+LOG(ITEMP*5)*15
3830 IF ETEMP>STEMP THEN ETEMP=STEMP-5
3840 IF ALLOY=316 THEN STEMP2=820+(2000*CW) ELSE STEMP2=770+(2000*CW)
3850 IF STEMP>STEMP2 THEN STEMP=STEMP2
3860 IF IHAZ>0 THEN ETEMP=575
3870 NTEMP=(STEMP-ETEMP)/5
3880 IF NTEMP<1 THEN NTEMP=1
3890 TTIME = NTEMP:NTIME = 1:ITIME = 1:KKK=1
3900 CRADJ = (LOG(ITEMP)+4)/(CW*30) + TMAX
3910 IF ITEMP<1 THEN ITEMP1=1 ELSE ITEMP1=ITEMP
3920 IF ALLOY=304 THEN CRADJ=TMAX+(LOG(ITEMP1)+.05)
3930 IF IHAZ>0 OR SIMSTR>2 THEN CRADJ=CRADJ/(30*(CW+.04))
3940 GOTO 1320
3950 REM   *****  Setup Analysis Conditions Heading for Hard-Copy Output  *****
3960 IF JJJ>1 THEN GOTO 4100
3970 LPRINT "-------------------------------------------------------------------"
3980 LPRINT "PROGRAM SSDOS.V8            ANALYSIS LABEL : ",A$
3990 LPRINT "-------------------------------------------------------------------"
4000 IF INCON=1 THEN LPRINT "SS ALLOY : ",ALLOY,"SOL. ANNEALED CONDITION":GOTO 4
020
4010 LPRINT "SS ALLOY : ",ALLOY,"MILL ANNEALED CONDITION"
4020 LPRINT "GRAIN SIZE :",GSNO,"INIT. EPR VALUE C/cm2  :",EPRIN
4030 GOTO 4050
4040 LPRINT "SOL. ANNEALED CONDITION     INITIAL EPR VALUE C/cm2  :",EPRIN
4050 IF ISTR=0 THEN GOTO 4070:IF KkK=1 THEN GOTO 4070
4060 LPRINT "SIMULTANEOUS STRAIN DURING THERMAL TREATMENT  %      :",SIMSTR
4070 LPRINT "-------------------------------------------------------------------"
4080 LPRINT "CARBON WT%  =",CW,"CHROMIUM WT%     =",CRB:LPRINT "NICKEL WT%  =",N
I,"MOLYBDENUM WT%   =",MO:LPRINT "NITRO. WT%  =",NIT,"PHOSPHORUS WT%   =",P1
4090 LPRINT "-------------------------------------------------------------------"
4100 ON CHOICE GOTO 4110,4110,4110,4110,4110,4110,4110,4110,4110
4110 IF IJK=1 THEN GOTO 4350
4120 LPRINT:LPRINT "Temperature     Time        Min. GB       Cr Depletion
DOS-EPR Value"
```

```
4130 IF KKK=1 THEN LPRINT "    deg C           s          Cr, wt%          Width, A
          C/cm2":GOTO 4150
4140 LPRINT "    deg C          hr          Cr, wt%          Width, A              C/c
m2"
4150 LPRINT "  -------       ------       -------          --------              ----
---"
4160 LPRINT
4170 FOR J=0 TO NTEMP
4180 IF ICCS>0 THEN GOTO 4240
4190 IF T(J)>1098 THEN S(0)=0:S(1)=360:S(2)=1080:S(3)=1800:S(4)=3600:S(5)=18000:
S(6)=36000!:S(7)=180000!
4200 IF T(J)<1098.1 AND T(J)>948 THEN S(0)=0:S(1)=360:S(2)=1800:S(3)=3600:S(4)=3
6000!:S(5)=180000!:S(6)=360000!:S(7)=900000!
4210 IF T(J)<948.1 AND T(J)>872.9 THEN S(0)=0:S(1)=1080:S(2)=3600:S(3)=36000!:S(
4)=180000!:S(5)=360000!:S(6)=900000!:S(7)=1800000!
4220 IF T(J)<873.1 THEN S(0)=0:S(1)=360000!:S(2)=1800000!:S(3)=3600000!:S(4)=1.8
E+07:S(5)=3.6E+07:S(6)=1.8E+08:S(7)=3.6E+08
4230 IF T(J)<873 AND T(J)>673 THEN S(0)=0:S(1)=3600:S(2)=36000!:S(3)=180000!:S(4
)=360000!:S(5)=900000!:S(6)=1800000!:S(7)=3600000!
4240 FOR I=1 TO KKJ
4250 LPRINT USING "########"; T(J)-273;
4260 IF KKK=1 THEN LPRINT USING "###########.##"; S(I),CRW(J);
4270 IF KKK=1 THEN LPRINT USING "##################.#";WI(J,I)*1E+08,EPRI(J,I):GOT
O 4320
4280 IF CRW1(J,I)>CRW(J) THEN LPRINT USING "###########.##"; S(I)/3600,CRW1(J,I):
4290 IF CRW1(J,I)>CRW(J) THEN GOTO 4310
4300 LPRINT USING "###########.##"; S(I)/3600,CRW(J);
4310 LPRINT USING "##################.#";WI(J,I)*1E+08,EPRI(J,I)
4320 NEXT I
4330 NEXT J
4340 LPRINT "-----------------------------------------------------------------------
-------"
4350 IF JJJ>0 THEN LPRINT:LPRINT " CYCLE NO.  =",JJJ,"STRAIN, %      =",SIMSTR
4360 IF JJJ>0 THEN LPRINT:LPRINT "C.Rate,C/s  =",ITEMP,"Tmax,C  =",STEMP,"Tmin,C
  =";
4370 IF JJJ>0 THEN LPRINT USING "######";ETEMP
4380 IF KKK=1 THEN LPRINT:LPRINT "          CUMULATIVE GB CHROMIUM DELETION WIDTH
, A   = ";
4390 IF KKK=1 THEN LPRINT USING "#####.#";WICUM1*1E+08
4400 IF KKK=1 THEN LPRINT:LPRINT "          CUMULATIVE ESTIMATED DOS-EPR VALUE, C
/cm2  = ";
4410 IF KKK=1 THEN LPRINT USING "####.#";EPR1
4420 GOTO 2890
4430 PRINT:PRINT "       ***  DEFORMATION EFFECTS ON SENSITIZATION DEVELOPMENT
***"
4440 PRINT:PRINT "      Simultaneous or prior strain effects on sensitization -
a factor"
```

```
4450 PRINT "      is input which modifies the Cr diffusion rate. Simultaneous st
rain"
4460 PRINT "      during or prior strain before each thermal cycle must be input
 for HAZ"
4470 PRINT "      simulation.  Strain effects on carbide nucleation subroutines
are being "
4480 PRINT "      developed and correlated to experimental data. They are not "
4490 PRINT "      considered in the model at the present time."
4500 PRINT:PRINT "      Selection of this option enables strain to be input duri
ng"
4510 PRINT "      parameter setups for the isothermal or continuous cooling"
4520 PRINT "      sensitization prediction.  Strains below 0.5% do not effect"
4530 PRINT "      Cr diffusivity and the effect of strain saturates above 20% an
d then"
4540 PRINT "      decreases.  This option must be set each time to include strai
n effects."
4550 PRINT:PRINT:INPUT "Enter 1 to Include Strain in Subsequent Predictions, RET
URN to cancel - ",ISTR:GOTO 2950
4560 CLS:PRINT:PRINT "BACKGROUND INFORMATION "
4570 PRINT "----------------------":PRINT
4580 PRINT "    The options listed in MENU 2 - MICROSTRUCTURAL DEVELOPMENT PREDI
CTION"
4590 PRINT "    FROM THERMOMECHANICAL HISTORY - enable the user to evaluate the"
4600 PRINT "    expected sensitization development as a function of material com
posi-"
4610 PRINT "    tion, initial condition and thermomechanical history in Type 304
 and"
4620 PRINT "    316 stainless steels.  Model predictions result from a combinati
on of"
4630 PRINT "    theoretical equations and empirical data correlations.  Componen
ts of"
4640 PRINT "    the model include determination of the equilibrium Cr concentrat
ion at"
4650 PRINT "    at carbide/matrix interfaces based on the thermodynamics of carb
ide"
4660 PRINT "    formation, Cr concentration gradients based on effective diffusi
vities,"
4670 PRINT "    and an empirical correlation between Cr depletion and degree of
sensiti-"
4680 PRINT "    zation as measured by the electrochemical potentiokinetic reacti
vation"
4690 PRINT "    (EPR) test.  Modifications to the model have been made based on"
4700 PRINT "    extensive isothermal sensitization experiments.  Comparisons bet
ween"
4710 PRINT "    measured and predicted microstructural development after more co
mplex"
4720 PRINT "    thermal and thermomechanical treatments are ongoing.  This infor
mation"
```

```
4730 PRINT "    is being used to modify and validate model predictions."
4740 PRINT:PRINT:PRINT "                          HIT RETURN TO CONTINUE        "
4750 INPUT " ",IBACK
4760 CLS:PRINT "BACKGROUND INFORMATION"
4770     PRINT "----------------------":PRINT
4780 PRINT "    This is a preliminary version of the model and is not intended f
or"
4790 PRINT "    general release or use.  Several of the options listed in the Mi
cro-"
4800 PRINT "    structural Development Menu are not available for use at this ti
me."
4810 PRINT "    These options require further evolution and comparison to existi
ng and"
4820 PRINT "    future data bases.  Both the impurity segregation prediction and
 the"
4830 PRINT "    stress corrosion cracking prediction have insufficient experimen
tal"
4840 PRINT "    data bases to allow more than qualitative comparisons.  As a res
ult of"
4850 PRINT "    removing these options certain material parameter entries have n
o"
4860 PRINT "    effect on model predictions (e.g., yield strength, etc.).  The e
ntry"
4870 PRINT "    statements remain since they indicate some additional important"
4880 PRINT "    parameters for microstructural and SCC prediction."
4890 PRINT:PRINT:PRINT:PRINT:PRINT "                              HIT RETURN TO CONTI
NUE "
4900 PRINT:INPUT " ",IBACK
4910 CLS:PRINT "BACKGROUND INFORMATION"
4920     PRINT "----------------------":PRINT
4930 PRINT "    An important aspect of the model is the prediction of sensitizat
ion in a"
4940 PRINT "    form that enables straightforward comparison to experiment.  Thu
s,"
4950 PRINT "    existing model capabilities can be evaluated using an inexpensiv
e, yet"
4960 PRINT "    quantitative technique (i.e. EPR).  The user is referred to the
following"
4970 PRINT "    publications for more information concerning the EPR test techni
que and"
4980 PRINT "    more specifics concerning the development of this model.
4990 PRINT:PRINT:PRINT "EPR TEST TECHNIQUE:"
5000 PRINT "    *  S.M.Bruemmer,L.A.Charlot and D.G.Atteridge.NUREG/CR-3918,1984
."
5010 PRINT "    *  W.L.Clarke.NUREG-0251-1,1976."
5020 PRINT "    *  A.P.Majidi AND M.A.Streicher.Corrosion, Vol.40, p.393 and 445
,1984."
5030 PRINT:PRINT "MODEL DEVELOPMENT:"
```

```
5040 PRINT "     *  S.M.Bruemmer, NUREG/GR-     , 1988."
5050 PRINT "     *  D.G.Atteridge,S.M.Bruemmer and R.E.Page.NUREG/CR-3613, Vol.1-
3,1983-85."
5060 PRINT:PRINT:PRINT:PRINT "                                   HIT RETURN TO CONTINUE
  ":INPUT " ",JBAC
5070 CLS:PRINT:PRINT "EXAMPLE PROBLEMS"
5080 PRINT "----------------":PRINT:PRINT
5090 PRINT "     This section allows the user to obtain example calculations of s
ensiti-"
5100 PRINT "     zation development in Type 304 or 316 stainless steel.  The purp
ose of"
5110 PRINT "     these examples is to indicate the output format of the model and
 "
5120 PRINT "     illustrate predictive capabilities.
5130 PRINT:PRINT:PRINT "MENU 2.1"
5140 PRINT "--------":PRINT
5150 CCNT=0:DDF=0:IEXAMP=1:IJK=0:JJJ=0:IWELD=0:JABC=0:ISTR=0:IHAZ=0:IGSCC=0:ITBL
E=0:KISOTT=0:TMH=0:CNT=0:WICUM=0:TZERO=0:NDF=0
5160 PRINT 1 "Isothermal Sensitization Prediction Example"
5170 PRINT 2 "Continuous Cooling Sensitization Prediction Example"
5180 PRINT 3 "Weld HAZ Sensitization Prediction Example"
5190 PRINT 4 "Exit to Microstructural Development Prediction Menu"
5200 PRINT:PRINT:INPUT "            Choice from Menu  -  ",CHOIC
5210 IF CHOIC=0 THEN GOTO 5070
5220 G$="COMPOSITION, Wt% :  .06 C; 18.5 Cr; 9.0 Ni; 0.1 Mo; .02 N"
5230 H$="COMPOSITION, Wt% :  .02 C; 17.0 Cr; 11.0 Ni; 2.1 Mo; .07 N"
5240 ON CHOIC GOTO 6300,5250,6660,5280
5250 CLS:PRINT:PRINT:PRINT "   Continuous cooling sensitization example problems
 are not available"
5260 PRINT "   at this time.  The weld HAZ example (option 3) uses a similar set
up"
5270 PRINT "   and output format.":PRINT:PRINT:PRINT:GOTO 6490
5280 GOTO 2960
5290 PRINT "             ***   IMPURITY SEGREGATION PREDICTION   ***"
5300 PRINT:PRINT "   Impurity segregation to grain boundary interfaces in stainl
ess steels"
5310 PRINT "   is determined using a modified surface adsorption analogue (trunc
ated"
5320 PRINT "   BET model).  The primary impurity segregant in austenitic stainle
ss"
5330 PRINT "   steels is phosphorus.  At the present time, thermodynamic and kin
etic"
5340 PRINT "   information is in place only for phosphorus and only phosphorus"
5350 PRINT "   segregation can be predicted.  It is important to note that the d
ata"
5360 PRINT "   base available for grain boundary segregation in stainless steels
 "
```

```
5370 PRINT "   is extremely limited.  Therefore, model predictions should be use
d to"
5380 PRINT "   indicate the potential for segregation until a better data base i
s"
5390 PRINT "   available for model verification.
5400 PRINT:PRINT "   Model setup for segregation prediction tied to the thermome
chanical"
5410 PRINT "   histories listed in the main menu is not complete at this time. "
5420 PRINT "   Segregation predictions can be made separately using a computer p
rogram"
5430 PRINT "   entitled SOLSEG which has been developed under Department of Ener
gy,"
5440 PRINT "   Basic Energy Sciences funding.  Contact S.M.Pruemmer for more inf
ormation."
5450 PRINT:PRINT:INPUT "        Hit RETURN for Microstructural Development Menu
", SEGEND
5460 GOTO 2960
5470 PRINT "     ***   STRESS CORROSION CRACKING SUSCEPTIBILITY PREDICTION   ***
"
5480 PRINT:PRINT "  Potential for IGSCC is assessed based on calculated EPR-DOS"
5490 PRINT "  values.  At the present time this SCC prediction is only "
5500 PRINT "  qualitative.  Slow-strain-rate (laboratory) SCC test data and limi
ted "
5510 PRINT "  field data has been correlated to measured EPR-DOS values.  A more
"
5520 PRINT "  extensive data base is being generated within the present program
at PNL."
5530 PRINT "  This data base will include correlations between Cr depletion,EPR-
DOS and"
5540 PRINT "  IGSCC.  Other variables such as material bulk composition, conditi
on,"
5550 PRINT "  and mechanical properties will also be considered in the final pre
diction."
5560 PRINT:PRINT "  General comments are made concerning the relative SCC suscep
tibility"
5570 PRINT "  of a component after some thermomechanical treatment.  These comme
nts"
5580 PRINT "  only appear on the monitor and are present to give the operator mo
re"
5590 PRINT "  insight into the quantitative prediction of degree of sensitizatio
n."
5600 PRINT:PRINT:PRINT:PRINT:INPUT "        Hit RETURN for Microstructural Devel
opment Menu  ",JJSCC
5610 IGSCC = 1
5620 GOTO 2960
5630 PRINT:PRINT " ***   SENSITIZATION DEVELOPMENT PREDICTION - 24 in. dia. WELD
MENT   ***"
```

```
5640 PRINT:PRINT "Thermomechanical (TM) histories for a 24-in.-dia., schedule 80
 pipe weld"
5650 PRINT "are input and sensitization development in the HAZ calculated.  TM i
nputs"
5660 PRINT "are based on detailed measurements of temperatures and strains at th
e pipe"
5670 PRINT "ID surface during TIG welding at PNL.  Maximum temperatures inputs r
eflect"
5680 PRINT "actual measurements while cooling rates are slower than measured to
approxi-"
5690 PRINT "mate the combined effects of heating rates, time near maximum temper
ature,"
5700 PRINT "and cooling rates on sensitization development.  TIG welding paramet
ers were"
5710 PRINT "comparable to those used for reactor piping systems, however TM hist
ories can"
5720 PRINT "vary significantly depending on specific welding and component param
eters."
5730 PRINT:PRINT "TM histories are input for the first 8 passes at a HAZ locatio
n"
5740 PRINT "about 0.2 cm from the fusion line and sensitization development dete
rmined on"
5750 PRINT "a pass by pass basis.  This option illustrates sensitization develop
ment"
5760 PRINT "that may occur in a weld HAZ and allows the response of various mate
rials"
5770 PRINT "and conditions to be compared.  Detailed predictions for specific we
ldments"
5780 PRINT "require measured or calculated TM histories pertinent to weldment of
"
5790 PRINT "interest.  Models are being developed and evaluated to calculate HAZ
-TM"
5800 PRINT "histories from welding parameters as part of this project.  These mo
dels"
5810 PRINT "will be an intregal part of the overall HAZ-SCC prediction capabilit
y."
5820 PRINT:PRINT:INPUT "                    HIT RETURN TO SET MATERIAL PARAMETERS"
,J1
5830 CCNT=0
5840 RESTORE
5850 TMH=1:NCC=0:CNT=1:IHAZ=1
5860 CLS:IF CCNT=1 GOTO 5890
5870 IF CCNT=2 GOTO 5960
5880 CLS:GOTO 260
5890 IF NCC>0 GOTO 5960
5900 FOR N=1 TO 8
5910 FOR J=1 TO 2
5920 READ B(N,J)
```

```
5930 NEXT J
5940 NEXT N
5950 DATA 990,40:DATA 845,27:DATA 810,12:DATA 795,6:DATA 805,4:DATA 760,3.5:DATA
 685,4:DATA 580,4
5960 NC=0:NCC=8
5970 NC=NC+1:IF NC=NCC+1 THEN GOTO 6100
5980 PRINT:PRINT:PRINT:PRINT "                              *** Program Running ***"
:PRINT:PRINT
5990 IF CCNT=1 THEN PRINT E$:PRINT G$
6000 IF CCNT=2 THEN PRINT F$:PRINT H$
6010 ITEMP=B(NC,2):DF(2,NDF)=ITEMP
6020 STEMP=B(NC,1):DF(3,NDF)=STEMP
6030 ETEMP=480
6040 IF NC>1 GOTO 6060
6050 WICUM=0:IJK=1:JABC=0
6060 JJJ=JJJ+1:DF(1,NDF)=JJJ
6070 IWELD=1
6080 IF NC=NCC+1 GOTO 6100
6090 GOTO 3680
6100 CLS:PRINT
6110 IF CCNT=0 THEN PRINT A$
6120 IF CCNT=1 THEN PRINT E$:PRINT G$
6130 IF CCNT=2 THEN PRINT F$:PRINT H$
6140 PRINT
6150 PRINT "WELD PASS     MAX. PASS      COOLING RATE    Cr DEPLETION   EPR VALU
E"
6160 PRINT " NUMBER        TEMP.,C        deg. C/sec       WIDTH, A       C/cm2
6170 PRINT "---------     ---------      ------------     ----------     -------
":PRINT
6180 FOR NDF=0 TO (NCC-1)
6190 PRINT "    ";DF(1,NDF),"    ";DF(3,NDF);
6200 PRINT USING "           ###.#";DF(2,NDF);
6210 PRINT USING "              ####";DF(5,NDF)*10^8;
6220 PRINT USING "    ######.#";DF(6,NDF)
6230 NEXT NDF
6240 PRINT:PRINT:ITBLE=1:NDF=0:ISTR=0:SIMSTR=0
6250 IF IGSCC>0 GOTO 2690
6260 PRINT:INPUT "          Hit RETURN to continue   ",IIII
6270 IF CCNT=1 THEN GOTO 6870
6280 IF CCNT=2 GOTO 6490
6290 IF CCNT=0 THEN ISTR=0:GOTO 2950
6300 CLS:PRINT:PRINT "A high carbon Type 304 and a low carbon Type 316L stainles
s steel are evaluated"
6310 PRINT "at three temperatures and at three times to illustrate isothermal se
nsiti-"
6320 PRINT "zation prediction.  The example runs the 304 case first and then the
 316L "
6330 PRINT "case.  Input compositions are shown along with the predictions."
```

```
6340 PRINT:PRINT:INPUT "     Hit RETURN to continue   ",IIII
6350 A(1,1)=.06:A(1,2)=18.5:A(1,3)=9:A(1,4)=.1:A(1,5)=.02
6360 A(2,1)=.02:A(2,2)=17:A(2,3)=11:A(2,4)=2.1:A(2,5)=.07
6370 KKK=5:JABC=1:ISOTH=1:CCNT=0:JJJ=0
6380 C$= "Isothermal Sensitization of Type 304 SS"
6390 D$= "Isothermal Sensitization of Type 316L SS"
6400 CLS:PRINT C$:DDF=1
6410 IF DDF=1 GOTO 6430
6420 CLS:PRINT D$:DDF=2
6430 CW=A(DDF,1):CRB=A(DDF,2):CRB1=CRB:NI=A(DDF,3):NI1=NI:MO=A(DDF,4):NIT=A(DDF,
5):NITRO=NIT*.56/14
6440 GOTO 460
6450 INCON=0:JPRED=1
6460 GSNO=5
6470 IF CCNT>0 GOTO 5840
6480 KKK=5:JABC=1:STEMP=800:KTEMP=600:ITEMP=100:GOTO 800
6490 PRINT:INPUT "                    Hit RETURN for Example Problem Menu",IIII:C
LS:GOTO 5130
6500 IF DDF<1 OR DDF>1 THEN GOTO 6560
6510 PRINT:PRINT:PRINT "Sensitization is predicted to increase with increasing t
ime at 600 and "
6520 PRINT "700 deg. C.  At 800 deg. C, healing occurs within several hours.  He
aling "
6530 PRINT "is accounted for by adjusting the minimum Cr content, thereby reduci
ng the"
6540 PRINT "Cr depletion width and the EPR-DOS value.  Healing is just beginning
 "
6550 PRINT "after 100 hours at 700 deg. C."
6560 IF DDF<2 THEN GOTO 6630
6570 PRINT:PRINT:PRINT "Sensitization is predicted to increase with increasing t
ime at 600 and 700 C."
6580 PRINT "Predicted DOS levels are much smaller for the 316L heat than for the
 304 heat"
6590 PRINT "primarily due to the difference in bulk carbon contents. No sensitiz
ation"
6600 PRINT "is predicted at 800 C because the calculated minimum Cr content at t
he"
6610 PRINT "grain boundaries is greater that the critical level for attack in th
e"
6620 PRINT "EPR test (i.e. 13.5 wt%)."
6630 PRINT:INPUT "                    Hit RETURN to continue    ",IIII
6640 IF DDF=1 GOTO 6420
6650 IF DDF=2 GOTO 6490
6660 CLS:PRINT:PRINT "A high carbon Type 304 and a low carbon Type 316 stainless
 steel are evaluated"
6670 PRINT "to illustrate the model's ability to calculate sensitization develop
ment"
```

```
6680 PRINT "during and after a typical HAZ thermal history.  Thermal histories f
or"
6690 PRINT "eight passes are automatically input and DOS reported after each pas
s.  The"
6700 PRINT "example runs the 304 case first and then the 316L case.  Maximum tem
peratures"
6710 PRINT "input reflect actual measured values, while cooling rates input are
slower"
6720 PRINT "than those measured to better approximate HAZ sensitization developm
ent."
6730 PRINT "HAZ sensitization development results from the entire thermal cycle
"
6740 PRINT "including heat-up, time near the peak temperature and a changing coo
ling"
6750 PRINT "rate with temperature.  The simple linear cooling rates used in the
present"
6760 PRINT "model cannot simulate the measured thermal cycle without separately
input-"
6770 PRINT "ting the various different segments of the overall cycle.  A number
of more"
6780 PRINT "exact methods of inputting thermal histories are being developed."
6790 PRINT:PRINT:INPUT "            Press RETURN to continue    ",IIII
6800 A(1,1)=.06:A(1,2)=18.5:A(1,3)=9:A(1,4)=.1:A(1,5)=.02
6810 A(2,1)=.02:A(2,2)=17:A(2,3)=12:A(2,4)=2.1:A(2,5)=.06
6820 E$="Weld HAZ Sensitization of 304 SS"
6830 F$="Weld HAZ Sensitization of 316L SS"
6840 DDF=0:IHAZ=0:ICCS=1
6850 CLS:PRINT E$:CCNT=1
6860 IF CCNT=1 GOTO 6900
6870 CLS:PRINT F$:CCNT=2
6880 IF CCNT=2 THEN JJJ=0:ITBLE=0
6890 IF CCNT=2 THEN NDF=0
6900 CW=A(CCNT,1):CRB=A(CCNT,2):CRB1=CRB:NI=A(CCNT,3):NI1=NI:MO=A(CCNT,4):NIT=A(
CCNT,5)
6910 GOTO 460
6920 PRINT:PRINT:PRINT "    ***   RESTART ANALYSIS - SAME MATERIAL CONDITIONS
***"
6930 PRINT:PRINT:PRINT "This option simplifies the input required to run consecu
tive analyses"
6940 PRINT "on the same heat of material.  Material parameters must be input usi
ng"
6950 PRINT "options 2,3 or 4 initially, however after the first predictions iden
tical"
6960 PRINT "bulk compositions and material conditions are assumed if this option
 is "
6970 PRINT "selected.  The purpose is to enable repetitive predictions illustrat
ing"
```

```
6980 PRINT "the sensitization response of a particular heat.  Once a composition
 is"
6990 PRINT "selected only the input for the TM history will be required.  To can
cel"
7000 PRINT "this setup and examine other materials, it is necessary to recall th
is"
7010 PRINT "option and reset the following flag."
7020 PRINT:PRINT:PRINT:INPUT "     Enter 1 to set, RETURN to cancel    ",IREPET
7030 IF CW=0 THEN PRINT:PRINT "     Material Parameters have not been Defined '!
"
7040 PRINT:INPUT "     Hit RETURN for Microstructural Development Menu   ",JRS
7050 CLS:GOTO 2980
```

APPENDIX B

ISOTHERMAL SENSITIZATION DATA BASE

B1 EPR-DOS DATA SUMMARY - AVERAGE VALUES (C/cm^2)

	Isothermal Heat Treatment Temperature and Times (h)							
	480 C		500 C			600 C		
Heat	5000	10	100	500	1.0	10	100	500
SS-1	-	-	0	-	0	8.2	18	-
SS-2	-	-	0	-	0	3.9	13	-
SS-3	-	0	0	-	0	6.3	20	-
SS-4	-	0.6	4.7	-	1.9	9.2	31	-
SS-5	-	4.5	13	-	0	22	50	-
SS-6	-	0.1	3.3	-	2.3	21	42	-
SS-7	-	1.0	12	-	5.6	44	65	-
SS-11	-	-	-	0.5	0	0.6	8.1	45
SS-12	-	-	-	0	0	0.2	2.4	16
SS-13	-	-	-	0	0	0	0.9	12
SS-14	-	-	0	1.1	0	0.5	8.0	42
SS-15	-	0	0	-	0	0.2	24	-
SS-16	7.3	0	0	-	0	13	47	-
SS-17	-	1.1	0.9	-	0	16	62	-
C-1	-	0	1.7	-	-	1.0	5.1	-
C-2	13	0	0.2	-	0	3.3	32	-
C-3	-	0	0.3	-	0.2	6.9	45	-
C-4	-	3.2	7.9	-	6.9	16	64	-
C-5	-	-	5.1	-	-	-	35	-
C-6	66	6.8	16	-	8.7	19	56	-
C-7	34	8.0	27	-	10	25	70	-
C-8	-	-	-	-	-	7.2	37	-
C-9	-	-	-	-	-	21	57	-
C-10	15	0	0	-	0	2.0	51	-
C-11	-	-	-	-	-	-	0	-
C-12	-	-	-	-	-	0	0	-
N-1	0	-	-	-	-	0	0.5	1.5
N-2	1.7	-	-	-	-	0.5	5.1	18
N-3	-	-	-	-	-	0.5	1.3	20
N-4	-	-	-	-	-	0	0.6	8.3
N-5	-	-	-	-	-	0.3	6.9	34
N-6	-	-	-	-	-	0.2	1.1	12
N-7	-	-	-	-	-	0	0.1	-

	Isothermal Heat Treatment Temperature and Times (h)								
	650 C		700 C				800 C		
Heat	20	500	0.1	1.0	10	100	0.1	1.0	10
SS-1	-	-	0	0.5	1.3	6.6	1.7	1.3	0
SS-2	-	-	0	0.9	0.2	0.4	0.2	0	0
SS-3	-	-	0	0	1.5	8.4	1.8	0	0
SS-4	-	-	0.4	11	18	2.9	0	2.2	0
SS-5	-	-	3.8	24	79	86	33	6.3	1.6
SS-6	-	-	0.3	17	44	32	11	2.9	1.0
SS-7	-	-	1.0	23	53	93	7.3	14	2.3
SS-11	4.2	7.0	0	0	0	4.0	0	0	0
SS-12	5.8	15	0	0	0.3	3.9	1.7	0	0
SS-13	0.9	1.7	0	0	0	3.2	1.2	0	0
SS-14	1.8	73	0	1.2	11	30	0	0	0
SS-15	-	-	0	0.5	24	58	0	0.6	2.0
SS-16	-	-	0	20	68	102	0.6	50	2.9
SS-17	-	-	0	14	83	181*	2.4	61	76
C-1	9.9	26	0	0	0	0	0	0	0
C-2	0	33	0	0	0	1.5	0	0	0
C-3	-	-	-	-	-	-	-	-	-
C-4	31	70	5.0	20	70	149*	0.5	1.1	1.1
C-5	-	49	-	-	-	-	-	-	-
C-6	-	-	9.2	14	60	82	0.4	1.0	0.9
C-7	-	-	4.0	19	69	94	7.7	8.1	1.2
C-8	-	-	-	38	47	0.5	-	-	-
C-9	-	-	-	36	57	8.7	-	-	-
C-10	-	-	0	3.0	35	100	1.2	21	35
C-11	-	-	-	-	-	1.3	-	-	-
C-12	-	-	-	0	0	16	-	-	-
N-1	4.0	10	-	0	0	0.6	-	-	-
N-2	9.0	44	-	0	0.5	15	-	-	-
N-3	9.1	50	-	0	0.3	16	-	-	-
N-4	1.6	13	-	0	0	1.1	-	-	-
N-5	20	60	-	0	1.1	20	-	-	-
N-6	8.2	24	-	0	0	1.8	-	-	-
N-7	-	-	-	0	0.4	4.7	-	-	-

* Specimens exhibitted significant transgranular attack during EPR test. Reported EPR-DOS values overestimate actual DOS.

B2 ESTIMATED TIMES-TO-SENSITIZE

Data listing summarizing times-to-sensitize for many Type 304 and 316 stainless steel heats. Heat compositions are reported along with estimated times-to-sensitize in hours at 600, 650 and 700 C. These temperatures were selected because of the available literature data. Only DOS measurements using the Strauss, modified Strauss or EPR test techniques were compiled and evaluated. Times-to-sensitize were extrapolated or simply estimated from the reported DOS as a function of time at temperature for the heats. An EPR-DOS value of about 5 C/cm^2 was used to represent initial sensitization, while any significant intergranular attack in the Strauss test was considered to indicate a sensitized condition.

Isothermal Sensitization : Data Table

Heat[a]	Type	Composition, wt%										Time to Sensitize, h		
		C	Cr	Ni	Mo	Mn	Si	P	S	N	B	700°C	650°C	600°C
SS1	304L	0.013	18.21	10.34	0.07	1.54	0.58	0.012	0.008	0.039	0.001	--	5	8
SS2	304L	0.013	18.20	10.54	0.25	1.82	0.45	0.009	0.022	0.046	0.002	--	5	10
SS3	304L	0.019	18.30	10.33	0.20	1.51	0.45	0.012	0.001	0.018	0.001	--	3	8
SS4	304	0.044	18.35	9.18	0.31	1.63	0.36	0.012	0.001	0.049	0.002	.5	1.0	4
SS5	304	0.054	18.42	8.47	0.08	1.01	0.53	0.012	0.011	0.062	0.001	.2	.3	2
SS6	304	0.050	18.67	8.78	0.16	1.89	0.38	0.012	0.002	0.059	0.001	.3	.5	2
SS7	304	0.060	19.17	9.54	0.12	1.31	0.42	0.013	0.015	0.041	0.001	.2	.3	.8
SS11	316L	0.015	17.93	12.73	2.11	0.89	0.65	0.014	0.001	0.020	0.001	80	100	200
SS12	316L	0.014	17.77	12.64	2.18	0.89	0.60	0.014	0.005	0.023	0.001	100	100	200
SS13	316L	0.013	17.53	12.70	2.10	1.39	0.59	0.014	0.001	0.027	0.001	100	100	200
SS14	316L	0.020	16.92	12.90	2.30	1.66	0.38	0.014	0.002	0.011	0.001	20	25	50
SS15	316	0.035	17.32	10.91	2.15	1.71	0.63	0.013	0.012	0.062	0.002	3	5	20
SS16	316	0.058	17.11	11.43	2.26	1.77	0.41	0.014	0.005	0.008	0.002	.3	1	3
SS17	316	0.067	16.81	11.21	2.20	1.46	0.28	0.016	0.020	0.071	0.003	.3	1	3
C1	304L	0.016	18.55	8.91	0.14	1.81	0.46	0.019	0.004	0.083	--	--	10	100
C2	304L	0.020	18.38	9.03	0.23	1.65	0.51	0.033	0.009	0.067	--	--	10	15
C3	304	0.034	18.25	8.77	0.29	1.70	0.59	0.024	0.009	0.075	--	.05	.03	1
C4	304	0.052	18.16	8.26	0.19	1.72	0.77	0.018	0.006	0.088	--	.1	.2	1
C5	304	0.050	18.64	8.92	0.17	1.80	0.61	0.022	0.007	0.098	--	.1	.2	1
C6	304	0.062	18.48	8.75	0.20	1.72	0.39	0.013	0.013	0.065	--	0.5	.1	.5
C7	304	0.072	18.53	9.33	0.43	1.74	0.46	0.046	0.017	0.036	--	0.5	.1	.5
C10	316	0.050	17.40	12.50	2.17	1.30	0.66	.0032	0.018	--	--	1	1	10

Isothermal Sensitization : Data Table

Heat[a]	Type	Composition, wt%										Time to Sensitize, h		
		C	Cr	Ni	Mo	Mn	Si	P	S	N	B	700°C	650°C	600°C
N1	316L	0.011	16.50	10.18	2.06	1.67	0.62	0.030	0.013	0.086	--	--	300	700
N2	316L	0.019	16.20	10.35	2.15	1.70	0.42	0.030	0.013	0.087	--	30	50	150
N3	316LN	0.023	17.00	10.48	2.16	1.84	0.61	0.025	0.003	0.154	--	20	40	150
N4	316LN	0.014	16.80	10.34	2.16	1.63	0.59	0.026	0.009	0.145	--	--	100	500
N5	316LN	0.024	16.75	10.49	2.10	1.62	0.54	0.023	0.018	0.163	--	20	25	70
N6	316LN	0.012	16.63	10.60	2.10	1.69	0.52	0.022	0.006	0.190	--	--	100	300
A	304L	.034	18.02	8.63	--	1.51	0.64	.04		.002		0.3	0.4	2
A	304LN	.029	18.13	11.68	--	1.54	0.52	.03		.13		6	3	2
B	304LN	.030	18.58	7.86	--	1.6	0.36	.03		.108		1	1	3
C	304LN	.036	20.22	9.52	--	1.59	0.49	.03		.083		0.8	0.8	2
HP1	304	0.069	18.6	9.4	--	--				0.002		.2	.15	0.8
HP2	304	0.045	17.22	9.51	--	--				0.003		.8	.6	2
HP3	304L	0.028	18.5	9.2	--	--				0.010		8	6	10
HP4	304L	0.013	18.5	9.5	--	--				0.010		15	15	80
HCN1	304	0.066	17.47	8.59	--	--				0.038		.1	.15	.6
HCN2	304	0.061	17.10	8.52	--	--				0.067		.15	.2	1.0
HCN3	304N	0.064	17.38	8.53	--	--				0.124		.3	.4	2
LCN1	304L	0.013	17.30	8.49	--	--				0.037		50	15	20
LCN2	304L	0.027	16.70	9.02	--	--				0.065		20	25	25
LCN3	304LN	0.015	17.96	8.77	--	--				0.097		60	40	100

Isothermal Sensitization : Data Table

Heat[a]	Type	Composition, wt%										Time to Sensitize, h		
		C	Cr	Ni	Mo	Mn	Si	P	S	N	B	700°C	650°C	600°C
	304	0.44	17.2	10.7		1.48	0.46	.027	.009				0.3	
		.10	18.0	7.7		0.5	0.51	.017	.009			0.03		
		.06	18	8		1.5	0.5					1	0.8	5
	304	.05	18.1	8.5	.16	.47	.44	.019	.009			4/8	1/3	1/7
	304	.077	18.2	8.43	--	1.12	.40	.025	.025			0.01/ 0.05	0.05/ 0.2	3/1
	304	.053	18.07	8.84		1.26	.52	.031	.006	.018		.05	.1	1.0
	304	.052	18.5	9.15	.09	1.61	.50	.027	.007			.2	.5	3
	304	0.050	18.4	9.34		1.5	0.62					.5	.5	1.5
	304	0.038	18.4	9.2	0.52	1.60	0.45	0.021	0.019			0.5	0.5	1.0
3A37	304L	0.018	18.64	8.66	0.23	1.82	0.59	0.023	0.013					
1H32	304L	0.028	18.26	8.50	0.36	1.71	0.36	0.028	0.013			.3	.4	.5
1E98	304	0.057	18.92	8.51	0.35	1.59	0.46	0.035	0.013			.05	.1	.5
3754	304	0.053	19.27	8.49	0.36	1.77	0.008	0.031	0.41			.05	.1	.5
3751	304	0.044	18.87	8.59	0.36	1.77	0.46	0.034	0.007			.2	.25	.4
3A39	304	0.044	18.20	8.43	0.23	1.83	0.55	0.023	0.006			.3	.5	.7
3752	304	0.043	18.80	8.63	0.38	1.78	0.41	0.028	0.008			0.9	.9	1.2
3753A	304	0.046	18.90	8.89	0.38	1.37	0.40	0.030	0.008			.2	.4	.9
1E97	302	0.092	18.98	8.55	0.35	1.63	0.46	0.035	0.012			.005	.01	.03
3753	302	0.090	18.80	8.59	0.36	1.74	0.39	0.030	0.007			.01	.02	.05
	304	.051	18.67	8.38	.13	1.52	.67	.022	.028	.04			0.5	
	304	.052	19.08	9.00	.22	1.77	.61	.034	.009	--		.05	0.1	0.5
	302	0.10	17.82	10.50		1.22	0.52					.01	.02	.08
	304	0.07	18.12	10.25		1.36	0.64					.03	.04	.2

Isothermal Sensitization : Data Table

Heat[a]	Type	Composition, wt%										Time to Sensitize, h		
		C	Cr	Ni	Mo	Mn	Si	P	S	N	B	700°C	650°C	600°C
A	304	0.061	18.38	8.32	0.04	1.56	0.62	0.021	0.018	0.045			.1	.2
B	304	0.042	18.56	8.83	0.19	1.46	0.45	0.019	0.029	0.042			1	3
C	304	0.061	18.23	8.14	0.16	1.55	0.62	0.022	0.022	0.031			.1	.2
H	304	0.044	18.69	8.24	0.30	1.55	0.58	0.024	0.017	0.039			.2	.5
I	304	0.057	18.55	8.18	0.18	1.46	0.55	0.023	0.021	0.092			1	3
K	304	0.060	18.20	8.10	0.21	1.42	0.53	0.023	0.025	0.074			1	3
	304	0.050	18.22	10.95						0.049		.02	.05	.2
	304L	0.027	18.35	10.75						0.043		.1	.3	1
	304L	0.021	18.51	10.66						0.047		.1	1	3
	304L	0.027	18.02	14.97						0.027		.02	.05	.3
	304L	0.025	18.30	9.72						0.062		.1	1	4
	304LN	0.026	18.62	9.35						0.156		.1	1	8
K380	304L	0.018	18.54	9.86		1.23	0.48			0.044			10	
K652	304L	0.022	17.83	9.21		1.2	0.4			0.016			2	
K17	304L	0.025	17.99	9.71		0.98	0.30			0.015			2	
L376	304L	0.027	18.92	9.70		1.26	0.39			0.032			1.0	
K382	304	0.042	18.36	9.97		1.36	0.50			0.027			.2	
K383	304	0.045	18.61	9.90		1.26	0.40			0.026			.2	
K197	304L	0.020	18.57	10.31		1.14	0.33			0.031			10	
K634	304L	0.021	18.51	10.66		1.32	0.37			0.047			2	
K198	304L	0.024	18.37	10.88		1.09	0.32			0.029			2	
K638	304L	0.026	18.35	10.75		1.40	0.36			0.054			1.5	
K385	304L	0.027	18.48	10.41		1.33	0.51			0.043			2	
L379	304	0.032	18.54	10.39		1.22	0.42			0.037			0.8	

Isothermal Sensitization : Data Table

Heat[a]	Type	Composition, wt%										Time to Sensitize, h		
		C	Cr	Ni	Mo	Mn	Si	P	S	N	B	700°C	650°C	600°C
K384	304	0.049	18.48	10.34		1.24	0.44			0.041			.2	
K388	304	0.050	18.22	10.95		1.50	0.46			0.049			.05	
K199	304L	0.018	18.40	11.50		1.09	0.32			0.036			10	
K393	304L	0.023	17.83	11.38		1.40	0.52			0.040			2	
K395	304L	0.023	18.51	11.82		1.32	0.51			0.026			2	
L382	304L	0.031	18.05	11.24		1.23	0.44			0.031			.6	
K776	304L	0.056	18.19	11.10		0.75	0.42			0.015			0.3	
K765	304	0.005	19.30	12.14		0.82	0.46			0.024				
K394	304L	0.022	17.92	12.64		1.27	0.50			0.027			5	
L3	304L	0.026	20.29	12.80		1.42	0.51			0.030			1.0	
L14	304L	0.028	20.52	12.71		1.24	0.54			0.039			.2	
L722	304L	0.025	18.3	6.5		1.2	0.4			0.089			1.5	
L723	304L	0.030	18.3	6.5		1.2	0.4			0.115			1.5	
L725	304L	0.033	18.3	6.5		1.2	0.4			0.132			.8	
L724	304L	0.033	18.3	6.5		1.2	0.4			0.146			1.0	
L348	304	0.034	18.16	7.65		1.30	0.52			0.088			2	
L347	304	0.036	18.47	7.63		1.22	0.43			0.031			2	
L349	304	0.041	17.80	7.38		1.22	0.49			0.136			.9	
L726	304L	0.030	18.3	8.0		1.2	0.4			0.113			2.5	
L727	304L	0.032	18.3	8.0		1.2	0.4			0.144			2	
K380	304L	0.018	18.54	9.86		1.23	0.48			0.044			10	
K17	304L	0.025	17.99	9.71		0.98	0.30			0.015			2.5	
K652	304L	0.022	17.83	9.21		1.2	0.4			0.016			2	
L376	304L	0.027	18.92	9.70		1.26	0.39			0.032			.9	

Isothermal Sensitization : Data Table

Heat[(a)]	Type	Composition, wt%										Time to Sensitize, h		
		C	Cr	Ni	Mo	Mn	Si	P	S	N	B	700°C	650°C	600°C
K381	304LN	0.025	18.30	9.72		1.38	0.48			0.062			2.5	
L385	304LN	0.024	18.62	9.36		1.07	0.42			0.089			1.0	
L388	304LN	0.028	18.16	9.33		1.22	0.42			0.145			1.0	
L729	304LN	0.029	18.3	9.0		1.4	0.4			0.147			2.5	
L386	304LN	0.025	18.25	9.61		1.32	0.44			0.148			1.0	
L378	304LN	0.026	18.62	9.35		1.25	0.40			0.156			1.0	
K119	304L	0.031	18.36	9.43		1.25	0.39			0.057			.6	
L387	304	0.032	18.78	9.42		1.27	0.50			0.036			.9	
L377	304N	0.034	18.54	9.25		1.18	0.46			0.105			.7	
L728	304N	0.039	18.3	9.0		1.2	0.4			0.115			2	
K198	304L	0.024	18.37	10.88		1.09	0.32			0.029			2	
K197	304L	0.020	18.57	10.31		1.14	0.33			0.031			10	
K385	304L	0.027	18.48	10.41		1.33	0.51			0.043			2.5	
K634	304L	0.021	18.51	10.66		1.32	0.37			0.047			2.5	
K638	304L	0.026	18.35	10.75		1.40	0.36			0.054			2.0	
L380	304LN	0.030	18.25	10.15		1.24	0.40			0.100			0.8	
K636	304LN	0.022	18.22	10.88		1.28	0.39			0.118			1.0	
K641	304LN	0.030	18.02	10.97		1.27	0.40			0.149			0.9	
K637	304LN	0.024	18.60	10.66		1.36	0.38			0.150			1.0	
L381	304	0.028	18.21	10.62		1.16	0.44			0.156			5	
L379	304	0.032	18.54	10.39		1.22	0.42			0.037			0.7	
K123	304N	0.033	18.35	10.47		1.20	0.40			0.153			0.4	
K121	304N	0.035	18.29	10.53		1.24	0.45			0.127			0.5	
K386	304	0.041	18.29	10.60		1.35	0.38			0.039			0.6	

Isothermal Sensitization : Data Table

Heat[(a)]	Type	Composition, wt%										Time to Sensitize, h		
		C	Cr	Ni	Mo	Mn	Si	P	S	N	B	700°C	650°C	600°C
K384	304	0.049	18.48	10.34		1.24	0.44			0.041			0.2	
K388	304	0.050	18.22	10.95		1.50	0.46			0.049			.05	
K117	304	0.054	18.36	10.56		1.38	0.44			0.038			0.8	
K395	304L	0.023	18.51	11.82		1.32	0.51			0.026			2	
K393	304L	0.023	17.83	11.38		1.40	0.52			0.040			2	
K387	304L	0.030	17.90	11.04		1.22	0.44			0.066			1.5	
K639	304LN	0.026	18.32	11.44		1.35	0.36			0.078			1.0	
K640	304LN	0.028	18.08	11.22		1.21	0.35			0.120			1.5	
L382	304	0.031	18.05	11.24		1.23	0.44			0.031			0.9	
K392	304	0.033	18.78	11.32		1.26	0.47			0.028			1.5	
K776	304	0.056	18.19	11.10		0.75	0.42			0.015			.05	
L384	304N	0.033	18.31	12.50		1.22	0.46			0.176			0.9	
C6	304	.063	18.5	11.4	.08	1.66	.60	.008	.011	.029		.05	.02	0.5
C4	304	.043	18.4	9.4	.22	1.24	.58	.010	.012	.029		.5	.3	0.7
C2	304L	.023	18.5	10.3	.29	1.31	.46	.020	.003	.064		3	5	20
C2N	304LN	.023	18.6	10.2	.12	1.24	.63	.010	.008	.20			10	30
	304	.052	9.08	9.00	.22	1.77	0.61	.034	.009	--		.05	.05	.1
ELC	304L	.014	18.40	10.50	.27	1.69	.33	.034	.014	.03			10	25
ELN	304LN	.014	18.49	8.92	.23	1.68	.35	.034	.010	.095			10	13
ELN	316LN	.014	17.70	13.89	2.29	1.72	.39	.024	.010	.090		50	100	200
	304	.05	18.4	9.3		1.58	0.44	.027	.0065			.05	.05	1
	316	.046	16.9	13.2	2.06	1.74	.70	.026	.006			.5	2	20
	316L	.009	17.10	12.75	2.48	1.44	.43	.022	.005	.08			300	500
	304	.052	18.5	9.15		1.61	0.5	.027	.007			.05	.05	3

Isothermal Sensitization : Data Table

Heat[a]	Type	Composition, wt%										Time to Sensitize, h		
		C	Cr	Ni	Mo	Mn	Si	P	S	N	B	700°C	650°C	600°C
	304-1	0.06	18.56	8.78	--	1.19	0.49	0.025	0.010			.2	.3	.7
	304L	0.018	18.96	9.91	--	0.96	0.59	0.025	0.015			2.5	2.5	4
	316-1	0.05	17.40	13.02	2.48	0.60	0.96	0.029	0.006			0.6	3	20
	316L	0.014	17.58	12.48	2.40	1.00	0.72	0.029	0.004			2	15	100
	304	0.05	18.17	8.29		1.20	0.59	0.031	0.014			.02	.1	.5
	316	0.05	17.01	10.86	2.13	1.02	0.63	0.033	0.004			0.5	2	20
	304L	0.018	18.18	10.04		1.47	0.64	0.032	0.008				100	
	316L	0.018	17.26	12.21	2.07	1.33	0.64	0.035	0.005				200	
AISI	304	0.05	18.5	8.5	0.10	1.28	0.65	0.025	0.010				0.1	
	302	0.09	17.21	8.05		0.66	0.56					.01	.05	.1
	304	0.04	18.71	10.76		1.40	0.39					5	5	10
	304	0.06	17.13	9.13		1.06	0.35					.5	.6	2
	316	0.03	16.54	14.05	2.23	1.58	0.34					1.5	3	20
	316	0.05	17.76	13.38	2.28	1.53	0.40					.1	1	10
	317	0.04	18.14	14.36	3.03	1.66	0.35					50	50	200
	317	0.10	18.30	13.62	3.09	1.59	0.37					.5	1	20
	316	0.057	17.14	12.77	2.21	1.67	0.54	0.035	0.025			.08/.5	.2/1.0	1/5
	304	0.078	18.1	8.49	--	1.12	0.41	0.025	0.027			.05/.2	.08/1	.1/3
4UL	304L	0.012	18.30	10.12	0.03	1.52	0.56	0.036	0.004			10	10	30
4L	304L	0.022	18.80	10.34	--	1.05	0.59	0.023	0.009			5	5	10
	304	0.054	18.2	8.5	--							.5	.3	0.9
	316	0.054	17.7	12.2	2.52							.3	.5	5
	304L	0.020	18.4	10.7	--								30	30

Isothermal Sensitization : Data Table

Heat[(a)]	Type	Composition, wt%										Time to Sensitize, h		
		C	Cr	Ni	Mo	Mn	Si	P	S	N	B	700°C	650°C	600°C
	316L	0.025	16.9	13.4	2.50							10	8	12
	304L	.022	19.31	9.39	--	1.74	.34	0.21	.018	.053		3	3.5	5
	316L	.023	18.42	12.62	3.00	1.40	.32	.018	.013	.020		2	1	10
MO1	316	0.077	18.08	11.6	2.0	--				0.002		.2	.5	2
MO2	316L	0.025	16.17	10.1	2.0	--				0.002		8	100	200
MON1	316	0.067	17.67	8.76	2.0	--				0.035		2	2	5
MON2	316N	0.067	17.65	8.80	2.03	--				0.096		2	2	10
MN1	316N	0.068	17.72	8.67	--	1.89				0.091		.2	.5	5
1	316LN	0.028	16.29	9.78	2.53	1.64	0.34	0.03		0.078		10	20	200
2	316LN	0.025	15.77	9.82	2.58	1.66	0.45	0.03		0.121		10	15	60
3	316LN	0.026	16.32	9.81	2.52	1.66	0.47	0.03		0.161		10	30	200
C	316	0.057	17.14	12.77	2.21	1.67	0.54	0.035		0.06		.7	1	5
	316L	0.022	17.0	13.3	2.25	1.80	0.38	0.021	0.020	0.032	18		1000	2000
	316L	0.023	17.4	12.1	2.44	1.70	0.40	0.029	0.008	0.078	38		1000	2000
	316	0.032	17.2	12.2	2.32	1.60	0.34	0.022	0.025	0.072	26	20	30	200
	316	0.030	17.5	12.3	2.47	1.84	0.44	0.021	0.002	0.075	11	20	40	200
A1	304	0.051	18.4	9.6	--	1.81	0.68	0.021	0.017	0.062	<10	.5	.5	10
SQ	316	0.030	17.5	12.3	2.47	1.84	0.44	0.021	0.002	0.075	11	5	10	30
	316LN	.018	16.2	13.4	2.37	1.43	0.51	.005	.002	.108			20	50
	316L	.017	16.8	13.7	2.38	1.36	0.53	.012	.017	.026			20	30
	316	.054	16.46	12.43	2.28	1.69	.64	.025	.006		13.3	.6	1.0	8
	316	.057	16.62	12.44	2.32	1.65	.0685	.025	.007			.8	2	10

Isothermal Sensitization : Data Table

Heat[a]	Type	Composition, wt%										Time to Sensitize, h		
		C	Cr	Ni	Mo	Mn	Si	P	S	N	B	700°C	650°C	600°C
	316L	.023	17.3	13.1	2.66	1.74	0.73					2	10	100
	316	.066	17.4	12.3	2.05	1.57	0.21					.1	.3	2

V I T A

June 22, 1953	Born - St. Louis, Missouri
1975	B.S. Metallurgical Engineering University of Illinois Urbana, Illinois
1977	M.S. Metallurgical Engineering University of Illinois Urbana, Illinois
1977 - present	Senior Research Scientist Material Sciences Department Battelle Northwest Laboratories Richland, Washington
1986 - 1987	Visiting Research Scientist Department of Materials Science and Engineering Oregon Graduate Center Beaverton, Oregon

RESEARCH EXPERIENCE AND PUBLICATIONS

Areas of research have included environment-induced material degradation, microstructural/microchemical effects on structural properties and interfacial phenomena in metallic materials. This work has led to more than 60 technical publications.